ROLE OF CT IN PATIENTS WITH PROSTHETIC HEART VALVES

Dominika Suchá

ROLE OF CT IN PATIENTS WITH PROSTHETIC HEART VALVES
PhD thesis, Utrecht University, the Netherlands

Copyright © D. Suchá 2016
All rights reserved. No part of this publication may be reproduced or transmitted in any form or by any means without permission from the author. The copyright of articles that have been published or accepted for publication has been transferred to the respective journals.

Financial support for the publication of this thesis was generously provided by: ABN AMRO Bank, Chipsoft and Guerbet Nederland.

Cover: Geoff Naylor
Lay out: Roy Sanders
Print: GVO drukkers & vormgevers B.V.
ISBN: 978-90-6464-982-0

ROLE OF CT IN PATIENTS WITH PROSTHETIC HEART VALVES

DE ROL VAN CT IN PATIËNTEN
MET EEN KUNSTHARTKLEP
(*met een samenvatting in het Nederlands*)

PROEFSCHRIFT

ter verkrijging van de graad van doctor aan de Universiteit Utrecht
op gezag van de rector magnificus, prof. dr. G.J. van der Zwaan,
ingevolge het besluit van het college voor promoties
in het openbaar te verdedigen
op woensdag 16 maart 2016 des middags te 2.30 uur

door

Dominika Suchá
geboren op 30 april 1987
te Praag, Tsjechoslowakije

Promotoren:	Prof. dr. W.P.Th.M. Mali
	Prof. dr. L.A. van Herwerden
Copromotoren:	Dr. R.P.J. Budde
	Dr. P. Symersky

Financial support by the Dutch Heart Foundation for the publication of this thesis is gratefully acknowledged.

The research described in this thesis was supported by a grant of the Dutch Heart Foundation (DHF grant number 2009B014).

To my parents

CONTENTS

Chapter 1	General introduction	9
Chapter 2	Multimodality imaging assessment of prosthetic heart valves: a systematic review	21
	PART ONE In vitro studies	
Chapter 3	Multidetector-row CT allows accurate measurement of mechanical prosthetic heart valve leaflet closing angles compared with fluoroscopy: an in vitro study	57
Chapter 4	The impact of a novel model-based iterative reconstruction algorithm on prosthetic heart valve related artifacts at reduced radiation dose multidetector-row CT	73
Chapter 5	Mock circulation loop for CT and MR imaging of prosthetic heart valves: a technical note	91
	PART TWO In vivo studies	
Chapter 6	Does the aortic annulus undergo conformational change throughout the cardiac cycle? A systematic review	109
Chapter 7	Baseline MDCT findings after prosthetic heart valve implantation provide important complementary information to echocardiography for follow-up purposes	135
Chapter 8	Diagnostic work-up and treatment strategy in patients with suspected prosthetic heart valve dysfunction: the incremental value of MDCT	157
Chapter 9	Reliability, agreement, and presentation of a reference standard for implanted heart valve sizes by multidetector-row computed tomography	183

Chapter 10	Aortic bioprostheses deform after implantation: insights from multidetector-row computed tomography	205
Chapter 11	MDCT diagnosis of early severe structural degeneration of a Mitroflow aortic bioprosthesis	219
Chapter 12	Multidetector-row computed tomography for prosthetic heart valve dysfunction: is concomitant non-invasive coronary angiography possible before redo-surgery?	227
Chapter 13	General discussion	245
Chapter 14	Dutch summary (Nederlandse samenvatting)	262
	Review committee	278
	List of abbreviations	280
	Biography	282
	List of publications	284
	Acknowledgements (Dankwoord)	290

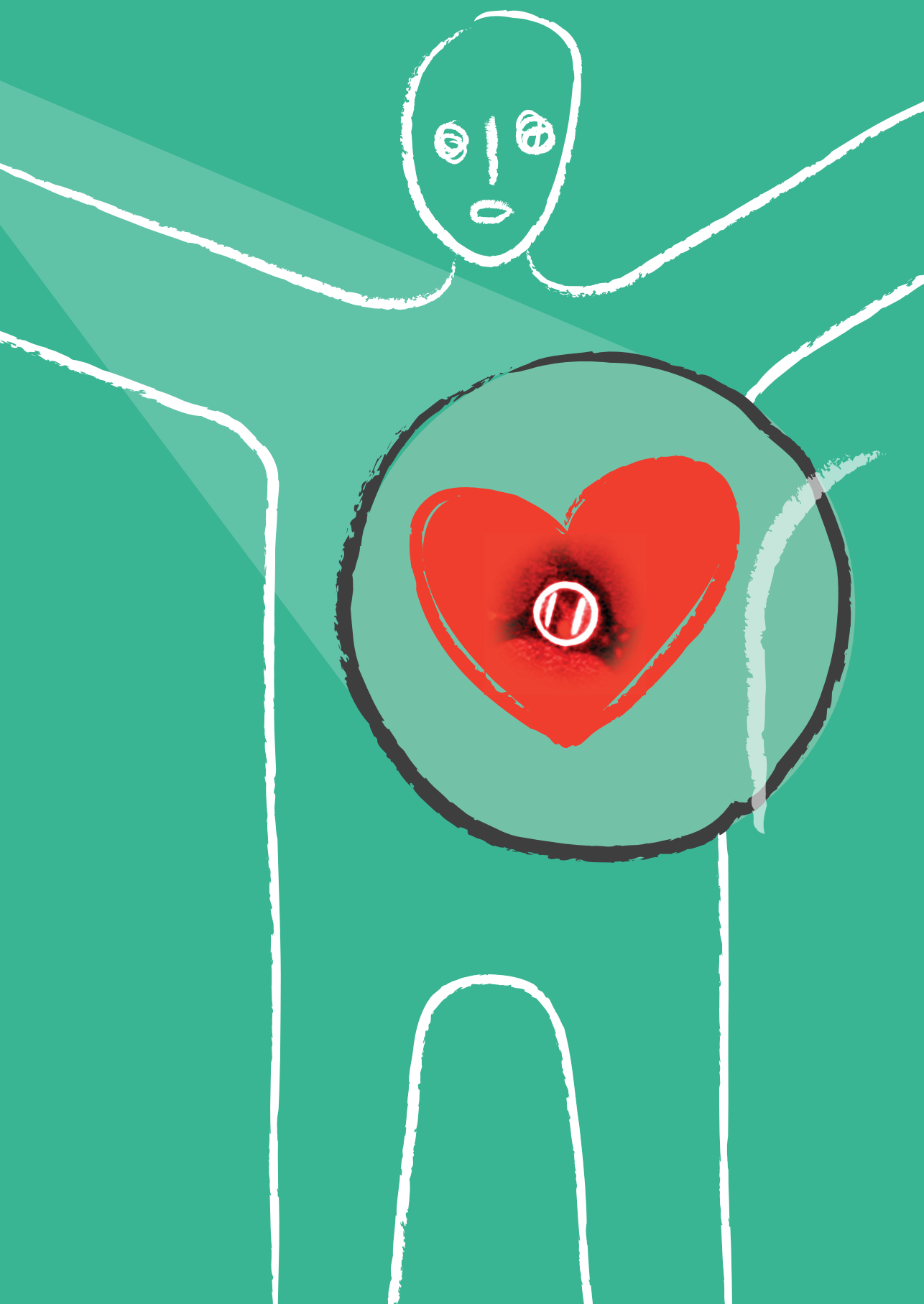

CHAPTER 1
General introduction

VALVULAR HEART DISEASE

Valvular heart disease accounts for a substantial part of the cardiovascular disease worldwide and has an estimated prevalence of 2.5% in the Western population aged <65 years and over 13% in the population aged >75 years[1]. Valvular heart disease may be due to congenital pathology such as bicuspid aortic valve disease or may be acquired and occur as a result of rheumatic disease or valve degeneration. The most common types of valvular heart disease are aortic stenosis, mitral regurgitation and aortic regurgitation. Valvular regurgitation may be caused by (primary) valve insufficiency or (secondary) perivalvular, ventricular and/or aortic root pathology. Aortic valve stenosis can be caused by congenital valve pathology or rheumatic valve disease, though the most common cause in industrialized countries is progressive aortic valve degeneration resulting in calcific aortic stenosis.

HEART VALVE REPLACEMENT

Whereas valve repair is the preferred technique in mitral valve disease, surgical aortic valve replacement is indicated in severe aortic stenosis and/or symptomatic patients[2]. As both the world population and elderly population are increasing, approximately 850.000 patients are expected to require heart valve replacement surgery in 2050[3]. Over the last decade, transcatheter heart valve replacement has been introduced as the alternative treatment for selected high-risk patients not eligible for surgical valve replacement[4]. Transcatheter valve replacement is a minimally invasive procedure in which the diseased valve can be accessed, typically, by transfemoral or transapical approach. The patient population, procedure related complications, implanted valves and related complications differ substantially between surgical and transcatheter procedures. For surgical valve replacement two main types of prosthetic heart valves are currently available: biological (stented and stentless) and mechanical (monoleaflet and bileaflet) valves. Biological valves are usually constructed from porcine or bovine tissue transplants, also known as xenografts. A special subgroup of biological valves comprises homografts and autografts, which are human valve tissue transplants. Biological valves have limited durability due to structural valve deterioration and require redo surgery at some point, whereas mechanical valves require lifelong anticoagulation therapy. Choosing the most appropriate surgical prosthesis type depends on several factors including the patients' age, comorbidity, specific indications and contraindications[2]. Transcatheter valves are balloon-expandable or self-expandable biological valves with a stent frame. Since the introduction of transcatheter procedures, more and

more transcatheter valves and sizes have become commercially available. A new type of prosthetic valves being developed concerns tissue-engineered (living) valves, which can be constructed for either surgical or transcatheter procedures. The aim for these valves is to simulate native valve physiology and have the ability to grow and regenerate[5].

PROSTHETIC HEART VALVE RELATED COMPLICATIONS

The estimated risk of valve related complications after surgical valve replacement is 0.5 to 6% per patient per year[6-8]. Apart from complications that are related to the use of anticoagulants, prosthetic heart valve (PHV) related complications include structural valve deterioration, regurgitation, endocarditis and obstruction. Biological valves are subject to degeneration, which becomes most apparent after the first ten years. Acquired PHV obstruction is mostly caused by valve thrombosis or pannus (fibrous subprosthetic tissue), whereas valve obstruction presenting early after implantation may be caused by patient prosthesis mismatch. Depending on the cause and severity of dysfunction, the treatment may include antibiotic therapy, anticoagulant therapy, fibrinolysis, redo valve surgery or valve-in-valve implantation. Regardless, complications and required therapy in PHV patients are associated with high morbidity and mortality. Baseline and follow-up imaging after PHV implantation is important to detect and differentiate between these potentially life-threatening complications.

ROUTINE IMAGING MODALITIES

Whilst the first heart valve replacement surgery was introduced in 1960[9, 10], echocardiography was establishing its role as the main diagnostic tool in clinical cardiology[11, 12]. More than 50 years later, transthoracic echocardiography (TTE) is still the primary diagnostic screening tool in PHV patients. Throughout the decades the technique has evolved substantially with the introduction of two-dimensional and echo-Doppler imaging allowing both anatomical and functional assessment. Furthermore, TTE is valued for its non-invasive character and bedside availability. Therefore, TTE is routinely performed in all patients shortly after valve replacement to create a baseline reference of the PHV anatomy and function[2, 4, 13]. If, over time, PHV dysfunction is suspected or biological valve function follow-up is required, TTE is repeated and the results are compared to patient specific baseline references. Although TTE is valuable because it provides crucial information on valve function, it may however not provide sufficient information to detect the underlying pathological mechanism in PHV dysfunction because of its limited

acoustic windows[14]. In that case, transesophageal echocardiography (TEE) comes into play, which is a semi-invasive technique that, overall, will increase the diagnostic accuracy because of its higher spatial resolution and better anatomical visualization[13, 15, 16]. TEE can also be especially helpful in the assessment of mitral prostheses. Nevertheless, echocardiography remains operator-dependent and susceptible to valve-related reverberations and acoustic shadowing which may significantly hamper diagnostic evaluation[13].

Cinefluoroscopy imaging is recommended as an additional modality since it can be helpful for the evaluation mechanical leaflet excursions[17]. With suspected PHV dysfunction, fluoroscopy may detect restricted leaflet motion as a result of PHV obstruction by thrombus or pannus. However, restricted leaflet excursions are not always present or may be very subtle[18]. Moreover, the diagnostic procedure may be very challenging in certain prosthetic valve orientations because the X-ray beam requires to be positioned exactly perpendicular to the valve leaflets[19]. Also, fluoroscopy is only potentially helpful in mechanical valves, since mechanical PHV leaflets are radiopaque. Biological PHV leaflets are radiolucent and cannot be visualized using fluoroscopy imaging.

NOVEL IMAGING MODALITIES

As routine imaging modalities may not provide satisfactory results because of the specific limitations briefly stressed above, additional evaluation using imaging modalities relatively novel to this field might be helpful.

Cardiac magnetic resonance imaging (MRI) was introduced by Goldman et al. in 1980 as a non-invasive, potential diagnostic tool for the evaluation of cardiovascular disease[20, 21]. In the following years, MRI showed its ability to assess the cardiac anatomy, pathology and its use for dynamic imaging. The benefits of cardiac MRI include the absence of biological tissue harming radiation or the use of potentially nephrotoxic, ionized contrast agents. The latter can be a contraindication in patients with cardiovascular disease because of the relatively higher prevalence of impaired renal function. Contrast-enhanced imaging is based on gadolinium administration, a paramagnetic agent considered relatively safe compared to ionized media. Furthermore, dynamic time-resolved imaging, also known as cine imaging, allows functional assessment and does not require administration of contrast media. The drawbacks of cardiac MRI include relatively long acquisition times and susceptibility to cardiac and breathing motion artifacts. Nowadays,

cardiac MRI is routinely performed using 1.5 Tesla magnet systems, but 3.0 Tesla scanners may be preferred in some cases. MRI is commonly performed in the evaluation of native heart valves for three-dimensional anatomic measurements, quantification of valvular regurgitation and assessment of left ventricular function and remodeling[4, 22]. However, its use in PHV patients has been limited because most PHVs contain metal components. Metal structures may potentially be hazardous because of the risk for dislodgment or heating of the metal due to the magnetic field and radiofrequency pulses. Furthermore, metal structures give rise to signal voids that can substantially disturb the image quality. With the development of new valve prostheses using different materials and the advances in image acquisition protocols, MRI may be successful in PHV evaluation.

Computed tomography (CT) of the heart was first performed approximately 40 years ago, soon after the introduction of first generation CT systems developed by Hounsfield in the early 1970s[23]. CT is an imaging technique that is based on the measurement of X-ray beam energy (photons) passing the body. The interaction of incoming X-rays with tissue atoms results in two main effects: the photoelectric effect (photon absorption) and Compton scatter (photon deflection). The threshold for each effect to occur is tissue (atom) specific, and the photoelectric effect also strongly depends on proton energy levels. Both effects result in (some) absorption of the photon energy (radiation dose) and the ionization of atoms. Low-energy photons are absorbed more quickly than high-energy photons. The more tissue the X-ray beam has passed the harder (higher energy) the beam gets (beam-hardening). As the absorption (attenuation) effects differ between tissues, this difference can be used for tissue differentiation and visualization. The first CT-scanners were constructed of a single X-ray source and detector. At that time, it was not possible to correct for cardiac motion and hence motion-related artifacts substantially distorted the image quality. Fundamental progress was made already in 1977 when two important techniques for cardiac CT imaging were introduced: prospective ECG-triggering[24] and retrospective ECG-gating[25]. With prospective triggering, images are acquired during one pre-specified phase of the cardiac cycle, e.g. at 75% of the RR-interval. This acquisition technique is associated with a relatively low effective radiation dose, though cardiac arrhythmias and high heart rates are problematic and result in poor image quality. With retrospective ECG-gating, images are acquired over multiple cardiac cycles and reconstructed for each phase of the RR-interval, e.g. at 5% or 10% increments. Whereas the advantage is that dynamic information throughout the cardiac cycle is provided, the offset is the

high effective radiation dose[26]. In the 1990s an important step was taken by the introduction of single-slice helical CT. This new CT technique allowed continuous image acquisition and was the beginning of a CT era in which technology evolved remarkably within a few years from 4-slice CT systems up to current 256-slice and 320-detector row CT systems[27, 28]. CT of PHVs was already presented in 1987 by Wachspress et al[29], but it took over 20 years for CT to be re-evaluated as potential tool for PHV assessment. Although the first studies were based on retrospective study designs and small sample sizes, they showed potential for the use of CT in patients with PHVs and especially in mechanical PHVs[30-34]. These initial results were the basis for this thesis.

THESIS OUTLINE

In this thesis the role of CT as additional imaging modality in patients with PHVs is evaluated. The work in this thesis is focused on stented biological and mechanical heart valves with an emphasis on non-endocarditis PHV pathology. First, an overview of the current literature on novel imaging modalities for PHV assessment is presented in *Chapter 2*. In this chapter, a systematic literature review is conducted to evaluate the potential role of CT and MRI for the evaluation of PHV patients in comparison with the current routine guidelines. Hereafter, this thesis is divided into two parts: Part I – In vitro studies and Part II – In vivo studies.

PART I – IN VITRO STUDIES

Current guidelines suggest CT for the evaluation of mechanical valves in case diagnostic work-up with echocardiography and fluoroscopy is inconclusive, though the accuracy of CT for this is not known. In *Chapter 3*, the reliability and agreement of CT to assess mechanical valve leaflet opening and closing angles is evaluated and compared with cinefluoroscopy, the reference test. For this, normal functioning and dysfunctional valves are assessed using a simplified pulsatile phantom set-up. *Chapter 4* explores the improvement of CT image quality and reduction of radiation dose by the implementation of iterative reconstruction techniques compared with conventional filtered-back image reconstruction in a non-pulsatile phantom setting. In order to improve in vitro studies by creating a more realistic PHV setting, an advanced piston pump driven mock circulation loop was developed that allows both CT and MRI compatible PHV assessment (*Chapter 5*).

PART II – IN VIVO STUDIES

A change of the geometric shape of the aortic annulus throughout the cardiac cycle may have implications for (transcatheter) prosthetic valve sizing. *Chapter 6* presents a systematic literature review of all imaging studies (echocardiography, CT and MRI) to assess whether the aortic annulus undergoes such a conformational change. To be able to differentiate between physiologic and pathologic conditions in patients with suspected PHV dysfunction, it is essential to appreciate normal CT aspects. *Chapter 7* presents the results from a prospective study in which patients were imaged with CT early after surgical PHV replacement in addition to echocardiography as baseline reference. In *Chapter 8*, the incremental value of CT in addition to routine diagnostic work-up (echocardiography +/-fluoroscopy) is evaluated in a prospective study in patients with suspected PHV dysfunction based on obstruction or abnormal (peri)prosthetic leakage. For the diagnostic work-up and planning of redo valve surgery and valve-in-valve transcatheter procedures, knowledge of the current implanted PHV size is essential. In *Chapter 9*, the reliability and agreement of CT for non-invasive assessment of the PHV size is evaluated and based on derived PHV dimensions a CT reference standard is presented. *Chapter 10* shows insights on the prevalence and degree of deformation of biological PHVs after surgical implantation, which may be associated with suboptimal PHV performance and may result in early structural valve deterioration. A patient showing remarkably early and severe degeneration of the biological Mitroflow valve in aortic position was evaluated with echocardiography and CT and this case is presented in *Chapter 11*. CT images acquired for the evaluation of PHV dysfunction may provide concomitant information on coronary artery disease. The performance of CT to rule out coronary artery disease before redo valve surgery compared to invasive coronary angiography is presented in *Chapter 12*. Finally, this thesis is concluded with a general summary and discussion in *Chapter 13*.

REFERENCES

1. Iung B, Vahanian A. Epidemiology of valvular heart disease in the adult. *Nat Rev Cardiol.* 2011;8:162-172
2. Vahanian A, Alfieri O, Andreotti F, Antunes MJ, Baron-Esquivias G, Baumgartner H, et al. Guidelines on the management of valvular heart disease (version 2012): The joint task force on the management of valvular heart disease of the european society of cardiology (ESC) and the european association for cardio-thoracic surgery (EACTS). *Eur J Cardiothorac Surg*. 2012;42:S1-44
3. Yacoub MH, Takkenberg JJ. Will heart valve tissue engineering change the world? *Nat Clin Pract Cardiovasc Med.* 2005;2:60-1
4. Nishimura RA, Otto CM, Bonow RO, Carabello BA, Erwin JP, 3rd, Guyton RA, et al. 2014 AHA/ACC guideline for the management of patients with valvular heart disease: Executive summary: A report of the american college of cardiology/american heart association task force on practice guidelines. *J Am Coll Cardiol*. 2014;63:2438-2488
5. Cheung DY, Duan B, Butcher JT. Current progress in tissue engineering of heart valves: Multiscale problems, multiscale solutions. *Expert Opin Biol Ther*. 2015;15:1155-1172
6. Chikwe J, Filsoufi F, Carpentier AF. Prosthetic valve selection for middle-aged patients with aortic stenosis. *Nat Rev Cardiol*. 2010;7:711-719
7. Stassano P, Di Tommaso L, Monaco M, Iorio F, Pepino P, Spampinato N, et al. Aortic valve replacement: A prospective randomized evaluation of mechanical versus biological valves in patients ages 55 to 70 years. *J Am Coll Cardiol*. 2009;54:1862-1868
8. Hammermeister K, Sethi GK, Henderson WG, Grover FL, Oprian C, Rahimtoola SH. Outcomes 15 years after valve replacement with a mechanical versus a bioprosthetic valve: Final report of the veterans affairs randomized trial. *J Am Coll Cardiol.* 2000;36:1152-1158
9. Harken DE, Soroff HS, Taylor WJ, Lefemine AA, Gupta SK, Lunzer S. Partial and complete prostheses in aortic insufficiency. *J Thorac Cardiovasc Surg*. 1960;40:744-762.
10. Starr A, Edwards ML. Mitral replacement: Clinical experience with a ball-valve prosthesis. *Ann Surg*. 1961;154:726-740
11. Edler I, Hertz CH. The use of ultrasonic reflectoscope for the continuous recording of the movements of heart walls. 1954. *Clin Physiol Funct Imaging*. 2004;24:118-136
12. Lalani AV, Lee SJ. Clinical echocardiography - an overview. *Can Med Assoc J*. 1976;114:46-47, 50-44.
13. Zoghbi WA, Chambers JB, Dumesnil JG, Foster E, Gottdiener JS, Grayburn PA, et al. Recommendations for evaluation of prosthetic valves with echocardiography and doppler ultrasound: A report from the american society of echocardiography's guidelines and standards committee and the task force on prosthetic valves, developed in conjunction with the american college of cardiology cardiovascular imaging committee, cardiac imaging committee of the american heart association, the european association of echocardiography, a registered branch of the european society of cardiology, the japanese society of echocardiography and the canadian society of echocardiography, endorsed by the american college of cardiology foundation, american heart association, european association of echocardiography, a registered branch of the european society of cardiology, the japanese society of echocardiography, and canadian society of echocardiography. *J Am Soc Echocardiogr*. 2009;22:975-1014
14. Faletra F, Constantin C, De Chiara F, Masciocco G, Santambrogio G, Moreo A, et al. Incorrect echocardiographic diagnosis in patients with mechanical prosthetic valve dysfunction: Correlation with surgical findings. *Am J Med*. 2000;108:531-537

15. Barbetseas J, Nagueh SF, Pitsavos C, Toutouzas PK, Quinones MA, Zoghbi WA. Differentiating thrombus from pannus formation in obstructed mechanical prosthetic valves: An evaluation of clinical, transthoracic and transesophageal echocardiographic parameters. *J Am Coll Cardiol*. 1998;32:1410-1417
16. Pibarot P, Dumesnil JG. Doppler echocardiographic evaluation of prosthetic valve function. *Heart*. 2012;98:69-78
17. Cianciulli TE, Lax JA, Beck MA, Cerruti FE, Gigena GE, Saccheri MC, et al. Cinefluoroscopic assessment of mechanical disc prostheses: Its value as a complementary method to echocardiography. *J Heart Valve Dis*. 2005;14:664-673
18. Tanis W, Habets J, van den Brink RB, Symersky P, Budde RP, Chamuleau SA. Differentiation of thrombus from pannus as the cause of acquired mechanical prosthetic heart valve obstruction by non-invasive imaging: A review of the literature. *Eur Heart J Cardiovasc Imaging*. 2014;15:119-129
19. Montorsi P, Arena V, Muratori M, Lavarra F, Cavoretto D, Repossini A, et al. Fluoroscopic functional evaluation of bileaflet prostheses: Effect of different intraoperative valve orientation. *Am J Card Imaging*. 1996;10:101-107
20. Goldman MR, Pohost GM, Ingwall JS, Fossel ET. Nuclear magnetic resonance imaging: Potential cardiac applications. *Am J Cardiol*. 1980;46:1278-1283
21. Geva T. Magnetic resonance imaging: Historical perspective. *J Cardiovasc Magn Reson*. 2006;8:573-580
22. Capoulade R, Pibarot P. Assessment of aortic valve disease: Role of imaging modalities. *Curr Treat Options Cardiovasc Med*. 2015;17:49
23. Hounsfield GN. Computerized transverse axial scanning (tomography). 1. Description of system. *Br J Radiol*. 1973;46:1016-1022
24. Sagel SS, Weiss ES, Gillard RG, Hounsfield GN, Jost GT, Stanley RJ, et al. Gated computed tomography of the human heart. *Invest Radiol*. 1977;12:563-566
25. Harell GS, Guthaner DF, Breiman RS, Morehouse CC, Seppi EJ, Marshall WH, Jr., et al. Stop-action cardiac computed tomography. *Radiology*. 1977;123:515-517
26. Hsiao EM, Rybicki FJ, Steigner M. CT coronary angiography: 256-slice and 320-detector row scanners. *Curr Cardiol Rep*. 2010;12:68-75
27. Hurlock GS, Higashino H, Mochizuki T. History of cardiac computed tomography: Single to 320-detector row multislice computed tomography. *Int J Cardiovasc Imaging*. 2009;25 Suppl 1:31-42
28. Goldman LW. Principles of CT: Multislice CT. *J Nucl Med Technol*. 2008;36:57-68
29. Wachspress JD, Untereker WJ, Kraushaar BT. Prosthetic valve visualization by cine-computed tomography: A case report. *Heart Vessels*. 1987;3:223-226
30. Grunenfelder J, Plass A, Alkadhi H, Genoni M. Evaluation of biological aortic valve prostheses by dual source computer tomography and anatomic measurements for potential transapical valve-in-valve procedure. *Interact Cardiovasc Thorac Surg*. 2008;7:195-200
31. Symersky P, Budde RP, de Mol BA, Prokop M. Comparison of multidetector-row computed tomography to echocardiography and fluoroscopy for evaluation of patients with mechanical prosthetic valve obstruction. *Am J Cardiol*. 2009;104:1128-1134
32. Teshima H, Hayashida N, Fukunaga S, Tayama E, Kawara T, Aoyagi S, et al. Usefulness of a multidetector-row computed tomography scanner for detecting pannus formation. *Ann Thorac Surg*. 2004;77:523-526

33. Konen E, Goitein O, Feinberg MS, Eshet Y, Raanani E, Rimon U, et al. The role of ECG-gated MDCT in the evaluation of aortic and mitral mechanical valves: Initial experience. *AJR. American Journal of Roentgenology*. 2008;191:26-31
34. LaBounty TM, Agarwal PP, Chughtai A, Bach DS, Wizauer E, Kazerooni EA. Evaluation of mechanical heart valve size and function with ECG-gated 64-MDCT. *AJR. American Journal of Roentgenology*. 2009;193:W389-396

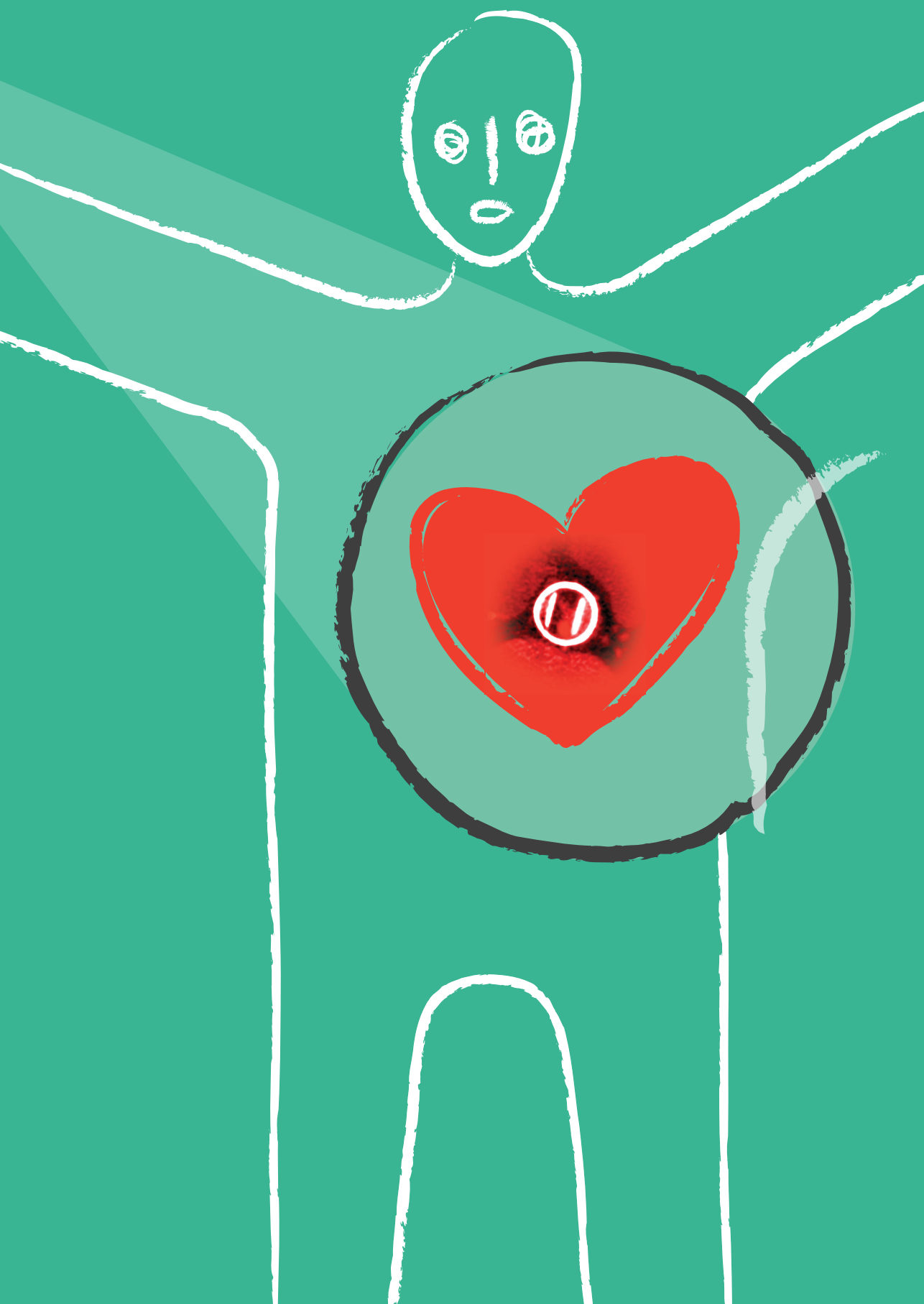

CHAPTER 2

Multimodality imaging assessment of prosthetic heart valves: a systematic review

Dominika Suchá
Petr Symersky
Wilco Tanis
Willem P.Th.M. Mali
Tim Leiner
Lex A. van Herwerden
Ricardo P. J. Budde

Published in Circulation: Cardiovascular Imaging, 2015

ABSTRACT

Echocardiography and fluoroscopy are the main techniques for prosthetic heart valve (PHV) evaluation, but due to specific limitations they may not identify the morphological substrate or the extent of PHV pathology. Cardiac computed tomography (CT) and magnetic resonance imaging (MRI) have emerged as new potential imaging modalities for valve prostheses. We present an overview of the possibilities and pitfalls of CT and MRI for PHV assessment based on a systematic literature review of all experimental and patient studies. For this, a comprehensive systematic search was performed in Pubmed and Embase on March 24th 2015 containing CT/MRI and PHV synonyms. Our final selection yielded 82 articles on surgical valves. CT allowed adequate assessment of most modern PHVs and complemented echocardiography in detecting the obstruction cause (pannus or thrombus), bioprosthesis calcifications and endocarditis extent (valve dehiscence and pseudoaneurysms). No clear advantage over echocardiography was found for the detection of vegetations or periprosthetic regurgitation. Whereas MRI metal artifacts may preclude direct prosthesis analysis, MRI provided information on PHV-related flow patterns and velocities. MRI demonstrated abnormal asymmetric flow patterns in PHV obstruction and allowed prosthetic regurgitation assessment. Hence, CT shows great clinical relevance as a complementary imaging tool for the diagnostic work-up of patients with suspected PHV obstruction and endocarditis. MRI shows potential for functional PHV assessment, though more studies are required to provide diagnostic reference values to allow discrimination of normal from pathological conditions.

INTRODUCTION

The number of patients requiring heart valve replacement is increasing rapidly as the population is aging[1]. Monitoring and follow-up of prosthetic heart valve (PHV) patients is important due to the numerous and potentially life-threatening complications such as infective endocarditis, thrombosis, pannus, (peri)prosthetic regurgitation, patient prosthesis mismatch and structural failure. The reported incidence of these complications varies from 0.5 to 6% per year[2, 3] and depends on prosthesis type, position and the modalities used for patient monitoring that may impact the diagnostic accuracy. Current imaging modalities include fluoroscopy, which is limited to the assessment of mechanical PHV leaflet motion, and echocardiography[4]. Echocardiography is the mainstay for evaluation of PHV function providing both functional (Doppler) and anatomical information. However, echocardiography may not identify the morphological cause of PHV dysfunction or provide information on its extent due to acoustic shadowing, complex anatomy and limited viewing windows[4-6].

Computed tomography (CT) and magnetic resonance imaging (MRI) have established their role in cardiac imaging. Several, yet diverse studies have advocated MRI and more prominently CT as new imaging techniques for PHV assessment to complement echocardiography[7-15]. This review provides a complete, systematic evidence-based literature overview on CT and MRI imaging of PHVs to determine their usefulness as additional imaging modalities for PHV evaluation with an emphasis on imaging feasibility, diagnostic potential and added value in relation to established techniques.

LITERATURE REVIEW

The search and manuscript were prepared according to the PRISMA statement for reporting systematic reviews and meta-analyses[16]. A comprehensive systematic literature search was performed in Pubmed and Embase databases on March 24th, 2015 to acquire all studies describing CT/MRI imaging of PHVs, using the algorithm presented in *Supplement 1*. In Embase, conference abstracts and papers, letters, notes and editorials were excluded from the search. No language or other restrictions were imposed. After manual removal of duplicates, articles were selected by screening titles and abstracts based on predefined criteria (*Figure 1*). The titles and abstracts of selected articles were screened independently by two reviewers. Consensus was reached for discordant judgments. Full texts of selected articles were screened and references of relevant articles and reviews were checked. Articles dealing with homografts or autografts only, experimental CT/MRI systems,

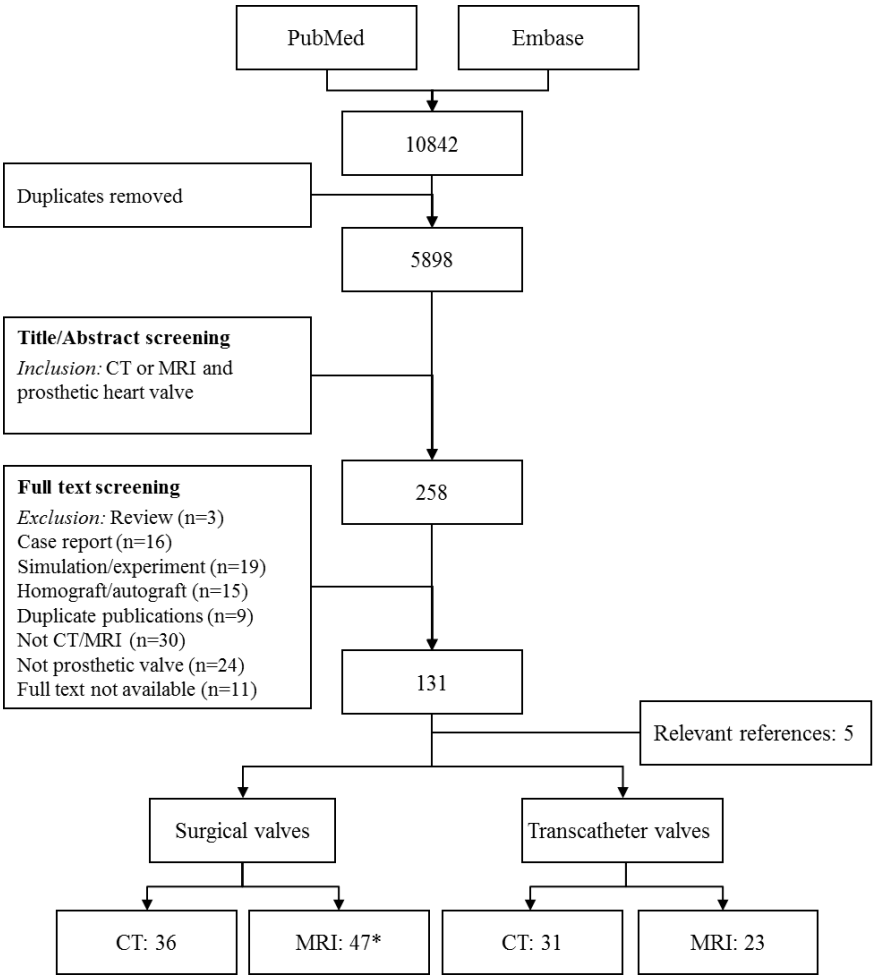

Figure 1 | Flowchart of systematic selection of relevant articles
* One study included performed both MRI and CT imaging

simulation studies based on CT/MRI data, duplicate publications and studies without available full text were excluded. Reference and citation check yielded five additional articles[17-21], since PHV or CT was not mentioned in title/abstract as defined in the syntax. The selection yielded 136 unique articles including 36 CT and 47 MRI studies on surgical valves and 54 studies on transcatheter prostheses (*Figure 1*). Based on these results, only articles on surgical valves were included for this review. The study characteristics of the included CT and MRI articles are presented in *Supplement 2 and 3*, respectively. Study results were compared with current imaging standards as retrieved from PHV guidelines.

CURRENT GUIDELINES

Table 1 provides a summarized overview on the current cardiology guidelines for PHV evaluation (AHA/ACC[22], ESC[23], Zoghbi et al.[4]). Transthoracic (TTE) and transesophageal (TEE) echocardiography are the key modalities for both baseline and dysfunction diagnostic work-up. Whereas TTE is readily available and non-invasive, TEE often provides better image quality due to its higher spatial resolution and thus it allows improved detection of PHV-related pathology. The main advantage of echocardiography is that it can provide functional information and baseline postoperative TTE is always available as reference for follow-up purposes. In contrast, detailed anatomical evaluation remains problematic due to acoustic shadowing and PHV metal reverberations. Moreover, operator experience is crucial for proper echocardiographic PHV assessment. The incremental value of fluoroscopy is limited to the assessment of mechanical valve leaflet excursions. As yet, CT is only mentioned briefly in the guidelines as a potential additional imaging tool, while MRI is not mentioned at all.

PROSTHETIC VALVES

Numerous surgical PHV types are available and may be separated into two main groups; biological and mechanical valves. Mechanical valves include monoleaflet (tilting disk) and bileaflet valves. Biological valves include porcine and pericardial bovine valves (xenografts) which can be stentless, or contain a metal ring and/or metal struts. Homografts and autografts are human tissue valves and will not be discussed in this review. Mechanical valves require lifelong anticoagulation therapy, whereas biological valves have limited durability due to structural deterioration. The choice of prosthesis type depends on the patients' age, comorbidity and specific contraindications[23].

COMPUTED TOMOGRAPHY

Acquisition

Most studies used retrospective ECG-gated acquisition protocols, which in general, are favoured over prospective ECG-triggering because they allow cardiac phase reconstructions at 5-10% intervals and offer dynamic information on leaflet movement. The radiation dose however is relatively high (range (mean) 4±0.5 - 18.8±3.8 mSv[24, 25]). For aortic valves, systolic 20-40% and diastolic 70-90% reconstructions usually yield the best images[25, 26]. Adjusted double oblique planes provide short axis views in plane with the prosthesis ring, and two views parallel and perpendicular to the prosthetic leaflets[27]. Short-acting beta-blockers

Table 1 | Current guidelines on PHV evaluation

Indication	Modality	Purpose
Baseline	TTE	6-12 weeks after implantation, consider prior to discharge
		Annually after the first 5-10 years for bioprostheses or earlier in young patients
Suspected dysfunction	TTE	With new clinical symptoms and/or suspected prosthesis dysfunction
	TEE	Consider if dysfunction suspected
Obstruction	TTE	To assess hemodynamic severity and compare with baseline studies
		To detect patient prosthesis mismatch
	TEE	To help distinct pannus and thrombus together with clinical parameters
		To assess thrombus size and valve motion
		For close monitoring follow-up of thrombosis
		In non-obstructive valve thrombosis
		After an embolic event
	Fluoroscopy	Only in mechanical valves, to assess valve motion
		For additional information if thrombus/pannus is suspected
	MDCT	Reasonable: to assess leaflet valve motion
		For additional information if thrombus/pannus is suspected
	Catheterization	If TTE/TEE is insufficient: to assess pressure gradients in aortic valves
Bioprosthesis degeneration	TTE	To detect early structural valve deterioration, leaflet stiffening, calcification, reduced effective orifice area and/or regurgitation
	TEE	Might be considered: If TTE is inconclusive for imaging biological valve cusps
	CT	Might be considered: If TTE/TEE is inconclusive for imaging biological valve cusps
Regurgitation	TTE	To detect hemodynamic severity of regurgitation
		To detect regurgitation and differentiate valvular from paravalvular regurgitation
	TEE	If TTE is inconclusive to diagnose regurgitation origin, cause and severity
		To detect associated complications

Table 1 | Continued

Indication	Modality	Purpose
Endocarditis	TTE	To identify vegetations, hemodynamic severity of regurgitation, ventricular function, pulmonary pressures
		To detect endocarditis complications, especially anterior aortic root, such as paravalvular extensions, aneurysms and abscesses
		To re-evaluate known endocarditis with clinical change or high risk-patients
	TEE	In combination with TTE highest diagnostic accuracy for vegetations and perivalvular extension
		If TTE is non-diagnostic or no significant findings but clinical suspicion
		To detect endocarditis complications such as perivalvular abscesses, valve dehiscence and to delineate fistulas and pseudoaneurysms
		Endocarditis if also intracardiac device present
		To re-evaluate known endocarditis with clinical change or high-risk patients
		Intra-operative in endocarditis valve surgery
		Reasonable: for diagnosis in patients with unknown source S. Aureus bacteremia
		Reasonable: for diagnosis in persistent fever without bacteremia or new murmur
		Might be considered: to detect concomitant endocarditis in S. Aureus bacteremia with known extracardiac entry source
	Catheterization	To delineate fistulas and pseudoaneurysms
	CT	Reasonable: to evaluate morphology/anatomy with suspected paraprosthetic infections if echocardiography insufficient for clear anatomical delineation
Valve dehiscence	Fluoroscopy	To detect abnormal tilting or rocking of the base ring (only in extensive dehiscence)
	Catheterization	For diagnosis of small or moderate valve dehiscence

Based on the guidelines of ESC , AHA /ACC, Zoghbi et al.[22, 23, 4]
CT= computed tomography; TEE= transesophageal echocardiography, TTE= transthoracic echocardiography

have been administered to reduce patients' heart rate and improve image quality, although no paper reported on potential complications[11, 12, 25, 28-30].

Image quality

Depending on the type of components, PHVs can cause hyperdense (blooming and bright streak) and/or hypodense (beam-hardening and dark streak) artifacts that may affect image quality (*Figure 2*). In vitro, artifact reduction was achieved with prospective ECG-triggering compared to retrospective ECG-gating[31] and with increased tube voltage (140kV versus 100-120kV)[32]. Iterative reconstruction techniques allowed 50-75% dose reduction [33] and improved objective image quality[34]. Pre-processing filters improved bioprosthetic image quality and semi-automatic segmentation methods allowed degenerated valve tissue discrimination[30]. In total, ten patient studies evaluated 307 mechanical[11, 12, 24, 28, 35-38] and 151 biological PHVs[25, 28, 35, 37, 39]. For most mechanical valves, image quality was excellent for leaflets and good-excellent for periprosthetic regions (*Table 2*). Artifacts were least in closed valve position and increased with rapid leaflet motion[26]. Sorin and Björk-Shiley monoleaflet valves consistently displayed severe artifacts related to their cobalt-chrome components, precluding assessment in 14/15 and 4/7 patients, respectively[12, 35-38]. Compared with fluoroscopy, non-enhanced CT showed greater leaflet visibility in 40 unspecified bileaflet valve patients[24]. Results for biological prostheses were less consistent. One study found sufficient image quality for evaluation of 47/50 unspecified biological valves[39]. Other studies showed leaflet and periprosthetic image quality to differ strongly between valve types (*Table 2*).

MAGNETIC RESONANCE IMAGING

Acquisition

Depending on the clinical context and imaging purpose different MRI sequences are required including T_1-weighed spin echo and gradient echo sequences, comprising steady-state free-precession (SSFP) and fast gradient echo (FGRE). SSFP is the workhorse sequence for cardiac MRI and provides high blood-tissue contrast allowing biological valve delineation and orifice area assessment[40]. FGRE is less susceptible to turbulent flow and was used for flow-related artifact reduction[9, 41]. Spin echo sequences showed less PHV-related artifacts[42-45]. For flow and velocity measurements phase-contrast sequences can be used[46-48] and motion-sensitized acquisitions are being developed to allow turbulent flow assessment[49]. Recently, 4D-flow MRI was introduced which may provide quantification and comprehensive characterization of flow patterns and offer insights in hemodynamics after valve replacement[50].

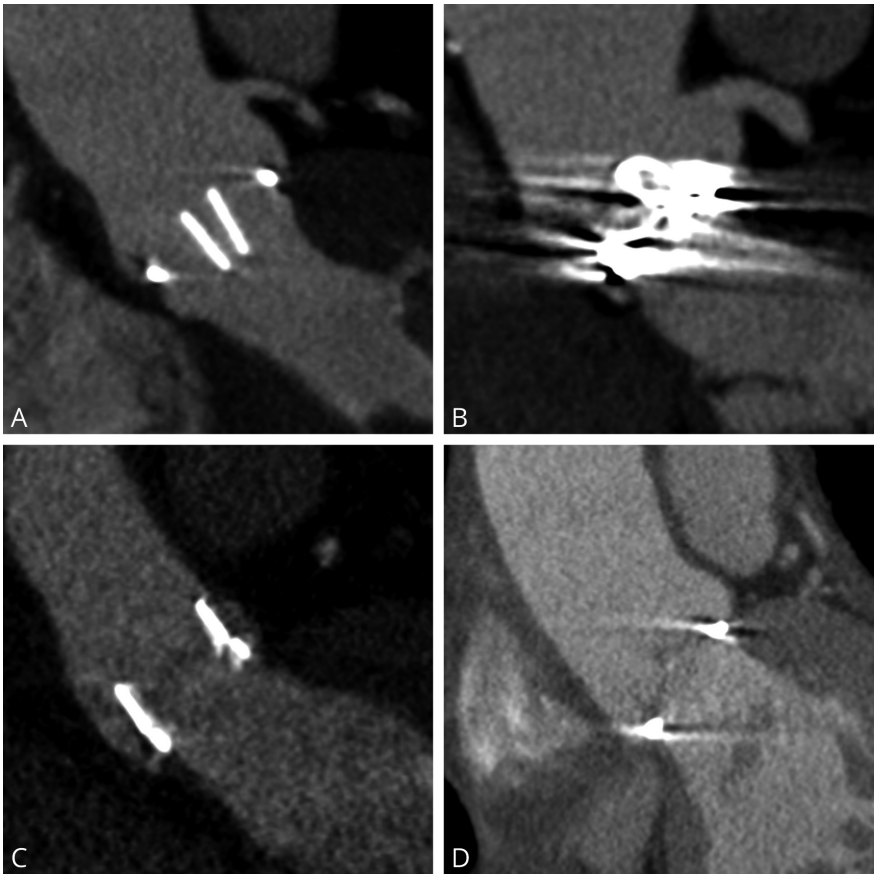

Figure 2 | Prosthetic heart valve related artifacts on CT
(A) St. Jude bileaflet valve; (B) Björk-Shiley monoleaflet valve; (C) Perimount biological valve; (D) Mitroflow biological valve

Image quality

MRI valve-related artifacts appear as localized signal voids ranging from mild to severe, depending on the amount and type of metal (*Figure 3*, *Table 3*)[42, 43, 51, 52]. Bileaflet and titanium-containing PHVs caused fewer artifacts than monoleaflet valves or cobalt-chromium alloys[43, 53]. PHV artifacts were evaluated in 124 patients with 115 biological and only 10 mechanical valves[9, 41, 52, 54, 55]. Signal voids precluded assessment of the mechanical prosthesis itself including the valve leaflets. Biological valves containing a simple ring showed no disturbing artifacts, unlike valves with metal struts[55]. Of 83 patients with various biological valves, 62 showed

Table 2 | CT image quality and artifacts of studied prosthetic heart valves

	Type	Artifacts				Image quality - (peri)prosthetic				Image quality - leaflets			
Valves		None	Minor	Moderate	Severe	ND	Fair	Good	Excellent	ND	Fair	Good	Excellent
Stentless valves*[25, 35, 37]	B	●							●		●		
Carbomedics[11, 12, 35-38, 97]	BM	●	●					●	●				●
ON-X[12, 28, 35, 37, 97]	BM	●	●					●	●				●
St. Jude Standard[28]	BM	●	●										
Medtronic Mosaic[25, 35, 37]	B		●						●		●	●	
Mitroflow[35, 37]	B		●				●	●			●		
St. Jude Epic[35,37]	B		●					●	●	●	●		
CE Perimount/Magna[25, 28, 35, 37]	B		●	●				●	●		●		
ATS[28, 38]	BM		●	●									●
St. Jude Regent[28, 38]	BM		●	●									●
St. Jude unspecified[12, 35-38]	BM		●	●				●				●	●
Duromedics[11, 35, 37]	BM			●			●	●				●	
Sorin bicarbon[11,35,37]	BM			●				●	●				●
St. Jude HP[28, 97]	BM			●				●					●
Omnicarbon[38]	MM			●									●
Medtronic Hall[11, 12, 35,37, 97]	MM	●	●	●				●				●	●
Björk-Shiley[11, 12, 35-38,97]	MM				●	●				●			
Sorin[35-37]	MM				●	●				●	●		
Medtronic Intact[35]	B							●		●	●		

Image quality was assessed using similar 4-5 point scales[35, 36, 38, 97, 98] or by volumetric artifact quantification[26]. The remaining studies reported the artifact extent and whether PHV (region) evaluation was possible. Image quality is summarized in this table as non-diagnostic, fair, good, excellent and artifacts as : none, minor, moderate, severe

* Medtronic Freestyle, St. Jude Toronto, Sorin Freedom Solo;

B= biological; BM=bileaflet mechanical; CB=caged-ball; MM=monoleaflet mechanical; ND=non-diagnostic.

Italicized valve types have been discontinued

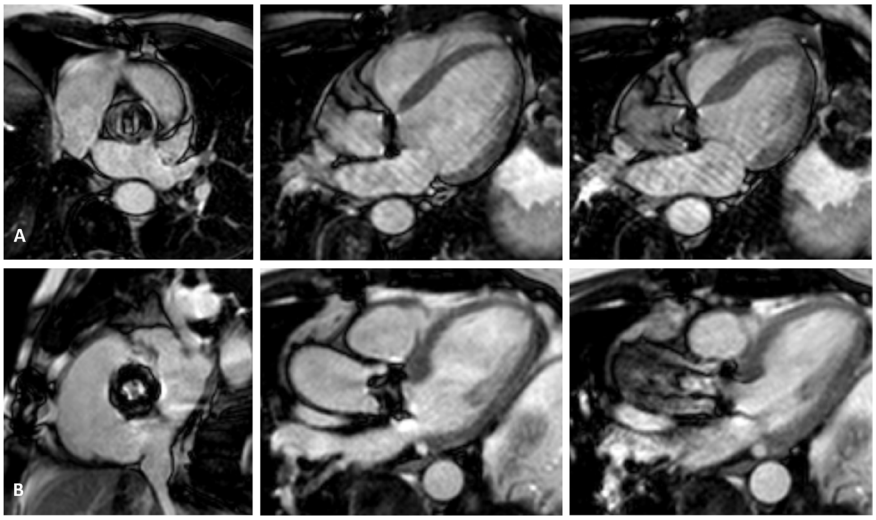

Figure 3 | MRI in prosthetic heart valves
Magnetic resonance steady-state free precession images of the mechanical Carbomedics (A; upper row) and biological Perimount (B; lower row) aortic prosthetic valves in plane and perpendicular in diastole and systole, respectively.

excellent image quality, 16 moderate and 5 non-diagnostic due to flow-related artifacts, stent material, arrhythmias or patient movement[9, 41]. One study improved PHV visualization by integrating resonant conduits in experimental setting[56].

Relevant risks of CT and MRI

Compared with routine echocardiography, CT and MRI in PHVs bear certain risks. The administration of iodinated contrast agents for contrast-enhanced CT may cause adverse reactions including contrast-induced nephropathy. Patients with known contrast medium allergy or impaired renal function may therefore not be eligible for contrast-enhanced CT imaging. MRI may entail severe complications related to the presence of metal devices. Pacemakers and ICDs in general, are an absolute contraindication. MRI safety has extensively been studied at 0.35-4.7T in 105 mechanical and 59 biological PHVs[19, 42-44, 51-53, 57-60]. The MRI force exerted on studied PHVs unto 4.7T was less than gravity or the beating heart[43, 57, 58] and temperature changes (max. +0.7°C) were considered safe as well[19, 42-44, 51-53]. None of included studies reported incidents related to MRI exposure in PHV patients. Three 0.5-1.5T MRI studies including 115 patients specifically observed no rhythm disturbances, clinical symptoms, discomfort or safety problems[45, 52, 61]

Table 3 | MRI artifacts of studied prosthetic heart valves

Valves	Type	Artifacts				F/L
		None	Minor	Moderate	Severe	
Hancock Vascor[53]	B	●				
St. Jude Toronto SPV[42]	B		●			
Biocor[42]	B		●			
St. Jude bioimplant[44]	B		●			
Tascon porcine[42]	B		●			
Wessex porcine[42]	B		●			
Xenofic pericardial[42]	B		●			
Edwards Mira[43,44]	BM		●			
CE Porcine[43, 52-55]	B		●	●		
Hancock Pericardial[44,53,54]	B		●	●		F/L
Sorin Pericarbon[42]	B		●	●		
Ionescu-Shiley[52, 53]	B		●	●		
Sorin bicarbon[44, 54]	BM		●	●		F
St. Jude unspecified[53, 54]	BM		●	●		F
Aortech[42]	MM		●	●		
Medtronic Hall (Kaster)[53, 54]	MM		●	●		F
Omniscience[44, 53]	MM		●	●		
Smeloff-Cutter[42,53,54]	CB		●	●		F
ON-X[44]	BM			●		
Duromedics[54]	BM			●		F
Lillehei-Kaster[52]	MM			●		
Ultracor[44]	MM			●		
Medtronic Intact[42]	B		●	●	●	
Mitroflow[42,44]	B		●	●	●	
St. Jude Masters/HP[42,44,52]	BM		●	●	●	
St. Jude Regent[42]	BM		●	●	●	
CE Perimount/Magna[40,43,44,55]	B			●	●	
ATS[42]	BM			●	●	
Jyros[42]	BM			●	●	
Beall[42]	MM			●	●	
Björk-Shiley[42,44,52,53,54]	MM			●	●	F
Omnicarbon[53]	MM			●	●	
Sorin allcarbon[42]	MM			●	●	
Starr-Edwards[51,53]	CB				●	

Artifacts: none, minor=smaller than the prosthesis, moderate=same or slightly larger than prosthesis, severe=larger than prosthesis or precluding assessment of adjacent structures
B= biological; BM=bileaflet mechanical; CB=caged-ball; F = in vivo flow assessment possible; L= in vivo leaflet assessment possible; MM=monoleaflet mechanical
Italicized valve types have been discontinued

Anatomy and function

Additional CT imaging can be helpful in the assessment of the periprosthetic anatomy, structural prosthetic integrity and pathology[11, 18, 62]. CT has been used to estimate the PHV size and function by evaluating diameters, orifice areas and leaflet motion and to measure anatomical dimensions such as the left ventricular outflow tract (LVOT), sinotubular junction and coronary ostium heights in biological valves as pre-assessment for transcatheter valve-in-valve implantation[55].

MRI provided cardiac dimensions including the aortic diameter after mechanical PHV implantation[13], pulmonary conduit diameter [63] and ventricular function[64] and allowed assessment of aortic root distensibility and annulus area throughout the cardiac cycle in bioprostheses in animals (n=19)[65] and stentless valves in patients (n=10)[66]. MRI and CT showed good agreement for geometric area, aortic root, LVOT and annulus diameter measurements in patients with bioprostheses (max. mean difference 1.4±2.3mm)[55]. Furthermore, MRI phantom studies extensively evaluated normal PHV flow patterns which depended on valve size, design, vessel geometry and distance of downstream measurements[21, 40, 46, 47, 49, 67-71]. In animals, flow patterns were also affected by prosthesis type[72] and orientation[73]. In patients, mechanical valves demonstrated more skewed and complex flow patterns[13, 46, 50, 68, 74].

Stented and smaller PHVs showed greater velocities than stentless and larger valves[40, 67, 75]. Velocity measurements were performed ≥1.0 valve-diameter downstream for flow and motion artifacts[13, 15, 46, 74], though mitral prostheses showed no significant flow artifacts[41]. Valve-related signal loss hampered Starr-Edwards flow assessment at <40mm downstream[21]. Only two studies performed measurements at 0.25-diameter downstream[68, 69]. Laser Doppler anemometry and MRI showed good agreement (<15% difference) for vessel center velocity measurements[68, 69, 71]. Furthermore, in vitro MRI phase-contrast measurements showed excellent correlation with the flow transducer (reference test)[70]. Phase-contrast MRI (*Figure 4*) was used in one study in addition to TTE as standard work-up after valve surgery[76]. A single study visualized flow profiles in time with 4D-flow and successfully assessed jet eccentricity and hemodynamic vortex formation from the sinotubular junction onwards[50].

PATHOLOGY

Structural deterioration

In aortic valves, the effective valve orifice area (EOA) estimated with TTE is used as a measure for stenosis evaluation. CT planimetric geometric orifice area (GOA)

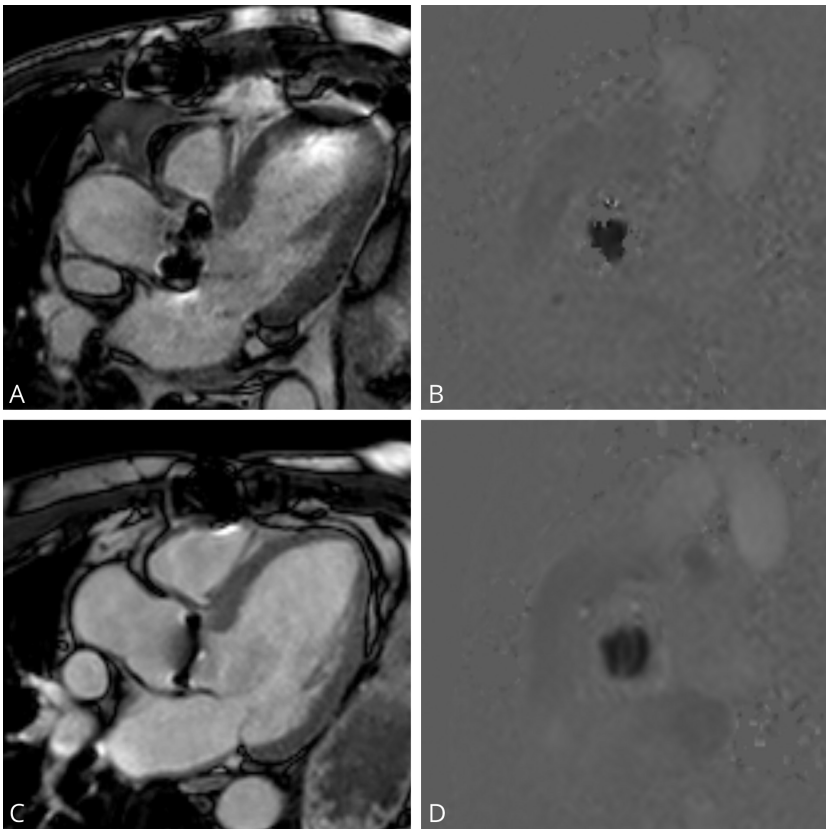

Figure 4 | MRI flow assessment
Left ventricular outflow tract steady-state free precession images (A and C) and in plane phase-contrast images (B and D) of a biological CE Perimount and a mechanical St. Jude aortic prosthetic heart valve, respectively. Note the single opening orifice of the biological valve (B) and the three opening orifices of the mechanical valve (D).

and TTE functional EOA measurements are distinct non-interchangeable entities[77]. Nevertheless, several studies compared them[25, 39, 78]. For biological valves, the leaflet GOA was measured in maximal systolic phase in 100 patients[25, 39] and correlated well with the EOA[25]. CT detected moderate stenosis using the GOA[39], but the GOA was consistently higher than the EOA (mean 0.06cm^2)[25, 39]. Aortic biological valve degeneration was evaluated in five CT studies[25, 39, 79-81]. Despite the variable leaflet image quality, one study detected restricted leaflet opening in all 34 patients with severe bioprosthetic dysfunction (EOA <0.65cm^2/m^2)[25]. CT also detected thickened leaflets (*Figure 5*) and hypoattenuating masses related to thrombus formation[25] and visualized valve ring or leaflet calcifications[39, 79-81].

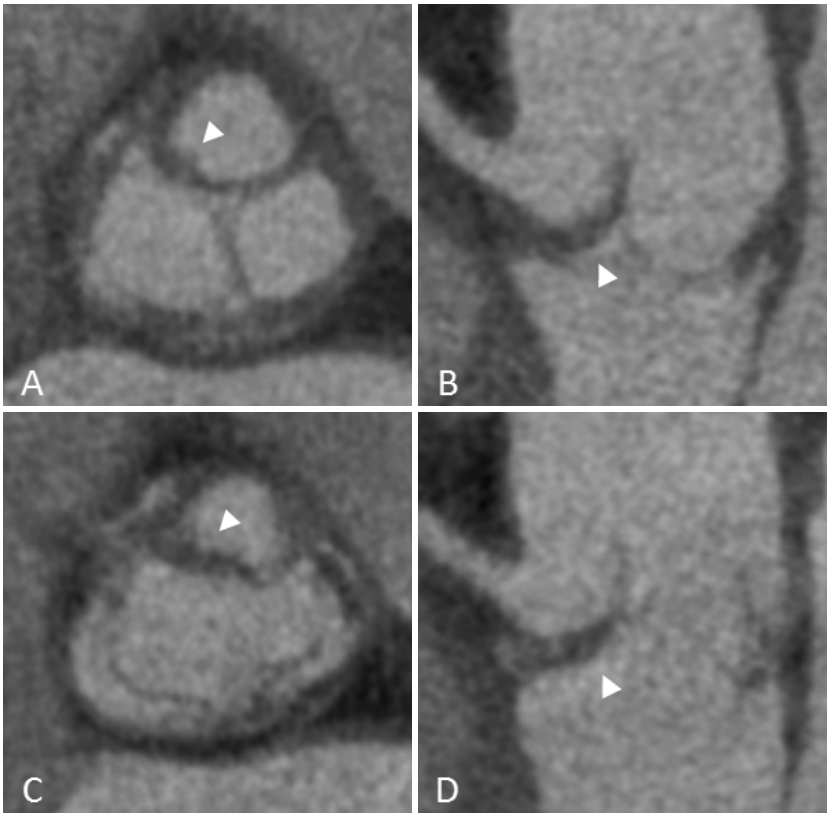

Figure 5 | Structural deterioration
CT images of a Sorin Freedom Solo stentless 23mm bioprosthesis in aortic position. Note the thickening of the right coronary cusp (arrowheads) presented in systole (A and B) and in diastole (C and D) with leaflet opening restriction.

Degenerative valves showed higher CT calcification volumes (181±33mm^3) compared to non-degenerative (75±37mm^3) valves[80, 81] and were significantly associated with patient-prosthesis mismatch and higher TTE transprosthetic gradients and regurgitation[81]. CT also allowed evaluation of pulmonary tissue-engineered[82, 83] and stentless[84] valve morphology. For MRI, the measured aortic biological GOA (*Figure 6*) was within the EOA standard deviations[40], despite the fundamental differences discussed, and showed strong agreement between MRI and TTE (mean difference 0.02±0.24cm^2) and MRI and TEE (mean difference 0.05±0.15cm^2) in 65 patients[9]. For mitral GOA, MRI overestimated the echocardiographic EOA in all PHV types[70] and a mean difference of 0.06±0.11cm^2 was reported[41].

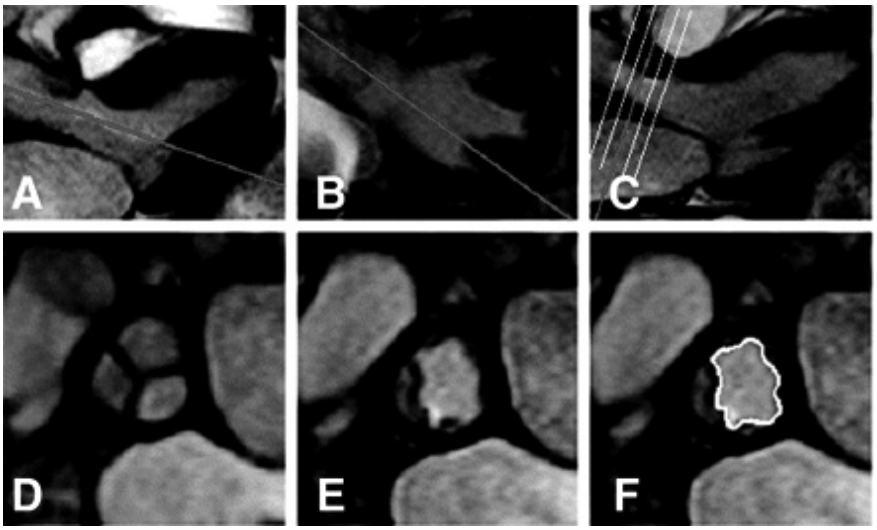

Figure 6 | Assessment of the geometric orifice area
Magnetic resonance views of the left ventricular outflow tract (A, B, C) are used to reconstruct images perpendicular to the transprosthetic flow jet of a biological aortic prosthetic valve in diastole (D) and systole (E). The prosthetic geometric orifice area is derived by planimetry of the greatest orifice in systole (F). *Copyrights Von Knobelsdorff et al. – Circ Cardiovasc Imaging. 2009;2:397-404*

Despite atrial fibrillation, mitral measurements could be obtained successfully[41]. MRI detected stenosis in 12/17 patients with tissue-engineered pulmonary valves by showing high peak velocities (3.5-4.0m/s) and mild to severe insufficiency (10-40%)[48]. In addition, MRI allowed cusp motion evaluation in tissue-engineered and biological left and right sided PHVs in sheep[63] and man[41, 64, 85] and detected leaflet restriction[41,63]. Moreover, significant wall thickening and PHV-conduit enhancement were visualized in all stenosis patients, which correlated histologically with severe inflammation and fibrosis.

Regurgitation

Important for patient follow-up is evaluation of regurgitation (*Figure 7 A-B*). Compared with TTE, CT performance for detecting aortic biological valve regurgitation was poor[39]. Periprosthetic regurgitation (non-endocarditis) in mechanical valves was detected by CT and echocardiography in 10 cases[11, 12, 28]. Selected CT protocols did allow discrimination of periprosthetic contrast-enhanced blood from surgical Teflon pledgets[86].The performance of MRI, compared with TEE, was systematically assessed by one group in 47 unique patients with 48 mechanical and 7 biological valves[45, 87].

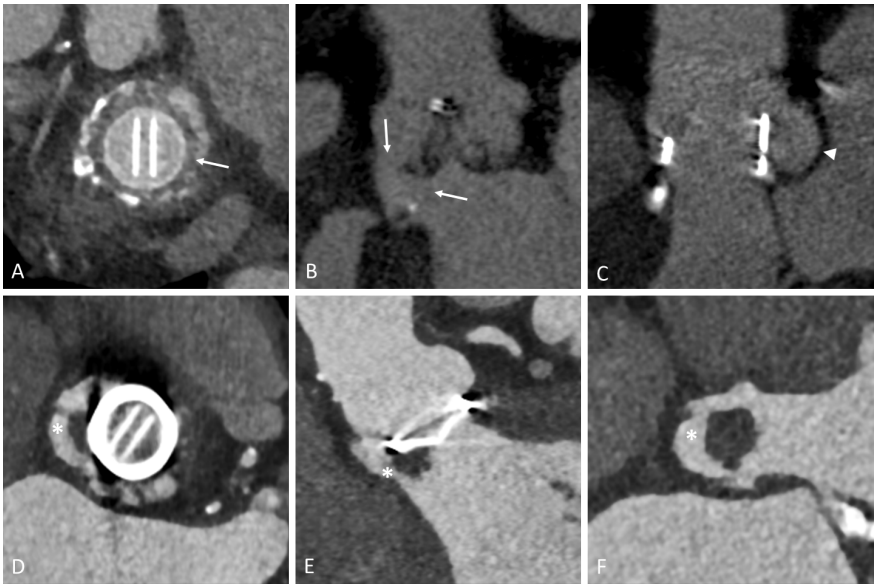

Figure 7 | CT in periprosthetic leakage and prosthetic valve endocarditis
(A) Periprosthetic leakage (arrows) in a patient with the mechanical St. Jude valve (B) Periprosthetic leakage (arrows) in a patient with the Medtronic Mosaic valve; (C) Pseudoaneurysm (arrows) in a patient with the Perimount biological prosthesis. (D-F) Endocarditis in a patient with a mechanical St. Jude prosthesis in aortic position. CT showed a large vegetation and provided information on mycotic aneurysm extension ((D) short axis view - valve level, (E) perpendicular plane - valve level, (F) short axis view - subprosthetic level).

Physiological regurgitation was found in 17/55 PHVs and both modalities detected regurgitation missed by the other technique in four (MRI) and five (TEE) patients[87]. Pathological regurgitation introduced more signal loss and/or turbulence and showed greater insufficiency jets[45, 54, 87]. MRI distinguished periprosthetic from transprosthetic regurgitation in all, but disagreed with TEE in four aortic valves[87].
TEE was unable to detect the origin of regurgitation in two PHVs. Surgical confirmation showed that MRI was correct in 11/13 and TEE in 12/13 patients. MRI regurgitation quantification correlated well with TEE, despite overestimation (4/32) and underestimation (3/32) of TEE classifications. For pulmonary PHVs, MRI was used in 144 patients to assess follow-up regurgitation and regurgitation fractions[64, 88-90].
MRI distinguished minimal and mild pulmonary valve incompetence better than echocardiography (n=13)[88]. In 20 patients MRI was also used to assess forward flow in biological pulmonary PHVs[91].

Prosthetic valve endocarditis

Endocarditis detection was systematically evaluated in three CT studies including 61 patients with 31 mechanical and 30 biological PHVs[17, 18, 92]. Two studies found no advantage over TEE for vegetation detection, irrespective of valve type[17, 18]. In a third study, CT detected vegetations missed by echocardiography in two biological and one mechanical PHV[92]. CT was better in depicting mycotic aneurysms and abscesses compared with TTE/TEE (11 versus 4, not detected by the other modality)[17, 92]. Moreover, CT provided surgically relevant additional information on aneurysm extension[18, 92], changed the treatment to surgery (n=1) and resulted in an alternative surgical strategy (n=6)[92]. *Figure 7 D-F* shows an example of CT in endocarditis. Altogether, diagnosis in patients suspected of PHV endocarditis was most accurate when CT and TEE were combined[17, 92]. MRI performance was not studied in patients with suspected PHV endocarditis.

Thrombosis and pannus formation

One of the main findings in suspected PHV obstruction is restricted leaflet motion. CT was highly accurate in measuring mechanical leaflet angles in normal and restricted valves and showed a maximal in vitro difference between CT and fluoroscopy of 2 degrees[93]. A good correlation between CT and fluoroscopy leaflet angles was also found in three patient studies (n=101)[10, 24, 36] and bileaflet valve angles corresponded to the manufacturers' data[36, 94]. For monoleaflet valves CT did not allow angle measurements in 6/7 Björk-Shileys[36, 38] and slightly underestimated Medtronic-Hall opening angles (67.4° versus 75° by manufacturer)[10]. Fluoroscopy did not allow angle measurements in 8/115 patients (due to high heart rate and/or difficult beam positioning) and was incorrect in 5/115 cases[10, 11, 24].Suspected mechanical PHV obstruction was systematically evaluated using CT in 70 patients[11, 12, 62, 95, 96]. CT detected the morphological substrate of obstruction in 21/25 selected patients with surgical confirmation in 18[11, 12, 62]. Of those, sixteen patients showed a subprosthetic mass from the interventricular septum to the pivot guard defined as pannus (n=12), pannus and thrombus (n=3) or a calcified rim (n=1) and two patients showed LVOT obstruction by a mitral PHV. In one patient with an increased transprosthetic gradient CT showed a tilted PHV position[11]. An example is presented in *Figure 8*. Another group evaluated patients with obstructed aortic valves (based on TTE/fluoroscopy) and detected pannus using CT in 19/23 patients and 7/29 controls[95, 96] and thrombus in 3/7 selected patients[96]. Pannus and thrombus were confirmed in all reoperated cases (n=6, n=2 resp.)[95, 96]. In contrast, echocardiography only detected an obstructive mass in 2/13 patients with CT masses[96].

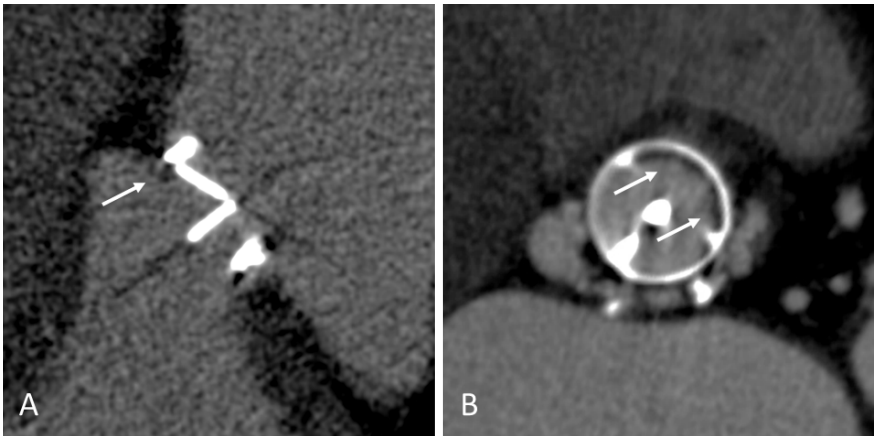

Figure 8 | Prosthetic valve pathology detected with CT
(A) Obstruction of a ATS mitral valve due to hypodense tissue (arrow) based on thrombus formation; (B) Pannus tissue (arrows) underneath a Medtronic Hall monoleaflet valve.

It is however unclear whether CT allows discrimination of pannus and thrombus based on attenuation values. Pannus had a significantly higher mean CT attenuation than the interventricular septum in one study[62] (170 and 108 Hounsfield units; HU, resp.) but equal attenuation in another[95]. A mean attenuation value for pannus of 153 HU (n=9) and 60 and 99 HU for thrombus (n=2) were also reported[96]. Moreover, no attenuation difference was found between pure pannus (n=3) and pannus with thrombus (n=2)[11]. CT could support patient prosthesis mismatch diagnosis in 10 patients with mechanical valves by showing a normal PHV function and small GOA, in combination with a small EOA (TTE)[78]. The correlation between mechanical GOA and EOA in 41 patients was moderate and mean GOA was 1.4cm^2 higher[78]. Overall, CT measurements of the prosthetic diameter (internal and external)[10, 24, 94] and GOA[10, 94] correlated well with the manufacturer specifications and between readers in mechanical valves. The correlation for both diameter and GOA was better with sinus rhythm and for aortic compared to mitral valves[10, 94]. Motion artifacts precluded CT measurements in six PHVs[10]. MRI was able to distinguish restricted from normal PHVs in vitro by central/lateral velocity jet ratios at low and high flow rates, whereas transprosthetic gradients were only discriminative at high flow rates[14]. Restricted valves showed higher velocities, merged or far-reaching asymmetric jets and reversed flow in the stenosed region[21, 49, 71]. Due to high velocities, flow measurements were less accurate and often only possible at 40mm downstream[21]. Still, velocity measurements showed good agreement with laser Doppler anemometry for the Björk-Shiley and St. Jude valve[71]. No MRI study reported on the evaluation of pannus or thrombus using MRI.

CONSIDERATIONS

Patient selection and study methods differ considerably between most studies, which makes head-to-head comparison of results difficult. For instance, MRI studies were published between 1985 and 2015 using different field strengths (0.2-3.0T) and acquisition sequences. MRI acquisition has changed and improved significantly over the years and many PHVs studied in the early years have been discontinued. Hence, their specific image quality is less relevant in the present clinical practice. Furthermore, most study sample sizes are small due to the relatively low incidence of complications in PHV patients. Results presented thus show clinical relevance for *specific* PHVs, patients and/or complications. Also, several studies excluded patients with impaired left ventricular function, arrhythmias, impaired renal function, clinically unstable patients or patients in whom echocardiography was not possible.

Based on available results, we have summarized the potentials of CT and MRI for clinical PHV assessment in *Table 4*.

CONCLUSIONS

The use for newer imaging modalities for the evaluation of PHVs may be given in by the limitations of current techniques. For example, echocardiography may not detect abnormalities due to acoustic shadowing caused by prosthetic components and limited viewing planes. CT and MRI may provide incremental information in selected patients by uncoupling image analysis and acquisition and providing a complete anatomical overview. CT can identify morphological correlates of obstruction such as (peri)prosthetic masses, restricted leaflet motion, LVOT obstruction and thickening and calcification of leaflets, which could be of importance for valve-in-valve procedures. Although no clear advantage over echocardiography was found for the detection of vegetations and periprosthetic regurgitation in general, CT showed incremental value for the assessment of endocarditis extension (pseudoaneurysms and valve dehiscence). Hence, the most important clinical indications in which CT provides additional information to echocardiography are suspected PHV obstruction in mechanical valves as well as endocarditis in biological and mechanical valves. Limitations for CT evaluation are excessive metal artifacts caused by older mechanical cobalt-chromium PHVs and limited visibility of normal biological leaflets. In addition, arrhythmias and high heart rates may impair image quality or induce artifacts. Experimental studies demonstrated promising results for artifact and radiation dose reduction, although

Table 4 | The role of CT and MRI for prosthetic heart valve evaluation

Indication	Modality	Potentials	Notes
Baseline	CT	Provide overview of cardiac anatomy and prosthesis related structures	Periprosthetic image quality valve type dependent
		Assess prosthetic inner diameter	
		Assess prosthetic GOA	Planimetric measurements, not interchangeable with EOA
		Measure leaflet opening and closing angles for mechanical valves	Poor image quality in Björk-Shiley monoleaflet valves
		Assess overall leaflet motion for some biological valves	Only if leaflets visible
	MRI	Assess cardiac dimensions and GOA in specific biological prostheses	
Suspected dysfunction			
Obstruction	CT	Detect restricted leaflet excursions independent of valve orientation or position	
	CT	Detect the morphological substrate of valve obstruction	Limited value for the Sorin and Björk-Shiley monoleaflets
	MRI	Measure velocities and detect abnormal flow patterns	
Thrombus	CT	Detect subprosthetic or supraprosthetic mass, often attached to leaflet and restricted leaflet motion	Tissue differentation based on CT attenuation not yet established
Pannus	CT	Detect (semi)circular subprosthetic mass along valve ring, mostly attached to the pivot guard, leaflet function may be normal	Tissue differentation based on CT attenuation not yet established
Second prosthesis	CT	Detect LVOT obstruction by protruding mitral prosthesis	
Prosthesis angulation		Detect angulated position of implanted prosthesis in relation to LVOT	
Patient prosthesis mismatch		Support echocardiography diagnosis by showing normal leaflet function, absent masses and small GOA	

Table 4 | Continued

Indication	Modality	Potentials	Notes
Bioprosthesis	CT	Detect leaflet thickening	
degeneration		Detect leaflet and valve calcifications	
		Show distribution of calcifications	
	MRI	Assess overall biological valve leaflet motion and detect restricted leaflets	Only if leaflets visible
Paraprosthetic regurgitation	CT	Limited, detect contrast agent extravasation in combination with echocardiography	Sensitivity of CT alone is moderate
	MRI	Detect paraprosthetic regurgitation	TEE required
Regurgitation	CT	Limited	Poor CT performance
	MRI	Detect valvular regurgitation and quantify regurgitation fraction	Clinically used for pulmonary biological prostheses
Endocarditis	CT	Limited, detect vegetations in combination with echocardiography	Sensitivity of CT alone is moderate
		Detect mycotic aneurysms and their extent	
Valve dehiscence	CT	Detect valve dehiscence	
Pseudoaneurysm	CT	Detect pseudoaneurysm formation and show their extent	
Pre surgical procedure	CT	Evaluate anatomical structures and pathology extent relevant for surgical planning including coronary arteries and relation of the bypass grafts to sternum	
Pre valve-in-valve procedure	CT	Measure aortic root, LVOT, bioprosthetic diameter, coronary ostia height	

EOA= effective orifice area; GOA= geometric orifice area; HU= Hounsfield Units; LVOT= left ventricular outflow tract

no clinical studies have been performed to assess these results in patients. MRI has shown to be safe and overall PHV-related artifacts remained localized, but mechanical details of the PHV could not be assessed. MRI allowed annular and orifice area measurements in biological valves with good agreement to echocardiography and assessment of flow and velocity patterns in biological and mechanical valves. MRI may potentially demonstrate abnormal asymmetric flow patterns in PHV obstruction, though leaflet angle measurements may not be possible. No studies have been published on the diagnostic performance for detecting PHV abnormalities such as pseudoaneurysms and abscesses. However, MRI was a useful tool for regurgitation assessment, especially in the follow-up of pulmonary valves. Future studies in non-selected populations may further specify the usefulness for CT and/or MRI in the overall PHV population. Contemporary studies are mandatory to optimize acquisition protocols and to present reference values to discriminate normal from pathological conditions for clinical implementation.

REFERENCES

1. Yacoub MH, Takkenberg JJ. Will heart valve tissue engineering change the world? *Nat Clin Pract Cardiovasc Med*. 2005;2:60-61
2. Hammermeister K, Sethi GK, Henderson WG, Grover FL, Oprian C, Rahimtoola SH. Outcomes 15 years after valve replacement with a mechanical versus a bioprosthetic valve: Final report of the veterans affairs randomized trial. *J Am Coll Cardiol*. 2000;36:1152-1158
3. Vongpatanasin W, Hillis LD, Lange RA. Prosthetic heart valves. *N Engl J Med*. 1996;335:407-416
4. Zoghbi WA, Chambers JB, Dumesnil JG, Foster E, Gottdiener JS, Grayburn PA, et al. Recommendations for evaluation of prosthetic valves with echocardiography and doppler ultrasound: A report from the american society of echocardiography's guidelines and standards committee and the task force on prosthetic valves, developed in conjunction with the american college of cardiology cardiovascular imaging committee, cardiac imaging committee of the american heart association, the european association of echocardiography, a registered branch of the european society of cardiology, the japanese society of echocardiography and the canadian society of echocardiography, endorsed by the american college of cardiology foundation, american heart association, european association of echocardiography, a registered branch of the european society of cardiology, the japanese society of echocardiography, and canadian society of echocardiography. *J Am Soc Echocardiogr*. 2009;22:975-1014
5. Girard SE, Miller FA, Jr., Orszulak TA, Mullany CJ, Montgomery S, Edwards WD, et al. Reoperation for prosthetic aortic valve obstruction in the era of echocardiography: Trends in diagnostic testing and comparison with surgical findings. *J Am Coll Cardiol*. 2001;37:579-584
6. Faletra F, Constantin C, De Chiara F, Masciocco G, Santambrogio G, Moreo A, et al. Incorrect echocardiographic diagnosis in patients with mechanical prosthetic valve dysfunction: Correlation with surgical findings. *Am J Med*. 2000;108:531-537
7. Habets J, Tanis W, Reitsma JB, van den Brink RB, Mali WP, Chamuleau SA, et al. Are novel non-invasive imaging techniques needed in patients with suspected prosthetic heart valve endocarditis? A systematic review and meta-analysis. *Eur Radiol*. 2015;25:2125-2133
8. Tanis W, Habets J, van den Brink RB, Symersky P, Budde RP, Chamuleau SA. Differentiation of thrombus from pannus as the cause of acquired mechanical prosthetic heart valve obstruction by non-invasive imaging: A review of the literature. *Eur Heart J Cardiovasc Imaging*. 2014;15:119-129
9. von Knobelsdorff-Brenkenhoff F, Rudolph A, Wassmuth R, Bohl S, Buschmann EE, Abdel-Aty H, et al. Feasibility of cardiovascular magnetic resonance to assess the orifice area of aortic bioprostheses. *Circ Cardiovasc Imaging*. 2009;2:397-404
10. LaBounty TM, Agarwal PP, Chughtai A, Bach DS, Wizauer E, Kazerooni EA. Evaluation of mechanical heart valve size and function with ecg-gated 64-mdct. *AJR Am J Roentgenol*. 2009;193:W389-396
11. Symersky P, Budde RP, de Mol BA, Prokop M. Comparison of multidetector-row computed tomography to echocardiography and fluoroscopy for evaluation of patients with mechanical prosthetic valve obstruction. *Am J Cardiol*. 2009;104:1128-1134
12. Tsai IC, Lin YK, Chang Y, Fu YC, Wang CC, Hsieh SR, et al. Correctness of multi-detector-row computed tomography for diagnosing mechanical prosthetic heart valve disorders using operative findings as a gold standard. *Eur Radiol*. 2009;19:857-867
13. Botnar R, Nagel E, Scheidegger MB, Pedersen EM, Hess O, Boesiger P. Assessment of prosthetic aortic valve performance by magnetic resonance velocity imaging. *MAGMA*. 2000;10:18-26

14. Garcia J, Marrufo O, Rodriguez AO, Pibarot P, Kadem L. A new index measured by cardiovascular magnetic resonance imaging to detect mechanical heart valve malfunction. *Conf Proc IEEE Eng Med Biol Soc*. 2011;2011:1347-1350
15. Pennekamp W, Geyhan N, Soeren P, Volkmar N. Determination of flow profiles of different mechanical aortic valve prostheses using phase-contrast mri. *J Cardiovasc Surg*. 2011;52:277-284
16. Liberati A, Altman DG, Tetzlaff J, Mulrow C, Gotzsche PC, Ioannidis JP, et al. The prisma statement for reporting systematic reviews and meta-analyses of studies that evaluate healthcare interventions: Explanation and elaboration. *BMJ*. 2009;339:b2700
17. Fagman E, Perrotta S, Bech-Hanssen O, Flinck A, Lamm C, Olaison L, et al. Ecg-gated computed tomography: A new role for patients with suspected aortic prosthetic valve endocarditis. *Eur Radiol*. 2012;22:2407-2414
18. Feuchtner GM, Stolzmann P, Dichtl W, Schertler T, Bonatti J, Scheffel H, et al. Multislice computed tomography in infective endocarditis: Comparison with transesophageal echocardiography and intraoperative findings. *J Am Coll Cardiol*. 2009;53:436-444
19. Frank H, Buxbaum P, Huber L, Globits S, Glogar D, Wolner E, et al. In vitro behaviour of mechanical heart valves in a 1.5 t superconducting magnet. *Eur Radiol*. 1992;2:555-558
20. Gurvitch R, Wood DA, Tay EL, Leipsic J, Ye J, Lichtenstein SV, et al. Transcatheter aortic valve implantation: Durability of clinical and hemodynamic outcomes beyond 3 years in a large patient cohort. *Circulation*. 2010;122:1319-1327
21. Walker PG, Pedersen EM, Oyre S, Flepp L, Ringgaard S, Heinrich RS, et al. Magnetic resonance velocity imaging: A new method for prosthetic heart valve study. *J Heart Valve Dis*. 1995;4:296-307
22. Nishimura RA, Otto CM, Bonow RO, Carabello BA, Erwin JP, 3rd, Guyton RA, et al. 2014 aha/acc guideline for the management of patients with valvular heart disease: Executive summary: A report of the american college of cardiology/american heart association task force on practice guidelines. *J Am Coll Cardiol*. 2014;63:2438-2488
23. Vahanian A, Alfieri O, Andreotti F, Antunes MJ, Baron-Esquivias G, Baumgartner H, et al. Guidelines on the management of valvular heart disease (version 2012): The joint task force on the management of valvular heart disease of the european society of cardiology (esc) and the european association for cardio-thoracic surgery (eacts). *Eur J Cardiothorac Surg*. 2012;42:S1-44
24. Bazeed MF, Moselhy MS, Rezk AI, Al-Murayeh MA. Low radiation dose non-contrast cardiac ct: Is it of value in the evaluation of mechanical aortic valve. *Acta Radiol*. 2012;53:389-393
25. Chenot F, Montant P, Goffinet C, Pasquet A, Vancraeynest D, Coche E, et al. Evaluation of anatomic valve opening and leaflet morphology in aortic valve bioprosthesis by using multidetector ct: Comparison with transthoracic echocardiography. *Radiology*. 2010;255:377-385
26. Symersky P, Budde RP, Westers P, de Mol BA, Prokop M. Multidetector ct imaging of mechanical prosthetic heart valves: Quantification of artifacts with a pulsatile in-vitro model. *Eur Radiol*. 2011;21:2103-2110
27. Suchá D, Daans CG, Symersky P, Planken RN, Mali WP, van Herwerden LA, et al. Reliability, agreement, and presentation of a reference standard for assessing implanted heart valve sizes by multidetector-row computed tomography. *Am J Cardiol*. 2015;116:112-120
28. Hara M, Nishino M, Taniike M, Makino N, Kato H, Egami Y, et al. Impact of 64 multi-detector computed tomography for the evaluation of aortic paraprosthetic regurgitation. *J Cardiol*. 2011;58:294-299

29. Tsai IC, Hsieh SR, Chern MS, Huang HT, Chen MC, Tsai WL, et al. Pseudoaneurysm in the left ventricular outflow tract after prosthetic aortic valve implantation: Evaluation upon multidetector-row computed tomography. *Tex Heart Inst J*. 2009;36:428-432
30. Ruggieri VG, Haigron P, Wang Q, Esneault S, Madeleine R, Heautot JF, et al. Ct-scan images preprocessing and segmentation to improve bioprosthesis leaflets morphological analysis. *Med Hypotheses*. 2013;81:86-93
31. Symersky P, Habets J, Westers P, de Mol BA, Prokop M, Budde RP. Prospective ecg triggering reduces prosthetic heart valve-induced artefacts compared with retrospective ecg gating on 256-slice ct. *Eur Radiol*. 2012;22:1271-1277
32. Habets J, Symersky P, Leiner T, de Mol BA, Mali WP, Budde RP. Artifact reduction strategies for prosthetic heart valve ct imaging. *Int J Cardiovasc Imaging*. 2012;28:2099-2108
33. Habets J, Symersky P, de Mol BA, Mali WP, Leiner T, Budde RP. A novel iterative reconstruction algorithm allows reduced dose multidetector-row ct imaging of mechanical prosthetic heart valves. *Int J Cardiovasc Imaging*. 2012;28:1567-1575
34. Suchá D, Willemink MJ, de Jong PA, Schilham AMR, Leiner T, Symersky P, et al. The impact of a new model-based iterative reconstruction algorithm on prosthetic heart valve related artifacts at reduced radiation dose mdct. *Int J Cardiovasc Imaging*. 2014;30:785-793
35. Habets J, Symersky P, van Herwerden LA, de Mol BA, Spijkerboer AM, Mali WP, et al. Prosthetic heart valve assessment with multidetector-row ct: Imaging characteristics of 91 valves in 83 patients. *Eur Radiol*. 2011;21:1390-1396
36. Konen E, Goitein O, Feinberg MS, Eshet Y, Raanani E, Rimon U, et al. The role of ecg-gated mdct in the evaluation of aortic and mitral mechanical valves: Initial experience. *AJR Am J Roentgenol*. 2008;191:26-31
37. Habets J, van den Brink RB, Uijlings R, Spijkerboer AM, Mali WP, Chamuleau SA, et al. Coronary artery assessment by multidetector computed tomography in patients with prosthetic heart valves. *Eur Radiol*. 2012;22:1278-1286
38. Numata S, Tsutsumi Y, Monta O, Yamazaki S, Seo H, Yoshida S, et al. Mechanical valve evaluation with four-dimensional computed tomography. *J Heart Valve Dis*. 2013;22:837-842
39. Grunenfelder J, Plass A, Alkadhi H, Genoni M. Evaluation of biological aortic valve prostheses by dual source computer tomography and anatomic measurements for potential transapical valve-in-valve procedure. *Interact Cardiovasc Thorac Surg*. 2008;7:195-200
40. von Knobelsdorff-Brenkenhoff F, Dieringer MA, Greiser A, Schulz-Menger J. In vitro assessment of heart valve bioprostheses by cardiovascular magnetic resonance: Four-dimensional mapping of flow patterns and orifice area planimetry. *Eur J Cardiothorac Surg*. 2011;40:736-742
41. von Knobelsdorff-Brenkenhoff F, Rudolph A, Wassmuth R, Schulz-Menger J. Assessment of mitral bioprostheses using cardiovascular magnetic resonance. *J Cardiov Magn Reson*. 2010;12:36
42. Edwards MB, Taylor KM, Shellock FG. Prosthetic heart valves: Evaluation of magnetic field interactions, heating, and artifacts at 1.5 t. *J Magn Reson Imaging*. 2000;12:363-369
43. Shellock FG. Prosthetic heart valves and annuloplasty rings: Assessment of magnetic field interactions, heating, and artifacts at 1.5 tesla. *J Cardiov Magn Reson*. 2001;3:317-324
44. Pruefer D, Kalden P, Schreiber W, Dahm M, Buerke M, Thelen M, et al. In vitro investigation of prosthetic heart valves in magnetic resonance imaging: Evaluation of potential hazards. *J Heart Valve Dis*. 2001;10:410-414

45. Bachmann R, Deutsch HJ, Jungehulsing M, Sechtem U, Hilger HH, Schicha H. [magnetic resonance tomography in patients with a heart valve prosthesis]. *Rofo*. 1991;155:499-505
46. Hasenkam JM, Ringgaard S, Houlind K, Botnar RM, Stodkilde-Jorgensen H, Boesiger P, et al. Prosthetic heart valve evaluation by magnetic resonance imaging. *Eur J Cardiothorac Surg*. 1999;16:300-305
47. Ringgaard S, Botnar RM, Djurhuus C, Stodkilde-Jorgensen H, Hasenkam JM, Boesiger P, et al. High-resolution assessment of velocity fields and shear stresses distal to prosthetic heart valves using high-field magnetic resonance imaging. *J Heart Valve Dis*. 1999;8:96-103
48. Voges I, Brasen JH, Entenmann A, Scheid M, Scheewe J, Fischer G, et al. Adverse results of a decellularized tissue-engineered pulmonary valve in humans assessed with magnetic resonance imaging. *Eur J Cardiothorac Surg*. 2013;44:e272-279
49. Adegbite O, Kadem L, Newling B. Purely phase-encoded mri of turbulent flow through a dysfunctional bileaflet mechanical heart valve. *MAGMA*. 2014;27:227-235
50. von Knobelsdorff-Brenkenhoff F, Trauzeddel RF, Barker AJ, Gruettner H, Markl M, Schulz-Menger J. Blood flow characteristics in the ascending aorta after aortic valve replacement--a pilot study using 4d-flow mri. *Int J Cardiol*. 2014;170:426-433
51. Soulen RL, Budinger TF, Higgins CB. Magnetic resonance imaging of prosthetic heart valves. *Radiology*. 1985;154:705-707
52. Randall PA, Kohman LJ, Scalzetti EM, Szeverenyi NM, Panicek DM. Magnetic resonance imaging of prosthetic cardiac valves in vitro and in vivo. *Am J Cardiol*. 1988;62:973-976
53. Hassler M, Le Bas JF, Wolf JE, Contamin C, Waksmann B, Coulomb M. [effects of the magnetic field in magnetic resonance imaging on 15 tested cardiac valve prostheses]. *J Radiol*. 1986;67:661-666
54. Di Cesare E, Enrici RM, Paparoni S, Castaldo F, Alagia MG, Splendiani A, et al. Low-field magnetic resonance imaging in the evaluation of mechanical and biological heart valve function. *Eur J Radiol*. 1995;20:224-228
55. Quail MA, Nordmeyer J, Schievano S, Reinthaler M, Mullen MJ, Taylor AM. Use of cardiovascular magnetic resonance imaging for tavr assessment in patients with bioprosthetic aortic valves: Comparison with computed tomography. *Eur J Radiol*. 2012;81:3912-3917
56. Immel E, Gilbert FJ, Melzer A. Experimental mri visible resonant prosthetic heart valves. *Minim Invasive Ther Allied Technol*. 2009;18:149-155
57. Edwards MB, Ordidge RJ, Hand JW, Taylor KM, Young IR. Assessment of magnetic field (4.7 t) induced forces on prosthetic heart valves and annuloplasty rings. *J Magn Reson Imaging*. 2005;22:311-317
58. Edwards MB, Ordidge RJ, Thomas DL, Hand JW, Taylor KM. Translational and rotational forces on heart valve prostheses subjected ex vivo to a 4.7-t mr system. *J Magn Reson Imaging*. 2002;16:653-659
59. Shellock FG. Biomedical implants and devices: Assessment of magnetic field interactions with a 3.0-tesla mr system. *J Magn Reson Imaging*. 2002;16:721-732
60. Shellock FG, Crues JV. High-field-strength mr imaging and metallic biomedical implants: An ex vivo evaluation of deflection forces. *AJR Am J Roentgenol*. 1988;151:389-392
61. Biere L, Pinaud F, Delepine S, Grall S, Viot N, Mateus V, et al. Cmr assessment after a transapical-transcatheter aortic valve implantation. *Eur J Radiol*. 2014;83:303-308
62. Ueda T, Teshima H, Fukunaga S, Aoyagi S, Tanaka H. Evaluation of prosthetic valve obstruction on electrocardiographically gated multidetector-row computed tomography--identification of subprosthetic pannus in the aortic position. *Circ J*. 2013;77:418-423

63. Gottlieb D, Kunal T, Emani S, Aikawa E, Brown DW, Powell AJ, et al. In vivo monitoring of function of autologous engineered pulmonary valve. *J Thorac Cardiovasc Surg*. 2010;139:723-731
64. Lee C, Lee CH, Kwak JG, Song JY, Shim WS, Choi EY, et al. Bicuspid pulmonary valve implantation using polytetrafluoroethylene membrane: Early results and assessment of the valve function by magnetic resonance imaging. *Eur J Cardiothorac Surg*. 2013;43:468-472
65. Funder JA, Ringgaard S, Frost MW, Wierup P, Klaaborg KE, Hjortdal V, et al. Aortic root distensibility and cross-sectional areas in stented and subcoronary stentless bioprostheses in pigs. *Interact Cardiovasc Thorac Surg*. 2010;10:976-980
66. O'Brien MF, Gardner MA, Garlick B, Jalali H, Gordon JA, Whitehouse SL, et al. Cryolife-o'brien stentless valve: 10-year results of 402 implants. *Ann Thorac Surg*. 2005;79:757-766
67. Kvitting JP, Dyverfeldt P, Sigfridsson A, Franzen S, Wigstrom L, Bolger AF, et al. In vitro assessment of flow patterns and turbulence intensity in prosthetic heart valves using generalized phase-contrast mri. *J Magn Reson Imaging*. 2010;31:1075-1080
68. Kozerke S, Hasenkam JM, Nygaard H, Paulsen PK, Pedersen EM, Boesiger P. Heart motion-adapted mr velocity mapping of blood velocity distribution downstream of aortic valve prostheses: Initial experience. *Radiology*. 2001;218:548-555
69. Kozerke S, Hasenkam JM, Pedersen EM, Boesiger P. Visualization of flow patterns distal to aortic valve prostheses in humans using a fast approach for cine 3d velocity mapping. *J Magn Reson Imaging*. 2001;13:690-698
70. Jackson MS, Igo SR, Lindsey TE, Maragiannis D, Chin KE, Autry K, et al. Development of a multi-modality compatible flow loop system for the functional assessment of mitral valve prostheses. *Cardiovasc Eng Technol*. 2014;5:13-24
71. Fontaine AA, Heinrich RS, Walker PG, Pedersen EM, Scheidegger MB, Boesiger P, et al. Comparison of magnetic resonance imaging and laser doppler amemometry velocity measurements downstream of replacement heart valves: Implications for in vivo assessment of prosthetic valve function. *J Heart Valve Dis*. 1996;5:66-73
72. Funder JA, Frost MW, Ringgaard S, Klaaborg KE, Wierup P, Hjortdal V, et al. In-vivo blood velocity and velocity gradient profiles downstream of stented and stentless aortic heart valves. *J Heart Valve Dis*. 2010;19:292-303
73. Machler H, Reiter G, Perthel M, Reiter U, Bergmann P, Zink M, et al. Influence of a tilting prosthetic mitral valve orientation on the left ventricular flow - an experimental in vivo magnetic resonance imaging study. *Eur J Cardiothorac Surg*. 2007;32:102-107
74. Houlind K, Eschen O, Pedersen EM, Jensen T, Hasenkam JM, Paulsen PK. Magnetic resonance imaging of blood velocity distribution around st. Jude medical aortic valves in patients. *J Heart Valve Dis*. 1996;5:511-517
75. Matsue H, Sawa Y, Matsumiya G, Matsuda H, Hamada S. Mid-term results of freestyle aortic stentless bioprosthetic valve: Clinical impact of quantitative analysis of in-vivo three-dimensional flow velocity profile by magnetic resonance imaging. *J Heart Valve Dis*. 2005;14:630-636
76. Crouch G, Bennetts J, Sinhal A, Tully PJ, Leong DP, Bradbrook C, et al. Early effects of transcatheter aortic valve implantation and aortic valve replacement on myocardial function and aortic valve hemodynamics: Insights from cardiovascular magnetic resonance imaging. *J Thorac Cardiovasc Surg*. 2015;149:462-470
77. Garcia D, Kadem L. What do you mean by aortic valve area: Geometric orifice area, effective orifice area, or gorlin area? *J Heart Valve Dis*. 2006;15:601-608

78. LaBounty TM, Agarwal PP, Chughtai A, Kazerooni EA, Wizauer E, Bach DS. Hemodynamic and functional assessment of mechanical aortic valves using combined echocardiography and multidetector computed tomography. *J Cardiovasc Comput Tomogr*. 2009;3:161-167
79. Cereijo JM, Alvarez JR, Quiroga JS, de Alegria AM, Suarez Penaranda JM. Is distortion of the bioprosthesis ring a risk factor for early calcification? *J Cardiothorac Surg*. 2010;5:77
80. Mahjoub H, Mathieu P, Senechal M, Larose E, Dumesnil J, Despres JP, et al. Apob/apoa-i ratio is associated with increased risk of bioprosthetic valve degeneration. *J Am Coll Cardiol*. 2013;61:752-761
81. Mahjoub H, Mathieu P, Larose E, Dahou A, Senechal M, Dumesnil JG, et al. Determinants of aortic bioprosthetic valve calcification assessed by multidetector ct. *Heart*. 2015;101:472-477
82. Dohmen PM, Lembcke A, Holinski S, Kivelitz D, Braun JP, Pruss A, et al. Mid-term clinical results using a tissue-engineered pulmonary valve to reconstruct the right ventricular outflow tract during the ross procedure. *Ann Thorac Surg*. 2007;84:729-736
83. Dohmen PM, Lembcke A, Holinski S, Pruss A, Konertz W. Ten years of clinical results with a tissue-engineered pulmonary valve. *Ann Thorac Surg*. 2011;92:1308-1314
84. Hechadi J, Gerber BL, Coche E, Melchior J, Jashari R, Glineur D, et al. Stentless xenografts as an alternative to pulmonary homografts in the ross operation. *Eur J Cardiothorac Surg*. 2013;44:E32-E39
85. Dohmen PM, Hotz H, Lembcke A, Kivelitz D, Hamm B, Konertz W. Magnetic resonance imaging of stentless xenografts for reconstruction of right ventricular outflow tract. *Semin Thorac Cardiovasc Surg*. 2001;13:24-27
86. Habets J, Meijer TS, Meijer RC, Mali WP, Vonken EJ, Budde RP. Ct attenuation measurements are valuable to discriminate pledgets used in prosthetic heart valve implantation from paravalvular leakage. *Br J Radiol*. 2012;85:e616-621
87. Deutsch HJ, Bachmann R, Sechtem U, Curtius JM, Jungehulsing M, Schicha H, et al. Regurgitant flow in cardiac valve prostheses: Diagnostic value of gradient echo nuclear magnetic resonance imaging in reference to transesophageal two-dimensional color doppler echocardiography. *J Am Coll Cardiol*. 1992;19:1500-1507
88. Nunn GR, Bennetts J, Onikul E. Durability of hand-sewn valves in the right ventricular outlet. *J Thorac Cardiovasc Surg*. 2008;136:290-296
89. Schreiber C, Horer J, Vogt M, Fratz S, Kunze M, Galm C, et al. A new treatment option for pulmonary valvar insufficiency: First experiences with implantation of a self-expanding stented valve without use of cardiopulmonary bypass. *Eur J Cardiothorac Surg*. 2007;31:26-30
90. Hallbergson A, Gauvreau K, Powell AJ, Geva T. Right ventricular remodeling after pulmonary valve replacement: Early gains, late losses. *Ann Thorac Surg*. 2015;99:660-666
91. Pijuan-Domenech A, Pineda V, Castro MA, Sureda-Barbosa C, Ribera A, Cruz LM, et al. "Pulmonary valve replacement diminishes the presence of restrictive physiology and reduces atrial volumes": A prospective study in tetralogy of fallot patients. *Int J Cardiol*. 2014;177:261-265
92. Habets J, Tanis W, van Herwerden LA, van den Brink RB, Mali WP, de Mol BA, et al. Cardiac computed tomography angiography results in diagnostic and therapeutic change in prosthetic heart valve endocarditis. *Int J Cardiovasc Imaging*. 2014;30:377-387
93. Suchá D, Symersky P, Vonken EJ, Provoost E, Chamuleau SA, Budde RP. Multidetector-row computed tomography allows accurate measurement of mechanical prosthetic heart valve leaflet closing angles compared with fluoroscopy. *J Comput Assist Tomogr*. 2014;38:451-456

94. Lee DH, Youn HJ, Shim SB, Lee SH, Jung JI, Jung SE, et al. The measurement of opening angle and orifice area of a bileaflet mechanical valve using multidetector computed tomography. *Korean Circ J*. 2009;39:157-162
95. Teshima H, Hayashida N, Fukunaga S, Tayama E, Kawara T, Aoyagi S, et al. Usefulness of a multidetector-row computed tomography scanner for detecting pannus formation. *Ann Thorac Surg*. 2004;77:523-526
96. Teshima H, Aoyagi S, Ueda T, Takagi K, Shojima T, Tanaka H. Evaluation of advancing the standard valve dysfunction by multidetector-row ct. *J Artif Organs*. 2014;17:162-168
97. Symersky P, Budde RP, Prokop M, de Mol BA. Multidetector-row computed tomography imaging characteristics of mechanical prosthetic valves. *J Heart Valve Dis*. 2011;20:216-222
98. de Heer LM, Habets J, Kluin J, Stella PR, Mali WP, van Herwerden LA, et al. Assessment of a transcatheter heart valve prosthesis with multidetector computed tomography: In vitro and in vivo imaging characteristics. *Int J Cardiovasc Imaging*. 2013;29:659-668

SUPPLEMENTARY MATERIAL

Supplement 1 | Search strategy performed in Pubmed* and Embase† on March 24th, 2015

#1:	"heart valves" OR "heart valve" OR "cardiac valves" OR "cardiac valve" OR "aortic valve" OR "aortic valves" OR "mitral valve" OR "mitral valves" OR "pulmonary valve" OR "pulmonary valves" OR "tricuspid valve" OR "tricuspid valves" OR "valvular disease" OR "valvular diseases" OR "cardiac valve prostheses" OR "cardiac valve prosthesis" OR "heart valve prostheses" OR "heart valve prosthesis" OR "prosthetic heart valves" OR "prosthetic heart valve" OR "mechanical valve" OR "mechanical valves" OR "mechanical prosthesis" OR "mechanical prostheses" OR PHV OR "aortic valve prosthesis" OR "aortic valve prostheses" OR "mitral valve prosthesis" OR "mitral valve prostheses" OR "biological valves" OR "biological valve" OR "biological prosthesis" OR "biological prostheses" OR bioprostheses OR bioprosthesis OR TAVI OR TAVR OR "transcatheter valve" OR "percutaneous valve" OR PPVI OR PPVR
#2:	CT OR CTs OR "computer tomography" OR "computed tomography" OR "computerized tomography" OR "CAT scan" OR "CAT scans" OR MDCT OR MSCT OR CTA OR "computer assisted tomography" OR "computed assisted tomography"
#3:	"magnetic resonance imaging" OR MRI OR MR OR NMR OR NMRI OR CMR
#4:	(#1 AND #2)
#5:	(#1 AND #3)

* In Title/Abstract

† In Title/Abstract: no conference abstract, letter, note or editorial

Supplement 2 | Main characteristics of CT studies evaluating prosthetic heart valves

Author, year	Study	No. PHVs	No. Mech.	Position	CT System	Protocol	Contrast	Dose	β-block.	IQ / Artifacts	Area / Diameter	Leaflet angles	Obstruction	Bioprosthesis degeneration	PVR	Endocarditis	Sx
Teshima[95], 2004	patients	28	28	A, M	8-slice	retro	yes	ns	ns				✓				2
Dohmen[82], 2007	patients	23	0	A	16-slice	retro	yes	ns	ns					✓			
Grunenfelder[39], 2008	patients	50	0	A	64-slice	retro	yes	ns	ns	✓	✓			✓	✓		
Konen[36], 2008	patients	23	23	A, M	40 or 64	retro	yes*	ns	ns	✓		✓					1
Feuchtner[18], 2009	patients	6	3	A, M	64-slice	retro	yes	ns	yes†							✓	6
LaBounty[10], 2009	patients	64	64	A, M	64-slice	retro	yes	44±8.3‡	no		✓	✓					
LaBounty[78], 2009	patients	41	41	A	64-slice	retro	yes	41.9±9.2‡	no		✓						
Lee[94], 2009	patients	30	30	A, M	64-slice	retro	yes	ns	no		✓	✓					
Symersky[11], 2009	patients	15	15	A, M	64-slice	retro	yes	ns	Yes >70	✓		✓	✓		✓		8
Tsai[29], 2009	patients	20	18	A	40-slice	retro	yes	ns	Yes >60				✓				
Tsai[12], 2009	patients	31	31	A, M, T	40-slice	retro	yes	15.8±3.1	Yes >60	✓			✓		✓		6
Cereijo[79], 2010	patients	4	0	A	64-slice	retro	ns	ns	ns					✓			
Chenot[25], 2010	patients	54	0	A	64-slice	retro	yes	18.8±3.8	Yes >75	✓	✓	✓		✓			
Dohmen[83], 2011	patients	11	0	P	8-slice	retro	ns	ns	ns					✓			
Habets[35], 2011	patients	91	70	A, M, T, P	16,64, 256	retro	yes	ns	ns	✓							
Hara[28], 2011	patients	20	15	A	64-slice	retro	yes	ns	yes	✓					✓		2
Symersky[97], 2011	in vitro	5	5	-	64-slice	retro	no	ns	-	✓							
Symersky[26], 2011	in vitro	4	4	-	64-slice	retro	no	ns	-	✓							
Bazeed[24], 2012	patients	40	40	A	64-slice	retro	no	4±0.5	no	✓	✓	✓					
Fagman[17], 2012	patients	27	10	A	64-slice	retro	yes	19	no							✓	16
Habets[86], 2012	both	23	18	A, M, T, P	64 or 256	retro	yes	ns	ns						✓		
Habets[33], 2012	in vitro	4	4	-	64-slice	retro	no	-	-	✓							
Habets[32], 2012	in vitro	2	2	-	64-slice	retro	no	-	-	✓							
Habets[37], 2012	patients	89	68	A, M, T, P	64 or 256	both	yes	15.6±5.5§	ns	✓							
Quail[55], 2012	patients	21	0	A	64-slice	retro	yes	ns	no		✓						
Symersky[31], 2012	in vitro	2	2	-	256-slice	both	no	-	-	✓							
Hechadi[84], 2013	patients	11	0	P	256-slice	prosp	no	ns	ns					✓			
Mahjoub[80], 2013	patients	194#	0	A	64-slice	prosp	no	ns	ns					✓			
Numata[38], 2013	patients	45	45	A, M	16 or 256	retro	no	ns	no	✓		✓					2
Ruggieri[30], 2013	patients	4	0	A	64-slice	retro	yes	6.4-7``	Yes >75	✓							
Ueda[62], 2013	patients	9	9	A	16-slice	retro	yes	ns	no				✓				9
Habets[92], 2014	patients	28	18	A, M	64 or 256	retro	yes	11.8	ns							✓	16
Suchá[93], 2014	in vitro	4	4	-	64-slice	retro	no	ns	-			✓					
Suchá[34], 2014	in vitro	3	2	-	256-slice	retro	yes	-	-	✓							
Teshima[96], 2014	patients	30	30	A, M, T	8,16,256	retro	yes	14.5``	no				✓				5
Mahjoub[81], 2015	patients	194#	0	A	64-slice	prosp	no	ns	ns					✓			

*in n=15; † in 8/37 of cohort including native valves; ‡= for thoraco-abdominal (±pelvic) CTA; §17.6±4.2 voor thoraco-abdominal CTA; `` calculated from provided dose-length product; # same patients; *IQ=image quality; Mech=mechanical prostheses; ns=not specified; PHV=prosthetic heart valve; prosp=prospective ECG-triggered; PVR=paravalvular regurgitation; retro=retrospective ECG-gated; Sx=surgical confirmation*

Supplement 3 | Main characteristics of MRI studies evaluating prosthetic heart valves

Author, year	Study	No. PHVs	No. Mech.	Position	MR System (T)	Safety	IQ / Artifacts	Area / Diameter	Flow/ velocity	Restriction/ Stenosis	Regurg.
Soulen[51], 1985	In vitro	9	7	-	0.35, 1.5, 2.35	✓	✓				
Hassler[53], 1986	In vitro	15	10	-	0.5, 2.35	✓	✓				
Randall[52], 1988	In vitro / Patients	11	3	A	0.5, 2.0	✓	✓				
Shellock[60], 1988	In vitro	7	5	-	1.5	✓					
Bachmann[45], 1991	Patients	100	84	A, M, T	1.5						✓
Deutsch[87], 1992	Patients	55	48	A, M, T	1.5						✓
Frank[19], 1992	In vitro	7	7	-	1.5	✓					
Di Cesare[54], 1995	Patients	16	7	A, M	0.2		✓				✓
Walker[21], 1995	In vitro	4	3	-	1.5				✓	✓	
Fontaine[71], 1996	In vitro	4	3	-	1.5				✓	✓	
Houlind[74], 1996	Patients	6	6	A	1.5				✓		
Hasenkam[46], 1999	In vitro/ Patients	7	7	A	1.5, 7.0				✓		
Ringgaard[47], 1999	In vitro	1	1	-	7.0				✓		
Botnar[13], 2000	Patients	7	7	A	1.5				✓		
Edwards[42], 2000	In vitro	32	16	-	1.5	✓	✓				
Dohmen[85], 2001	Patients	7	0	A, P	1.5						
Kozerke[68], 2001	Patients	10	10	A	1.5				✓		
Kozerke[69], 2001	In vitro/ Patients	7	7	A	1.5				✓		
Pruefer[44], 2001	In vitro	17	12	-	1.5	✓	✓				
Shellock[43], 2001	In vitro	3	1	-	1.5	✓	✓				
Edwards[58], 2002	In vitro	60	35	-	4.7	✓					
Shellock[59], 2002	In vitro	9	7	-	3.0	✓					
Edwards[57], 2005	In vitro	11	3	-	4.7	✓					
Matsue[75], 2005	Patients	26	0	A	1.5				✓		
O'Brien[66], 2005	Patients	10	0	A	1.5			✓			
Machler[73], 2007	Animals	10	10	M	1.5				✓		
Schreiber[89], 2007	Patients	6	0	P	1.5						✓
Nunn[88], 2008	Patients	13	0	P	ns						✓
Immel[56], 2009	In vitro	2	1	-	1.0, 1.5, 3.0		✓				
Von Knobelsdorff[9], 2009	Patients	65	0	A	1.5		✓	✓			
Funder[72], 2010	Animals	27	0	A	1.5				✓		
Funder[65], 2010	Animals	19	0	A	1.5			✓			
Gottlieb[63], 2010	Animals	9	0	P	1.5			✓			
Kvitting[67], 2010	In vitro	4	2	-	1.5				✓		
Von Knobelsdorff[41], 2010	Patients	18	0	M	1.5		✓	✓			
Garcia[14], 2011	In vitro	1	1	-	3.0					✓	
Pennekamp[15], 2011	Patients	60	60	A	1.5				✓		
von Knobelsdorff[40], 2011	In vitro	10	0	-	1.5		✓	✓	✓		
Quail[55], 2012	Patients	21	0	A	1.5		✓	✓			
Lee[64], 2013	Patients	24	0	P	1.5						✓
Voges[48], 2013	Patients	17	0	P	1.5					✓	
Adegbite[49], 2014	In vitro	2	1	-	1.5				✓	✓	
Jackson[70], 2014	In vitro	3	1	-	1.5			✓	✓		
Pijuan-Domenech[91], 2014	Patients	20	0	P	1.5						✓
Von Knobelsdorf[50], 2014	Patients	31	9	A	1.5				✓		
Crouch[76], 2015	Patients	21	0	A	1.5						✓
Hallbergson[90], 2015	Patients	101	0	P	1.5						✓

IQ=image quality; Mech=mechanical prostheses; ns=not specified; PHV=prosthetic heart valve; Regurg=regurgitation

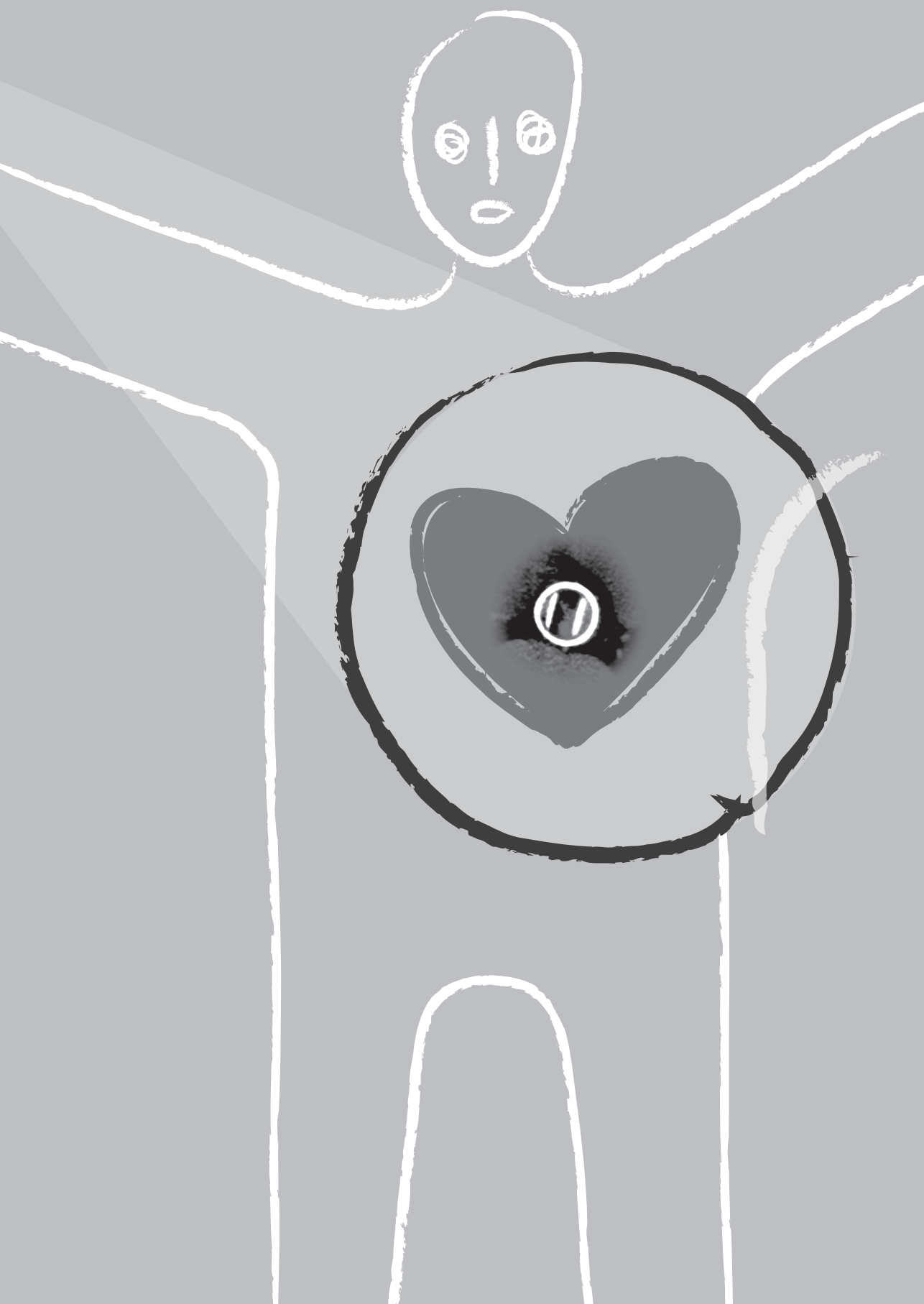

PART I
In vitro studies

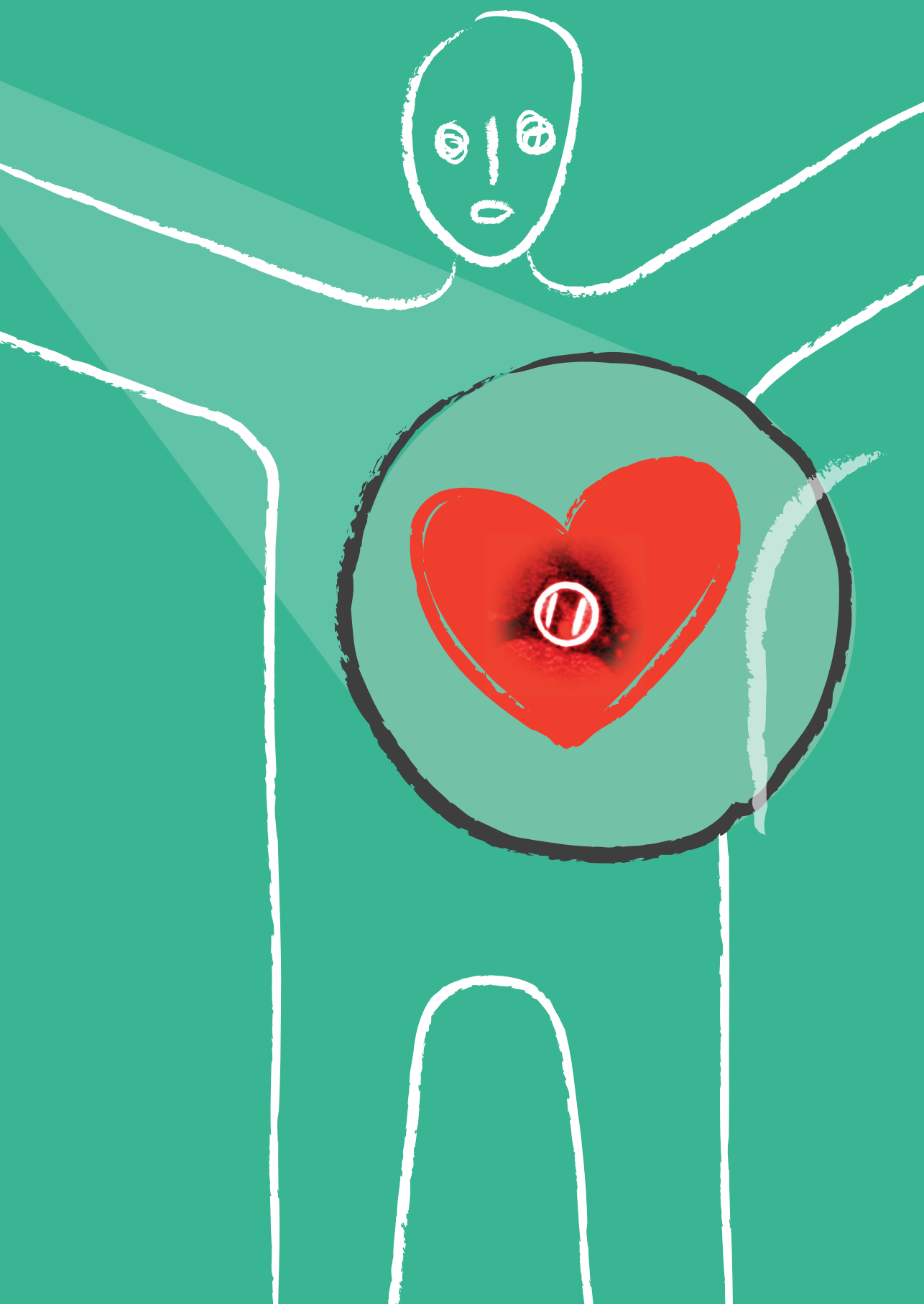

CHAPTER 3

Multidetector-row CT allows accurate measurement of mechanical prosthetic heart valve leaflet closing angles compared with fluoroscopy

Dominika Suchá
Petr Symersky
Evert-Jan P.A. Vonken
Esther Provoost
Steven A.J. Chamuleau
Ricardo P.J. Budde

Published in the Journal of Computer Assisted Tomography, 2014

ABSTRACT

PURPOSE

To compare multidetector-row computed tomography (MDCT) leaflet restriction measurements with fluoroscopy in commonly used mechanical prosthetic heart valves (PHV).

METHODS

Four mechanical PHVs (ON-X, Carbomedics, St. Jude, Medtronic Hall) were imaged in a pulsatile model using fluoroscopy and 64-detector-row CT. Five image acquisitions were made of each PHV without (one) and with (four) restricted leaflet closure. Three observers measured closure angles on fluoroscopy and MDCT. Data was analyzed using intraclass correlation coefficients (ICC) and Bland-Altman plots.

RESULTS

Interobserver agreement was high in restricted and non-restricted leaflets on both modalities (ICCs >0.995). MDCT and fluoroscopy showed high agreements (ICCs >0.989). Median MDCT closure angle measurements differed at most -2 to +2 degrees from fluoroscopy in restricted and -1 to +2 degrees in non-restricted leaflets.

CONCLUSIONS

MDCT allows measurement of leaflet motion with a maximal median discrepancy of 2 degrees. Both MDCT and fluoroscopy detect restricted leaflet closure with great accuracy.

INTRODUCTION

Prosthetic valve obstruction is one of the most serious complications after mechanical prosthetic valve replacement and has an incidence of 0.5 to 6% per year[1,2]. Echocardiography and fluoroscopy are the primary diagnostic modalities for the evaluation of mechanical prosthetic heart valves (PHV)[3,4]. Echocardiography provides valuable anatomical as well as functional information, whereas fluoroscopy allows assessment of mechanical prosthetic leaflet motion due to addition of tungsten to the carbon substrate of the leaflets. Although the experience with fluoroscopy is extensive, it only is possible by positioning the X-ray beam exactly perpendicular to the valve leaflets. In certain prosthetic valve orientations such as an anatomically oriented mitral prosthesis and aortic prostheses orientated parallel to the ventricular septum, fluoroscopy is not possible as the X-ray beam would be directed obliquely through the width of the thorax[5]. Hence, leaflet motion cannot be assessed with conventional modalities in all patients.

Multidetector-row computed tomography (MDCT) has shown potential as a non-invasive technique to evaluate prosthetic heart valves[6-10]. Electrocardiographically (ECG) gated image reconstructions allow dynamic visualization and assessment of prosthetic leaflet motion[7-9]. Little is known about the diagnostic accuracy of MDCT to assess leaflet motion and detect restricted leaflet excursions[8, 11, 12]. Potential advantages of MDCT are the possibility of assessing the valve leaflets in any desired imaging plane and, with a full cardiac acquisition, to assess the coronary arteries, the periprosthetic anatomy and possible obstructive masses. Possibly, cardiac MDCT may provide a comprehensive anatomic examination for the follow-up of patients with prosthetic heart valves.

Currently, European guidelines recommend the use of cardiac MDCT for the evaluation of prosthetic valve dysfunction if results with echocardiography and fluoroscopy are inconclusive[13]. The drawbacks that restrict widespread use are the radiation dose and, for evaluation of leaflet motion, the lack of validation of MDCT for the detection of leaflet motion restriction. Although clinical studies have found good correlation between MDCT and fluoroscopy, the accuracy of MDCT leaflet restriction measurements is unknown.

The main causes of prosthetic valve obstruction are thrombus and pannus (fibrous semicircular subprosthetic tissue) which may both cause gross systolic or diastolic abnormalities that can easily be detected with several modalities. However, sometimes only subtle leaflet restriction is present and normal leaflet motion may be found in up to 17% of patients with pannus imaged with fluoroscopy[14]. Hence, the evaluation of leaflet motion with MDCT may only be justified for suspected

valve dysfunction if it performs at least as accurate as fluoroscopy. The objective of this study was to compare MDCT detecting leaflet motion restriction to fluoroscopy in four different commonly used mechanical heart valve prostheses in optimal in vitro circumstances and to evaluate if MDCT has potential to detect even small leaflet restrictions with various standardized restriction grades.

MATERIALS AND METHODS

Valves

Four different mechanical aortic valve prostheses were studied: St. Jude HP (SJ; St. Jude Medical Inc., St. Paul MN), Medtronic Hall tilting disc (MH; Medtronic Inc., Minneapolis MN), Carbomedics standard (CM; Carbomedics Inc., Austin TX), and ON-X (ON-X; ON-X Life Technologies Inc., Austin, TX). For each valve various grades of leaflet closure restriction were simulated. Closure restriction was achieved by placing a suture around the valve ring at the middle of one of the leaflets (*Figure 1*). To create different standardized and reproducible grades of restriction, different thicknesses of sutures were used; Prolene 1 (thickest), 2-0, 4-0 (thinnest) and Ticron 2-0. Hence, five image acquisitions were obtained of each valve either without (one) or with (four) various grades of leaflet closure restriction.

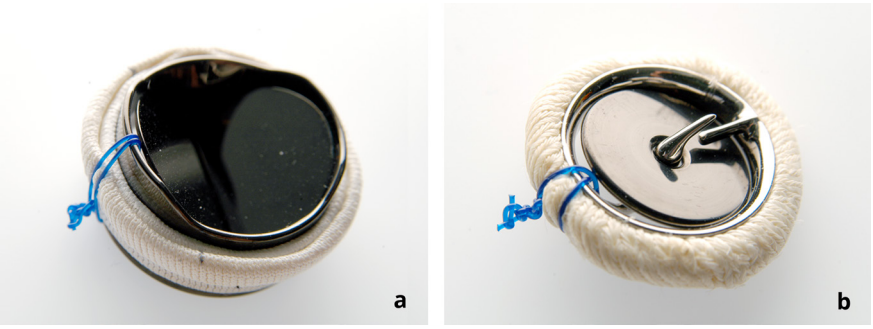

Figure 1 | An ON-X bileaflet (A) and a Medtronic Hall tilting disc (B) aortic valve with a Prolene 1 suture (maximal thickness) placed around the valve ring. Note the incomplete closure of the leaflet.

In vitro set-up

The valves were mounted in a previously described custom-made in vitro model which was filled with water[7]. Briefly, the valve was placed in a polymethyl methacrylate valve chamber connected by an inlet and outlet portion to the computer controlled piston pump mock loop. The valve chamber was placed in a commercially available anthropomorphic thoracic phantom (QRM GmbH,

Möhrendorf, Germany) to simulate radiation absorption of the human thorax. The piston pump was set at 60 beats per minute and an artificial ECG signal was generated by the software to enable image acquisition.

Computed tomography

Image acquisition was performed using a 64-detector-row CT scanner (Brilliance 64-channel, Philips Medical Systems, Cleveland, Ohio). Retrospectively ECG-gated scans were acquired using the following parameters: slice collimation of 64 x 0.625 mm, gantry rotation time of 420 milliseconds; matrix size of 512 x 512 pixels, a pitch of 0.2, tube voltage 120kV and tube current-time product 600mAs. Images were reconstructed at 10% increments of the RR-interval throughout the full cardiac cycle, generating 10 datasets of each acquisition. Assessment of the images was performed on a dedicated workstation (Philips Brilliance 3.0, Philips medical Systems, Cleveland, Ohio). Imaging planes were set to obtain reconstruction planes directly perpendicular to the valve leaflets. The reconstruction phase in which the valve was completely closed was determined visually and from this phase a batch of images (thickness of 0.9 mm) containing the entire valve was saved. Subsequently, by looping all reconstruction phases, a cine loop of valve leaflet motion through the middle of the prosthesis was obtained.

Fluoroscopy

Fluoroscopy cine images were made using a fluoroscopy C-arm (Pulsera; Philips Nederland BV Medical Systems, Eindhoven, The Netherlands). The in vitro model was placed on a standard angiography table. The x-ray beam was positioned perpendicular to the valve ring and leaflets and fluoroscopy images were recorded during approximately five seconds.

Image analysis

The images were scored by three independent observers (an experienced radiologist, cardiologist and cardiothoracic surgeon). CT and fluoroscopy images were saved and supplied on DVD. For evaluation and scoring a commercially available analysis software (Philips Brilliance 3.0 and Philips DICOM Viewer R2.5, Philips Medical Systems, Cleveland, Ohio) was used, which was supplied on the DVD as well. The observers were blinded for number and amount of restriction in each valve. Before the scoring, observers received instructions on MDCT and fluoroscopy evaluation of PHVs regarding normal valve anatomy, window levelling and angle measurements. The software enabled the observers to scroll through the images and change window width and level settings as one pleased.

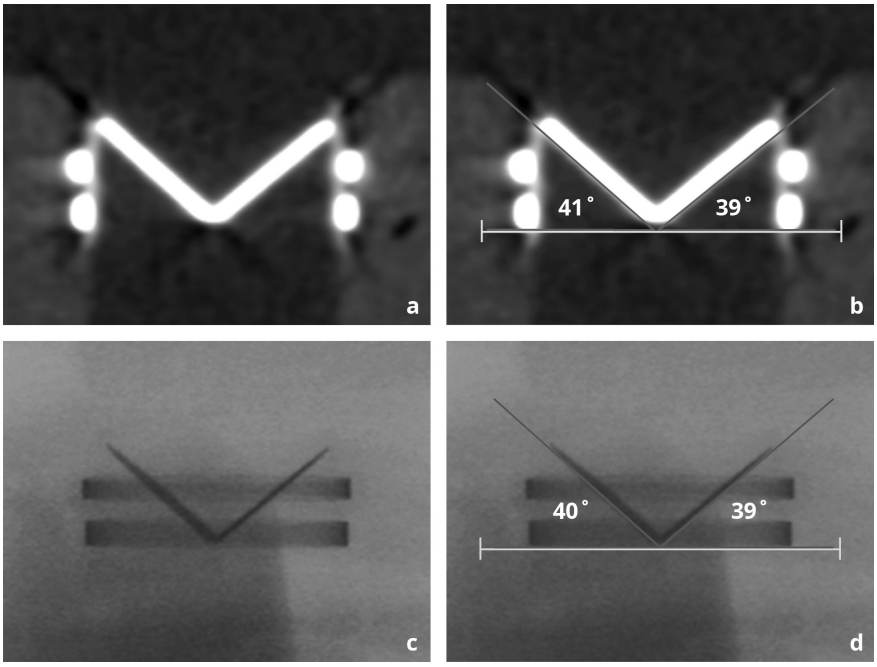

Figure 2. MDCT (A,B) and fluoroscopy (C,D) images with closure angle measurements in a bileaflet ON-X prosthetic valve with restriction of the left leaflet due to a Prolene 4.0 (thinnest) suture (not visible).

Both MDCT and fluoroscopy images could be viewed in cine mode. The still and cine loop images per valve were scored together. For each valve five scans (one normal, four with restriction) were scored. The scoring was performed by using standardized scoring forms. For each valve, each individual valve leaflet was scored as either completely closed or not. The angle between the valve leaflet and valve ring was measured in closed position using the angle measurement tools available in the image display program. First a line parallel to the valve ring was drawn (baseline). Second a line parallel to the valve leaflet followed by a line parallel to the baseline was drawn (*Figures 2 and 3*). The program automatically measured the angle between the two lines. This procedure was repeated for all leaflets.

Statistical Analysis

Statistical analysis was performed using the SPSS 20.0 version for Windows. Intraclass correlation coefficients (ICC) were calculated for interobserver agreements on angle measurements. Also, ICCs were calculated to determine the agreements between angle measurements on MDCT and fluoroscopy. An ICC value of 1.0

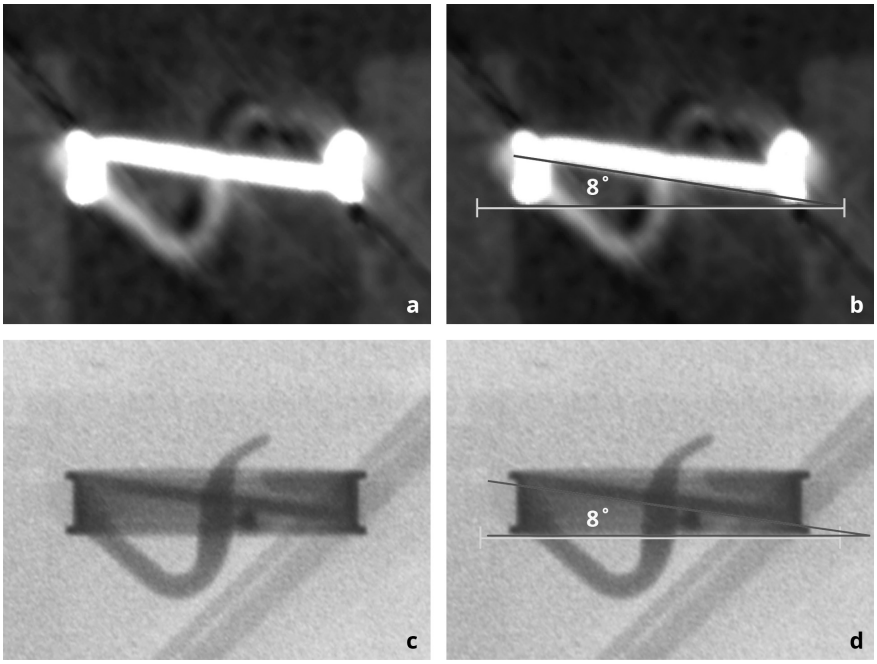

Figure 3. MDCT (A,B) and fluoroscopy (C,D) images of closing angle measurements in the Medtronic Hall tilting disc due to a Prolene 1 suture (not visible).

indicates perfect correlation. For comparison of MDCT and fluoroscopy angle closure measurements Bland-Altman plots were performed. The results of scoring individual leaflets on the presence of restriction on MDCT and fluoroscopy images were compared to the restriction key file. Sensitivity, specificity, positive predictive value and negative predictive value of both imaging modalities were calculated for each observer separately per leaflet and per valve.

RESULTS

Interobserver agreement was excellent for MDCT in both the restriction and non-restriction group (ICC 0.996 and 0.995 respectively). Also, interobserver agreement for fluoroscopy measurements was high in both groups (ICC 0.998 and 0.996 respectively).

Agreements between MDCT and fluoroscopy closing angle measurements were analyzed per observer and showed high correlations in all observers (ICCs > 0.989) (*Table 1*). Bland-Altman plots showed MDCT leaflet closure angle measurements to differ at most -2 to +3 degrees from fluoroscopy measurements when analyzed

per observer separately (*Figure 4*). Median closing angle measurements on MDCT differed at most -2 to +2 degrees from fluoroscopy measurements in restricted leaflets. In non-restricted leaflets the median MDCT measurements differed at most -1 to +2 degrees from fluoroscopy measurements (*Table 2*).

All observers missed one same restricted leaflet with MDCT (ON-X, Prolene 4-0; *Figure 2*), one observer missed an additional restricted leaflet (ON-X, Prolene 2-0). With fluoroscopy two observers missed one leaflet restriction (ON-X, Prolene 4-0), the other observer missed one leaflet restriction (Carbomedics 2-0) and misdiagnosed restriction in two normal functioning leaflets (Carbomedics). The positive and negative predictive values for leaflet restriction detection with MDCT as well as sensitivity and specificity are presented in *Table 3*.

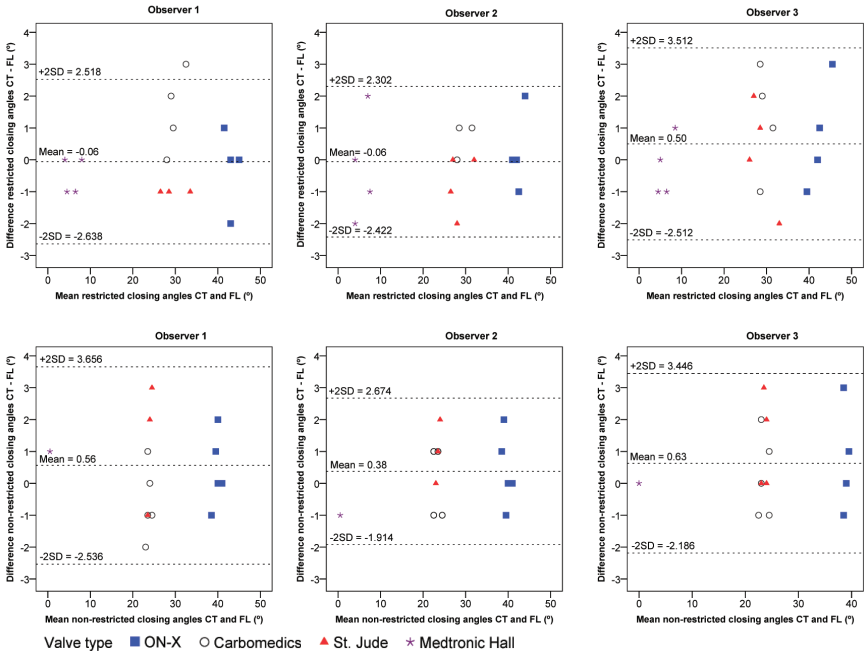

Figure 4 | Bland-Altman plots of leaflet closing angle measurements with computed tomography (CT) and fluoroscopy (FL).

Table 1 | CT and fluoroscopy agreement for leaflet closing angle measurements in restricted and non-restricted leaflets

	CT – FL agreement*		
	Observer 1	Observer 2	Observer 3
Restriction	.996	.996	.994
Non-restriction	.989	.994	.990

* Intraclass correlation coefficients
CT= computed tomography; FL= fluoroscopy

Table 2 | The overall difference between leaflet closure angle measurements with CT and FL per valve type

	Difference in angle measurements CT – FL (°)	
	Restricted leaflets	Non-restricted leaflets
ON-X, median (*)	-1 to 0 (-2 to 3)	0 to 2 (-1 to 3)
Carbomedics	-1 to 2 (-1 to 3)	-1 to 2 (-2 to 2)
St. Jude	-2 to 0 (-2 to 2)	0 to 2 (-1 to 3)
Medtronic-Hall	-1 to 0 (-2 to 2)	0 (-1 to 1)

* within all observers

Table 3 | Sensitivity, specificity, PPV, NPV of CT and FL for detecting leaflet closure restriction by three observers per leaflet and per valve

	Obs	Sensitivity	Specificity	PPV	NPV
Leaflets					
CT	1	0.94	1.0	1.0	0.95
	2	0.94	1.0	1.0	0.95
	3	0.88	1.0	1.0	0.90
FL	1	0.94	1.0	1.0	0.95
	2	0.94	0.89	0.88	0.94
	3	0.94	1.0	1.0	0.95
Valve					
CT	1	0.94	1.0	1.0	0.80
	2	0.94	1.0	1.0	0.80
	3	0.88	1.0	1.0	0.67
FL	1	0.94	1.0	1.0	0.80
	2	1.0	0.75	0.88	1.0
	3	0.94	1.0	1.0	0.80

Obs= observer; PPV= positive predictive value; NPV= negative predictive value

DISCUSSION

Fluoroscopy is the gold standard for determining mechanical PHV leaflet motion[4, 13]. In this in vitro study MDCT was used to assess closing angle measurements in restricted and non-restricted mechanical PHV leaflets and compared to fluoroscopy. The main finding of this study is that MDCT can measure leaflet closing angles with high agreement to fluoroscopy measurements with a maximal median difference of -2 to +2 degrees in restricted leaflets and -1 to +2 degrees in non-restricted leaflets. Hence, in controlled in vitro conditions, there exists a very small margin of error when performing leaflet angle measurements with MDCT.

Since the introduction of MDCT as an imaging technique in patients with PHVs, leaflet opening and closing angles of mechanical PHVs have been assessed with MDCT in patient studies[6, 11, 15-17]. Clinical studies found strong correlations for leaflet angles between MDCT and fluoroscopy and between MDCT and manufacturer specifications. However, a large margin of error was observed. For example, LaBounty et al. found differences between MDCT and fluoroscopy of up to 20 degrees. The authors explained this wide distribution by pointing out that fluoroscopy had not yielded a perfectly perpendicular view of the leaflets in two cases[16]. Konen et al. found a distribution of about 10 degrees when comparing MDCT with fluoroscopy[11]. Bazeed et al. failed to assess eight of 40 opening angles with fluoroscopy whereas MDCT was able to assess angles in all patients[15]. Based on these studies, MDCT may only be suitable to detect grossly impaired leaflet motion. However, some limitations may account for these discrepancies. First, the gold standard (fluoroscopy) may not be possible in certain valve orientations and therefore may in itself be a source of error[5, 16]. Secondly, several older prostheses such as the Björk-Shiley tilting disc and the Sorin tilting disc prostheses, do not have tungsten impregnated leaflets and are made of a cobalt chrome alloy which is associated with severe artifacts on MDCT[7, 8, 11]. Hence several confounding factors may have hampered the clinical comparison of MDCT and fluoroscopy. In order to compare the performance of each modality for leaflet motion a controlled in vitro model was chosen for this study. Furthermore, different suture thicknesses were used to evaluate if MDCT and fluoroscopy can detect even small restriction grades. Our results demonstrated excellent agreement for closing angle measurements between observers and between CT and fluoroscopy. The maximal median difference of 2 degrees found in our study indicates that in controlled setup both modalities are comparable and that the difference found in the clinical setting cannot be explained by the different imaging techniques. It also serves as an in vitro benchmark for the margin of error that is acceptable for each modality. Restricted

leaflet motion as assessed with fluoroscopy has been defined as more than 10% of the angles provided by manufacturers[4]. MDCT studies defined closure restriction as more than 0 degrees for monoleaflet PHVs, incomplete disc apposition for bileaflet PHVs or simply angles greater than specified by manufacturer[11, 16]. Also, MDCT reading errors for angle measurements have been estimated at 4 degrees[6]. Despite that the 10% limit was set for opening angles on fluoroscopy, the 2 degree margin of error found with MDCT should not lead to misdiagnoses in patients and is still even within the range of reading errors.

In vitro, the majority of missed restricted leaflets in this study concerned the ON-X PHV with 4-0 Prolene suture. This suture is probably too thin (0.15 mm) to simulate relevant leaflet restriction, since it was the thinnest suture used in this study and restriction was missed on both MDCT and fluoroscopy. In vivo leaflet restriction caused by thrombus tissue will probably show a greater and clinically more relevant restriction grade than restriction with a suture. However, even small leaflet angle restrictions have been detected with MDCT in a patient with leaflet restriction due to an inverted suture knot which was confirmed at reoperation[6]. In our study, with exclusion of the specific thinnest suture restricted PHV, MDCT showed only one wrong diagnosis in one observer but fluoroscopy three, confirming the adequacy of MDCT to assess PHV leaflet closure. In a previous study of our group, MDCT was able to detect seven patients with leaflet restriction whereas fluoroscopy failed to detect three of these[6]. The current study showed that MDCT is able to measure closing angles adequately not only in normal functioning valves but also in PHVs with restriction and with high interobserver correlations. Clinical factors which may hamper the evaluation are non-perpendicular view and torsion of the prosthesis during the cardiac cycle for fluoroscopy and excessive artifacts and, possibly, a limited temporal resolution for MDCT. All these factors may contribute to suboptimal clinical diagnostic images and a larger margin of error.

This study has several limitations. First, PHVs were studied in a pulsatile in vitro model with fixation of the PHV annulus. Therefore no annular motion was present which may influence MDCT image quality. Second, the piston pump was set at 60 beats per minute without beat alterations or arrhythmias. Since arrhythmias or higher heart rates can induce more artifacts and poorer image quality they might result in altered leaflet angle measurements. Third, prostheses associated with severe artifacts, such as the Sorin and Björk-Shiley tilting disc, were excluded from this study. However, most frequently implanted PHVs including the Medtronic-Hall tilting disc were assessed in this study. Fourth, only five scans were retrieved per

PHV type. Therefore no analysis was possible to identify closing angle measurement differences between various valve types. On the other hand, all imaged PHVs showed only minimal differences for angle measurements from fluoroscopy measurements diminishing the relevance of per type analysis.

CONCLUSIONS

MDCT has shown to adequately assess leaflet closing angles in PHVs compared to fluoroscopy in controlled in vitro circumstances with maximal median differences of -2 degrees to +2 degrees in restricted leaflets and -1 to +2 degrees in non-restricted leaflets. Both MDCT and fluoroscopy detect incomplete leaflet closure with great accuracy.

REFERENCES

1. Cannegieter SC, Rosendaal FR, Briet E. Thromboembolic and bleeding complications in patients with mechanical heart valve prostheses. *Circulation*. 1994;89:635-641
2. Vongpatanasin W, Hillis LD, Lange RA. Prosthetic heart valves. *N Engl J Med*. 1996;335:407-416
3. Zoghbi WA, Chambers JB, Dumesnil JG, Foster E, Gottdiener JS, Grayburn PA, et al. Recommendations for evaluation of prosthetic valves with echocardiography and doppler ultrasound: A report from the american society of echocardiography's guidelines and standards committee and the task force on prosthetic valves, developed in conjunction with the american college of cardiology cardiovascular imaging committee, cardiac imaging committee of the american heart association, the european association of echocardiography, a registered branch of the european society of cardiology, the japanese society of echocardiography and the canadian society of echocardiography, endorsed by the american college of cardiology foundation, american heart association, european association of echocardiography, a registered branch of the european society of cardiology, the japanese society of echocardiography, and canadian society of echocardiography. *J Am Soc Echocardiogr*. 2009;22:975-1014
4. Cianciulli TE, Lax JA, Beck MA, Cerruti FE, Gigena GE, Saccheri MC, et al. Cinefluoroscopic assessment of mechanical disc prostheses: Its value as a complementary method to echocardiography. *J Heart Valve Dis*. 2005;14:664-673
5. Montorsi P, Arena V, Muratori M, Lavarra F, Cavoretto D, Repossini A, et al. Fluoroscopic functional evaluation of bileaflet prostheses: Effect of different intraoperative valve orientation. *Am J Card Imaging*. 1996;10:101-107
6. Symersky P, Budde RP, de Mol BA, Prokop M. Comparison of multidetector-row computed tomography to echocardiography and fluoroscopy for evaluation of patients with mechanical prosthetic valve obstruction. *Am J Cardiol*. 2009;104:1128-1134
7. Symersky P, Budde RP, Prokop M, de Mol BA. Multidetector-row computed tomography imaging characteristics of mechanical prosthetic valves. *J Heart Valve Dis*. 2011;20:216-222
8. Tsai IC, Lin YK, Chang Y, Fu YC, Wang CC, Hsieh SR, et al. Correctness of multi-detector-row computed tomography for diagnosing mechanical prosthetic heart valve disorders using operative findings as a gold standard. *Eur Radiol*. 2009;19:857-867
9. Teshima H, Hayashida N, Fukunaga S, Tayama E, Kawara T, Aoyagi S, et al. Usefulness of a multidetector-row computed tomography scanner for detecting pannus formation. *Ann Cardiothorac Surg*. 2004;77:523-526
10. Habets J, Budde RP, Symersky P, van den Brink RB, de Mol BA, Mali WP, et al. Diagnostic evaluation of left-sided prosthetic heart valve dysfunction. *Nat Rev Cardiol*. 2011;8:466-478
11. Konen E, Goitein O, Feinberg MS, Eshet Y, Raanani E, Rimon U, et al. The role of ecg-gated mdct in the evaluation of aortic and mitral mechanical valves: Initial experience. *AJR Am J Roentgenol*. 2008;191:26-31
12. Habets J, Symersky P, van Herwerden LA, de Mol BA, Spijkerboer AM, Mali WP, et al. Prosthetic heart valve assessment with multidetector-row ct: Imaging characteristics of 91 valves in 83 patients. *Eur Radiol*. 2011;21:1390-1396
13. Vahanian A, Alfieri O, Andreotti F, Antunes MJ, Baron-Esquivias G, Baumgartner H, et al. Guidelines on the management of valvular heart disease (version 2012): The joint task force on the management of valvular heart disease of the european society of cardiology (esc) and the european association for cardio-thoracic surgery (eacts). *Eur J Cardiothorac Surg*. 2012;42:S1-44

14. Tanis W, Habets J, van den Brink RB, Symersky P, Budde RP, Chamuleau SA. Differentiation of thrombus from pannus as the cause of acquired mechanical prosthetic heart valve obstruction by non-invasive imaging: A review of the literature. *Eur Heart J Cardiovasc Imaging*. 2014;15:119-129
15. Bazeed MF, Moselhy MS, Rezk AI, Al-Murayeh MA. Low radiation dose non-contrast cardiac ct: Is it of value in the evaluation of mechanical aortic valve. *Acta Radiol*. 2012;53:389-393
16. LaBounty TM, Agarwal PP, Chughtai A, Bach DS, Wizauer E, Kazerooni EA. Evaluation of mechanical heart valve size and function with ecg-gated 64-mdct. *AJR Am J Roentgenol*. 2009;193:W389-396
17. Lee DH, Youn HJ, Shim SB, Lee SH, Jung JI, Jung SE, et al. The measurement of opening angle and orifice area of a bileaflet mechanical valve using multidetector computed tomography. *Korean Circ J*. 2009;39:157-162

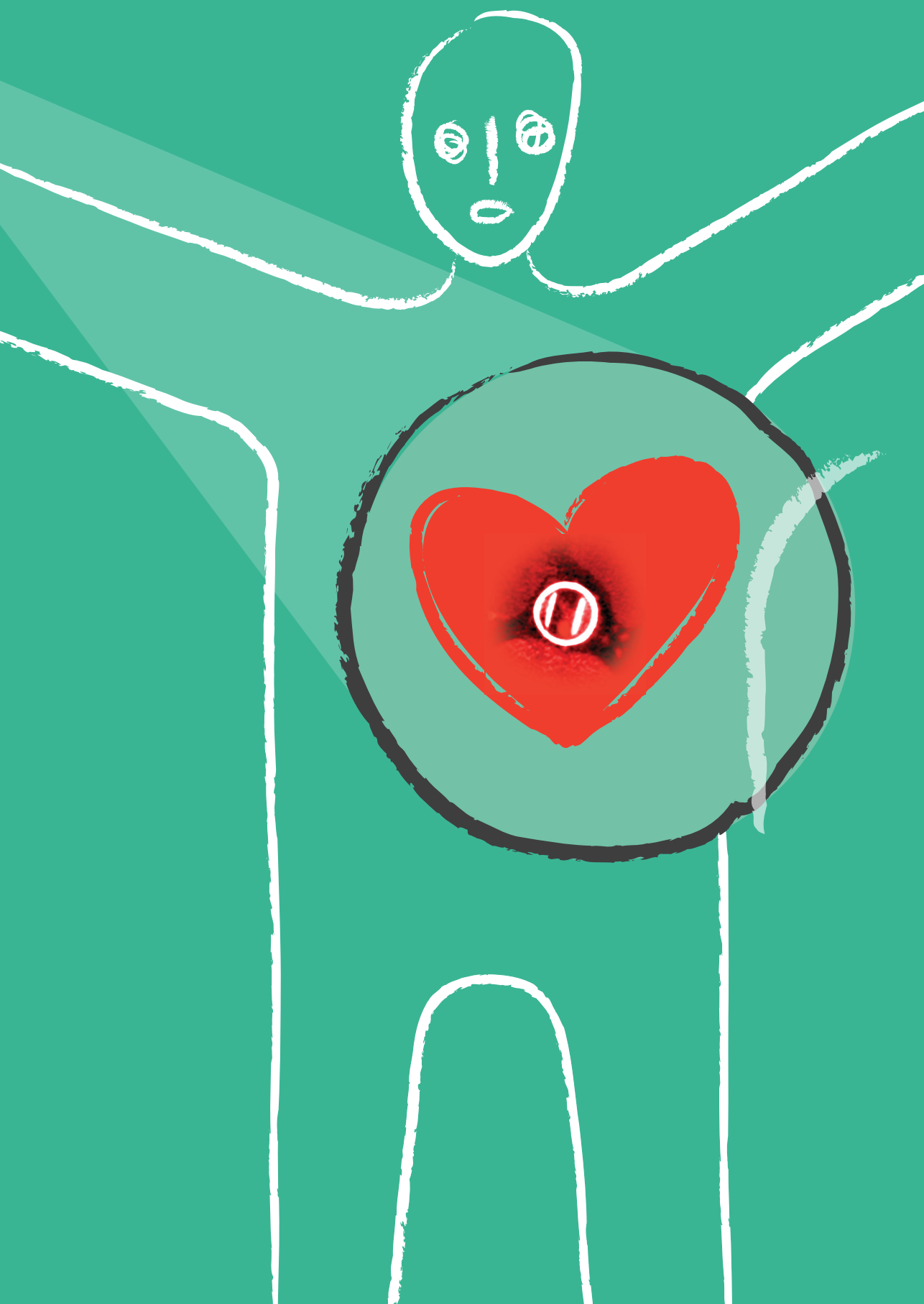

CHAPTER 4

The impact of a new model-based iterative reconstruction algorithm on prosthetic heart valve related artifacts at reduced radiation dose MDCT

Dominika Suchá
Martin J. Willemink
Pim A. de Jong
Arnold M.R Schilham
Tim Leiner
Petr Symersky
Ricardo P.J. Budde

Published in the International Journal of Cardiovascular Imaging, 2014

ABSTRACT

PURPOSE

To assess the impact of hybrid iterative reconstruction (IR) and novel model-based iterative reconstruction (IMR) and dose reduction on prosthetic heart valve (PHV) related artifacts and objective image quality.

METHODS

One transcatheter and two mechanical PHVs were embedded in diluted contrast-gel, inserted in an anthropomorphic phantom and imaged stationary with retrospectively ECG-gated computed tomography. Eight acquisitions were obtained of each PHV at 120 kV, 600 mAs (routine), 300 mAs and 150 mAs (reduced-dose). Data were reconstructed with filtered back-projection (FBP), IR and IMR. Hypodense and hyperdense artifact volumes were quantified using two threshold-filters. Signal-to-noise (SNR) and contrast-to-noise (CNR) ratios were calculated.

RESULTS

Artifact volumes differed significantly between reconstruction algorithms for all PHVs ($P<0.005$). Compared to FBP, iterative reconstruction decreased overall hypodense and hyperdense artifact volumes; at 150 mAs by 53% and 20% (IR) and 67% and 23% (IMR), respectively and significantly increased SNR and CNR at all doses ($P<0.012$). Even at reduced-dose, IMR resulted in higher image quality than routine-dose FBP and IR.

CONCLUSIONS

Iterative reconstruction and particularly IMR significantly reduce PHV-related artifacts and improve objective image quality in non-pulsatile conditions, even in reduced-dose images. Also, this study suggests that IMR allows for more radiation dose reduction in comparison to hybrid IR while maintaining high image quality.

INTRODUCTION

Over the last decade, prosthetic heart valve (PHV) assessment with multidetector-row computed tomography (MDCT) has expanded. MDCT has shown significant benefits complementary to echocardiography and cinefluoroscopy, since it may detect periprosthetic masses, false aortic aneurysms and leaflet motion restriction that cannot be found otherwise[1-6]. However, diagnostic analysis with retrospectively gated MDCT remains hampered by the PHV-related artifacts which limit the interpretation of PHV images and is associated with relatively high radiation doses which may exceed 15 mSv per acquisition[7, 8]. Artifacts may hamper assessment of valve related disease by obscuring the periprosthetic anatomy, thereby impairing accurate diagnosis of pannus or thrombus as PHV obstruction cause, periprosthetic leakage and endocarditis vegetations, pseudoaneurysms and valve dehiscence.

Multiple techniques have become commercially available in order to reduce the radiation dose for cardiac MDCT[9]. One part of these techniques concerns the reconstruction of MDCT data into images. The conventional filtered back projection (FBP) is a robust algorithm for MDCT image formation, however this fairly simple technique is hampered by increased amounts of image noise at reduced radiation doses[10]. Therefore, iterative reconstruction algorithms have been developed, which allow imaging at reduced radiation doses while preserving image quality. By now, all major MDCT vendors offer iterative reconstruction algorithms ranging from basic hybrid algorithms to more advanced model-based algorithms[11]. The basic hybrid iterative reconstruction algorithms iterate within the raw data and/or in the image domain and compare the updated data to the original data and/or image. Herewith an optimized image with reduced noise is generated. Numerous studies have investigated the impact of hybrid iterative reconstruction algorithms on image quality[11, 12], but only few have investigated the effects of a more sophisticated model-based iterative reconstruction algorithm (Veo, GE Healthcare)[13-16]. With relation to PHV-related artifacts, only hybrid iterative reconstruction was evaluated and compared to FBP in solely two studies[17, 18]. All studies suggested that iterative reconstruction may achieve significant MDCT radiation dose reduction without reduction of image quality.

Recently a new model-based iterative reconstruction algorithm has been introduced called Iterative Model Reconstruction (IMR, Philips Healthcare, Best, The Netherlands)[11, 19]. The most important difference between hybrid and model-based iterative reconstruction methods is that in the latter approach not only the quantum noise statistics but also non-random noise intrinsic to the geometry and optics of the imaging system are modeled. Furthermore, model-based algorithms

are fully iterative with forward and backward reconstructions, which could result in reduced cone-beam, spiral or other artifacts[11, 20]. However, to our knowledge the effects of the new model-based iterative reconstruction algorithms on PHV-related artifacts have never been evaluated. Therefore, the purpose of this study was to investigate the impact of this novel model-based iterative reconstruction technique in comparison with a hybrid iterative reconstruction technique and FBP on PHV-related artifacts and objective image quality with routine and reduced dose MDCT.

MATERIALS AND METHODS

Heart valve prostheses

Three different PHVs were studied: (1) St. Jude mechanical bileaflet (SJ; St. Jude Medical Inc., St Paul MN, USA), (2) Medtronic Hall tilting disc (MH; Medtronic Inc., Minneapolis MN, USA) and (3) Edwards Sapien XT transcatheter valve (ES; Edwards Lifesciences, Irvine, CA, USA). All valves were inserted and attached in open position in the center of a plastic holder containing diluted contrast gel; a mixture of contrast (Ultravist 300mg/ml; Bayer B.V., Mijdrecht, The Netherlands) and gel in a ratio of 1:20 (*Figure 1*). The PHVs were attached to the holder by sutures under an angle of 45 degrees to simulate the same aortic PHV position in relation to the tube angle as in patients. For simulation of human thoracic radiation absorption, the PHV holder was placed in a commercially available anthropomorphic thoracic phantom (QRM GmbH, Möhrendorf, Germany).

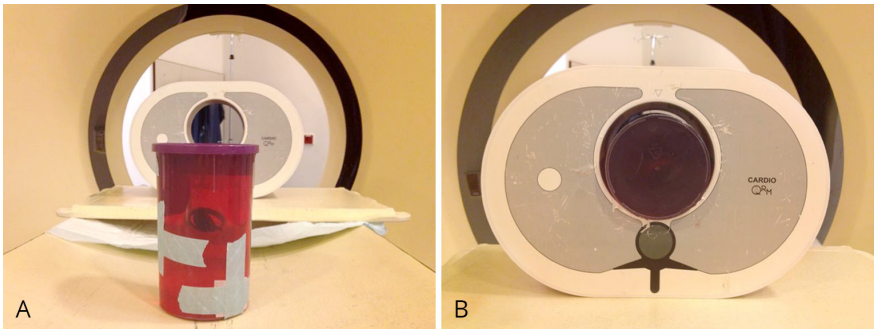

Figure 1 | A prosthetic heart valve mounted in a static contrast gel containing holder (A) placed in the commercially available anthropomorphic thoracic phantom (B) (QRM GmbH, Möhrendorf, Germany)

MDCT

MDCT images were acquired on a 256-slice MDCT scanner (Brilliance iCT, Philips Healthcare, Best, The Netherlands) with retrospective ECG-gating. For all three valves (SJ, MH and ES) eight image acquisitions were performed. The acquisition protocol was based on the standard clinical retrospectively ECG-gated MDCT protocol for PHV evaluation: slice collimation of 128 x 0.625 mm, gantry rotation time of 0.27 seconds, matrix size of 512 x 512 pixels, pitch of 0.16, tube voltage of 120 kV and tube current-time product of 600 mAs. All acquisitions were also repeated at tube current-time products of 300 mAs and 150 mAs to examine the effects of reduced radiation doses compared to routine radiation dose. The volume CT dose index ($CTDI_{vol}$) was registered. Thus, eight series with three different radiation dose acquisitions were obtained resulting in a total of 24 acquisitions for each of the three PHVs. For retrospective ECG-gating an ECG-generator was used to simulate a heart rate of 75 beats per minute.

Data reconstruction

Raw data were transferred to a dedicated CT workstation with a prototype software package of a novel model-based iterative reconstruction algorithm (IMR prototype release 7, Philips Healthcare, Best, The Netherlands). Herewith, MDCT data could be reconstructed in three different ways: FBP, hybrid iterative reconstruction (IR; iDose^4, Philips Healthcare) and model-based iterative reconstruction (IMR; IMR, Philips Healthcare). The strength of noise reduction ranges from 1 to 7 for iDose^4 and from 1 to 3 for IMR, in which higher levels result in less image noise. For the current study, we used iDose^4 level 4 as recommended by the vendor and used in a previous study[17, 21], and IMR level 3 to analyze the maximum achievable effect. Images were reconstructed using the cardiac routine filter. Furthermore, images were reconstructed in 75% of the RR interval, slice thickness was 0.9 mm with 0.45 mm increment and field of view was 250 x 250 mm, as is common in our clinical practice.

Image analysis

Reconstructed images were transferred to another dedicated workstation (Extended Brilliance Workstation version 4.5.5, Philips Healthcare, Best, The Netherlands) for objective analysis by one observer. Hypodense and hyperdense artifact volumes were measured automatically by the software in three-dimensional volume rendered images, after excision of the thoracic phantom, by applying two predefined threshold filters based on the attenuation of the surrounding structures according to previously described methods (*Figure 2*)[17, 22].

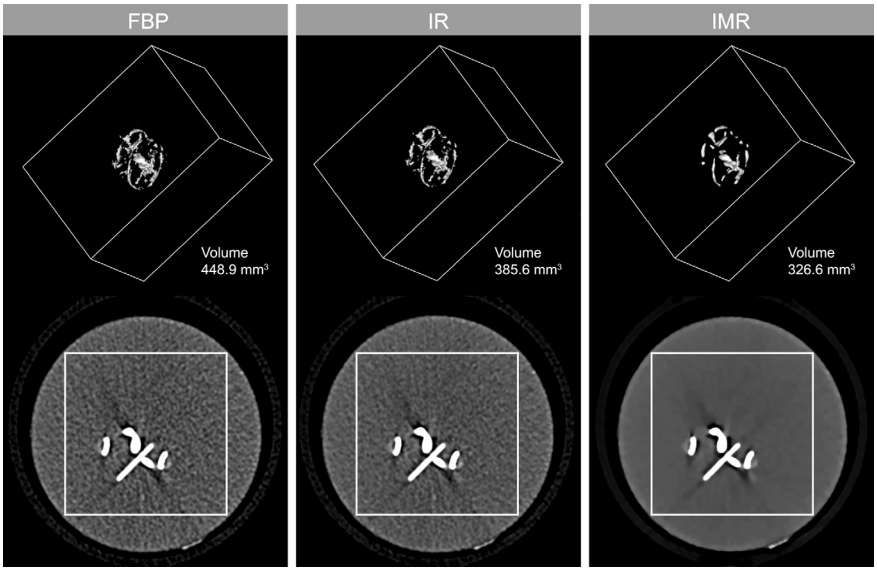

Figure 2 | Three-dimensional volume rendered images showing hypodense artifact volumes (top) measured and excised from reduced dose 300mAs MDCT images (bottom; axial view) of the Medtronic Hall tilting disc valve reconstructed with FBP, IR and IMR, respectively.
MDCT= multidetector-row computed tomography; FBP= filtered back projection; IR= hybrid iterative reconstruction; IMR= model-based iterative reconstruction

Accurately defined lower and upper thresholds include all required voxels based on Hounsfield unit (HU) values beneath and above the threshold, respectively. To enable solely artifact volume measurements, the surrounding structures needed to be excluded, in this case the contrast media. Therefore, the mean HU-value of the contrast agent was the basis for both thresholds. From this, the lower and upper thresholds were defined by subtracting and adding three times the standard deviation (SD) of the mean contrast HU-value, respectively. The PHVs were surrounded by diluted contrast gel with a mean density of 380 ± 85 Hounsfield units (HU ± standard deviation; SD) at 150mAs. Thus, the lower threshold value for hypodense artifacts was set at 125 HU (380 HU – 3SD) and the upper threshold value for hyperdense artifacts at 635 HU (380 HU + 3SD). PHV components were included in the hyperdense artifact measurements.

To evaluate objective image quality we used the signal-to-noise ratio (SNR) and contrast-to-noise ratio (CNR) as described before[21]. SNR and CNR are calculated by using the general equations:

$$SNR = \frac{Signal_1}{SD_1} \qquad CNR = \frac{Signal_1 - Signal_2}{\sqrt{\frac{1}{2} \times ({SD_1}^2 + {SD_2}^2)}}$$

in which signal is the mean signal of the tissue in HU and SD is the standard deviation of the signal as measure of noise. For reliable and reproducible results, a homogenous signal of sufficient volume is required. For this reason we used the contrast material and sternum of the thoracic phantom for signal measurements in this study.

In all acquisitions of the ES PHV regions of interest (ROI) with a diameter of 20 mm were drawn in the contrast and sternum at exactly the same locations to measure the mean image signal and SD as a measure of noise. From this signal-to-noise ratios (SNR) and contrast-to-noise ratios (CNR) were calculated.

Statistical analysis

Data were analyzed by two observers using the IBM SPPS Statistics software version 20.0 for Windows. Nonparametric data were presented as medians with interquartile range (IQR) and statistically analyzed using the Friedman test with the significance level set at $P<0.05$. The Wilcoxon signed-rank test was conducted for post-hoc analysis with appliance of the Bonferroni correction for multiple testing resulting in a significance level of $P<0.017$.

RESULTS

One complete MH series including three different radiation dose acquisitions was excluded due to technical failure during reconstruction of one 300 mAs scan, therefore 21 MH acquisitions were available for analysis. The $CTDI_{vol}$ values were 38.5, 19.3 and 9.6 mGy for 600 mAs, 300 mAs and 150 mAs, respectively.

Absolute artifact volumes measured are presented in *Table 1*. For all PHVs, significant artifact differences were found between the reconstruction algorithms (all $P<0.005$). *Figure 3A* shows the artifact volume decrease for the SJ PHV, related to the reconstruction algorithms. All PHVs showed similar volume decrease patterns. Decrease of artifact volumes was greatest for hypodense artifacts and reduced dose acquisitions. At routine dose, differences between absolute hypodense artifact volumes were relatively small.

Table 1| Artifact volume measurements in three prosthetic heart valves

Reconstruction algorithm	600 mAs			300 mAs			150 mAs		
	FBP	IR	IMR	FBP	IR	IMR	FBP	IR	IMR
Hypodense artifacts, median (IQR); mm^3									
St. Jude	899 (844-947)	866 (812-908)	865 (821-920)	910 (874-944)	802 (768-841)	763 (722-825)	2083 (2058-2175)	955 (920-1010)	777 (723-828)
Medtronic Hall	381 (370-411)	362 (349-388)	382 (370-412)	449 (426-468)	386 (368-413)	327 (316-346)	1053 (1021-1332)	439 (388-534)	258 (174-329)
Edwards Sapien	1522 (1464-1568)	1461 (1392-1516)	1507 (1443-1563)	1575 (1542-1646)	1410 (1383-1470)	1331 (1312-1371)	2672 (2549-2831)	1418 (1372-1598)	975 (916-1149)
Hyperdense artifacts, median (IQR); mm^3									
St. Jude	1868 (1865-1875)	1859 (1855-1866)	1836 (1832-1847)	1915 (1882-1937)	1888 (1855-1906)	1865 (1838-1891)	2331 (2266-2361)	1957 (1930-1987)	1934 (1873-1948)
Medtronic Hall	2207 (2169-2217)	2198 (2156-2206)	2096 (2048-2103)	2258 (2229-2263)	2228 (2193-2229)	2116 (2086-2123)	2782 (2778-2864)	2276 (2268-2285)	2174 (2152-2180)
Edwards Sapien	1613 (1563-1634)	1595 (1545-1615)	1525 (1468-1543)	1735 (1705-1767)	1675 (1638-1701)	1571 (1543-1596)	2302 (2247-2330)	1712 (1692-1771)	1587 (1568-1623)

FBP= filtered back projection; IR= hybrid iterative reconstruction; IMR= model-based iterative reconstruction; IQR= interquartile range

The effects of dose reduction on hypodense and hyperdense artifact volumes are given in *Table 1* as well. Artifact volumes increased significantly with FBP at reduced radiation dose in all PHVs (all P<0.002). In contrast, images reconstructed with IR and IMR showed less variation between artifact volumes at different radiation doses and even inclined to remain equal (*Figure 3B*). An example of the effects of different radiation doses and reconstruction techniques on prosthetic heart valve related artifacts is presented in *Figure 4*.

The noise measured in contrast is presented in *Table 2*. The SNR was significantly higher with IR and IMR when compared to FBP in both contrast and sternum, and in all acquisitions (all P<0.012). The SNR of the ROI placed within the contrast solution at 150 mAs is presented in *Figure 3C*. In all reconstructions IMR also resulted in higher SNR than IR (P<0.012) (*Table 2*). Likewise, the CNR was significantly higher in IMR reconstructions compared to FBP and IR (P<0.012) (*Table 2*).

The CNR and SNR differed significantly between all radiation doses with all reconstruction algorithms (all P<0.006). However, in post hoc analysis IMR showed no significant differences for the CNR and SNR between 600 and 300 mAs acquisitions and between 300 and 150 mAs acquisitions (P>0.034) (*Figure 3D*).

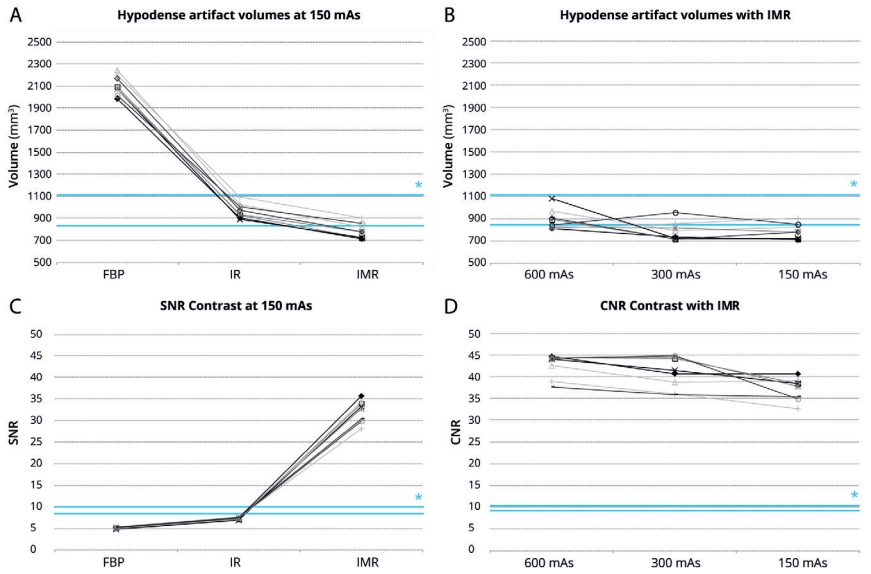

Figure 3 | Hypodense artifact volumes in the St. Jude prosthetic heart valve (A and B) and the effects of FBP, IR and IMR reconstructions at 150 mAs (A) and IMR reconstructions at 600 mAs, 300 mAs and 150 mAs (B). Also presented, the SNRs at 150 mAs for the three different reconstruction algorithms (C) and CNRs at 600 mAs, 300 mAs and 150 mAs for IMR (D). The reference lines (*) represent the minimal and maximal FBP values at 600 mAs.

FBP= filtered back projection; IR= hybrid iterative reconstruction; MR= model-based iterative reconstruction; SNR= signal-to-noise ratio; CNR= contrast-to-noise ratio

Table 2 | Noise, SNR and CNR in contrast at routine and reduced dose MDCT with three different reconstruction algorithms

Reconstruction algorithm	600 mAs			300 mAs			150 mAs		
	FBP	IR	IMR	FBP	IR	IMR	FBP	IR	IMR
Noise, median (IQR)	40.1 (39.4-41.9)	29.3 (28.9-30.5)	10.3 (10.2-10.7)	55.8 (54.0-58.0)	40.1 (38.5-42.1)	10.7 (10.0-12.0)	75.3 (75.0-77.3)	52.8 (52.2-53.7)	11.7 (11.3-12.8)
SNR	9.6 (9.2-9.8)	13.1 (12.6-13.4)	37.2 (36.0-37.4)	6.9 (6.7-7.2)	9.7 (9.2-10.0)	36.1 (32.2-38.4)	5.1 (5.0-5.2)	7.3 (7.2-7.4)	33.0 (30.2-34.0)
CNR	9.7 (9.5-9.8)	13.4 (13.2-13.5)	44.0 (41.6-44.3)	7.0 (6.9-7.1)	9.7 (9.5-9.9)	41.1 (38.0-44.2)	5.1 (5.0-5.2)	7.3 (7.2-7.4)	38.1 (35.2-38.6)

Noise= standard deviation of the mean contrast signal; IQR= interquartile range; SNR= signal-to-noise ratio; CNR= contrast-to-noise ratio; MDCT= multidetector-row computed tomography; FBP= filtered back projection; IR= hybrid iterative reconstruction; IMR= model-based iterative reconstruction

Table 3 | Relative change for artifact volumes and image quality presented for all radiation doses and reconstruction techniques compared to the reference standard (600mAs, filtered back projection)

	600 mAs		300 mAs		150 mAs	
	IR	IMR	IR	IMR	IR	IMR
Hypodense artifacts	- 4%	- 1%	- 12%	- 20%	- 53%	- 67%
Hyperdense artifacts	- 1%	- 4%	- 2%	- 6%	- 20%	- 23%
SNR	+ 40%	+ 560%	+ 41%	+ 729%	+ 43%	+ 903%
CNR	+ 38%	+ 353%	+ 40%	+ 490%	+ 44%	+ 649%

SNR= signal-to-noise ratio; CNR= contrast-to-noise ratio; IR= hybrid iterative reconstruction; IMR= model-based iterative reconstruction

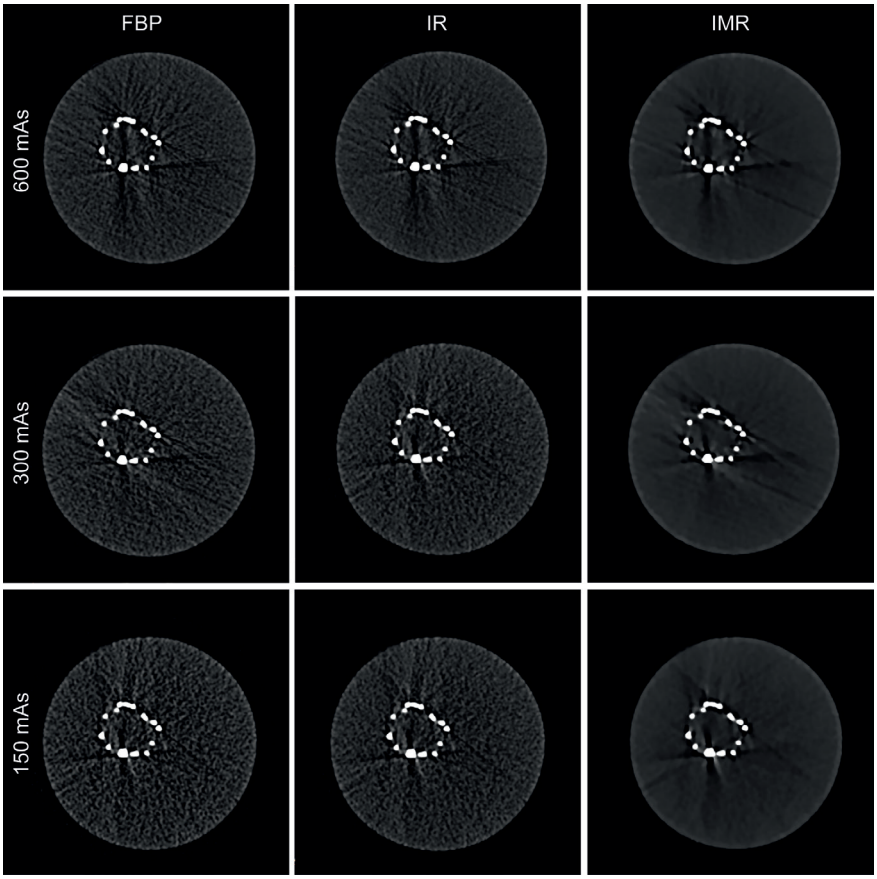

Figure 4 | Multidetector-row computed tomography images of the Edwards Sapien XT prosthetic heart valve reconstructed with FBP, IR and IMR at 600 mAs (routine dose) and 300 mAs and 150 mAs (reduced dose). *FBP= filtered back projection; IR= hybrid iterative reconstruction; IMR= model-based iterative reconstruction*

Table 3 provides an overview of the results presenting the relative change for artifact volume and image quality based on reconstruction technique and radiation dose.

DISCUSSION

The main findings of our study are twofold. First, PHV artifact volumes are significantly reduced in all PHVs by IR and particularly by IMR. Artifact volumes of FBP reconstructions increase significantly with reduced radiation doses, however artifact volumes remain relatively unchanged with IR and IMR at reduced radiation doses. Second, IMR significantly increases objective MDCT image quality as

quantified by SNR and CNR when compared to FBP and IR. Even at 75% reduced dose the objective image quality with IMR is higher than with FBP and IR at routine dose. Therefore this phantom study suggests that IMR allows radiation dose reduction while objective image quality is maintained and even can be improved. This is, to our best knowledge, the first study that evaluates the novel IMR algorithm and the impact of IMR on metal related artifacts in commonly implanted PHVs. Since IMR offers full iterative reconstruction and modeling of both quantum and non-random noise, a different and greater impact is expected on metal related artifacts compared to IR. Our study showed that this is indeed the case.

Previously, several studies have assessed the effects of various other reconstruction algorithms and artifact reduction filters on metal artifacts in MDCT images[17, 18, 23]. Our group previously found increased PHV-related hypodense and hyperdense artifact volumes with FBP at 50% reduced radiation dose in a pulsatile phantom set-up[17]. Furthermore, no significant artifact reduction was found with 50% reduced dose IR compared to routine dose FBP. In that study, image noise was also evaluated and equal results were found in 50% reduced dose IR and routine dose images reconstructed with FBP. In another study a metal artifact reduction filter was evaluated, but this filter introduced new interpolation artifacts[18]. In accordance with previous results, we found similar artifact volumes with 50% reduced dose IR and routine dose FBP. However, artifact volumes with routine dose FBP did not increase much with 50% reduced dose FBP, but artifacts increased considerably with 75% reduced radiation dose. Possibly this is due to the use of contrast agent rather than water. Since current threshold values are based on the attenuation of contrast agent they differ from the thresholds applied formerly which were based on the attenuation of water. Therefore the amount of noise included in artifact measurements could alter between studies. Also, in our study artifact volumes were even further reduced by IMR compared to IR, even at 75% reduced radiation dose.

Noise in projection data is believed to be an important cause of metal streak artifacts, next to beam hardening and patient motion[23]. Boas et al. studied the impact of linear interpolation, a metal detection technique and a selective algebraic reconstruction technique on metal streak artifacts with disturbance by Poisson noise, beam hardening and motion. With all techniques, Poisson noise showed greatest metal streak artifacts. Hence, by reducing noise in projection data one would presume reduction of metal streak artifacts which was emphasized in this study.

Reduction of PHV artifacts will likely improve diagnostic evaluation in patients with suspected prosthetic heart valve complications. By reducing both hypodense and

hyperdense artifacts one might visualize the periprosthetic anatomy as required to specify the underlying problem. For example, with high amounts of MDCT artifacts in a patient with PHV obstruction on echocardiography, it might not be possible to diagnose pannus tissue as the cause of obstruction. In addition, reduction of noise and increase of SNR and CNR might allow for more detailed evaluation of the periprosthetic region and might improve for instance evaluation of periprosthetic leakage.

As noted earlier, PHV evaluation with retrospectively ECG-gated MDCT involves patient exposure to high radiation doses. In this study IMR allowed even 75% radiation dose reduction while maintaining image quality and reducing PHV-related artifacts. Objective IMR image quality at 150 mAs acquisitions was even higher compared to routine FBP image quality at 600 mAs. By this means, IMR offers important potential for significant patient radiation dose reduction, even beyond the radiation dose reduction offered by IR.

Iterative reconstruction has one known disadvantage; its longer reconstruction time. However, several studies showed the reconstruction time delay with hybrid iterative reconstruction to be without clinical relevance[24, 25]. On the other hand, reconstruction time delay with model-based iterative reconstruction is significantly more time consuming[26]. With our protocol, it took approximately 20 minutes per reconstruction for acquired IMR data. It is stated that with the latest version, reconstruction times are reduced to 5 minutes. For application of IMR in emergency settings this could be a drawback, although outpatient imaging should not be hampered. Hence, the feasibility of the IMR algorithm in patient studies needs to be assessed more extensively.

This study has several limitations. First, a different kernel was used than the clinical cardiac B filter. Thus, artifact volumes reconstructed with FBP and IR might differ from volumes measured with the routine cardiac filter. However, since the same kernel was used for FBP, IR and IMR, the effects on artifact volume could still be evaluated. Second, only the objective image quality without subjective image quality or clinical diagnostic value was assessed since we performed a phantom study. Furthermore, images could not be evaluated in a blinded manner since the different reconstruction algorithms can easily be distinguished visually. Subjective evaluation could therefore introduce bias. Third, image noise could not entirely be excluded from artifact volume measurements. Complete exclusion of image noise might result in different artifact volume quantifications. Fourth, a static PHV model was used. For clinical implementation it would be valuable to evaluate the effect of IMR on motion artifacts in a pulsatile setting as well. Furthermore, a pulsatile

experiment would allow assessment of the impact of heart rate on artifacts and image quality, since a high heart rate might negatively affect both.

In conclusion, we evaluated a novel model-based iterative reconstruction algorithm and found in comparison to FBP and IR significantly decreased hypodense and hyperdense artifact volumes at reduced radiation doses in all PHVs. Furthermore, IMR increased objective MDCT image quality of all PHVs. Objective image quality with IMR was higher than at routine dose with FBP, even at a 75% reduced radiation dose.

REFERENCES

1. Caudron J, Fares J, Hauville C, Cribier A, Dacher JN, Tron C, et al. Evaluation of multislice computed tomography early after transcatheter aortic valve implantation with the edwards sapien bioprosthesis. *Am J Cardiol*. 2011;108:873-881
2. Willson AB, Webb JG, Labounty TM, Achenbach S, Moss R, Wheeler M, et al. 3-dimensional aortic annular assessment by multidetector computed tomography predicts moderate or severe paravalvular regurgitation after transcatheter aortic valve replacement: A multicenter retrospective analysis. *J Am Coll Cardiol*. 2012;59:1287-1294
3. LaBounty TM, Agarwal PP, Chughtai A, Bach DS, Wizauer E, Kazerooni EA. Evaluation of mechanical heart valve size and function with ecg-gated 64-mdct. *AJR Am J Roentgenol*. 2009;193:W389-396
4. Symersky P, Budde RP, de Mol BA, Prokop M. Comparison of multidetector-row computed tomography to echocardiography and fluoroscopy for evaluation of patients with mechanical prosthetic valve obstruction. *Am J Cardiol*. 2009;104:1128-1134
5. Tsai IC, Lin YK, Chang Y, Fu YC, Wang CC, Hsieh SR, et al. Correctness of multi-detector-row computed tomography for diagnosing mechanical prosthetic heart valve disorders using operative findings as a gold standard. *Eur Radiol*. 2009;19:857-867
6. Habets J, Budde RP, Symersky P, van den Brink RB, de Mol BA, Mali WP, et al. Diagnostic evaluation of left-sided prosthetic heart valve dysfunction. *Nat Rev Cardiol*. 2011;8:466-478
7. Hausleiter J, Meyer T, Hermann F, Hadamitzky M, Krebs M, Gerber TC, et al. Estimated radiation dose associated with cardiac ct angiography. *JAMA*. 2009;301:500-507
8. Symersky P, Budde RP, Westers P, de Mol BA, Prokop M. Multidetector ct imaging of mechanical prosthetic heart valves: Quantification of artifacts with a pulsatile in-vitro model. *Eur Radiol*. 2011;21:2103-2110
9. Lee TY, Chhem RK. Impact of new technologies on dose reduction in ct. *Eur J Radiol*. 2010;76:28-35
10. Willemink MJ, de Jong PA, Leiner T, de Heer LM, Nievelstein RA, Budde RP, et al. Iterative reconstruction techniques for computed tomography part 1: Technical principles. *Eur Radiol*. 2013;23:1623-1631
11. Kachelrieß M. Iterative reconstruction techniques: What do they mean for cardiac ct? *Curr Cardiovasc Imaging Rep*. 2013;6:268-281
12. Willemink MJ, Leiner T, de Jong PA, de Heer LM, Nievelstein RA, Schilham AM, et al. Iterative reconstruction techniques for computed tomography part 2: Initial results in dose reduction and image quality. *Eur Radiol*. 2013;23:1632-1642
13. Scheffel H, Stolzmann P, Schlett CL, Engel LC, Major GP, Karolyi M, et al. Coronary artery plaques: Cardiac ct with model-based and adaptive-statistical iterative reconstruction technique. *Eur J Radiol*. 2012;81:e363-369
14. Singh S, Kalra MK, Do S, Thibault JB, Pien H, O'Connor OJ, et al. Comparison of hybrid and pure iterative reconstruction techniques with conventional filtered back projection: Dose reduction potential in the abdomen. *J Comput Assist Tomogr*. 2012;36:347-353
15. Vardhanabhuti V, Loader RJ, Mitchell GR, Riordan RD, Roobottom CA. Image quality assessment of standard- and low-dose chest ct using filtered back projection, adaptive statistical iterative reconstruction, and novel model-based iterative reconstruction algorithms. *AJR Am J Roentgenol*. 2013;200:545-552

16. Katsura M, Matsuda I, Akahane M, Yasaka K, Hanaoka S, Akai H, et al. Model-based iterative reconstruction technique for ultralow-dose chest ct: Comparison of pulmonary nodule detectability with the adaptive statistical iterative reconstruction technique. *Invest Radiol*. 2013;48:206-212
17. Habets J, Symersky P, de Mol BA, Mali WP, Leiner T, Budde RP. A novel iterative reconstruction algorithm allows reduced dose multidetector-row ct imaging of mechanical prosthetic heart valves. *Int J Cardiovasc Imaging*. 2012;28:1567-1575
18. Habets J, Symersky P, Leiner T, de Mol BA, Mali WP, Budde RP. Artifact reduction strategies for prosthetic heart valve ct imaging. *Int J Cardiovasc Imaging*. 2012;28:2099-2108
19. Willemink MJ, De Jong PA. Pediatric chest computed tomography at a radiation dose approaching a chest radiograph. *Am J Respir Crit Care Med*. 2013;188:626-627
20. Nielsen T, Manzke R, Proksa R, Grass M. Cardiac cone-beam ct volume reconstruction using art. *Med Phys*. 2005;32:851-860
21. Willemink MJ, Habets J, de Jong PA, Schilham AM, Mali WP, Leiner T, et al. Iterative reconstruction improves evaluation of native aortic and mitral valves by retrospectively ecg-gated thoracoabdominal cta. *Eur Radiol*. 2013;23:968-974
22. van der Schaaf I, van Leeuwen M, Vlassenbroek A, Velthuis B. Minimizing clip artifacts in multi ct angiography of clipped patients. *AJNR Am J Neuroradiol*. 2006;27:60-66
23. Boas FE, Fleischmann D. Evaluation of two iterative techniques for reducing metal artifacts in computed tomography. *Radiology*. 2011;259:894-902
24. Gervaise A, Osemont B, Lecocq S, Noel A, Micard E, Felblinger J, et al. Ct image quality improvement using adaptive iterative dose reduction with wide-volume acquisition on 320-detector ct. *Eur Radiol*. 2012;22:295-301
25. Willemink MJ, Schilham AM, Leiner T, Mali WP, de Jong PA, Budde RP. Iterative reconstruction does not substantially delay ct imaging in an emergency setting. *Insights Imaging*. 2013;4:391-397
26. Yamada Y, Jinzaki M, Tanami Y, Shiomi E, Sugiura H, Abe T, et al. Model-based iterative reconstruction technique for ultralow-dose computed tomography of the lung: A pilot study. *Invest Radiol*. 2012;47:482-489

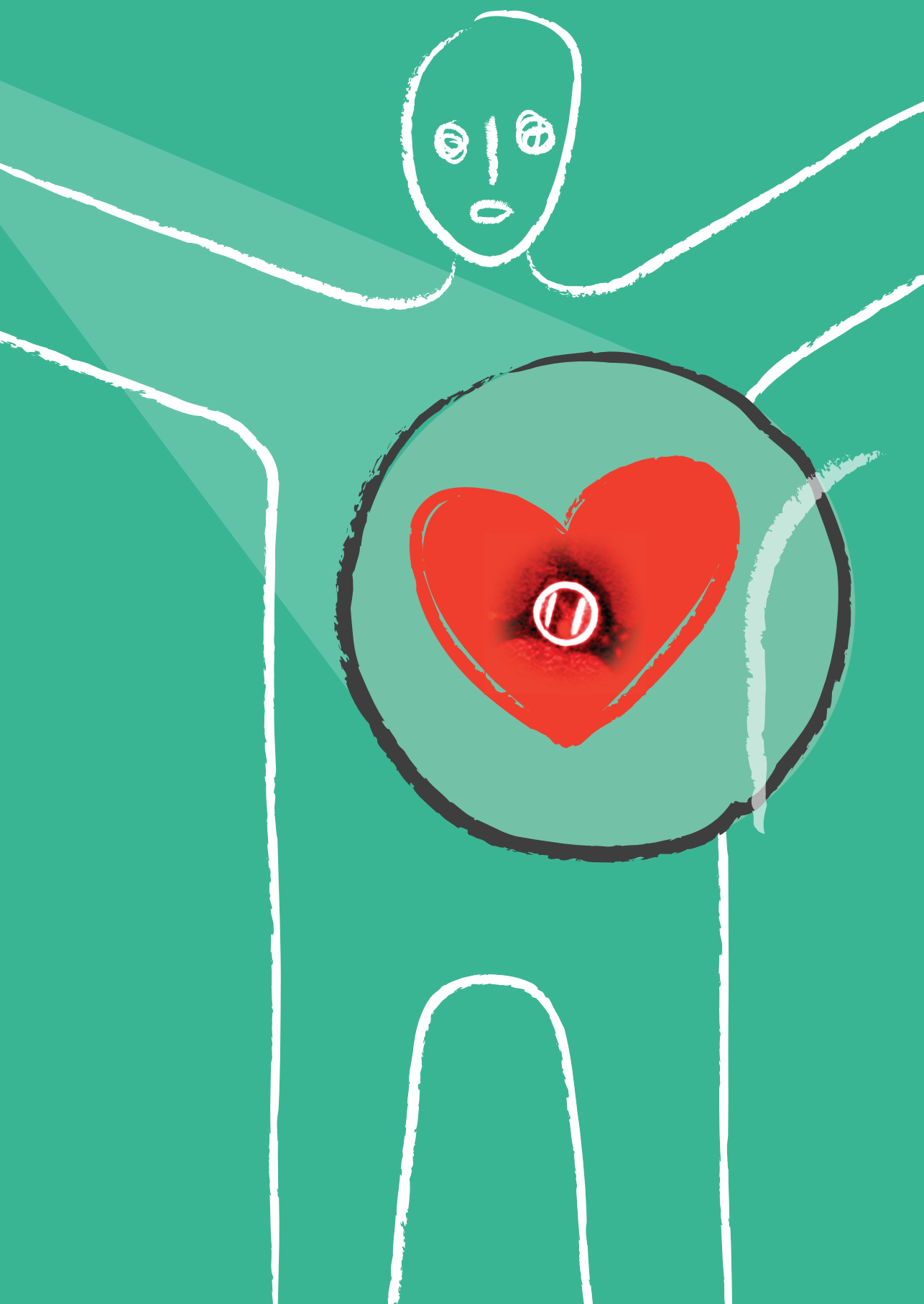

CHAPTER 5

Mock circulation loop for CT and MR imaging of prosthetic heart valves: a technical note

Dominika Suchá
Linda M. de Heer
Hanna Talacua
Lex A. van Herwerden
Marc P. Buijsrogge
Johannes M.A. Stijnen
Willem P.Th.M. Mali
Jolanda Kluin
Willem J.L. Suyker
Ricardo P.J. Budde

Manuscript draft

ABSTRACT

Computed tomography (CT) and magnetic resonance imaging (MRI) have established their role in cardiac imaging. Both may have potential for the evaluation of patients with prosthetic heart valves (PHVs), though in vitro studies are required to optimize image acquisition protocols. In addition, PHV-related measurements that may provide information on PHV performance require validation. Various pulsatile and non-pulsatile phantom models have been used for PHV evaluation in an in vitro setting. Typically, mock circulation loops have been used that allow for simulation of several cardiovascular characteristics including arterial vessel compliance and peripheral resistance. One of the challenges is to develop a mock circulation loop that is MRI safe and compatible, as metal objects may interact with the magnetic field and cause hazard or image distortion. In this technical note we present an advanced CT and MRI compatible mock circulation loop for the evaluation of biological and mechanical heart valves.

INTRODUCTION

Over the past years, prosthetic heart valves (PHV) have been subject to remarkable change with the development of improved models, new materials, the introduction of balloon-expandable and self-expandable transcatheter valves and even the development of tissue-engineered valves[1]. In addition, great advances in imaging techniques have been established over the last decade with improvement of the available three-dimensional imaging modalities and the introduction of modern reconstruction techniques. Cardiac computed tomography (CT) has shown its potential for prosthetic valve assessment revealing pathology not detected with other techniques[2,3], and magnetic resonance imaging (MRI) might provide detailed flow assessment but is yet limited by PHV-related artifacts[4]. All abovementioned developments call for in vitro evaluation of I. function and flow patterns in new valve models and II. acquisition protocol development to ensure optimal image quality. Phantom models have been used to study prosthetic valves in an in vitro setting for over 50 years[5-7]. Throughout the early years several in vitro phantoms have been used and the first mock circulation loop allowing controlled heart performance was presented in 1971[8]. In mock circulation loops, the heart is commonly represented using a mathematical model also known as the Windkessel model. It has first been initiated by Stephen Hales in 1733[9] and improved and described by Otto Frank in 1899[10]. As presented in its original form in the early days, the Windkessel model was a two-element system. This model takes into account the arterial compliance and peripheral resistance when simulating the cardiovascular system and creating cardiac output. Throughout the years, the Windkessel model has evolved into multiple-element systems[11]. With each element an extra component is introduced to the model. With the three-element model, the (proximal) aortic impedance was added, for a four-element model the inertia of the blood and a fifth element includes the venous compliance. Previously, we have described a mock circulation loop for the evaluation of mechanical PHVs in an in vitro setting[12]. In brief, this phantom consisted of a valve chamber with a simplified inlet and outlet portion connected to a computer driven piston pump. The afterload was regulated by a height-adjustable reservoir. Though this was a practical phantom for the assessment of mechanical PHVs in a pulsatile setting, imaging was only feasible with CT, as the mock circulation loop included ferromagnetic elements not suitable for MRI acquisition. In addition, it was a fairly simplified phantom allowing only a basic preset of aortic flow patterns. Developing a mock circulation loop compatible with MRI is demanding since strong magnetic fields will, in general, attract all magnetic objects present within the magnetic field. In other words, common ferromagnetic items such as bolts and bars may

cause severe hazard when moved around due to magnetic forces. Furthermore, ferromagnetic objects may result in severe signal voids and thus in poor image quality. To permit both CT and MRI compatible assessment of mechanical and biological prosthetic heart valves, a novel mock loop was developed using a five-element Windkessel model (LifeTec Group, Eindhoven, the Netherlands). In this technical note we present a part-by-part description of this mock circulation loop.

MOCK CIRCULATION LOOP

A schematic overview of the mock circulation loop is presented in *Figure 1* and the complete mock circulation loop including the control system is shown in *Figure 2*.

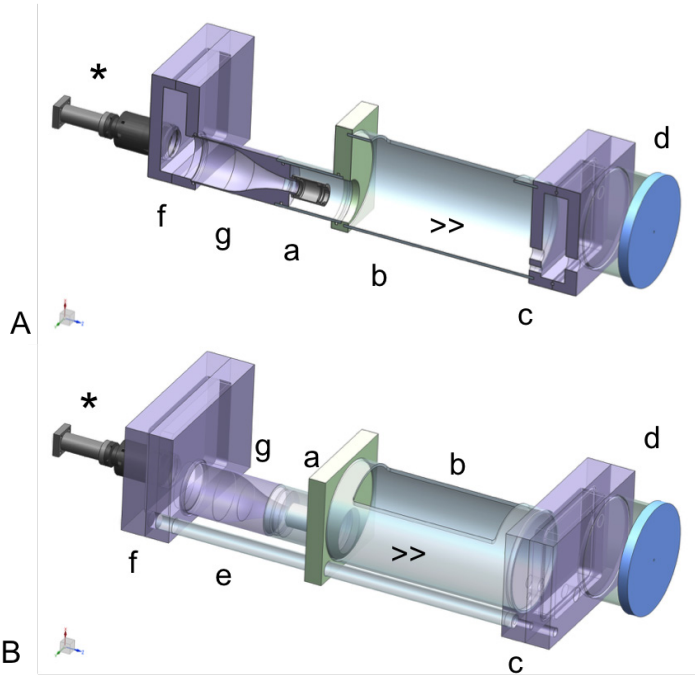

Figure 1 | Schematic overview of the mock circulation loop. A schematic overview of the mock circulation loop developed by LifeTec Group (Eindhoven, the Netherlands). The mock circulation loop consists of the following components represented in (A-G; A) the valve holder, (B) large container in which the silicon aorta (not shown, >>) connects the valve holder and afterload system, (C) the afterload compartment with (D) air compression chamber, (E) return path, (F) preload compartment with the atrial part and a biological valve connecting the ventricular component and piston pump (*) and (G) left ventricular outflow tract. Image courtesy of S. van Tuijl, LifeTec Group.

Figure 2 | Mock circulation loop and computer in the CT room. This figure shows the mock circulation loop in CT set-up with the main part on the CT table of the 256-detector row iCT scanner (Philips Healthcare) and the computer, motor and pressure system in front.

The central body

The main part of the mock loop system is the valve chamber, located in the center of the phantom. Currently, two valve chambers are available for this mock loop system: (I) a simple straight valve chamber and (II) an angulated valve chamber in which the valve is mounted at an angle of 45 degrees, approximating the patients' aortic valve position in relation to the CT X-ray beam (*Figure 3*). The individual components of the valve chamber are presented in *Figure 4*. Various types of prosthetic valve types can be mounted in the valve chamber including surgical mechanical, stented and stentless biological and transcatheter heart valves. The prosthetic valve is mounted in the valve chamber using a valve (stent) holder and ring structure. Different rings and stent holders are available that have been customized for each type and size of prosthesis to optimally mount the specific prosthesis in the valve chamber and thereby prevent undesired prosthetic motion which may induce motion-related imaging artifacts. The valve chamber itself is sealed using MR compatible (non-ferromagnetic) screws and connected to the artificial left ventricular outflow tract (LVOT) at the inflow side and the aorta at the outflow side. The central body of the mock loop is constructed in such a way that,

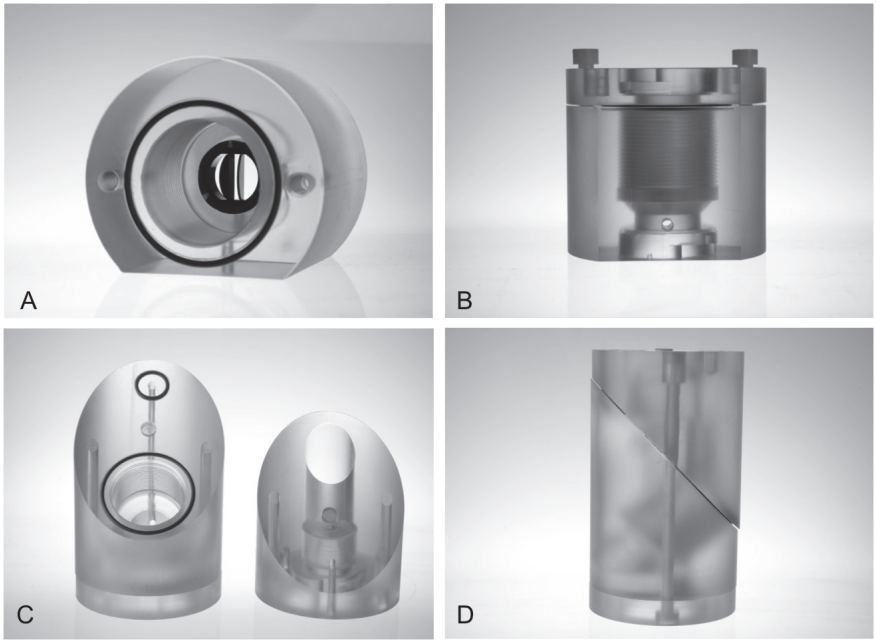

Figure 3 | Prosthetic heart valve chambers. Two different MRI compatible prosthetic valve holders were developed for the mock circulation loop: a straight valve holder (A and B) and valve holder in which the valve is mounted at an angle of 45 degrees (C and D).

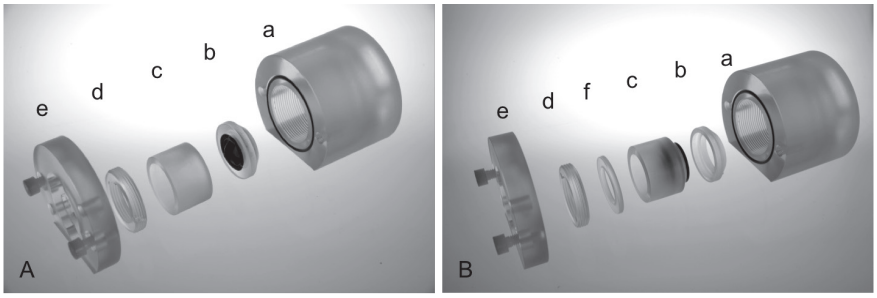

Figure 4 | Valve chamber components. The straight valve holder (A) and its sealing (E) including MRI compatible screws are shown in panels A and B. For each prosthetic valve type and size, different subparts have been customized to ensure an optimal fit of the prosthetic valve in the valve chamber. The prosthetic valve is either mounted in the funnel shaped ring (B) or a cylinder (C). One or more threaded rings (D, F) are used to fix the valve ring and valve holder within the valve chamber to prevent undesired movement.

if required, an anthropomorphic phantom simulating radiation dose absorption of the human thorax can be placed around the valve chamber.

The afterload system

The artificial aorta is made from a silicon tube, a compliant material in order to simulate physiological flow characteristics and vessel compliance as present in humans. A pressure sensor can be attached to both the valve chamber (prevalvular) and to the aorta (postvalvular) (*Figure 5*). With this, the simulated ventricular and aortic pressure can be measured and monitored as well as the pressure drop over the PHV. The valve chamber and aorta are located in a larger container that is used to fill the internal mock loop environment with fluid. This container also allows for assembling the valve chamber components submerged within the fluid in order to exclude all air and create an airless zone surrounding the prosthetic valve for optimal imaging. In addition, due to the container the modeled aorta is surrounded by fluid and can produce more consistent flow patterns since sporadic aortic tube movements are limited.

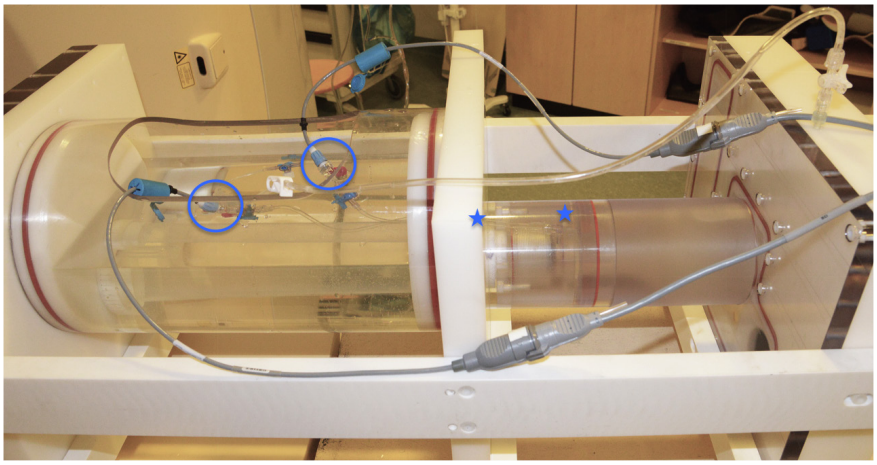

Figure 5 | Main body of the mock circulation loop. The central body of the mock circulation loop showing the left ventricular outflow tract and valve chamber on the right side and the large container including silicon aorta on the left side. Note the presence of the pressure sensors (encircled) connected to the ventricular and aortic side of the valve chamber (*).

The distal end of the artificial aorta is connected to the second part of the afterload system that represents the peripheral human circulation (*Figure 1*). This part consists of an air compliance chamber and two threaded pins functioning as resistances, connected by a fluid container (*Figure 6*). The fluid passes from the artificial aorta into the afterload fluid container. The air compliance chamber allows for simulation of blood vessel compliance since the creation of a high-pressure system by air compression will create more fluid volume capacity (*Figure 6A*). Two threaded pins control the passage of the fluid from the aorta and from the afterload container into the left atrium (the preload system). By inserting the pins further into the afterload container, more resistance is produced (*Figure 6B*). Herewith the systemic resistance can be simulated and manipulated. In humans, these vascular resistances are (auto) regulated by vasoconstriction and vasodilation, the capillary network, muscle activity and gravity. The first pin is used to balance between the compliance from the silicon aorta and the one produced by the air compliance chamber. From the afterload container, the fluid passes through the second pinhole into a long tube along the central body of the mock loop and into the arterial 'preload' compartment (*Figure 1*). This contains an atrial component that is connected by an artificial heart valve to the ventricular system.

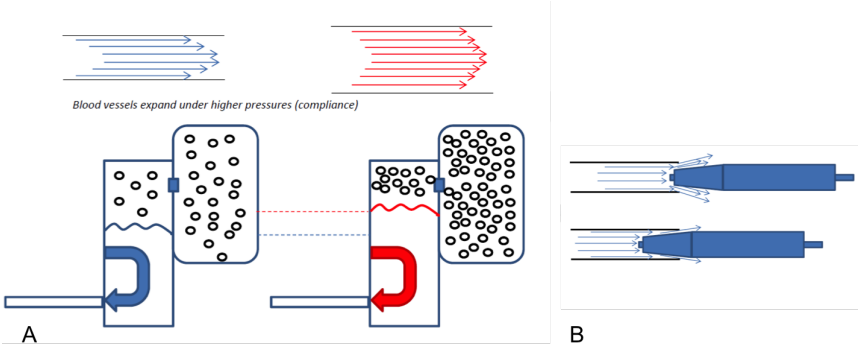

Figure 6 | Air compliance chamber and afterload resistance pins. A schematic overview is presented of the air compliance chamber (A) and threaded pins (B) present in the afterload system of the mock circulation loop. The air compliance chamber simulates blood vessel compliance by allowing compression of air and hence the creation of a high-pressure system which creates more fluid capacity (shown in A). The threaded pins (B) control the passage of the fluid from one compartment into the other, thereby harmonizing all different compliance components of the mock circulation loop. Insertion of the pins will overall, create more resistance, whereas retraction of the pins will decrease the resistance.

The ventricular system

The piston pump that drives the mock loop is connected to the ventricular part of the mock loop system (*Figure 1*). Backward and forward movements of the piston pump result in fluid displacement from the atrial into the ventricular component. Hereafter, the fluid is directed forwards through the artificial LVOT into the prosthetic valve chamber and the aorta, respectively. The LVOT is constructed in a bottleneck design to allow the fluid to merge into a more consistent, laminar flow while passing through the prosthetic valve mounted in the straight valve chamber.

Open versus closed system

The mock loop system has three (open) air access points: one at the afterload air compliance chamber and two at the arterial preload side (one atrial and one ventricular opening). These access points can be sealed using plugs. With this, the mock loop system can be run as an open pressure or closed pressure system. In general, the airlock of the afterload and compliance chamber remains sealed in order to allow the chamber to compress air and regulate pressures. By locking the air access point at the preload ventricular part, it is ensured the fluid passes through the LVOT and into valve chamber instead of out of the mock loop system. Since the air lock at the atrial preload site is separated from the ventricular chamber by an artificial heart valve, this lock can remain opened. If this air access point is open, we refer to the circulation loop as an open pressure system, when closed we refer to this as a closed pressure system. An advantage of using the open system is that the mock circulation loop pressures can be maintained relatively easily since small system leaks will have only minor or negligible effects. When using the closed pressure system, the initial circulation pressures have to be adjusted precisely by regulating the water and/or air levels within the mock loop. An advantage of using the closed system is that less fluid is required (e.g. when using expensive blood substitutes or imaging particles).

MRI set-up

The complete system as described above including all bolts, screws and pins is composed of non-ferromagnetic materials, e.g. MRI safe materials. The piston pump of the mock circulation loop however consists of components that are not MRI compatible. By using a MRI compatible shaft the piston pump can be extended with approximately 250 centimeters and placed outside the 5 Gauss line of the MRI system (*Figure 7*).

Figure 7 | Mock circulation loop in MRI compatible set-up. In this picture the mock circulation loop is shown after it has been assembled using the extension bar to place the motor out of the 5 Gauss line of the 1.5 Tesla MRI scanner (Philips Healthcare).

The total length of the mock loop system in MRI set-up is about 480 centimeters. Once placed inside the MRI room, the mock loop can be put together and the piston pump secured to a metal trolley at the far end of the system using supportive bars and titanium wing nuts. Furthermore, all cables running from the mock loop system are connected through a hatch in the MRI room to the mock loop motor and computer placed outside the MRI area.

Software

The mock loop system runs on two Labview scripts (LabVIEW Inc., Austin, TX, USA), which were developed to facilitate all user-friendly regulation of the mock loop device. With the first program the pressure system output can be read which can be used to optimize the baseline systemic pressures in non-pulsatile setting by adding fluid to the closed system. Furthermore, with this program the starting position of the piston pump can be controlled and altered (*Figure 8A*). After optimizing the pressures and piston pump starting position, the second program is used. This

Labview script allows mock loop system control with start and stop commands to initiate piston pump movement and allow for pressure refinement in pulsatile setting. The program allows for adjustment of the stroke volume (mL), heart rate (beats per minute), systolic fraction and thus cardiac output (L/min). Furthermore a delay in time can be set up as well for initiation of the mock loop system (*Figure 8B*).

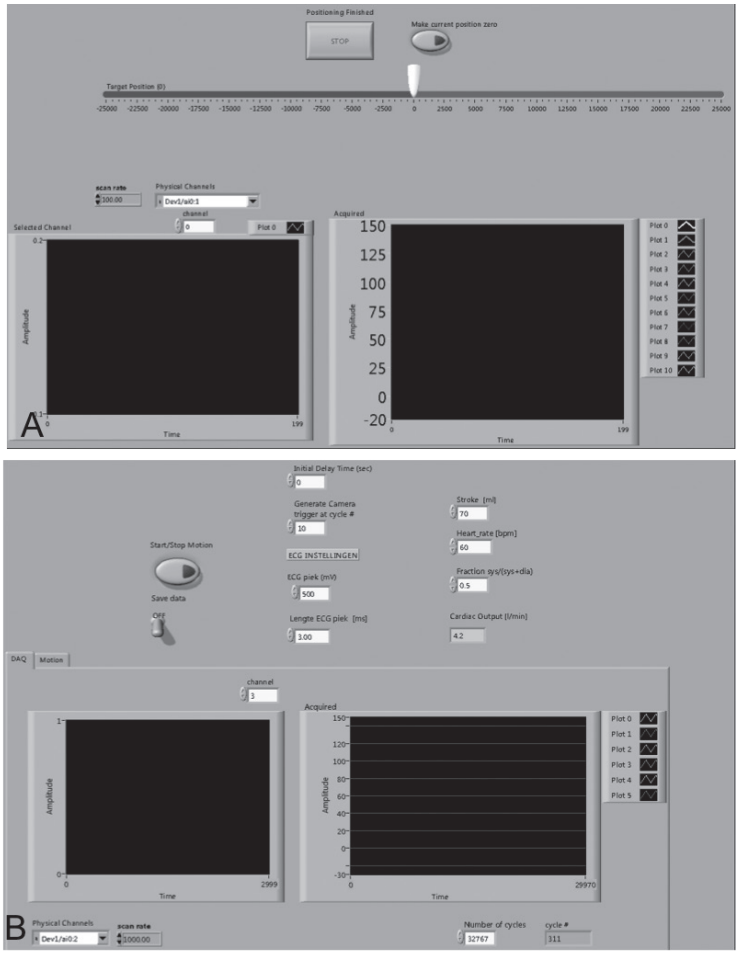

Figure 8 | Labview program software to control the mock circulation loop. Two Labview programs were developed to run the mock circulation loop. The first program (shown in A) controls the starting position of the piston pump and shows baseline pressures in non-pulsatile setting. In B, the program is shown that is used to start and stop the mock loop and adjust the stroke volume, heart rate, systolic fraction and cardiac output.

Also, the LabView program generates an (simulated) electrocardiography (ECG) signal synchronized with the piston pump motor that can be used for ECG-controlled image acquisitions. With the LabView program, the ECG peak height (mV) and length (ms) can be adjusted. Lastly, a high-speed camera can be inserted into the main container of the mock loop through the aorta using an endoscope, which allows en face evaluation of valve leaflet excursions. For this, a camera trigger can be set within the Labview program to start at recording a specific circulation cycle repetition. Within the Labview program, various output graphs can be created and displayed, for example for evaluation of the diastolic and systolic pressures. All recorded data during mock loop operations can be saved to external files.

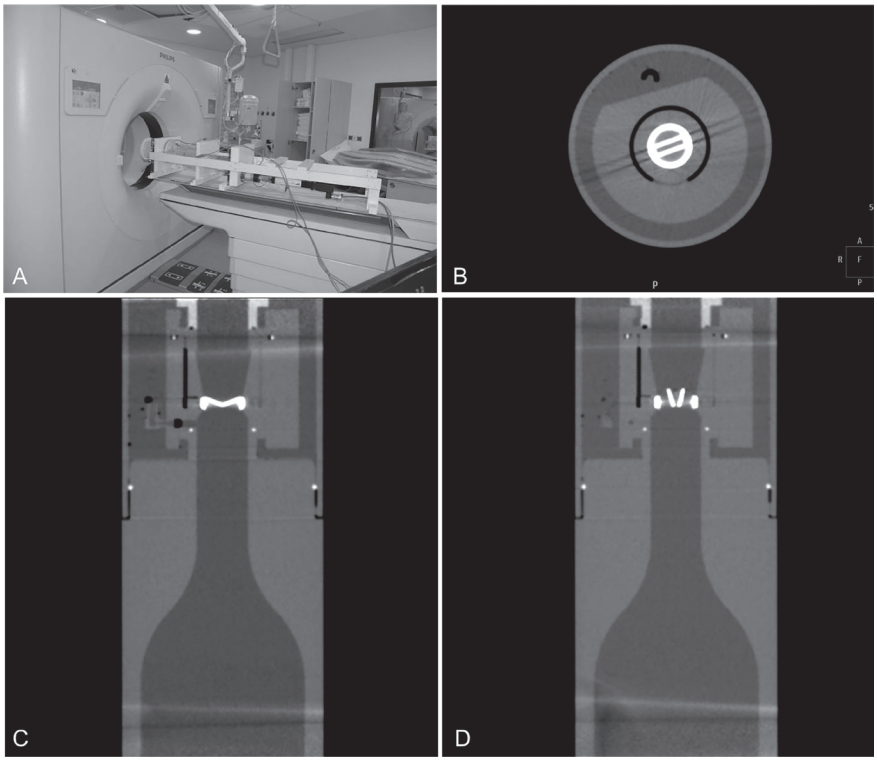

Figure 9 | CT images of prosthetic valve in the mock circulation loop . A bileaflet Carbomedics valve was mounted into the straight valve chamber, the mock circulation loop was filled with water and imaged using retrospectively ECG-gated imaging on a 256-slice multidetector-row iCT scanner (Philips Healthcare). Reconstructed CT images in plane with the prosthetic valve (B) and perpendicular to the valve leaflets are shown in diastolic (C) and systolic phase (D). Note the bottleneck design of the left ventricular outflow tract visualized in C and D.

Test run

An aortic bileaflet Carbomedics valve was mounted into the straight valve chamber. The mock loop system was filled with water and set up as an open pressure system. The mock loop was placed on the CT table and run with a simulated heart rate set at 60 beats per minute (*Figure 9*). CT imaging of the mock loop system was performed on a 256-slice multidetector-row CT scanner (iCT, Philips Healthcare, Best, The Netherlands). Retrospectively ECG-gated acquisitions were obtained using the following protocol: tube voltage 120 kV, tube current-time product 600 mAs, slice collimation of 128 x 0.625 mm, pitch of 0.18 and gantry rotation time of 0.33 seconds. No anthropomorphic phantom was used to simulate radiation dose absorption of the human thorax for this experiment. CT images were reconstructed in each 10% phase of the RR-interval using filtered back projection with a slice thickness of 0.90 mm and slice increment of 0.45 mm. Examples of the mounted Carbomedics valve in the running mock circulation loop and imaged with CT are presented in *Figure 9*.

DISCUSSION

In this technical note we described a mock circulation loop that allows assessment of prosthetic heart valves with both CT and MR imaging with a more advanced pulsatile system based on a five-element Windkessel model compared to our prior phantom which has been described previously[12]. The prior piston pump driven phantom was based on a three-element model and consisted of a 45-degree angulated valve chamber and a height-adjustable reservoir that allowed regulation of the afterload. In contrast to the basic phantom, the novel mock loop system allows for simulation of various flow conditions by enabling adjustment of the heart rate, stroke volume, systolic fraction and systolic and diastolic pressures. Since this system has a compliant afterload system, biological valves can be evaluated. The advantage of simulating different flow conditions is that both physiologic and pathologic conditions can be reproduced. In addition, both normal functioning and dysfunctional prosthetic heart valves can be evaluated. As imaging modalities, reconstruction techniques and software programs are advancing rapidly, the amount of information that can be obtained on valve function using solely imaging is increasing. Consequently, more realistic heart valve phantoms are required as well. Recently, one study presented a technical note on a comparable mock loop system primarily for the evaluation prosthetic mitral valves[13]. The mock circulation loop described in this report was designed for aortic valve prostheses. This novel system, which is based on a five-element Windkessel model, was

assembled without the use of metal components. Firstly, this allows for CT imaging without inducing metal-related artifacts that may hamper the diagnostic image quality. Secondly, the use of non-ferromagnetic materials allows for safe and MRI compatible imaging without metal-related image distortion and signal voids. Recently, four-dimensional (4D) MRI techniques have been introduced that allow flow assessment in native heart valves[14]. A first study showed that 4D-MRI might also be feasible for the assessment of flow in prosthetic heart valves[4]. The current mock circulation loop creates an excellent opportunity for the evaluation of 4D-MRI feasibility and reproducibility for the assessment of normal prosthetic flow patterns in a controlled, phantom setting. In addition, as (biological) transcatheter valves are associated with regurgitation and implanted more frequently, there is an increasing demand for reliable assessment of pathological prosthetic and periprosthetic regurgitation. Currently, regurgitation is evaluated using semi-quantitative methods and routine PHV imaging modalities such as echocardiography. New 4D-MRI techniques may allow for quantification of prosthetic and periprosthetic regurgitation. Furthermore, the effective valve area of PHVs could potentially be obtained using MRI flow-derived data and aid in the evaluation of recurrent valve stenosis. The mock circulation loop can be used to optimize imaging protocols and to establish reliable and reproducible evaluation of the PHV function using MRI. Similarly, the mock circulation loop can be used to optimize CT acquisition protocols and improve the diagnostic imaging quality for novel CT systems being clinically introduced such as dual-energy CT and photon-counting CT. Also, the additional value of novel, radiation dose reducing reconstruction techniques and various metal-artefact reduction filters for PHV assessment can be evaluated. Currently, significant differences exist not only between mechanical and biological valves but also between different PHV manufacturers for prosthesis design and type of alloys being used. All these different PHV features impact the diagnostic image quality. Hence, the feasibility of CT and MRI imaging may differ between valves and calls for valve specific acquisition protocol validation and optimization. To conclude, we have presented a mock circulation loop meeting the increasing demand for a more realistic heart valve phantom to allow for PHV function and imaging evaluation in a controlled and MRI safe setting. Future directions comprise several reproducibility studies to evaluate valve function related parameters that may aid in the clinical work-up of patients with suspected PHV dysfunction as well as optimize CT and MRI image acquisition and reconstruction protocols.

REFERENCES

1. Le Huu A, Shum-Tim D. Tissue engineering of autologous heart valves: A focused update. *Future Cardiol*. 2014;10:93-104
2. Suchá D, Symersky P, Vonken EJPA, Provoost E, Chamuleau SAJ, Budde RPJ. Multidetector-row computed tomography allows accurate measurement of mechanical prosthetic heart valve leaflet closing angles compared with fluoroscopy. *J Comput Assist Tomogr*. 2014;38:451-456
3. Makkar RR, Fontana G, Jilaihawi H, Chakravarty T, Kofoed KF, de Backer O, et al. Possible subclinical leaflet thrombosis in bioprosthetic aortic valves. *N Engl J Med*. 2015;373:2015-2024
4. von Knobelsdorff-Brenkenhoff F, Trauzeddel RF, Barker AJ, Gruettner H, Markl M, Schulz-Menger J. Blood flow characteristics in the ascending aorta after aortic valve replacement--a pilot study using 4d-flow mri. *Int J Cardiol*. 2014;170:426-433
5. Wright JT, Temple LJ. An improved method for determining the flow characteristics of prosthetic mitral heart valves. *Thorax*. 1971;26:81-88
6. Bjork VO, Intonti F, Meissl A. A mechanical pulse duplicator for testing prosthetic mitral and aortic valves. *Thorax*. 1962;17:280-283
7. Wieting DW, Hall CW, Kreisle LF, Liotta D, DeBakey ME. Design of a system for analyzing flow behavior of prosthetic human heart valves. *Cardiovasc Res Cent Bull.* 1966;5:41-56
8. Westerhof N, Elzinga G, Sipkema P. An artificial arterial system for pumping hearts. *J Appl Physiol*. 1971;31:776-781
9. Hales S. *Statistical essays ii haemostatics*. London, U.K.: Innays and Manby; 1733.
10. Frank O. Die grundform des arteriellen pulses. *Zeitung fur Biologie*. 1899;37:483–586
11. Westerhof N, Lankhaar JW, Westerhof BE. The arterial windkessel. *Med Biol Eng Comput*. 2009;47:131-141
12. Symersky P, Budde RP, Prokop M, de Mol BA. Multidetector-row computed tomography imaging characteristics of mechanical prosthetic valves. *J Heart Valve Dis*. 2011;20:216-222
13. Jackson MS, Igo SR, Lindsey TE, Maragiannis D, Chin KE, Autry K, et al. Development of a multi-modality compatible flow loop system for the functional assessment of mitral valve prostheses. *Cardiovasc Eng Technol*. 2014;5:13-24
14. Burris NS, Hope MD. 4d flow mri applications for aortic disease. *Magn Reson Imaging Clin N Am*. 2015;23:15-23

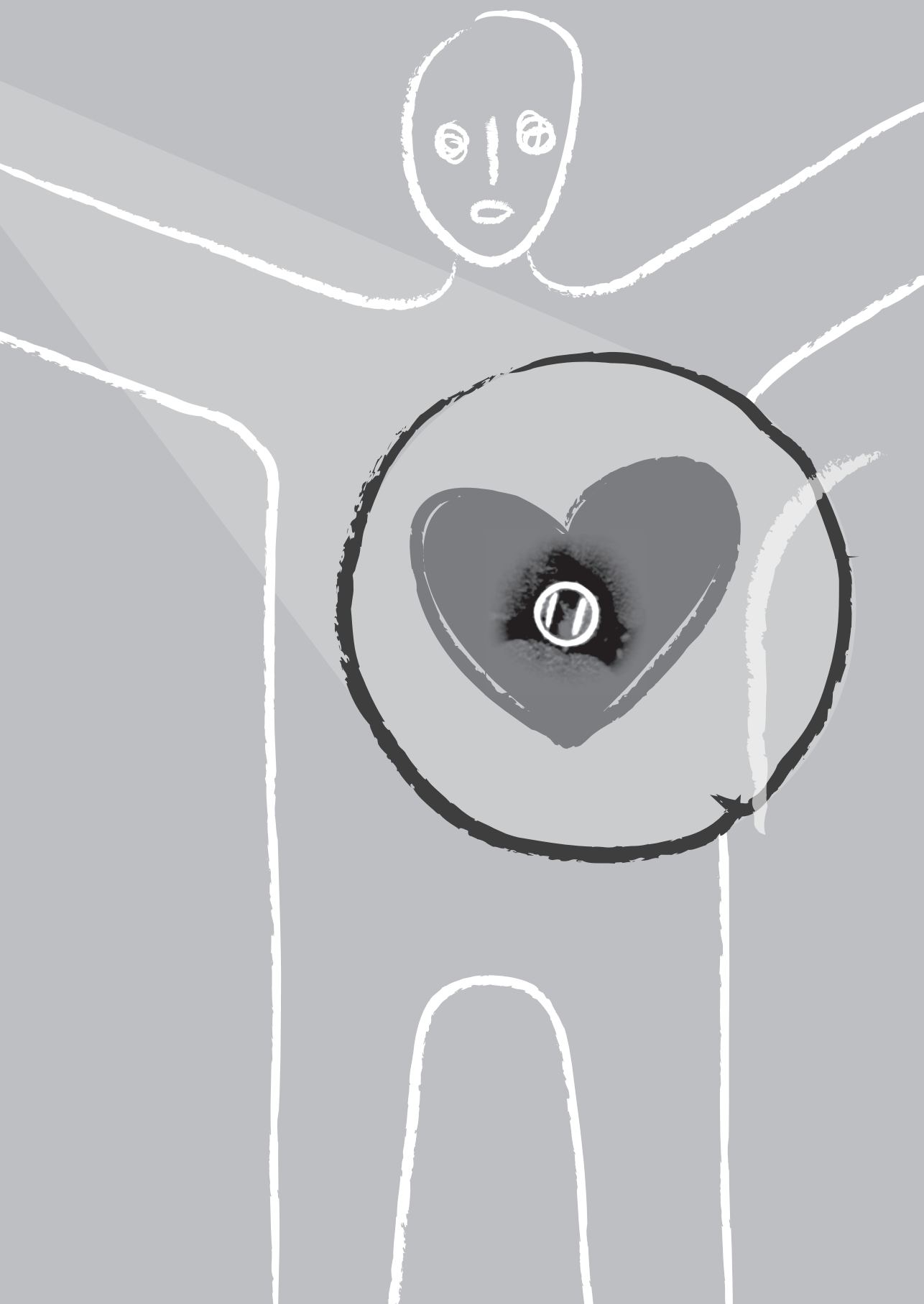

PART II
In vivo studies

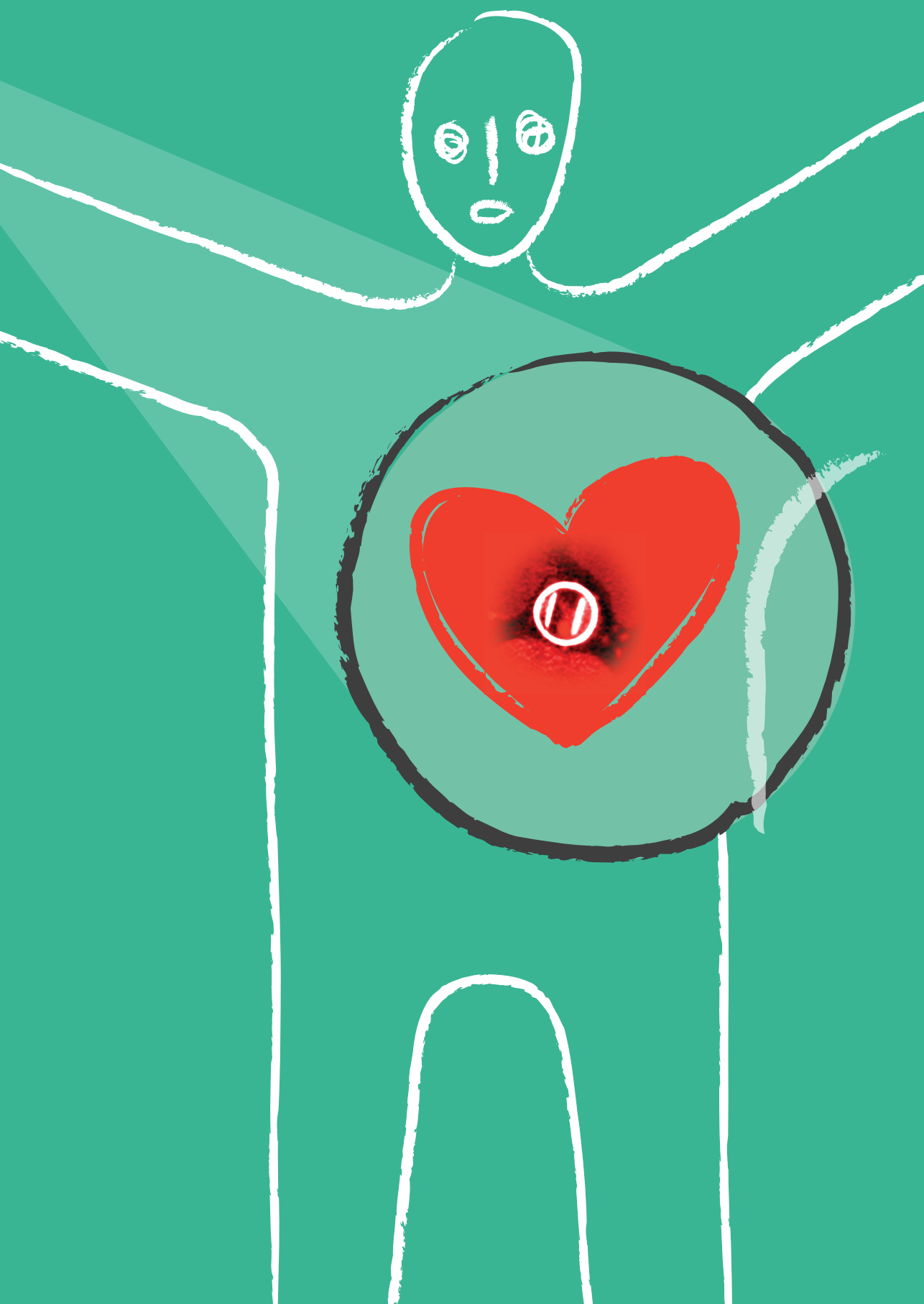

CHAPTER 6

Does the aortic annulus undergo conformational change throughout the cardiac cycle? A systematic review

Dominika Suchá*
Volkan Tuncay*
Niek H.J. Prakken
Tim Leiner
Peter M.A. van Ooijen
Matthijs Oudkerk
Ricardo P. J. Budde

* Both authors contributed equally to this paper

Published in the European Heart Journal - Cardiovascular Imaging, 2015

ABSTRACT

PURPOSE

Accurate annular sizing in transcatheter aortic valve implantation (TAVI) planning is essential. It is now widely recognized that the annulus is an oval structure in most patients, but it remains unclear if the annulus undergoes change in size and shape during the cardiac cycle that may impact prosthesis size selection. Our aim was to assess whether the aortic annulus undergoes dynamic conformational change during the cardiac cycle and to evaluate possible implications for prosthesis size selection

METHODS AND RESULTS

We performed a systematic search in Pubmed and Embase databases and reviewed all available literature on aortic annulus measurements in at least two cardiac phases. Twenty-nine articles published from 2001 to 2014 were included. In total, 2021 subjects with and without aortic stenosis were evaluated with a mean age ranging from 11±3.6 to 84.9±7.2 years. Two- and three-dimensional echocardiography was performed in six studies each, MRI was used in one and CT in 17 studies. In general, the aortic annulus was more circular in systole and predominantly oval in diastole. Whereas the annular long axis diameter shows insignificant change throughout the cycle, the short axis diameter, area and perimeter were significantly larger in systole compared to diastole.

CONCLUSION

The aortic annulus does undergo dynamic changes during the cardiac cycle. In patients with large conformational changes, diastolic compared to systolic measurements can result in undersizing TAVI prostheses. Due to the complex annular anatomy and dynamic change, three-dimensional assessment in multiple phases has utmost importance in TAVI planning to improve prosthesis sizing.

INTRODUCTION

In the elderly, the prevalence of moderate to severe aortic stenosis (AS) is approximately 3%[1]. About half of all patients with severe AS are referred for surgical aortic valve replacement (AVR)[2]. For selected high-risk patients, transcatheter aortic valve implantation (TAVI) has become a successful alternative to conventional valve surgery[3, 4].

In conventional AVR, the appropriate size of the prosthesis is determined by direct measurements of the annulus during surgery. In TAVI, assessment of the annular and prosthetic size relies entirely on preprocedural and/or periprocedural imaging. Precise aortic root measurement is essential for choosing the correct prosthesis size to minimize the risk of complications such as significant (> mild) paravalvular regurgitation, which has been reported in 1%-39% of TAVI patients[5-7]. Measurements of the aortic annulus were originally performed using transthoracic or transesophageal two-dimensional echocardiography (TTE and TEE, respectively). However, studies have found the aortic annulus to often have an ellipsoid shape rather than a circular structure[8-10]. Hence, three-dimensional echocardiography or computed tomography (CT) allows for more accurate assessment of the shape and size of the annulus by providing images in any desired imaging plane.

The ascending aorta is known to undergo conformational changes during the cardiac cycle[11, 12]. However, no consensus exists whether such changes are also present in the aortic annulus and in what way. If the annulus does undergo significant dynamic changes, this may affect selection of the most optimal cardiac phase for measurement and improve prosthesis sizing or even prosthesis design. In order to clarify this concern, we conducted a systematic review of all the literature investigating the dynamic behavior of the aortic annulus using echocardiography, CT and/or magnetic resonance imaging (MRI).

METHODS

Literature search

Pubmed and Embase databases were systematically searched on June 25th, 2014 using the search syntax presented in *Appendix 1*. In Embase, we included only articles, articles in press, reviews, and short surveys. No other limitations were applied. Two reviewers (DS, VT) screened all titles and abstracts independently. In total, 5637 articles were found and 2173 duplicates excluded manually (*Figure 1*).

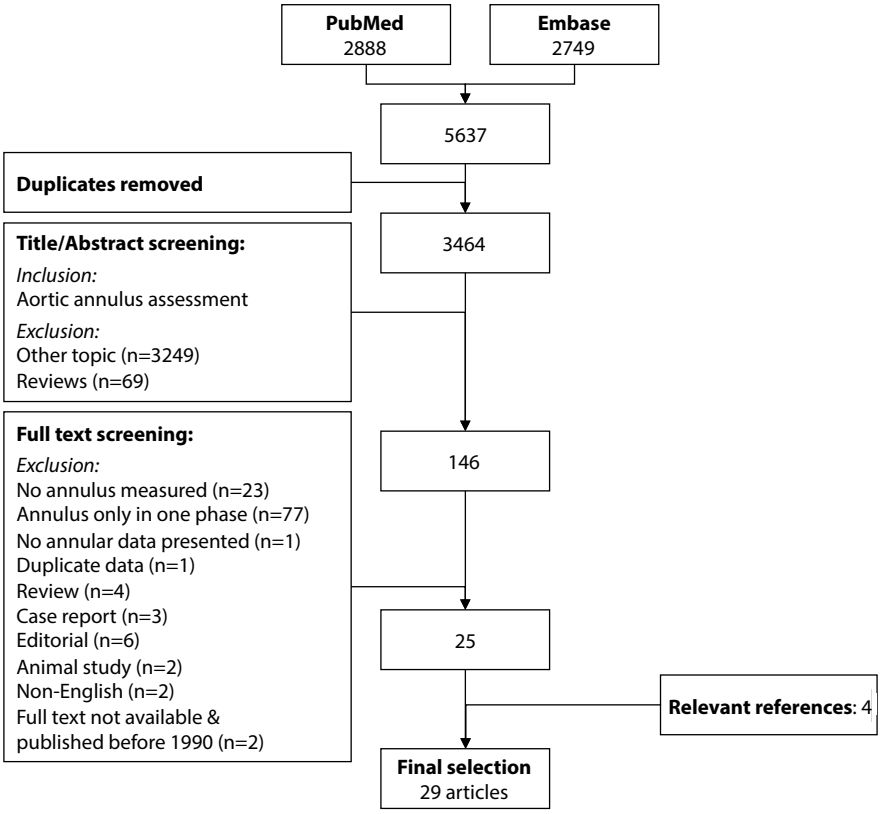

Figure. 1 | Literature search

Article selection

Only articles aimed at imaging and evaluation of the aortic annulus were included for further screening. In total, 146 articles were selected for full text screening. Both reviewers independently excluded studies evaluating the annulus only in one cardiac phase and articles on other aortic/cardiac dimensions than the annulus. Furthermore, studies on animals, case reports, reviews, editorials and non-English articles were excluded (*Figure 1*). A third reviewer (RB) settled discordant judgements. Our selection comprised 25 articles on aortic annulus change during the cardiac cycle. References and citations were screened for relevant articles not included in our search. This resulted in four additional articles[13-16], since annulus as defined in the search syntax was not mentioned in the title/abstract. The final selection included 29 articles.

Data extraction

We extracted the following data from the selected articles: first author, journal, publication year, number of patients, mean age, gender, number of patients with AS, definition of AS and mean aortic valve area, imaging modalities used for measurements including selected plane and imaging phase, definition of annulus, annulus measurement method (manual, semiautomatic) and annular parameters within the cardiac cycle.

RESULTS

Study characteristics

Twenty-nine original articles were included published from 2001 to 2014. Of these, seven evaluated annular dynamic changes in healthy subjects (e.g. no aortic root or valve disease), 10 compared a healthy population with AS patients and 12 studies included only AS patients. In total, 2021 subjects were evaluated with a mean age ranging from 11±3.6 to 84.9±7.2 years. Study and patient characteristics are summarized in *Table 1*.

Imaging characteristics

Two-dimensional echocardiography (TTE and/or TEE) in systole and diastole was performed in six studies, all using the parasternal long axis view. Three-dimensional modalities used for assessment of the annulus were echocardiography (6 studies), MRI (1 study) and CT (17 studies). The CT acquisition protocol comprised retrospective ECG-gating in 15 studies, wide-window (20-90%) dose-modulated prospective ECG-triggering in one study and one study did not specify the CT protocol. Of all three-dimensional modality studies, the MRI and four CT studies evaluated coronal and/or sagittal plane reconstructions[8, 10, 17-19] and one CT study used an undefined longitudinal view[20]. Reconstructed double oblique images in plane with the aortic annulus were evaluated in 19 studies. Since the annulus is not a true anatomical structure, the exact location of anatomical measurements had to be specified. The aortic annulus was defined in general as a virtual ring at the lowest, most caudal, insertion of the valve leaflets in 22 studies. Two studies measured the ventriculo-arterial junction[20, 21] and five studies did not specify aortic annulus[8, 13, 18, 22, 23]. Annular measurements were performed semi-automatically in six studies[15, 16, 23-26] and manually in the remaining 23 studies.

Table 1 | Study characteristics

			No aortic stenosis		
Author (ref)	Year	Patient population	N Patients	Mean age±SD	N Males (%)
Burman[18]	2008	Healthy subjects	120	49.3±17.2*	60 (50%)
de Heer[10]	2011	CAD screening	108	56.1±12.5	89 (82%)
Kazui[20]	2006	Normal aortic root/valve	25	60.1±14.8	17 (68%)
Martin[31]	2013	Cardiac murmur/pre chemotherapy	30	11±3.6	NA
de Paulis[13]	2001	Normal aortic root/valve	7	45.3±19	6 (86%)
Veronesi[16]	2009	Normal aortic root/valve	24	54±20	7 (29%)
Zhu[21]	2011	Healthy subjects	314	37.2±13.5	133 (42%)
de Heer[24]	2012	CAD screening vs TAVI indicated	15	53±12	12 (80%)
Hamdan[33]	2012	CAD screening vs TAVI indicated	11	56.2±11.8	5 (45%)
Izumi[22]	2012	Pre AF ablation vs AS	37	68±5	10 (27%)
Otani[43]	2010	TEE indicated non-AS vs AS	80	70±10	43 (54%)
Shabestari[32]	2013	CAD screening vs aortic calcification	52	50.5±11.3	27 (26%)
Shiran[14]	2009	TEE non-AS vs AS	30	62±13	18 (60%)
Tops[8]	2008	CAD screening no/mild AS vs AS	150	54±11‡	111 (66%)‡
Tsang[26]	2013	Stroke work-up vs TAVI indicated	16	80±5	7 (44%)
Tsang[15]	2013	Normal valves vs AS	20	59.2±17	10 (50%)
Yoshikawa[23]	2013	Stroke work-up vs AS	40	65.1±11.7	24 (60%)
Bertaso[17]	2012	TAVI indicated	-	-	-
Blanke[35]	2012	TAVI indicated	-	-	-
Bolen[27]	2012	TAVI indicated	-	-	-
Jilaihawi[25]	2012	TAVI indicated	-	-	-
Kempfert[44]	2012	Pre conventional AVR	-	-	-
Lehmkuhl[28]	2013	TAVI indicated	-	-	-
Lehmkuhl[34]	2013	TAVI indicated	-	-	-
Masri[42]	2014	Pre TAVI or conventional AVR	-	-	-
Peng[36]	2012	Severe AS	-	-	-
Pontone[29]	2011	TAVI indicated	-	-	-
Willson[30]	2012	TAVI indicated	-	-	-
Wood[19]	2009	TAVI indicated	-	-	-

* Of male subjects; † Of total group (n=52); ‡ Of total group (n=169); § 2D speckle tracking echocardiography; ‖ Of total group (n=96); ¶ Of total group (n=120)

Aortic stenosis						
N patients	Mean age±SD	N Males (%)	Definition stenosis	AVA (cm^2)	Mean gradient	Modality
-	-	-	-	-	-	MRI
-	-	-	-	-	-	CT
-	-	-	-	-	-	CT
-	-	-	-	-	-	TTE-2D-3D
-	-	-	-	-	-	TEE-2D
-	-	-	-	-	-	TEE-3D
-	-	-	-	-	-	TTE-2D
20	81±6	6 (30%)	not defined	NA	39±14	CT
35	80.1±7.4	16 (46%)	not defined	NA	NA	CT
23	73±5	10 (43%)	not defined	NA	NA	TTE-3D
71	73±8	41 (58%)	not defined	1.1±0.4	38±20	TEE-3D
30	66.58±8.90†	30 (58%)†	aortic valve calcifications >100 HU	NA	NA	CT
20	78±9	5 (25%)	not defined	NA	NA	TTE-2D, TEE-2D
17	54±11‡	111 (66%)‡	moderate to severe AS	0.8±0.2	50±21	CT
27	82±7	16 (59%)	AVA <1.0cm^2, mean PG>40mmHg	0.7±0.1	40±12	TEE-3D
20	72±9	14 (70%)	AVA <1.0cm^2, mean PG >40mmHg	0.9±0.2	47±11	TEE-3D
40	69.3±9.6	25 (63%)	AVA <1.0cm^2 or PG>40mmHg	0.8±0.4	43.2±18.4	TEE-2D§
59	82.4±5	29 (49%)	AVA <1cm^2, AVAi <0.6cm^2/m^2	0.7±0.2	NA	CT
110	82.9±7.9	27 (25%)	severe AS	0.7±0.2	43.6±14.1	CT
47	78±9.5	25 (53%)	not defined	CT:0.9±0.2	NA	CT
20	84.9±7.2‖	50 (52%)‖	not defined	NA	NA	CT
26	NA	NA	severe AS	NA	NA	TTE-2D, TEE-2D
56	81.6±6.8	16 (29%)	severe AS	0.91±0.14	NA	CT
27	82.3±11.2	6 (22%)	severe AS	NA	NA	CT
87	81±10	47 (54%)	symptomatic severe AS	0.6±0.1	46±13	CT
62	68.2±5.9	41 (66%)	not defined	0.8±0.2	61.6±20.9	CT
60	80±8	22 (37%)	not defined	0.7±0.2	51.9±15.2	CT
66	81.4±7.8¶	57 (48%)¶	not defined	0.7±0.2§	42.9±16.6§	CT
19	83.5	NA	symptomatic severe AS	0.6	50.7	CT

AVA(i)= aortic valve area (indexed); AS= aortic stenosis; CAD= coronary artery disease; CT= computed tomography; NA= not available; HU= CT Hounsfield units; MRI= magnetic resonance imaging; PG= pressure gradient; SD= standard deviation; TAVI= transcatheter aortic valve implantation; TEE= transesophageal echocardiography; TTE= transthoracic echocardiography

Deformation during the cardiac cycle

On parasternal long axis view, the annulus diameter was larger in systole than in diastole in nine out of ten studies (*Table 2*, largest mean difference 2.9±0.7mm). Only two studies performed paired T-tests[14, 20] of which one found a significant change for TEE-derived diameter throughout the cycle (mean difference 0.3±0.7mm, P=0.0005)[14]. No significant change was shown for TTE-derived diameter measurements.

Results on coronal view measurements were contradictory as the largest annulus diameter was found either in the systolic (n=3) or diastolic phase (n=3) (*Table 3*). One study evaluated the mean diameter difference between these phases (0.23mm) but no statistical significance was reached[17]. However, all results on sagittal view showed larger systolic than diastolic annulus diameters with significant difference (mean 0.42mm, P=0.008), though tested only by one study[17] (*Table 3*).

Table 4 shows all diameter measurements acquired using the double oblique in plane view. No evident pattern was found for change in maximal (long axis) annulus diameter since it was largest either in systole or diastole in seven patient groups each. Statistical analysis was performed by seven studies[10, 17, 25, 27-30] but only one found significant differences (mean 0.3±2.4mm in diastole, P<0.001)[10]. In contrast, the minimal (short axis) annulus diameter was largest in systole in the majority of patients (16 study groups) and in diastole in three studies (4 patient groups)[22, 31, 32]. The change in diameter (*Figure 2*) was significant in 11 patient groups[10, 17, 22, 25, 27, 28, 30, 33, 34] all showing a greater short-axis diameter in systole except for the two groups of Izumi et al.[22]. Pontone et al. did not find significant differences[29].

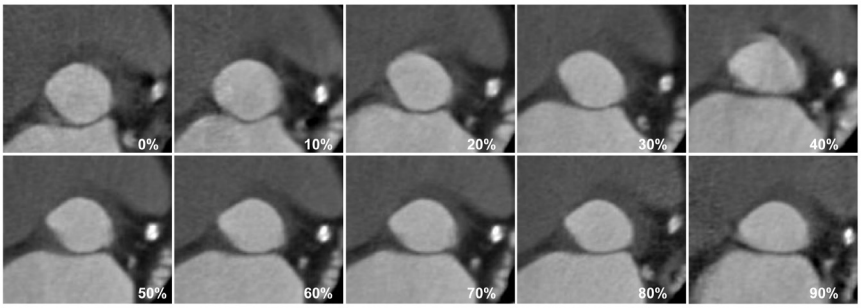

Figure 2 Dynamic deformation of the annulus. Cardiac ECG-gated multidetector-row computed tomography images reconstructed in each 10% phase of the RR-interval. Note the conformational change of the aortic annulus showing a more circular shape during systole and an oval shape during diastole. Whereas the long axis diameter remains relatively stable, the short-axis diameter undergoes significant change throughout the cycle.

Table 2 | Parasternal long axis annulus diameter measurements

Author	Imaging	Cardiac phase measured	Systole	Diastole	Mean difference	P-value
Patients without aortic valve stenosis						
Kazui[20]	CT*	40%, 80% RR-interval	22.5±2.2	22.1±2.2	-	NS
Martin[31]	TTE-2D	mid-systole, end-diastole	19.4	19.5	-	-
de Paulis[13]	TEE-2D	systole, diastole	22.2±1.6	20.6±1	7%±3.2%	-
Shiran†[14]	TTE-2D	mid-systole, end-diastole	21.1±2.1	21.0±1.8	0.2±0.8	P=0.2
	TEE-2D	mid-systole, end-diastole	21.6±2.2	21.3±2.1	0.3±0.7	P=0.0005
Yoshikawa[23]	TEE-2D‡	83 ms, 421 ms from ECG R-wave	22.9±2.7	20.0±2.9	2.9±0.7	-
Zhu[21]	TTE-2D	mid-systole, end-diastole	20.91±2.29	20.35±8.67	-	-
Patients with aortic valve stenosis						
Kempfert[44]	TTE-2D	end-systole, end-diastole	24.2±3.5	22.9±3.1	-	-
	TEE-2D	end-systole, end-diastole	24.5±2.7	23.8±2.7	-	-
Yoshikawa[23]	TEE-2D‡	99 ms, 435 ms from ECG R-wave	21.6±2.6	19.4±2.6	2.2±0.6	-

All annular measurements are presented in millimeters as mean±standard deviation
* In CT longitudinal view
† Results are similar for stenosis patients
‡ TEE speckle tracing
CT= computed tomography; NS= non-significant; ms= milliseconds; TEE= transesophageal echocardiography; TTE= transthoracic echocardiography

Table 3 | Coronal and sagittal axis annulus diameter measurements

			Coronal view				Sagittal view			
Author	Imaging	Cardiac phase measured	Systole	Diastole	Mean Δ	P-value	Systole	Diastole	Mean Δ	P-value
Patients without aortic valve stenosis										
Burman[18]	MRI	max systolic, end-diastolic	25.7±2.1 (M)	26.2±2.3	-	-	22.4±2.1	22.2±2.4	-	-
			23.0±2.0 (F)	23.0±2.1	-	-	21.0±2.1	19.9±1.9	-	-
de Heer[10]	CT	30-40%, 70-75% RR-interval	26.6±2.8	26.9±2.4	-	-	-	-	-	-
Tops[8]	CT	30%, 75% RR-interval	26.4±2.8	26.3±2.6	-	-	24.0±2.6	23.4±2.7	-	-
Patients with aortic valve stenosis										
Bertaso[17]	CT	30-40%. 70-80% RR-interval	25.3±2.7	25.5±2.7	0.23 (0.9%)	0.115	22±2.4	21.6±2.3	0.42 (1.9%)	0.008
Tops[8]	CT	30%, 75% RR-interval	27.3±3.7	26.7±3.9	-	-	24.7±3.0	24.2±3.0	-	-
Wood[19]	CT	30%, 70% RR-interval	25.7±1.5	25.5±2.5	-	-	22.4±1.3	21.5±2.1	-	-

All annular measurements are presented in millimeters as mean±standard deviation
(F)= in females; (M)= in males
Mean Δ= mean difference between systolic and diastolic measurement

Table 4 | Double oblique plane annulus diameter measurements

			Maximal diameter				Minimal diameter			
Author	Imaging	Cardiac phase measured	Systole	Diastole	Mean Δ	P-value	Systole	Diastole	Mean Δ	P-value
Patients without aortic valve stenosis										
Hamdan[33]	CT	all: max 30%, min 90-0%	-	-	-	-	21.7±1.8	19.0±2.6	12.3±7.3%	<0.001
de Heer[10]	CT	30-40%, 70-75%	29.7±3.4	30.1±3.0	0.3±2.4	<0.001	25.1±3.3	24.0±3.1	1.1±2.0	<0.001
Izumi[22]	TTE-3D	end-systole, end-diastole	-	-	-	-	20.6±1.4	22.4±1.6	7.8±3.4%	<0.0001
Martin[31]	TTE-3D	mid-systole, end-diastole	20.1	20.1	-	-	18.8	19.3	-	-
Otani[43]	TEE-3D	mid-systole, end-diastole	24.6±2.1	25.0±2.2	-	-	19.6±1.8	19.1±1.8	-	-
Shabestari[32]	CT	30-35%, 70-75%	26.69±2.72	27.85±3.09	0.59	-	20.80±2.47	20.86±1.81	0.05	-
Patients with aortic valve stenosis										
Bertaso[17]	CT	30-40%, 70-80%	28.7±2.7	28.4±2.7	0.24 (0.7%)	0.163	22.4±2.4	21.7±2.4	0.75 (3.4%)	0.004
Blanke[35]	CT	all: max 20%, min 60%	27.8*	26.8*	2%	-	22.0±1.9	19.8*	11%	-
Bolen[27]	CT	20-30%, 90%	28.4±3.5	28.7±3.4	-	0.67	22.9±2.4	21.4±2.5	-	0.006
Hamdan[33]	CT	all: max 30%, min 90-0%	-	-	-	-	22.6±2.9	20.4±2.7	9.8±3.4 %	<0.001
Izumi[22]	TTE-3D	end-systole, end-diastole	-	-	-	-	18.7±1.9	19.1±1.7	2.0±2.2%	<0.0001
Jilaihawi[25]	CT	mean at 16% and 54%	27.1±2.9	26.8±2.8	-	0.43	21.3±2.7	19.7±2.3	-	<0.0001
Lehmkuhl[28]	CT	40-50%, 90-0%	27.1±3†	27.0±3.0†	1.6±1.2	NS	24.8±2.9‡	23.0±3.2‡	2.2±1.6	<0.001
Lehmkuhl[34]	CT	end-systole, end-diastole	24.7±2.2†	24.8±2.0†	-	-	21.4±1.8‡	20.5±2.0‡	1.2±2.0	<0.01
Masri[42]	CT	all: max NA, min NA	26±3	25±3	1.2±0.5	-	21±3	20±3	1.2±0.5	-
Otani[43]	TEE-3D	mid-systole, end-diastole	25.2±2.8	25.2±2.6	-	-	19.5±2.3	19.2±2.3	-	-
Peng[36]	CT	all: max 0-10%, min 50%	28.2±4.0	27.1±3.7	3.2±1.4	-	23.1±2.6	21.1±2.8	3.6±1.4	-
Pontone[29]	CT	systole, diastole	25.1±2.8	25.4±2.7	-	NS	21.2±2.2	20.1±2.7	-	NS
Shabestari[32]	CT	30-35%, 70-75%	27.16±3.11	27.42±2.62	-	-	20.57±2.10	20.45±2.37	-	-
Willson[30]	CT	25-35%, 75%	26.6±2.84	26.2±2.90	-	0.22	20.8±2.24	20.2±1.99	-	0.01

All annular measurements are presented in millimeters as mean±standard deviation
* derived from graphs
† distance between basal attachment of left coronary cusp and opposite intercommissure
‡ distance between basal attachment of right coronary cusp and opposite intercommissure

Table 5 | Double oblique plane annulus area measurements

Author	Imaging	Cardiac phase measured	Area method	Area		P-value	Mean difference	P-value
				Systole	Diastole			
Patients without aortic valve stenosis								
De Heer[24]	CT	all: max 0-30%, min 50-70%	semi-automatic	NA	NA	-	122±33 (28%±10%)	<0.001
Veronesi[16]	TEE-3D	all: max 19%, min 57%	semi-automatic	3.7±1.1*	4.6±1.3*	<0.05	-	-
Hamdan[33]	CT	all: max 30%, min 90-0%	manual	448±81.8	398.7±93.7	<0.001	11.2±5.2%	<0.001
Otani[43]	TEE-3D	mid-systole, end-diastole	manual	391±66	390±65	-	-	-
Shabestari[32]	CT	30-35%, 70-75%	manual	457.71±82.86	460.24±79.70	-	2.53	-
Tsang[26]	TEE-3D	all: max NA, min NA	semi-automatic	5.3±1.1*	4.2±1.1*	-	-	-
Tsang[15]	TEE-3D	all: max NA, min NA	semi-automatic	5.4±1.0*	4.4±1.2*	-	-	-
Patients with aortic valve stenosis								
De Heer[24]	CT	all: max 0-30%, min 50-70%	semi-automatic	NA	NA	-	98±52 (21±10%)	<0.001
Hamdan[33]	CT	all: max 30%, min 90-0%	manual	480.9±108	438.8±103	<0.001	6.2±4.8%	<0.001
Otani[43]	TEE-3D	mid-systole, end-diastole	manual	397±89	396±88	-	-	-
Shabestari[32]	CT	30-35%, 70-75%	manual	437.82±92.44	438.31±79.25	-	6.92	-
Bertaso[17]	CT	30-40%, 70-80%	ellipse equation	509±12	488±12	-	4%	0.002
Blanke[35]	CT	all: max 20%, min 60%	manual	483.4±75.2	410.5±68.7	<0.001	72.9±22.6 (18.2%)	<0.001
Masri[42]	CT	all: max NA, min NA	manual	482±111	445±102	-	38±17	-
Pontone[29]	CT	systole, diastole	manual	410.5±81.4	409.2±97.1	NS	-	-
Tsang[26]	TEE-3D	all: max NA, min NA	semi-automatic	4.4±1.4 *	3.8±1.2*	-	-	-
Tsang[15]	TEE-3D	all: max NA, min NA	semi-automatic	5.1±1.1*	3.7±1.7*	-	-	-
Willson[30]	CT	25-35%, 75%	manual	4.7±0.8*	4.5±0.9*	<0.001	-	-

Measurements are presented in mm^2 or cm^2 if indicated with* as mean±standard deviation

NA= not available; NS= not significant

The annular area was evaluated in 18 patient groups using double oblique plane reconstructions (*Table 5*). The majority (n=15, 83%) showed the largest area during (early) systole, with a maximal mean difference of 122±33mm^2 throughout the cardiac cycle[24]. Nine groups were statistically evaluated[16, 17, 24, 29, 30, 33, 35] and the area was significantly larger during systole in seven, during diastole in one and not significantly different in one group[29].
The annular perimeter was largest during systole in five and during diastole in three groups (*Table 6*). This was tested and significant in four and one patient group, respectively. The largest mean difference between systole and diastole was 5.4±1.5mm[35].

Aortic stenosis versus non-stenosis

As presented in *Tables 3-6*, both non-AS patients (e.g. without aortic root disease) and AS patients showed significant annular change throughout the cycle. Five studies directly compared the extent of conformational change between AS and non-AS patients. Based on longitudinal parasternal view measurements, Shiran et al. found similar results for AS and non-AS patients. In contrast, Yoshikawa et al. detected significantly less absolute and relative diameter change in AS patients ($p \leq 0.0027$)[23]. Furthermore, the diameter reached its maximal value at a later point in the cardiac cycle than in non-AS patients (99 versus 83ms from the R-wave, resp. $P<0.0004$). Using double oblique plane images, Izumi et al. also found a significantly smaller annulus diameter deformation in AS patients (2 vs. 8% in controls, $p<0.0001$)[22]. In the study of Hamdan et al. AS patients showed higher annular stiffness compared to healthy subjects, based on the perimeter and left ventricular pressure change (23 versus 14 MPA, resp. $P=0.029$)[33]. No significant difference was found for dynamic changes between patients with and without aortic valve calcifications[32].

Other factors

Aortic root calcifications in general did not show a correlation with annular change[32] or circularity[28] during the cardiac cycle. But the location of the calcifications was related to annulus area change, showing the least change with both annular and commissural calcifications (6mm^2) and the greatest change with only commissural calcifications (23mm^2)[32]. Only one study evaluated the influence of age on annulus change within the cardiac cycle but found no age effect[32]. In this study, a weak linear correlation was found between diastolic blood pressure and annulus perimeter changes ($r=-0.25$, $P=0.01$), and between ejection fraction and minimal diameter changes ($r=-0.22$, $P=0.03$). Another study found the left ventricular outflow tract diameter and stroke volume to be associated with larger changes throughout the cycle[36].

Table 6 | Double oblique plane annulus perimeter measurements

			Perimeter			
Author	Imaging	Phase measured	Systole	Diastole	Mean difference	P-value
Patients without aortic valve stenosis						
Hamdan[33]	CT	all: max 30%, min 90-0%	76.1±6.7	74.1±7.6	2.2±2.2%	0.01
Shabestari[32]	CT	30-35%, 70-75%	86.64±7.40	88.12±8.90	1.48	-
Veronesi[16]	TEE-3D	all: max 19%, min 57%	69.5±10.6	78.1±11.5	-	<0.05
Patients with aortic valve stenosis						
Blanke[35]	CT	all: max 20%, min 60%	79.6±6.0	74.2±5.7	5.4±1.5 (7.3±2.1%)	<0.001
Hamdan[33]	CT	all: max 30%, min 90-0%	78.9±8.7	77.3±8.6	0.56±0.85%	0.01
Masri[42]	CT	all: max NA, min NA	80±9	77±9	3±1	-
Shabestari[32]	CT	30-35%, 70-75%	86.67±8.52	87.51±8.21	-	-
Willson[30]	CT	25-35%, 75%	78.5±8.2	77.2±8.0	-	0.01

All measurements are presented in millimeters as mean±standard deviation
NA= not available

Impact on prosthesis sizing

Blanke et al. evaluated the annulus in 5% steps throughout the full cardiac cycle and found the selected cardiac phase to affect prosthesis agreement[35]. Selection of the cardiac phase in which the area or perimeter-derived diameter reached its maximal value showed the highest agreement with the selected Edwards Sapien prosthesis and most relative oversizing (±10%). The area and perimeter were largest between 0-30% phases of the RR-interval. Measurements obtained in the clinically used 35%-systolic and 75%-diastolic cardiac phase showed only 76% prosthesis agreement (84/110 patients) and less relative oversizing (±7% and ±5%, resp.)[35]. In particular, 75%-diastolic phase area and diameter measurements led to (theoretical) undersizing in 15 (14%) and 6 (6%) patients. In this phase, the area and perimeter-derived diameters differed 2.7±1.4mm and 2.0±1.1mm with the prosthesis compared to 1.5±1.2mm and 1.1±1.2mm during maximal phase measurements, respectively. Likewise, Wilsson et al. found diastolic phase measurements to result in smaller Sapien XT prostheses in 13/66 patients and in larger in only 1/66 patients[30]. The patients with downsized prostheses showed significant larger conformational change in annulus diameter, area and perimeter compared to patients without a switch in prosthesis size. In contrast, the use of the diastolic diameter in another study resulted in a larger prosthesis in 2/34 patients (29 versus 26mm Corevalve)[17]. Some patients might show the largest area in the diastolic phase, as also found by de Heer et al. in 3/15 patients[24].

DISCUSSION

This systematic review clearly demonstrates that the aortic annulus does undergo dynamic conformational change during the cardiac cycle. The annulus becomes more circular in systole and has a predominantly oval shape in diastole. Using double oblique reconstructions perpendicular to the center lumen line of the left ventricular outflow tract the annulus has a significantly larger short axis diameter, area and perimeter in systole compared to diastole. A greater diameter is also found in systolic compared to diastolic phase on the parasternal long-axis and sagittal views, though each was statistically confirmed only by one study. In contrast, the double oblique long axis diameter suggests no significant change throughout the cardiac cycle and the same goes for the coronal diameter. Results on differences for the magnitude of conformational changes between AS and non-AS patients are contradictory.

The finding that the aortic annulus undergoes conformational changes during the cardiac cycle is important and may add to improved prosthesis design. In clinical

setting, this knowledge may add in selecting the optimal imaging phase and approximating the true annular dimensions. Blanke et al. showed better annular agreement with prosthetic sizes selected based on the maximal annular values throughout the cardiac cycle compared to prostheses based on routine predefined systolic (35%) or diastolic (75%) reconstructions[35]. Importantly, de Heer et al. found the cardiac phase for maximal annulus area to vary between patients from 0%-60% and 90% of the RR-interval and similar differences exist for the minimal area[24]. Apparently, the systolic phase does not represent the aortic annulus in its maximal dimensions in all patients. This might also be one of the reasons why some studies found larger diastolic diameters and/or no significant differences in the overall patient group. Assessment of the full cardiac cycle hence enables selection of the annulus in its ultimate dimensions, which may improve the annulus to prosthesis agreement.

Likewise, the choice of the measured parameter may affect prosthesis size selection as well since the annulus, in general, is an ellipsoid structure. The results show the minimal short diameter axis to significantly change in dimension, whereas the maximal diameter remains relatively unchanged. In addition, the perimeter changes throughout the cardiac cycle as well. These findings support the belief that the annular structure becomes less oval throughout the cycle. Studies using a so-called effective diameter, the diameter calculated from the measured area or perimeter, may induce an error if solely formulas for circular structures are applied. Evaluation of multiple parameters may be desirable in specific patients, for instance in patients whose annular dimensions are in the overlapping/borderzone prosthesis size recommendations. Multiphase assessment providing knowledge on the amount of annular distensibility may also be helpful in choosing the most optimal size in these patients.

Furthermore, the change in dimensions of the aortic annulus seems to urge the use of three-dimensional techniques for accurate annulus size assessment. *Table 7* provides an overview of current imaging modalities used for annulus measurements. An advantage of CT is that it provides an overview of the cardiac anatomy and calcifications present which may impact prosthesis size selection in borderzone patients[37]. TEE might be a helpful three-dimensional modality in patients not eligible for contrast-enhanced CT imaging[37-39]. However, compared with CT measurements 3D-TEE consistently displayed smaller dimensions, which may cause significant undersizing[38, 39]. Two-dimensional TEE showed even more undersizing compared with CT-based sizing[39]. Hence, the use of three-dimensional imaging modalities and CT in particular seems indispensable to reduce potential sizing error.

Table 7 | Imaging modalities

	Benefits	Drawbacks
2D-TTE	Non-invasive	Operator dependent
	Readily available and portable	Two-dimensional assessment
	No contrast agent required	Image quality limited (acoustic shadowing, obesity, chronic obstructive pulmonary disease)
2D-TEE	High spatial resolution	Semi-invasive
	No contrast agent required	Operator dependent
	Intra-operative use possible	Two-dimensional assessment
		Possible complications
		Might require sedation
		Specific contraindications (esophageal disease)
3D-TEE	Three-dimensional assessment	Semi-invasive
	No contrast agent required	Operator dependent
	Intra-operative use possible	Possible complications
		Might require sedation
		Specific contraindications (esophageal disease)
CT	High spatial resolution	Contrast agent required
	Non-invasive	Radiation exposure
	Three-dimensional assessment	Heart rate control may be required
	Short acquisition time	Specific contraindications (pregnancy, impaired renal function, contrast allergy)
	Anatomic overview	
	Allows calcium (distribution) assessment	
MRI	High contrast resolution	Long acquisition time
	Non-invasive	Patient breath-holding
	Three-dimensional assessment	Specific contraindications (claustrophobia, metal implants, pacemakers, hemodynamic instability)
	Anatomic overview	

Patient post-procedural outcome has often been related to the presence of relevant paravalvular regurgitation, although the direct association with mortality yet needs to be evaluated[40]. One of the key factors in paravalvular regurgitation is the relation with prosthesis oversizing and undersizing[28, 30, 41]. The purpose of this review was to assess whether the aortic annulus undergoes significant dynamic change and its possible implications for prosthesis size selection. Currently, TAVI prostheses are available in four sizes (23, 26, 29 and 31mm) for annular sizes of 18-29mm and the prosthesis size recommendations overlap for annulus dimensions. Results showed the systolic short axis diameter to differ significantly by (mean) 0.75mm minimum[17] to 2.7±1.6mm maximum[33] from the diastolic diameter. Maximal differences within the cycle ranged to even 8.7mm in Peng et al[36]. With little annular change, the impact on TAVI sizing may be small as was the case in the study of Bertaso et al[17]. With greater annular deformations, diastolic sizing can lead to a relevant change in prosthetic size selection, as 20% of patients in the study of Willson et al. received a smaller prosthesis[30]. The conformational change of the annulus showed to impact the annulus to prosthesis agreement[35], consequently it also may result in (undesired) oversizing or undersizing and thus in paravalvular leakage. Remarkably, one study found significantly less conformational change of the annulus in patients with clinically relevant paravalvular leakage, showing a mean area deformation of 32±10mm^2 versus 46±21mm^2 (P=0.003) in non-leakage patients and perimeter deformation of 2.6±0.8mm versus 3.6±1.3mm (P=0.001), respectively[42]. For paravalvular leakage prediction the same study showed 74% sensitivity and 72% specificity for conformational changes of less than 3mm in annular perimeter. Prosthesis to annular perimeter size ratio and annular calcifications were also independent predictors for paravalvular leakage.

As shown in this review, results vary remarkably between specific studies. The reported mean percentage change ranges from 4 to 28% for area, 2 to 12% for minimal diameter and 0.56 to 7.3% perimeter. Evidently, the heterogeneity between studies is substantial and likely accounts for the observed ranges. Significant differences are present for both study methods and patient characteristics. With regard to the first, study sample size and imaging modality may affect study results just like the assessment of two predefined versus all cardiac phases and manual versus semi-automatic measurements. Second, patient age, gender and degree and/or definition of stenosis differ between studies. The impact of gender on the amount of conformational change has not been evaluated and only one study reported on the effect of age without significant differences. No consensus exists on whether the annular conformational changes vary between AS patients and

non-AS patients. Furthermore, patients with aortic root calcifications in general did not show significant differences with the control group, whereas significant differences were found for annular area related to the distribution of calcifications[32]. More research and larger study samples are needed to provide basic insight on various potential factors affecting the annular distensibility and conformational changes. As for TAVI sizing and patient outcome, it is essential to take the dynamic deformation into consideration by selecting the optimal imaging modality, cardiac phase and annular parameter. Based on this review we can conclude that three-dimensional imaging is required for adequate annulus assessment. Despite its well-known drawbacks, CT provides the most comprehensive overview of cardiac structures and optimal imaging plane reconstructions and hence allows for reliable assessment of all annular dimensions. The use of two-dimensional imaging modalities on the other hand may lead to relevant prosthesis undersizing. Furthermore, selection of the cardiac phase in which the annulus shows the largest dimensions seems to prevent (theoretical) prosthesis undersizing, but the maximal phase is patient specific. Future studies are required to evaluate the effect of the use of different annular parameters on patient outcome and to prospectively assess the clinical impact of sizing based on different cardiac phases.

Limitations

In this study we did not take the effect of semiautomatic or manual measurements into account. Secondly, variability in the definition of annulus might impact study results, although the majority of included studies (76%) used the same definition. Thirdly, published results lack data on paired intra-patient analyses to be able to assess differences on patient level. Lumping the mean overall systolic and diastolic diameters reported will not provide the mean difference within patients. Hence, insufficient data was available to perform a meta-analysis to acquire the pooled difference for mean change of the annulus within the cardiac cycle. Lastly, evaluation of the accuracy of annulus measurements using different imaging modalities in comparison with true intraoperative measurements was beyond the scope of this review.

REFERENCES

1. Go AS, Mozaffarian D, Roger VL, Benjamin EJ, Berry JD, Blaha MJ, et al. Heart disease and stroke statistics--2014 update: A report from the american heart association. *Circulation*. 2014;129:e28-e292
2. Bach DS. Prevalence and characteristics of unoperated patients with severe aortic stenosis. *J Heart Valve Dis*. 2011;20:284-291
3. Kodali SK, Williams MR, Smith CR, Svensson LG, Webb JG, Makkar RR, et al. Two-year outcomes after transcatheter or surgical aortic-valve replacement. *N Engl J Med*. 2012;366:1686-1695
4. Toggweiler S, Humphries KH, Lee M, Binder RK, Moss RR, Freeman M, et al. 5-year outcome after transcatheter aortic valve implantation. *J Am Coll Cardiol*. 2013;61:413-419
5. Jerez-Valero M, Urena M, Webb JG, Tamburino C, Munoz-Garcia AJ, Cheema A, et al. Clinical impact of aortic regurgitation after transcatheter aortic valve replacement: Insights into the degree and acuteness of presentation. *JACC Cardiovasc Interv*. 2014;7:1022-1032
6. Chrysohoou C, Hayek SS, Spilias N, Lerakis S. Echocardiographic and clinical factors related to paravalvular leak incidence in low-gradient severe aortic stenosis patients post-transcatheter aortic valve implantation. *Eur Heart J Cardiovasc Imaging*. 2015;16:558-563
7. O'Sullivan KE, Gough A, Segurado R, Barry M, Sugrue D, Hurley J. Is valve choice a significant determinant of paravalular leak post-transcatheter aortic valve implantation? A systematic review and meta-analysis. *Eur J Cardiothorac Surg*. 2014;45:826-833
8. Tops LF, Wood DA, Delgado V, Schuijf JD, Mayo JR, Pasupati S, et al. Noninvasive evaluation of the aortic root with multislice computed tomography implications for transcatheter aortic valve replacement. *JACC Cardiovasc Imaging*. 2008;1:321-330
9. Messika-Zeitoun D, Serfaty JM, Brochet E, Ducrocq G, Lepage L, Detaint D, et al. Multimodal assessment of the aortic annulus diameter: Implications for transcatheter aortic valve implantation. *J Am Coll Cardiol*. 2010;55:186-194
10. de Heer LM, Budde RP, Mali WP, de Vos AM, van Herwerden LA, Kluin J. Aortic root dimension changes during systole and diastole: Evaluation with ecg-gated multidetector row computed tomography. *Int J Cardiovasc Imaging*. 2011;27:1195-1204
11. Albano AJ, Mitchell E, Pape LA. Standardizing the method of measuring by echocardiogram the diameter of the ascending aorta in patients with a bicuspid aortic valve. *Am J Cardiol*. 2010;105:1000-1004
12. van Prehn J, Vincken KL, Muhs BE, Barwegen GK, Bartels LW, Prokop M, et al. Toward endografting of the ascending aorta: Insight into dynamics using dynamic cine-cta. *J Endovasc Ther*. 2007;14:551-560
13. De Paulis R, De Matteis GM, Nardi P, Scaffa R, Buratta MM, Chiariello L. Opening and closing characteristics of the aortic valve after valve-sparing procedures using a new aortic root conduit. *Ann Thorac Surg*. 2001;72:487-494
14. Shiran A, Adawi S, Ganaeem M, Asmer E. Accuracy and reproducibility of left ventricular outflow tract diameter measurement using transthoracic when compared with transesophageal echocardiography in systole and diastole. *Eur J Echocardiogr*. 2009;10:319-324
15. Tsang W, Veronesi F, Sugeng L, Weinert L, Takeuchi M, Jeevanandam V, et al. Mitral valve dynamics in severe aortic stenosis before and after aortic valve replacement. *J Am Soc Echocardiogr*. 2013;26:606-614

16. Veronesi F, Corsi C, Sugeng L, Mor-Avi V, Caiani EG, Weinert L, et al. A study of functional anatomy of aortic-mitral valve coupling using 3d matrix transesophageal echocardiography. *Circ Cardiovasc Imaging*. 2009;2:24-31
17. Bertaso AG, Wong DT, Liew GY, Cunnington MS, Richardson JD, Thomson VS, et al. Aortic annulus dimension assessment by computed tomography for transcatheter aortic valve implantation: Differences between systole and diastole. *Int J Cardiovasc Imaging*. 2012;28:2091-2098
18. Burman ED, Keegan J, Kilner PJ. Aortic root measurement by cardiovascular magnetic resonance: Specification of planes and lines of measurement and corresponding normal values. *Circ Cardiovasc Imaging*. 2008;1:104-113
19. Wood DA, Tops LF, Mayo JR, Pasupati S, Schalij MJ, Humphries K, et al. Role of multislice computed tomography in transcatheter aortic valve replacement. *Am J Cardiol*. 2009;103:1295-1301
20. Kazui T, Izumoto H, Yoshioka K, Kawazoe K. Dynamic morphologic changes in the normal aortic annulus during systole and diastole. *J Heart Valve Dis*. 2006;15:617-621
21. Zhu D, Zhao Q. Dynamic normal aortic root diameters: Implications for aortic root reconstruction. *Ann Thorac Surg*. 2011;91:485-489
22. Izumi C, Miyake M, Takahashi S, Hayashi H, Miyanishi T, Matsutani H, et al. Usefulness of real-time three-dimensional echocardiography in evaluating aortic root diameters during a cardiac cycle. *J Echocardiogr*. 2012;10:8-14
23. Yoshikawa H, Suzuki M, Hashimoto G, Kusunose Y, Otsuka T, Hara H, et al. Assessment of cyclic changes in the diameter of the aortic annulus using speckle-tracking trans-esophageal echocardiography. *Ultrasound Med Biol*. 2013;39:2084-2090
24. de Heer LM, Budde RP, van Prehn J, Mali WP, Bartels LW, Stella PR, et al. Pulsatile distention of the nondiseased and stenotic aortic valve annulus: Analysis with electrocardiogram-gated computed tomography. *Ann Thorac Surg*. 2012;93:516-522
25. Jilaihawi H, Kashif M, Fontana G, Furugen A, Shiota T, Friede G, et al. Cross-sectional computed tomographic assessment improves accuracy of aortic annular sizing for transcatheter aortic valve replacement and reduces the incidence of paravalvular aortic regurgitation. *J Am Coll Cardiol*. 2012;59:1275-1286
26. Tsang W, Meineri M, Hahn RT, Veronesi F, Shah AP, Osten M, et al. A three-dimensional echocardiographic study on aortic-mitral coupling in transcatheter aortic valve replacement. *Eur Heart J Cardiovasc Imaging*. 2013;14:950-956
27. Bolen MA, Popovic ZB, Dahiya A, Kapadia SR, Tuzcu EM, Flamm SD, et al. Prospective ecg-triggered, axial 4-d imaging of the aortic root, valvular, and left ventricular structures: A lower radiation dose option for preprocedural tavr imaging. *J Cardiovasc Comput Tomogr*. 2012;6:393-398
28. Lehmkuhl L, Foldyna B, Von Aspern K, Lucke C, Grothoff M, Nitzsche S, et al. Inter-individual variance and cardiac cycle dependency of aortic root dimensions and shape as assessed by ecg-gated multi-slice computed tomography in patients with severe aortic stenosis prior to transcatheter aortic valve implantation: Is it crucial for correct sizing? *Int J Cardiovasc Imaging*. 2013;29:693-703
29. Pontone G, Andreini D, Bartorelli AL, Annoni A, Mushtaq S, Bertella E, et al. Feasibility and accuracy of a comprehensive multidetector computed tomography acquisition for patients referred for balloon-expandable transcatheter aortic valve implantation. *Am Heart J*. 2011;161:1106-1113

30. Willson AB, Webb JG, Freeman M, Wood DA, Gurvitch R, Thompson CR, et al. Computed tomography-based sizing recommendations for transcatheter aortic valve replacement with balloon-expandable valves: Comparison with transesophageal echocardiography and rationale for implementation in a prospective trial. *J Cardiovasc Comput Tomogr*. 2012;6:406-414
31. Martin R, Hascoet S, Dulac Y, Peyre M, Mejean S, Hadeed K, et al. Comparison of two- and three-dimensional transthoracic echocardiography for measurement of aortic annulus diameter in children. *Arch Cardiovasc Dis*. 2013;106:492-500
32. Shabestari A, Pourghorban R, Tehrai M, Pouraliakbar H, Faghihi Langroudi T, Bakhshandeh H, et al. Comparison of aortic root dimension changes during cardiac cycle between the patients with and without aortic valve calcification using ecg-gated 64-slice and dual-source 256-slice computed tomography scanners: Results of a multicenter study. *Int J Cardiovasc Imaging*. 2013;29:1391-1400
33. Hamdan A, Guetta V, Konen E, Goitein O, Segev A, Raanani E, et al. Deformation dynamics and mechanical properties of the aortic annulus by 4-dimensional computed tomography: Insights into the functional anatomy of the aortic valve complex and implications for transcatheter aortic valve therapy. *J Am Coll Cardiol*. 2012;59:119-127
34. Lehmkuhl LH, von Aspern K, Foldyna B, Grothoff M, Nitzsche S, Kempfert J, et al. Comparison of aortic root measurements in patients undergoing transapical aortic valve implantation (ta-avi) using three-dimensional rotational angiography (3d-ra) and multislice computed tomography (msct): Differences and variability. *Int J Cardiovasc Imaging*. 2013;29:417-424
35. Blanke P, Russe M, Leipsic J, Reinohl J, Ebersberger U, Suranyi P, et al. Conformational pulsatile changes of the aortic annulus: Impact on prosthesis sizing by computed tomography for transcatheter aortic valve replacement. *JACC Cardiovasc Interv*. 2012;5:984-994
36. Peng LQ, Yang ZG, Yu JQ, Chu ZG, Deng W, Shao H. Dynamic assessment of aortic annulus in patients with aortic stenosis throughout cardiac cycle with dual-source computed tomography. *Int J Cardiol*. 2012;158:304-307
37. Husser O, Holzamer A, Resch M, Endemann DH, Nunez J, Bodi V, et al. Prosthesis sizing for transcatheter aortic valve implantation--comparison of three dimensional transesophageal echocardiography with multislice computed tomography. *Int J Cardiol*. 2013;168:3431-3438
38. Jilaihawi H, Doctor N, Kashif M, Chakravarty T, Rafique A, Makar M, et al. Aortic annular sizing for transcatheter aortic valve replacement using cross-sectional 3-dimensional transesophageal echocardiography. *J Am Coll Cardiol*. 2013;61:908-916
39. Ng AC, Delgado V, van der Kley F, Shanks M, van de Veire NR, Bertini M, et al. Comparison of aortic root dimensions and geometries before and after transcatheter aortic valve implantation by 2- and 3-dimensional transesophageal echocardiography and multislice computed tomography. *Circ Cardiovasc Imaging*. 2010;3:94-102
40. Genereux P, Head SJ, Hahn R, Daneault B, Kodali S, Williams MR, et al. Paravalvular leak after transcatheter aortic valve replacement: The new achilles' heel? A comprehensive review of the literature. *J Am Coll Cardiol*. 2013;61:1125-1136
41. Willson AB, Webb JG, Labounty TM, Achenbach S, Moss R, Wheeler M, et al. 3-dimensional aortic annular assessment by multidetector computed tomography predicts moderate or severe paravalvular regurgitation after transcatheter aortic valve replacement: A multicenter retrospective analysis. *J Am Coll Cardiol*. 2012;59:1287-1294

42. Masri A, Schoenhagen P, Svensson L, Kapadia SR, Griffin BP, Tuzcu EM, et al. Dynamic characterization of aortic annulus geometry and morphology with multimodality imaging: Predictive value for aortic regurgitation after transcatheter aortic valve replacement. *J Thorac Cardiovasc Surg*. 2014;147:1847-1854
43. Otani K, Takeuchi M, Kaku K, Sugeng L, Yoshitani H, Haruki N, et al. Assessment of the aortic root using real-time 3d transesophageal echocardiography. *Circ J*. 2010;74:2649-2657
44. Kempfert J, Van Linden A, Lehmkuhl L, Rastan AJ, Holzhey D, Blumenstein J, et al. Aortic annulus sizing: Echocardiographic versus computed tomography derived measurements in comparison with direct surgical sizing. *Eur J Cardiothorac Surg*. 2012;42:627-633

SUPPLEMENTARY MATERIAL

Appendix 1.

Search strategy performed in Pubmed* and Embase† on June 25th, 2014	
#1:	Imaging OR CT OR CTs OR 'computer tomography' OR 'computed tomography' OR 'computerized tomography' OR 'CAT scan' OR 'CAT scans' OR MDCT OR MSCT OR CTA OR 'computer assisted tomography' OR 'computed assisted tomography' OR 'magnetic resonance imaging' OR 'magnetic resonance' OR MRI OR MR OR NMR OR NMRI OR CMR OR echocardiographies OR echocardiography OR TTE OR TEE OR ultrasound OR ultrasonographies OR ultrasonography OR ultrasonic OR echography OR echographies OR echotomography OR echotomographies
#2:	'aortic annulus' OR 'aortic annular' OR 'aortic root' OR TAVI OR TAVR OR 'transcatheter valve' OR 'percutaneous valve' OR 'transcatheter aortic valve' OR 'percutaneous aortic valve'
#3:	(#1 AND #2)

* In Title/Abstract

† In Title/Abstract: no conference abstract, letter, note or editorial

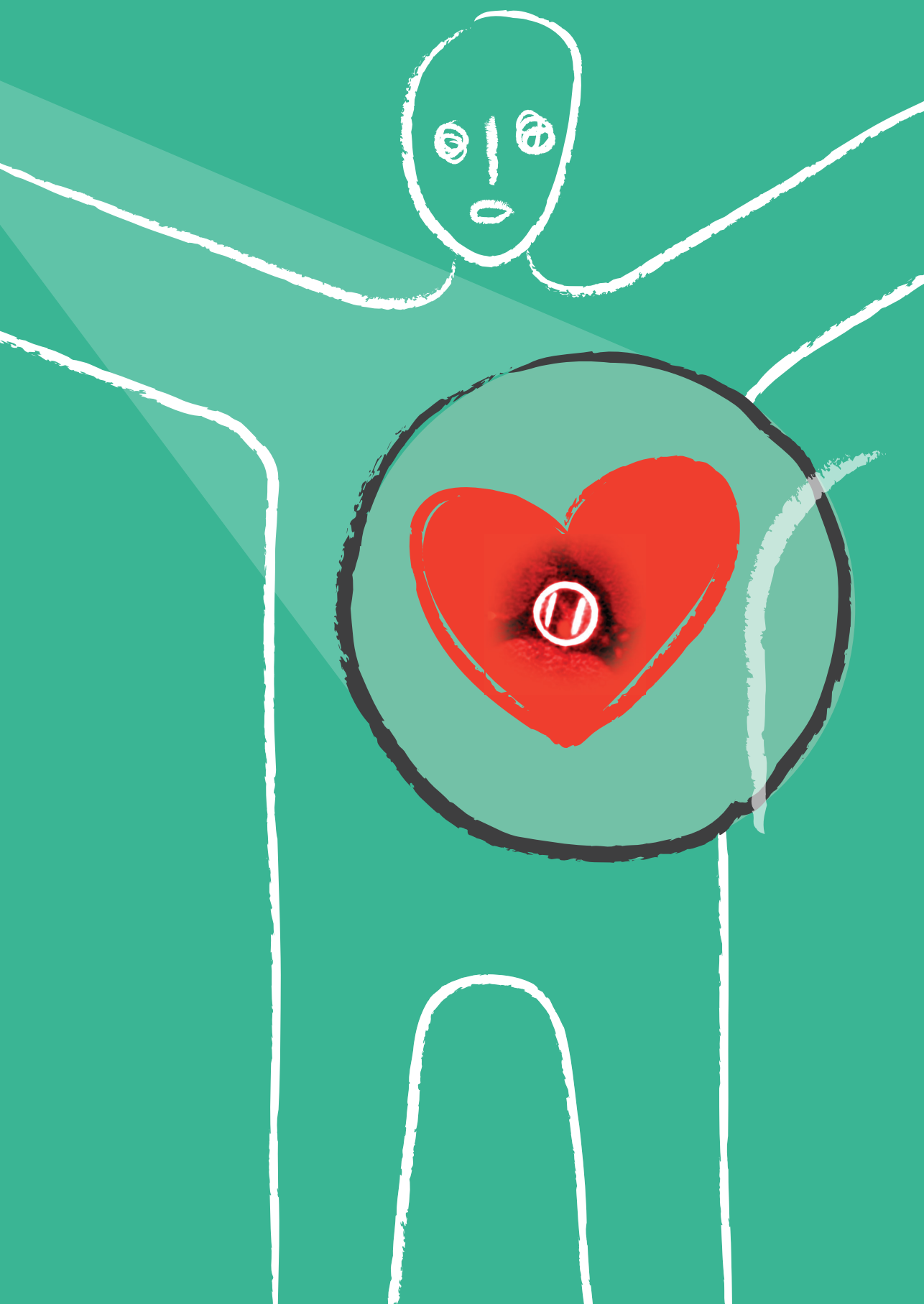

CHAPTER 7

Baseline MDCT findings after prosthetic heart valve implantation provide important complementary information to echocardiography for follow-up purposes

Dominika Suchá
Steven A.J. Chamuleau
Petr Symersky
Matthijs F.L. Meijs
Renee B.A. van den Brink
Bas A.J.M. de Mol
Willem P. Th. M. Mali
Jesse Habets
Lex A. van Herwerden
Ricardo P.J. Budde

Published in European Radiology, 2015

ABSTRACT

PURPOSE

Recent studies have proposed additional multidetector-row CT (MDCT) for prosthetic heart valve (PHV) dysfunction. References to discriminate physiological from pathological conditions early after implantation are lacking. We present baseline MDCT findings of PHVs six weeks post-implantation.

METHODS

Patients were prospectively enrolled and TTE was performed according to clinical guidelines. 256-MDCT images were systematically assessed for leaflet excursions, image quality, valve-related artifacts, pathological and additional findings.

RESULTS

Forty-six patients were included comprising 33 mechanical and 16 biological PHVs. Overall, MDCT image quality was good and relevant regions remained reliably assessable despite mild-moderate PHV-artifacts. MDCT detected three unexpected valve related pathology cases: (1) prominent subprosthetic tissue, (2) pseudoaneurysm and (3) extensive pseudoaneurysms and valve dehiscence. The latter patient required redo valve surgery. TTE only showed trace periprosthetic regurgitation, and no abnormalities in the other cases. Additional findings were: tilted aortic PHV position (n=3), pericardial hematoma (n=3) and pericardial effusion (n=3). Periaortic induration was present in 33/40 (83%) aortic valve patients.

CONCLUSIONS

MDCT allowed evaluation of relevant PHV regions in all valves, revealed baseline postsurgical findings and, despite normal TTE findings, detected three cases of unexpected, clinically relevant pathology.

INTRODUCTION

Current cardiology guidelines recommend transthoracic echocardiography (TTE) six to twelve weeks after valve replacement surgery as a baseline for adequate patient follow-up[1, 2]. For mechanical valves, TTE is only repeated in case of suspected dysfunction whereas for biological valves annual TTE assessment should be planned after the first five years[1]. As additional modalities for the evaluation of prosthetic valve dysfunction, transesophageal echocardiography and cinefluoroscopy are advised. However, these imaging modalities often cannot identify the cause of obstruction or the extent of endocarditis related pathology[3, 4]. Several preliminary studies have shown the incremental value of ECG-gated multidetector-row computed tomography (MDCT) for the evaluation of patients with prosthetic heart valves (PHV)[4-8]. Recently, MDCT was added to the American College of Cardiology and European Society of Cardiology guidelines as a potential additional imaging modality for patients with suspected PHV thrombus[1, 2], pannus[1] or endocarditis[2]. Before MDCT can be fully implemented in daily clinical practice, it is essential to be able to discriminate normal from pathological conditions. As proposed with TTE imaging, follow-up results should be compared to the acquired baseline references[1]. Currently, normal references for MDCT findings early after PHV implantation are lacking. The purpose of this study was to evaluate the baseline MDCT imaging characteristics six weeks after PHV implantation and report incidental pathological findings.

METHODS

Study sample

A prospective study was conducted to acquire standardized TTE and MDCT images six weeks after PHV implantation. Patients were consecutively enrolled between June 2010 and September 2013 after surgical aortic or mitral heart valve replacement in the University Medical Center Utrecht and Academic Medical Center Amsterdam, the Netherlands. The inclusion criterion was successful implantation of one of the common surgical PHV types of the participating institutions: St. Jude Medical, Sorin Carbomedics, ON-X, Sorin Bicarbon, Carpentier-Edwards Perimount or Sorin Mitroflow. Exclusion criteria consisted of (1) known allergy to contrast media, (2) other contraindications for contrast use such as an estimated glomerular filtration rate <60 ml/min/1.73m^2, (3) contraindication for MDCT imaging, (4) possible pregnancy and (5) refusal to be informed about additional MDCT findings. This study was approved by the Institutional Review Board and all patients gave written informed consent before inclusion.

TTE imaging and analysis

TTE was performed on the principal investigation site (Utrecht) six weeks after implantation according to routine follow-up guidelines and by using standard clinical echocardiographic equipment. Images were evaluated by one independent observer (MM; cardiologist) with five years' experience in cardiac imaging. A second observer (SC; imaging cardiologist) with eight years' experience in PHV imaging evaluated all cases of abnormalities and pathological findings for a consensus score. Both observers were blinded for MDCT results. PHV assessment was conducted according to the guidelines[1, 9] and included measurements of the mean and peak transprosthetic gradients, velocity time integrals (VTI), calculation of effective orifice area (EOA) and evaluation of regurgitation. The VTI was measured through the left ventricular outflow tract (LVOT) and across the PHV (aortic or mitral). The EOA was calculated using the LVOT diameter and Doppler continuity equation for all PHVs[10, 11], as the pressure half-time method is not preferred in mitral PHVs[9]. Available guidelines specified per PHV manufacturer and PHV size were used as reference[9]. Periprosthetic regurgitation was scored on a visual scale as none, trace, mild, moderate or severe. Prosthetic regurgitation was scored as normal for PHV, trace, mild, moderate or severe. Additional (pathological) findings were reported. Left ventricular function was measured on available 3D full volume dataset, or 2D images by the Simpson biplane method and scored as normal (>55%), mild dysfunction (45-55%), moderate dysfunction (30-45%) or severe dysfunction (<30%). If measurements were not possible, the left ventricular function was estimated.

MDCT imaging

MDCT images were acquired on the same day as TTE imaging using a 256-slice MDCT scanner (iCT, Philips Healthcare, Best, The Netherlands). The acquisition protocol consisted of a non-enhanced prospectively ECG-triggered acquisition of the PHV region with the following parameters: collimation 128 x 0.625 mm, gantry rotation time 270 ms, tube voltage 120 kV and tube current-time product 30 mAs. For contrast-enhanced imaging a triphasic injection protocol was applied using iodinated contrast agent (Ultravist 300mg/ml; Bayer Healthcare Pharmaceutical Inc.). First, the contrast agent was administered followed by a mixture of contrast agent and saline in 30/70 ratio, respectively and a saline flush at last (mean flow rate 6-6.7 cc/s). Flow and volume injection were weight dependent and a threshold of 100 Hounsfield units in the descending aorta was used for acquisition. No beta-blockers were administered for heart rate control. The contrast-enhanced

retrospectively ECG-gated acquisition of the cardiac region was performed according to the following protocol: collimation 128 x 0.625 mm, gantry rotation time 270 or 330 ms, pitch 0.16 or 0.18, tube voltage 120 kV and tube current-time product 600 or 700 mAs. The rotation time and pitch were dependent on the heart rate (<62, 62-72 or >72 beats per minute; bpm) and the tube current-time product on the patients' body weight (65-80 or >80 kg). Images were reconstructed at each 10% phase of the RR-interval with a 0.45 increment and 0.9 mm slice thickness. The dose-length product (mGy*cm) extracted from the MDCT dose reports and the conversion factor for adult chest MDCT examinations (0.0145 mSv/mGy*cm) were multiplied to acquire the effective per patient radiation dose (mSv)[12].

MDCT analysis

Images were analyzed on a dedicated workstation (Extended Brilliance Workstation v4.5, Philips Healthcare, Best, The Netherlands). For each PHV, the best systolic and diastolic imaging phase was selected. Both phases were used to assess the image quality, PHV-related artifacts and leaflet motion. Image quality and PHV-related artifacts were assessed for five PHV-related regions as published previously[13, 14]: the supraprosthetic, periprosthetic, subprosthetic, prosthetic and valve leaflet region. Image quality was scored on a 4-point scale as follows: (1) non-diagnostic with no discernible detail widely beyond the prosthesis, (2) moderate with no details <5mm of the prosthesis, (3) good with some structure details <5mm of the prosthesis and (4) excellent visualization with perfect structure details. PHV-related artifacts were scored as: (1) virtually none, (2) mild artifacts <5mm beyond the prosthesis, (3) moderate artifacts >5mm beyond the prosthesis and (4) severe artifacts beyond the border of the valve chamber. For mechanical PHVs, the leaflet opening and closing angles were measured[15] and cine images reconstructed for evaluation of symmetrical leaflet excursions. Pericardial effusion was evaluated and scored as physiologic, mild or moderate. The fat tissue surrounding the aorta and aortic PHVs was assessed and tissue induration was reported when present. Polytetrafluoroethylene felt pledgets implanted during valve surgery were reported when visible. All PHVs were systematically evaluated and scored for unexpected pathology such as thrombus, pannus, vegetations, mycotic aneurysms, biological leaflet thickening, pseudoaneurysms, PHV dehiscence and PHV angulation in relation to the LVOT axis. For all patients possible additional findings were reported as well. One observer (DS) with two years' experience in PHV imaging performed all MDCT measurements independently. Image quality, artifacts and pathology were assessed by a second observer (RB) with seven years' experience additionally for a consensus score. Both observers were blinded for TTE results.

Statistical analysis

For analysis of the acquired data descriptive statistics were applied using SPSS version 20.0 for Windows. As measures of central tendency and dispersion, the mean ± standard deviation (SD) or median [interquartile range; IQR] are provided, based on the data distribution. For summary statistics the number and percentage are provided.

RESULTS

A total of 68 patients were consecutively included after valve surgery. Of these, 16 patients decided upon study withdrawal at six weeks, one patient died, one patient showed an impaired renal function, one patient underwent MDCT for clinical reasons and three patients were excluded because of imaging protocol violation. Hence, 46 patients with 49 valves were included. Patient characteristics are presented in *Table 1*. Median time between valve replacement surgery and TTE/MDCT imaging was 44 days [IQR 41-52]. TTE and MDCT examinations were performed on the same day in 45 patients and with an interval of two days in one patient.

TTE

The mean heart rate during TTE examinations was 74 ± 16 bpm. Six of 46 patients had atrial fibrillation during examination. Left ventricular ejection fraction was normal in 30 patients, showed mild dysfunction in seven patients, moderate dysfunction in six and severe dysfunction in three patients. Mean EOA was 2.00 ± 0.64 for aortic and 2.05 ± 0.41 for mitral PHVs. An overview of all TTE results on PHV assessment is presented in *Table 2*. One patient with a Carbomedics 27mm PHV showed mild to moderate prosthetic regurgitation but this was considered clinically insignificant. Hence, TTE results on prosthetic and periprosthetic regurgitation did not show any pathological findings requiring short-term interventions. Pericardial effusion was not present or scored as physiologic (<2 mm) in 42 patients on TTE imaging at six weeks. One patient showed pericardial effusion of 7 mm and three patients had greater pericardial effusion (12, 12 and 13 mm). An example of good quality TTE images for a biological and mechanical PHV is presented in *Figure 1*.

MDCT

The mean effective radiation dose was 11.3 ± 1.1 mSv. Heart rate during MDCT examinations was known in 38/46 patients and was 72 ± 16 bpm (mean ± SD). Two patients showed arrhythmias during MDCT acquisition, 36 patients had a normal sinus rhythm. The optimal MDCT reconstructions were 30%-40% systolic and 75%-

Table 1 | Patient characteristics at baseline

Study subjects	Patients N= 46	
Age, mean ± SD	61 ± 12	
Male, n (%)	37 (80%)	
Prior myocardial infarction	1 (2%)	
Prior cardiac surgery	8 (17%)	
BMI, mean ± SD	27.3 ± 4.8	
BSA	1.98 ± 0.22	
Concomitant bypass surgery	10 (22%)	
Concomitant other procedure	15 (33%)	
Medication at discharge		
Vitamin K antagonists	43 (94%)	
Antiplatelet drugs	16 (35%)	
Rate control drugs	39 (85%)	
PHV type implanted, n (%)	Aortic, N=40 (82%)	Mitral, N=9 (18%)
St. Jude Medical	8 (20%)	4 (44%)
Carbomedics	11 (28%)	1 (11%)
ON-X	3 (8%)	2 (22%)
Sorin Bicarbon	3 (8%)	1 (11%)
Perimount (biological)	11 (28%)	1 (11%)
Mitroflow (biological)	4 (10%)	-
PHV size		
21 mm	2 (5%)	-
23 mm	18 (45%)	-
25 mm	13 (33%)	2 (22%)
27 mm	6 (15%)	2 (22%)
29 mm	1 (3%)	1 (11%)
31 mm	-	3 (33%)
33 mm	-	1 (11%)

BMI= body mass index; BSA= body surface area; PHV= prosthetic heart valve; SD= standard deviation

Table 2 | Transthoracic echocardiography results: patient characteristics six weeks after prosthetic valve implantation

TTE	Aortic PHV = 40	Mitral PHV = 9
Effective orifice area*, mean ± SD	2.00 ± 0.64	2.05 ± 0.41
Mean transprosthetic gradient, median [IQR]	9.4 [6.0-12.7]	5.8 [4.1-6.6]
Peak transprosthetic gradient	17.5 [12.2-27.1]	14.7 [7.7-17.4]
Periprosthetic regurgitation, n (%)		
None	38 (95%)	9 (100%)
Trace	1 (3%)	-
Mild	1 (3%)	-
Moderate	-	-
Severe	-	-
Prosthetic regurgitation		
Normal for PHV	38 (95%)	9 (100%)
Trace	1 (3%)	-
Mild	-	-
Moderate	1 (3%)	-
Severe	-	-

* Based on the Doppler continuity equation and measured left ventricular outflow tract diameter
† Graded according to clinical routine based on mean and peak gradients, EOA, cardiac output and available PHV type and size specific reference values.
PHV= prosthetic heart valve; TTE= transthoracic echocardiography

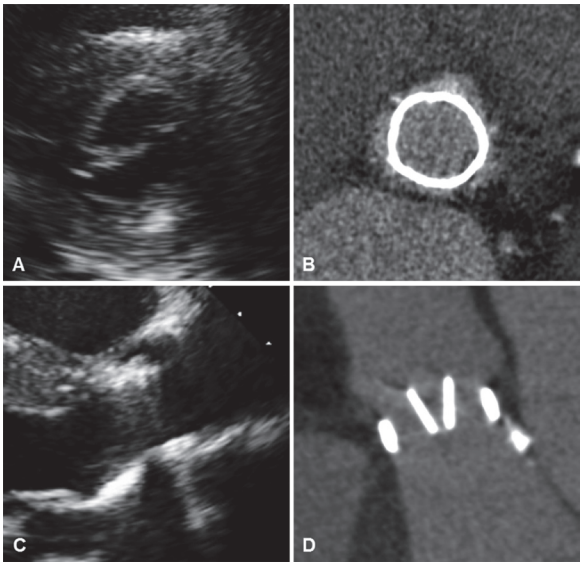

Figure 1 | Example of biological and mechanical prosthetic heart valve imaging. Transthoracic echocardiography images (A, C) and multidetector-row computed tomography images (B, D) of a normal functioning Perimount 25mm biological valve (A, B) and a normal functioning Carbomedics 23mm mechanical heart valve (C, D) in aortic position.

80%-90% diastolic phases (*Appendix 1*). Results on image quality and artifacts are presented in *Appendix 2* and *Appendix 3*, classified by manufacturer and anatomic region. For aortic valves in general, moderate artifacts and image quality were found for the periprosthetic region, and good image quality with only mild artifacts for the other regions. For mitral valves, mild to moderate artifacts with moderate to good image quality were present for the periprosthetic, subprosthetic and prosthetic region and good image quality with mild artifacts for the supraprosthetic region. All mechanical valves showed good to excellent leaflet image quality whereas the biological Mitroflow and Perimount showed moderate and non-diagnostic leaflet image quality, respectively (*Figure 1*). Mechanical leaflet excursions are presented in *Table 3*. The differences in angles between both leaflets of one PHV were assessed and a maximal median difference of 4 degrees for opening and 7 degrees for closing angles was found. Leaflet motion as assessed on cine images showed symmetrical leaflet excursions in all (n=33) mechanical PHVs.

Additional findings

MDCT detected moderate pericardial effusion in three patients, the same patients as those detected by TTE. MDCT also showed a slight aortic PHV angulation in three patients. Prominent hematoma at periaortic and/or pericardial position were present in three patients (*Figure 2*). Most importantly, the periaortic fat tissue in patients after aortic valve replacement showed induration in 33 patients. Of those, two patients showed severe periaortic fat tissue induration (*Figure 2F*).

Pathology

MDCT found PHV-related pathology in three patients. First, MDCT detected prominent subprosthetic tissue in one patient with an aortic biological Perimount 23mm (*Figure 3*). Differential diagnosis was a retracted annulus, native valve remnant or small thrombus. Second, a pseudoaneurysm (approximately 22 x9 x13mm) was found on the supraprosthetic site near the former left and non-coronary cusp in a patient with an aortic biological Perimount 25mm, requiring follow-up (*Figure 4*).
In addition, a malignant coronary anomaly was revealed in this patient showing the right coronary artery (RCA) deriving from the left ostium and coursing between the aorta and pulmonary trunk. Since MDCT showed RCA tapering, clinical evaluation and cardiac stress testing was required. Third, MDCT detected extended pseudonaneurysm formation and valve dehiscence in a patient with an aortic mechanical St. Jude 23mm (*Figure 5*). This patient eventually had to undergo redo surgery. In this patient, TTE only detected a trace of periprosthetic regurgitation stated as clinically not relevant. After the MDCT-based diagnosis, the patient underwent additional multimodality imaging[16]. *Table 4* provides an overview of all PHV morphology as detected by MDCT.

Table 3 | MDCT mechanical valve leaflet angles as measured and compared to manufacturers' values

	Opening angles (degrees)*					Closing angles (degrees)*				
	Aortic	Δ leaflets†	Mitral	Δ leaflets†	MFR	Aortic	Δ leaflets†	Mitral	Δ leaflets†	MFR
St. Jude, 19-25mm	84 (82-88)	4 (1-6)	n/a	n/a	85	30 (26-34)	5 (3-7)	n/a	n/a	30
St. Jude, 27-31mm	85 (83-87)	2 (1-4)	83 (80-85)	3 (1-5)	85	23 (22-27)	3 (0-5)	23 (22-27)	2 (0-5)	25
Carbomedics	80 (72-82)	2 (0-3)	73 (72-74)	2 (-)	78	24 (20-28)	3 (0-7)	24 (22-27)	5 (-)	25
Sorin Bicarbon	79 (78-80)	1 (1)	78 (77-78)	1 (-)	80	21 (19-22)	1 (1-3)	20 (19-20)	1 (-)	20
On-X	79 (76-84)	4 (1-6)	76 (75-80)	4 (2-6)	90	40 (39-42)	1 (0-2)	40 (39-41)	1 (1)	40

* Median and total range (minimum-maximum) in degrees provided

† Median difference between the both leaflet angles of a specific PHV in each single patient

MDCT= multidetector-row computed tomography; MFR= manufacturer; n/a= not available

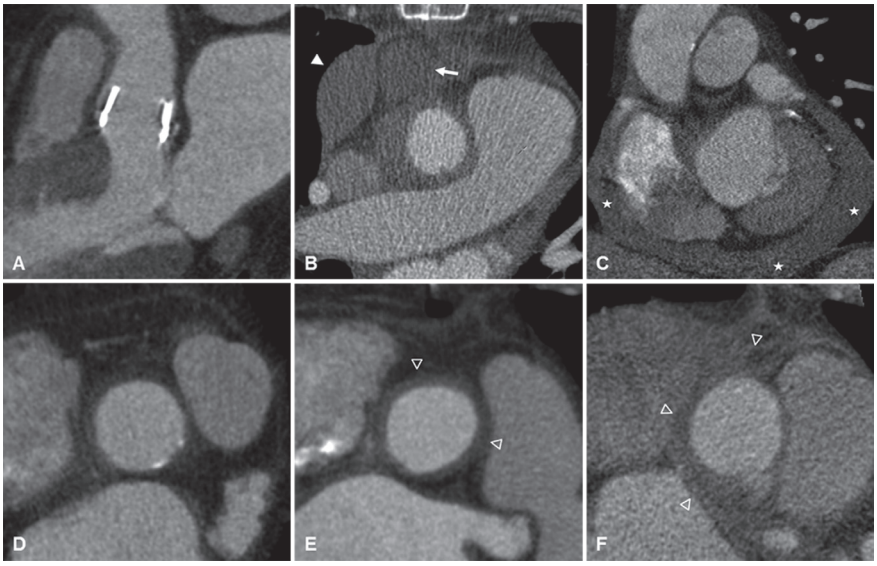

Figure 2 | Additional findings with multidetector-row computed tomography. A. Example of a patient with a slightly tilted position of an aortic Perimount prosthesis. B. Prominent pleural hematoma (35 Hounsfield Units; arrowhead) and pericardial hematoma (31 Hounsfield Units; arrow) in a patient six weeks after implantation of the aortic St. Jude valve. C. Prominent pericardial effusion (stars) at six weeks follow-up after biological Perimount implantation in the aortic position. D-F. MDCT images of the proximal ascending aorta in the short axis view in a patient without evident induration of the periaortic fat tissue (D), with moderate induration (E; empty arrowheads) and with severe induration of the periaortic tissue (F; empty arrowheads).

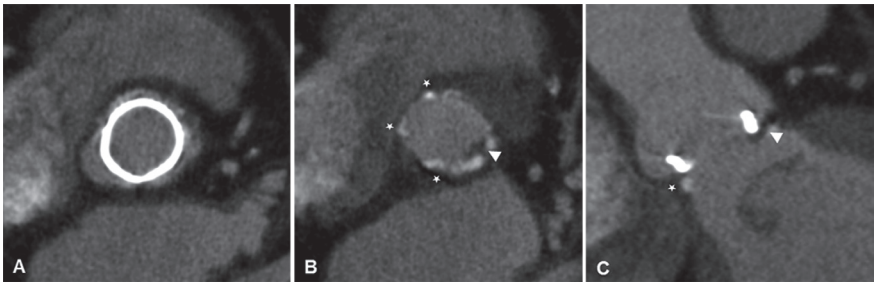

Figure 3 | Unexpected pathology detected with MDCT imaging. Multidetector-row computed tomography images (MDCT) of a 69-year old male patient six weeks after aortic Perimount 23mm implantation (A-C). Note the presence of the subprosthetic hypodense tissue (arrowhead) on both the in plane (B) and the perpendicular plane image (C). Differential diagnosis: retracted annulus, native valve remnant or small thrombus. Transthoracic echocardiography did not detect any abnormalities in this patient. The stars in the image indicate the present polytetrafluoroethylene felt pledgets.

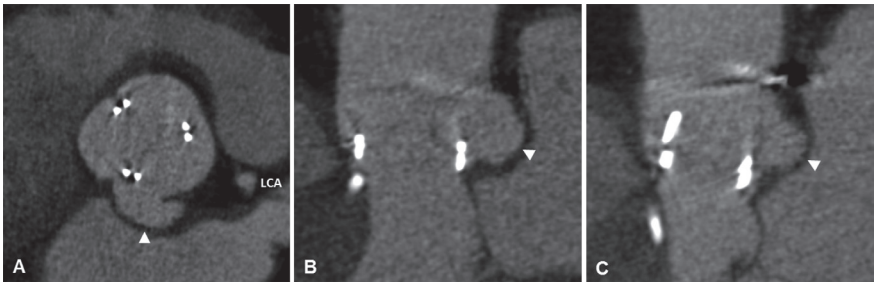

Figure 4 | Detection of a pseudoaneurysm. Multidetector-row computed tomography (MDCT) detected a pseudoaneurysm on the supraprosthetic site near the former left and non-coronary cusp in a 74-year old male patient six weeks after aortic Perimount 25mm implantation. The pseudoaneurysm (arrowheads) of approximately 22x 9x 13mm is presented on the in plane (A) and the perpendicular plane MDCT views (B, C). No pathology or periprosthetic regurgitation was found with transthoracic echocardiography. *LCA= left coronary artery.*

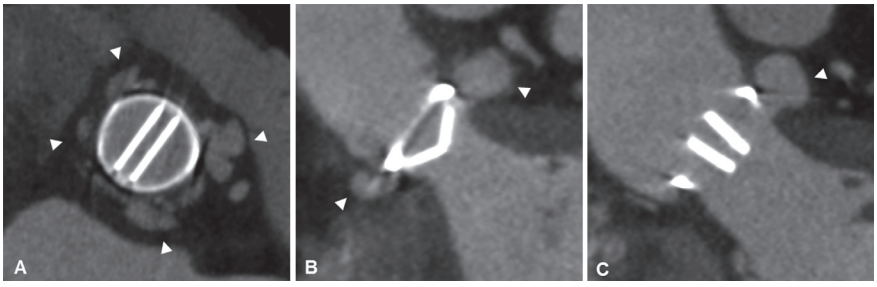

Figure 5 | Unexpected pathology requiring redo valve surgery. Fifty-one year old female patient after valve replacement surgery with the mechanical St. Jude 23mm prosthesis in aortic position. Multidetector-row computed tomography imaging (A-C) showed extended pseudoaneurysm formation (arrowheads) and valve dehiscence eventually requiring redo surgery. Transthoracic echocardiography detected only a trace of periprosthetic regurgitation, stated as clinically not relevant.

DISCUSSION

The current study demonstrates that MDCT is a feasible and valuable tool for PHV patient follow-up. We presented the baseline MDCT imaging characteristics and PHV morphology shortly after valve replacement surgery. The major finding was the detection of three cases of unexpected but clinically important valve related pathology that were missed by routine TTE imaging. Furthermore, MDCT showed that in the early postoperative stage 83% of aortic valve patients present induration of the periaortic fat tissue, which can be considered a normal finding at this stage. In this study, the presence of moderate valve-related artifacts did not hamper the image quality. Regions that are most relevant for clinical evaluation of PHV-related

Table 4 | Morphological prosthetic valve assessment by multidetector-row computed tomography

	Aortic PHV		Mitral PHV	
	Mechanical N=25	Biological N=15	Mechanical N=8	Biological N=1
Pledgets visible, n (%)	17 (68%)	12 (80%)	6 (75%)	1 (100%)
Periaortic fat tissue induration	22 (88%)	11 (73%)	n/a	n/a
Leaflet thickening	-	-	-	-
Thrombus	-	-	-	-
Subprosthetic tissue	-	1 (7%)	-	-
Vegetations	-	-	-	-
Abscesses	-	-	-	-
Pseudoaneurysms	1 (4%)	1 (7%)	-	-
Valve dehiscence	1 (4%)	-	-	-
Valve angulation*	1 (4%)	2 (13%)	-	-
Abnormal pericardial effusion	1 (4%)	2 (13%)	-	-
Pericardial hematoma	2 (8%)	1 (7%)	-	-

* to the left ventricular outflow tract axis
n/a= not applicable; PHV= prosthetic heart valve

pathology such as the periprosthetic and subprosthetic region remained visible and reliably assessable despite the presence of artifacts. In patients with a high body mass index (BMI), TTE imaging may be challenging and result in poor image quality whereas MDCT imaging may be hampered by higher image noise levels.
In this cohort though, mean BMI was 27.3 but did not preclude reliable MDCT assessment. Hence, MDCT imaging might be less affected by increased BMI than TTE imaging.
Leaflet motion can be evaluated with MDCT as demonstrated previously[15]. The maximal difference between the measured angles and manufacturer values was 15 degrees for the ON-X valve but only 6 degrees for all other mechanical valves. Although the leaflets of the ON-X valve are designed to open to 90 degrees, our study demonstrated a more reduced opening angle for this valve type in all patients, without any signs of dysfunction or elevated transprosthetic gradients.
This phenomenon has previously also been found using fluoroscopy in patients with aortic On-X valves[17] and in phantom setting in mitral ON-X valves[18]. For biological leaflets, Chenot et al. previously measured leaflet angles in a variety of biological valve types[5]. In our cohort, the leaflets of the biological Perimount valves

were not assessable. Whereas during follow-up the biological leaflets may thicken and become more visible, in normal setting early after implantation these leaflets showed too thin for MDCT assessment. Nevertheless, MDCT allowed assessment of both aortic and mitral valve leaflet angles while conventional fluoroscopy has shown significant problems in positioning the beam perpendicular to the valve leaflets in certain anatomical valve orientations[17, 19]. Another remarkable MDCT finding was the induration of the periaortic fat tissue in 83% of normal follow-up patients with aortic valves. In patients suspected of PHV endocarditis the appearance of this area is of paramount importance for diagnosis. Apparently, six weeks post uncomplicated aortic valve surgery, the periaortic fat tissue is still disturbed in the majority of patients and can be considered a normal baseline finding. However, it is not known how long this periaortic induration persists. In case of early postoperative endocarditis suspicion it might be difficult to distinguish a physiological state from pathological conditions based solely on the fat tissue's MDCT appearance. Further studies are needed to establish the duration of periaortic induration. In future setting, additional 18F-fluorodeoxyglucose positron emission tomography might possibly aid in the diagnostic work-up of endocarditis patients by showing increased metabolic uptake values[16].

Although TTE remains important for providing hemodynamic information, MDCT demonstrated several findings that were not detected by TTE. For example, MDCT found a tilted position of three aortic PHVs, which has been related to an increased transprosthetic gradient[4]. In patients with suspected PHV dysfunction MDCT may aid in diagnostic work-up by detecting a tilted position as the cause of obstruction. Furthermore, MDCT detected prominent subprosthetic tissue in one patient and a large pseudoaneurysm and malignant coronary anomaly in another patient. Above all, MDCT detected severe valve dehiscence requiring redo surgery while TTE only showed a trace of insignificant periprosthetic regurgitation. Thus, MDCT showed incremental value over echocardiography in the assessment of anatomical structures near the prosthesis and in the detection of related pathology such as pseudoaneurysms. Recently, we demonstrated the feasibility of MDCT for non-invasive coronary artery and bypass graft assessment in PHV dysfunction patients[20]. The incidental (pathological) findings in this study may need to be confirmed in larger series in order to assess their long-term significance and to clarify the role of MDCT as a screening modality. Because of the limitations of radiation exposure, screening with MDCT may only be possible with a certain amount of clinical suspicion. On the other hand, the utilization of dose reduction strategies such as iterative image reconstruction algorithms allows a far more widespread use of

MDCT. We did not incorporate these techniques in the current study. Prospectively ECG-triggered MDCT acquisitions may also save radiation exposure, but they do not provide dynamic information on leaflet excursions. As shown in this study, the optimal systolic and diastolic phases for PHV assessment differ substantially among patients. Hence, selecting the best phase in advance as required with prospectively triggered imaging can be very challenging.

A strength of this study is the prospective cohort. No selection was made based on clinical signs. Thus, a random sample of normal patients short after successful valve replacement surgery is presented. All patients underwent TTE and MDCT imaging in the same hospital center using the same devices and software in all patients. Furthermore, MDCT and TTE were performed on the same day in 98% of patients, thereby virtually excluding differences in results due to time effect and/or left ventricular filling conditions.

A limitation of the current study is that we could not assess all currently available prosthetic valves. However, based on available in vitro and in vivo MDCT studies we do not expect significant differences with other contemporary valves[14].

Furthermore, patients with an impaired renal function were excluded to reduce the risk of contrast-induced nephropathy. For logistic purposes, the renal function was assessed early after cardiothoracic surgery (before discharge). It is probable that at six weeks after implantation renal function has recovered and contrast-enhanced imaging can be performed in more patients. No beta-blockers were administered before MDCT acquisition, which may have affected image quality.

CONCLUSION

Six weeks after valve replacement surgery, MDCT allowed evaluation of relevant anatomical regions in all PHVs in both aortic and mitral position despite mild to moderate artifacts and presented baseline findings such as tilted aortic PHV positions and prominent pericardial hematoma. A major additional finding was induration of the periaortic fat tissue present in 83% of patients after uncomplicated aortic valve replacement. The use of MDCT as a complementary imaging tool for follow-up in postoperative patients is feasible and revealed three cases of clinically relevant pathology that were not detected by TTE imaging. Further studies are needed to assess whether early abnormalities with MDCT in seemingly normally functioning valves are as frequent as in this series.

REFERENCES

1. Vahanian A, Alfieri O, Andreotti F, Antunes MJ, Baron-Esquivias G, Baumgartner H, et al. Guidelines on the management of valvular heart disease (version 2012): The joint task force on the management of valvular heart disease of the european society of cardiology (esc) and the european association for cardio-thoracic surgery (eacts). *Eur J Cardiothorac Surg*. 2012;42:S1-44
2. Nishimura RA, Otto CM, Bonow RO, Carabello BA, Erwin JP, 3rd, Guyton RA, et al. 2014 aha/acc guideline for the management of patients with valvular heart disease: Executive summary: A report of the american college of cardiology/american heart association task force on practice guidelines. *J Am Coll Cardiol*. 2014;63:2438-2488
3. Habets J, Tanis W, van Herwerden LA, van den Brink RB, Mali WP, de Mol BA, et al. Cardiac computed tomography angiography results in diagnostic and therapeutic change in prosthetic heart valve endocarditis. *Int J Cardiovasc Imaging*. 2014;30:377-387
4. Symersky P, Budde RP, de Mol BA, Prokop M. Comparison of multidetector-row computed tomography to echocardiography and fluoroscopy for evaluation of patients with mechanical prosthetic valve obstruction. *Am J Cardiol*. 2009;104:1128-1134
5. Chenot F, Montant P, Goffinet C, Pasquet A, Vancraeynest D, Coche E, et al. Evaluation of anatomic valve opening and leaflet morphology in aortic valve bioprosthesis by using multidetector ct: Comparison with transthoracic echocardiography. *Radiology*. 2010;255:377-385
6. Fagman E, Perrotta S, Bech-Hanssen O, Flinck A, Lamm C, Olaison L, et al. Ecg-gated computed tomography: A new role for patients with suspected aortic prosthetic valve endocarditis. *Eur Radiol*. 2012;22:2407-2414
7. Teshima H, Hayashida N, Fukunaga S, Tayama E, Kawara T, Aoyagi S, et al. Usefulness of a multidetector-row computed tomography scanner for detecting pannus formation. *Ann Cardiothorac Surg*. 2004;77:523-526
8. Habets J, Tanis W, Reitsma JB, van den Brink RB, Mali WP, Chamuleau SA, et al. Are novel non-invasive imaging techniques needed in patients with suspected prosthetic heart valve endocarditis? A systematic review and meta-analysis. *Eur Radiol*. 2015;25:2125–2133
9. Zoghbi WA, Chambers JB, Dumesnil JG, Foster E, Gottdiener JS, Grayburn PA, et al. Recommendations for evaluation of prosthetic valves with echocardiography and doppler ultrasound: A report from the american society of echocardiography's guidelines and standards committee and the task force on prosthetic valves, developed in conjunction with the american college of cardiology cardiovascular imaging committee, cardiac imaging committee of the american heart association, the european association of echocardiography, a registered branch of the european society of cardiology, the japanese society of echocardiography and the canadian society of echocardiography, endorsed by the american college of cardiology foundation, american heart association, european association of echocardiography, a registered branch of the european society of cardiology, the japanese society of echocardiography, and canadian society of echocardiography. *J Am Soc Echocardiogr*. 2009;22:975-1014
10. Otto CM, Pearlman AS, Comess KA, Reamer RP, Janko CL, Huntsman LL. Determination of the stenotic aortic valve area in adults using doppler echocardiography. *J Am Coll Cardiol*. 1986;7:509-517
11. Zoghbi WA, Farmer KL, Soto JG, Nelson JG, Quinones MA. Accurate noninvasive quantification of stenotic aortic valve area by doppler echocardiography. *Circulation*. 1986;73:452-459
12. Deak PD, Smal Y, Kalender WA. Multisection ct protocols: Sex- and age-specific conversion factors used to determine effective dose from dose-length product. *Radiology*. 2010;257:158-166

13. de Heer LM, Habets J, Kluin J, Stella PR, Mali WP, van Herwerden LA, et al. Assessment of a transcatheter heart valve prosthesis with multidetector computed tomography: In vitro and in vivo imaging characteristics. *Int J Cardiovasc Imaging*. 2013;29:659-668
14. Habets J, Symersky P, van Herwerden LA, de Mol BA, Spijkerboer AM, Mali WP, et al. Prosthetic heart valve assessment with multidetector-row ct: Imaging characteristics of 91 valves in 83 patients. *Eur Radiol*. 2011;21:1390-1396
15. Suchá D, Symersky P, Vonken EJ, Provoost E, Chamuleau SA, Budde RP. Multidetector-row computed tomography allows accurate measurement of mechanical prosthetic heart valve leaflet closing angles compared with fluoroscopy. *J Comput Assist Tomogr*. 2014;38:451-456
16. Tanis W, Scholtens A, Habets J, van den Brink RB, van Herwerden LA, Chamuleau SA, et al. Ct angiography and (1)(8)f-fdg-pet fusion imaging for prosthetic heart valve endocarditis. *JACC Cardiovasc Imaging*. 2013;6:1008-1013
17. Cianciulli TE, Lax JA, Beck MA, Cerruti FE, Gigena GE, Saccheri MC, et al. Cinefluoroscopic assessment of mechanical disc prostheses: Its value as a complementary method to echocardiography. *J Heart Valve Dis*. 2005;14:664-673
18. Feng Z, Nakamura T, Fujimoto T, Umezu M. In vitro investigation of opening behavior and hydrodynamics of bileaflet valves in the mitral position. *Artif Organs*. 2002;26:32-39
19. Montorsi P, Arena V, Muratori M, Lavarra F, Cavoretto D, Repossini A, et al. Fluoroscopic functional evaluation of bileaflet prostheses: Effect of different intraoperative valve orientation. *Am J Card Imaging*. 1996;10:101-107
20. Tanis W, Suchá D, Laufer W, Habets J, van Herwerden LA, Symersky P, et al. Multidetector-row computed tomography for prosthetic heart valve dysfunction: Is concomitant non-invasive coronary angiography possible before redo-surgery? *Eur Radiol*. 2015;25:1623-1630

SUPPLEMENTARY MATERIAL

Appendix 1 | Most optimal cardiac phases for MDCT prosthetic valve assessment

MDCT	Aortic PHVs = 40	Mitral PHVs = 9
Best systolic phase		
20%	7 (18%)	1 (11%)
30%	17 (43%)	2 (22%)
40%	15 (38%)	6 (67%)
50%	1 (3%)	-
Best diastolic phase		
60%	1 (3%)	1 (11%)
70%	3 (8%)	2 (22%)
75%	15 (38%)	-
80%	11 (28%)	3 (33%)
90%	6 (15%)	3 (33%)
0%	4 (10%)	-

MDCT= multidector-row computed tomography; PHV= prosthetic heart valve

Appendix 2 | MDCT image quality and artifacts for aortic valves

	Supraprosthetic		Periprosthetic		Subprosthetic		Prosthetic		Leaflets		Overall	
	S	D	S	D	S	D	S	D	S	D	S	D
Image quality*												
St. Jude (n=8)	3 (2-4)	3 (3-4)	2 (1-3)	2 (2-3)	3 (2-4)	3 (2-4)	3 (2-3)	3 (2-4)	4 (2-4)	3.5 (3-4)	3 (2-4)	3 (3-4)
Carbomedics (n=11)	3 (2-4)	3 (2-4)	2 (2-3)	2 (1-3)	3 (2-4)	3 (2-4)	3 (2-4)	3 (2-4)	3 (3-4)	4 (3-4)	3 (2-4)	3 (2-4)
ON-X (n=3)	3 (3-4)	3 (3-4)	3 (2-3)	3 (3-4)	3 (3-4)	3 (3-4)	3 (2-4)	3 (-)	4 (3-4)	4 (3-4)	3 (-)	3 (3-4)
Sorin (n=3)	3 (2-3)	3 (3-4)	2 (2-3)	3 (2-3)	3 (2-3)	3 (-)	3 (2-3)	3 (2-3)	3 (3-4)	4 (3-4)	2 (2-3)	3 (2-3)
Perimount (n=11)	3 (3-4)	4 (3-4)	3 (2-4)	3 (2-4)	3 (2-4)	3 (3-4)	3 (2-4)	3 (2-4)	1 (-)	2 (1-2)	3 (2-4)	3 (3-4)
Mitroflow (n=4)	3 (-)	3 (-)	2 (-)	2 (-)	2.5 (2-3)	2.5 (2-3)	2 (2-3)	2 (-)	2.5 (2-4)	3 (1-3)	2 (2-3)	2.5 (2-3)
Artifacts†												
St. Jude	2 (1-3)	2 (1-3)	3 (2-4)	3 (2-3)	2 (1-2)	2.5 (1-3)	2 (2-3)	2 (2-3)	n/a	n/a	2 (2-3)	2.5 (2-3)
Carbomedics	3 (2-3)	2 (1-3)	3 (2-4)	3 (2-4)	2 (1-3)	2 (1-3)	3 (2-3)	2 (2-3)	n/a	n/a	3 (2-3)	2 (2-3)
ON-X	1 (1-3)	3 (2-3)	3 (1-3)	2 (1-3)	2 (1-2)	3 (1-3)	2 (1-3)	2 (1-2)	n/a	n/a	2 (1-3)	2 (1-2)
Sorin	2 (2-3)	2 (-)	3 (2-3)	3 (2-3)	2 (2-3)	2 (-)	2 (2-3)	2 (2-3)	n/a	n/a	3 (2-3)	2 (2-3)
Perimount	1 (1-2)	1 (1-2)	2 (1-4)	2 (2-3)	1 (1-3)	2 (1-2)	2 (2-3)	2 (1-2)	n/a	n/a	2 (1-3)	2 (1-3)
Mitroflow	2 (2-3)	2 (-)	3 (-)	3 (-)	2.5 (2-3)	3 (2-3)	2.5 (2-3)	3 (2-3)	n/a	n/a	2.5 (2-3)	3 (-)

* Image quality for the supra, peri and subprosthetic region: 1= non-diagnostic with no discernible details widely beyond the prosthesis; 2=moderate with no structure details <5mm of the prosthesis; 3=good with some structure details <5mm of the prosthesis; 4= excellent visualization with perfect structure details. Image quality for prosthetic and leaflets: 1= non-diagnostic, no prosthetic structure discernible; 2=moderate, prosthetic structure partially discernible; 3=good, prosthetic structure discernible but with deformation; 4= excellent visibility of prosthetic structure. Presented are the median and total range (minimum-maximum)

† Valve related artifacts: 1= virtually none; 2= mild artifacts <5mm beyond the prosthesis; 3= moderate artifacts >5mm beyond the prosthesis; 4= severe artifacts beyond the border of the valve chamber. Presented are the median and total range (minimum-maximum)

D= diastolic phase; MDCT= multidetector-row computed tomography; S= systolic phase

Appendix 3 | Mitral valves MDCT image quality and artifacts

	Supraprosthetic		Periprosthetic		Subprosthetic		Prosthetic		Leaflets		Overall	
	S	D	S	D	S	D	S	D	S	D	S	D
Image quality*												
St. Jude (n=4)	3 (2-3)	3 (2-3)	2 (2-3)	2 (-)	2.5 (2-3)	2.5 (2-3)	2.5 (2-4)	2 (2-3)	3.5 (3-4)	3 (3-4)	2.5 (2-3)	2.5 (2-3)
Carbomedics (n=1)	3 (-)	2 (-)	2 (-)	2 (-)	3 (-)	3 (-)	2 (-)	2 (-)	2 (-)	3 (-)	2 (-)	2 (-)
ON-X (n=2)	3 (-)	3 (-)	3 (-)	3.5 (3-4)	2.5 (2-3)	3 (-)	3 (-)	3 (-)	3.5 (3-4)	3.5 (3-4)	3 (-)	3 (-)
Sorin (n=1)	3 (-)	3 (-)	3 (-)	2 (-)	3 (-)	2 (-)	3 (-)	2 (-)	4 (-)	3 (-)	3 (-)	3 (-)
Perimount (n=1)	3 (-)	3 (-)	3 (-)	3 (-)	2 (-)	2 (-)	3 (-)	3 (-)	1 (-)	2 (-)	3 (-)	3 (-)
Artifacts†												
St. Jude	2.5 (2-3)	3 (2-3)	3 (-)	3 (-)	3 (2-3)	3 (2-3)	3 (2-3)	3 (2-3)	n/a	n/a	3 (2-3)	3 (2-3)
Carbomedics	3 (-)	3 (-)	4 (-)	3 (-)	3 (-)	3 (-)	3 (-)	3 (-)	n/a	n/a	3 (-)	3 (-)
ON-X	2 (-)	2.5 (2-3)	2 (-)	2 (-)	2.5 (2-3)	2.5 (2-3)	2 (-)	2 (-)	n/a	n/a	2 (-)	2.5 (2-3)
Sorin	2 (-)	2 (-)	2 (-)	3 (-)	3 (-)	3 (-)	2 (-)	3 (-)	n/a	n/a	2 (-)	3 (-)
Perimount	1 (-)	2 (-)	2 (-)	2 (-)	3 (-)	4 (-)	1 (-)	2 (-)	n/a	n/a	2 (-)	2 (-)

* Image quality for the supra, peri and subprosthetic region: 1= non-diagnostic with no discernible details widely beyond the prosthesis; 2=moderate with no structure details <5mm of the prosthesis; 3=good with some structure details <5mm of the prosthesis; 4= excellent visualization with perfect structure details. Image quality for prosthetic and leaflets: 1= non-diagnostic, no prosthetic structure discernible; 2=moderate, prosthetic structure partially discernible; 3=good, prosthetic structure discernible but with deformation; 4= excellent visibility of prosthetic structure. Presented are the median and total range (minimum-maximum)

† Valve related artifacts: 1= virtually none; 2= mild artifacts <5mm beyond the prosthesis; 3= moderate artifacts >5mm beyond the prosthesis; 4= severe artifacts beyond the border of the valve chamber. Presented are the median and total range (minimum-maximum)

D= diastolic phase; MDCT= multidetector-row computed tomography; S= systolic phase

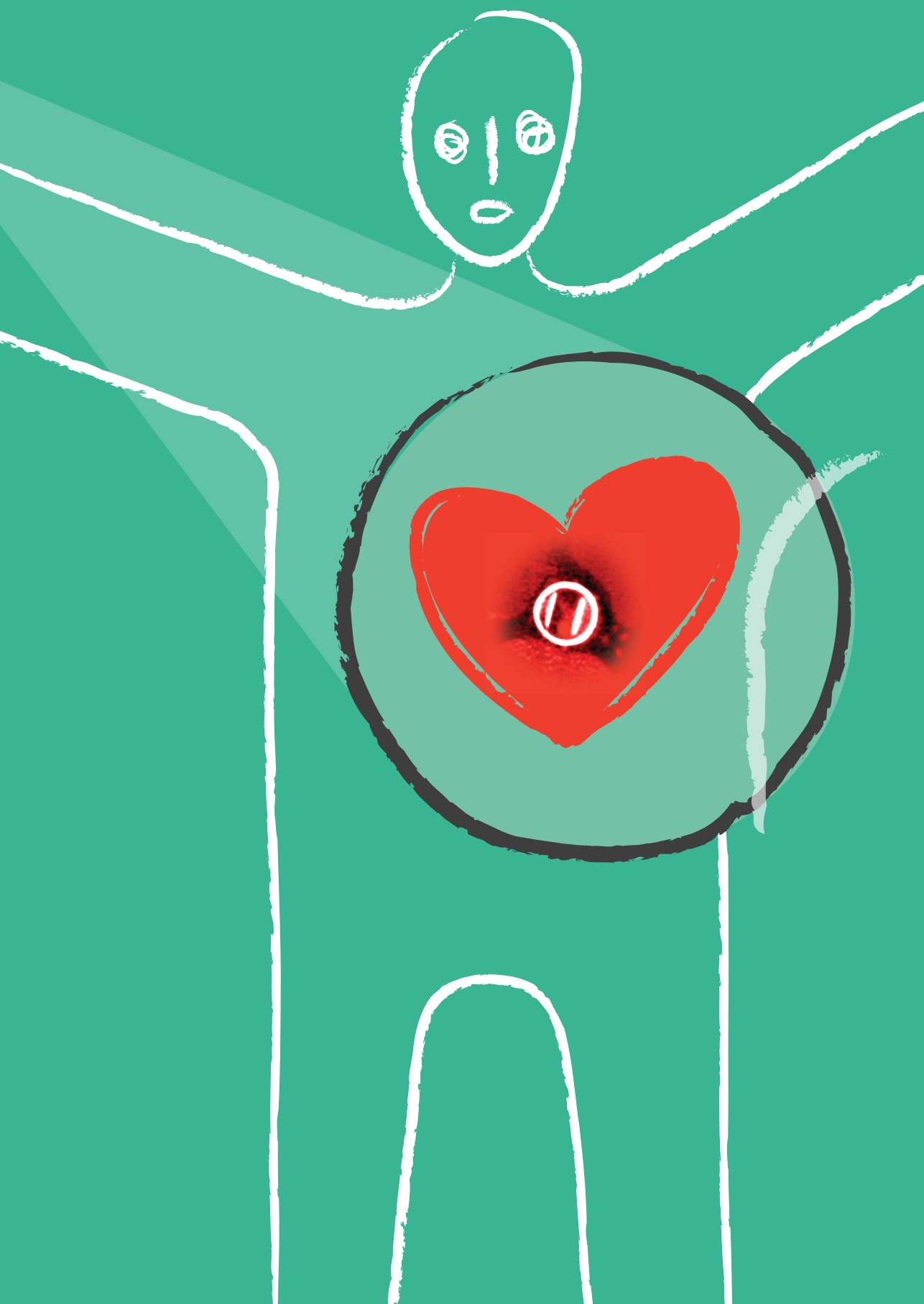

CHAPTER 8

Diagnostic work-up and treatment strategy in patients with suspected prosthetic heart valve dysfunction: the incremental value of MDCT

Dominika Suchá
Petr Symersky
Renee B.A. van den Brink
Wilco Tanis
Eduard M. Laufer
Matthijs F.L. Meijs
Jesse Habets
Bas A.J.M. de Mol
Willem P.Th.M. Mali
Steven A.J. Chamuleau
Lex A. van Herwerden
Ricardo P.J. Budde

Submitted

ABSTRACT

PURPOSE

In patients with suspected prosthetic heart valve (PHV) dysfunction, routine transthoracic (TTE) and transesophageal (TEE) echocardiography and fluoroscopy may be insufficient for the identification of the cause of dysfunction. The aim was to assess the value of MDCT as a routine complementary imaging modality in patients with suspected PHV-dysfunction for (1) diagnosing the cause of PHV obstruction and regurgitation and (2) proposing a treatment strategy.

METHODS

Patients with suspected PHV dysfunction were prospectively recruited based on signs of abnormal obstruction, abnormal (peri)prosthetic regurgitation (non-endocarditis) and/or clinical abnormalities likely due to PHV-dysfunction. All patients underwent routine diagnostic work-up (TTE, TEE, +/-fluoroscopy) and additional MDCT imaging. An expert panel reviewed all cases for study purposes and assessed for each case the most probable diagnosis and a treatment strategy, first based on routine work-up, second with additional MDCT information. The change in diagnosis and treatment strategy was evaluated to assess the incremental value of additional MDCT imaging.

RESULTS

Forty-two patients were included with suspected PHV obstruction (n=30) and PHV-regurgitation (n=12). MDCT showed incremental value to routine work-up in 26/30 obstruction cases for detecting the specific cause of obstruction and in 7/12 regurgitation patients for the assessment of complications and surgical planning. MDCT resulted in treatment strategy change in 8/30 and 3/12 patients, respectively.

CONCLUSIONS

As additional imaging modality, MDCT may identify the cause of PHV dysfunction and may alter treatment strategy. Routine MDCT may be considered in all patients with suspected PHV obstruction and in selected patients with suspected PHV-regurgitation.

INTRODUCTION

Following implantation of prosthetic heart valves (PHV), lifelong follow-up is required in order to detect possible dysfunction[1,2]. PHV dysfunction is a serious and potentially life-threatening condition that may manifest itself in various ways and requires careful evaluation. Abnormal obstruction of the prosthesis may be caused by tissue masses (thrombus, pannus), an angulated PHV position or obstruction of the left ventricular outflow tract (LVOT). Abnormal regurgitation may be due to structural valve deterioration, interference of leaflet motion, valve dehiscence or prosthetic endocarditis. Accurate diagnosis of the underlying pathological mechanism is mandatory for proper decision-making, though detecting the cause of dysfunction using routine echocardiography and fluoroscopy is challenging, even for experienced clinicians[3-5]. PHV-related reverberations, acoustic shadowing and limited viewing angles may hinder thorough evaluation of clinically relevant valve-related regions[6,7]. Over the last years, additional ECG-gated MDCT imaging has been suggested in patients with suspected PHV dysfunction[8-11]. Although its role in functional PHV assessment remains limited, MDCT can provide complementary information on PHV-related anatomy and underlying pathology due to its three-dimensional nature and high spatial resolution. In the routine diagnostic work-up of patients with suspected prosthetic valve endocarditis, MDCT was a valuable additional imaging modality for detecting complications of endocarditis and provided information relevant for surgical planning[12]. In suspected dysfunction other than endocarditis, the value of MDCT on top of the standard imaging care has not been evaluated systematically. We performed a cross-sectional study in patients with suspected PHV dysfunction to evaluate the incremental value of retrospectively ECG-gated MDCT as a routine additional imaging modality in a daily clinical practice setting with respect to diagnosing the cause of PHV dysfunction as well as its impact on treatment strategy.

METHODS

Patients

Patients with suspected PHV dysfunction were prospectively recruited from the outpatient clinic or upon hospital admission in two academic centers in the Netherlands (University Medical Center Utrecht and Academic Medical Center, Amsterdam) from May 2010 to December 2013. The inclusion criteria were: (1) signs of abnormal obstruction including an increase of the aortic peak transprosthetic pressure gradient (TPG) (>20mmHg), an elevated mitral mean TPG (>10mmHg) with normal heart rate, or leaflet motion restriction on fluoroscopy

(>5 degrees); (2) signs of abnormal (peri)prosthetic regurgitation (non-endocarditis); (3) abnormalities with a high clinical suspicion of prosthetic dysfunction (e.g. stroke, dyspnea). Patients under the age of 18, patients with contrast agent allergy or pregnant patients were not included. Patients without routine TTE or TEE imaging were excluded. The institutional review board approved this study and all patients provided written informed consent [IRB 10-008]. Patient characteristics were collected including age, gender, medical history, physical and laboratory examination and surgical records.

Routine diagnostic imaging

All patients underwent both transthoracic and transesophageal echocardiography (TTE and TEE, respectively) either in the primary hospital or, after referral, in one of the academic centers using clinically available probes. Depending on the suspected type and cause of PHV dysfunction, echocardiographic assessment included evaluation of the mean and peak gradients, effective orifice area, velocity time integrals, prosthetic leaflet motion, presence of (obstructive) masses and presence of prosthetic or periprosthetic regurgitation. Additional fluoroscopy imaging was performed in patients with mechanical valves upon the clinicians' request as part of the standard diagnostic work-up. Images were evaluated for leaflet motion restriction and/or rocking motion of the valve.

MDCT

Before MDCT imaging, prehydration (intravenous sodium chloride) was administered in patients with an impaired renal function to reduce the risk of contrast-induced nephropathy. Beta-blockers were administered after approval by the cardiologist in selected patients to reduce the heart rate during MDCT acquisition. A 256-slice or 64-slice MDCT scanner (iCT and Brilliance 64, Philips Healthcare, Best, The Netherlands) was used. Our image acquisition protocol was described previously[12]. In brief, patients underwent a scout view and a non-enhanced prospectively ECG-gated acquisition of the PHV region. Second, an iodinated contrast agent was administered (either a triphasic or biphasic protocol) and retrospective ECG-gated imaging was performed using the following acquisition parameters: tube voltage 120kV, tube current-time product 600 or 700mAs, collimation 128 or 64 x0.625mm and, depending on the heart rate, a gantry rotation time of 270 or 330ms and pitch of 0.16 or 0.18. The radiation exposure (mSv) was acquired from the scanners' dose-length product using a conversion factor 0.0145 mSv/mGy*cm[13]. Images were reconstructed at each 10% of the cardiac cycle with an increment of 0.45 and slice thickness of 0.9 mm and transferred to a dedicated workstation. Multiplanar

reformation images reconstructed in plane with the PHV and perpendicular to the PHV and valve leaflets were used for prosthesis evaluation[14]. For the assessment of leaflet excursions, mechanical leaflet angles were measured in systole and diastole and the cine mode was used to dynamically evaluate leaflet excursions. All images were clinically assessed for PVH-related pathology such as periprosthetic regurgitation, abscesses, thrombus and/or pannus and LVOT obstruction.

Diagnosis and treatment strategy

Routinely, clinical decisions regarding complex valve pathology are made in multidisciplinary cardiac teams. After patients were evaluated according to clinical routine, an expert panel retrospectively evaluated all cases for study purpose and assessed the cause of PHV dysfunction and proposed a treatment strategy after initial evaluation with echocardiography and fluoroscopy and, subsequently, with the additional information provided by MDCT imaging. The expert panel consisted of three cardiologists and three cardiothoracic surgeons with clinical experience in the care for PHV patients. Each patient was evaluated by two experts independently. A third expert reviewed all conflicting judgments and made a final decision. The primary study outcomes were: (A) did MDCT have incremental value in addition to routine clinical imaging and (B) did MDCT change the treatment strategy. Whether MDCT adds incremental value to routine imaging was based on the ability to diagnose the cause of dysfunction or propose a treatment strategy using the information provided by MDCT. All patient cases were assessed by the experts according to standardized scoring forms. Per case, the panel members indicated the cause of dysfunction and proposed a treatment strategy in two steps (*Figure 1 and Supplement*): first, based on clinical presentation, TTE and TEE (± fluoroscopy) and, subsequently, with the addition of the MDCT imaging results to the routine work-up. All cases were systematically assessed for a wide range of pathology including: pannus, thrombus, LVOT obstruction (subvalvular membrane, ventricular septal hypertrophy, mitral prosthesis), patient prosthesis mismatch, tilted PHV, biological structural valve deterioration, structural mechanical valve dysfunction, aneurysms, prosthetic and periprosthetic regurgitation. Therapeutic strategies included watchful waiting, additional imaging (TTE, TEE, magnetic resonance), intravenous heparin, fibrinolysis, antibiotics, percutaneous valve repair, emergency and elective surgery.

Figure 1 | Flowchart expert panel case assessment.
TEE= transesophageal echocardiography; TTE= transthoracic echocardiography; MDCT= multidetector-row computed tomography

Follow-up

After comprehensive diagnostic work-up in the clinical setting, patients were treated and monitored by their own clinician. In patients who underwent redo surgery, surgical findings were compared to the imaging results. In patients without redo surgery, the clinical course and echocardiographic follow-up was evaluated.

Data analysis

Data were entered in a Microsoft Access database and analysis was performed using SPSS version 20.0 for Windows. Patients were divided into two groups based on the suspected PHV dysfunction and study inclusion criteria as: (I) PHV obstruction and (II) PHV regurgitation. Group one included patients with an increase in aortic and/or mitral TPG, restricted leaflet motion and cerebral stroke or transient ischemic attack without a clinical suspicion of endocarditis. Group two included patients with suspected regurgitation based on echocardiography imaging. Since a reference test (surgery and/or pathology) was not available in the majority of patients, the judgment of the expert panel was used. The specific change in diagnosis and/or therapeutic strategy as determined by the panel was evaluated. Categorical data are presented as numbers and percentages and continuous data as mean (± standard deviation; SD) or median [interquartile range; IQR], depending on data distribution.

RESULTS

Forty-nine patients were prospectively enrolled in the study. Of those, seven patients were excluded since no TEE (n=6) or no TEE and MDCT (n=1) imaging could be performed. Hence, forty-two patients with suspected dysfunction were included for analysis with overall 49 PHVs. Patient characteristics are presented in *Table 1*.

Table 1 | Patients

Characteristic	Patients (N=42)
Age, years	61.8 ± 13.1
Male gender	20 (48%)
Increase max. TPG aortic >20mmHg	21 (50%)
Elevated mean TPG mitral >10mmHg*	3 (7%)
Abnormal (peri)prosthetic regurgitation	12 (29%)
>5° leaflet restriction on fluoroscopy	6 (14%)
Cerebral stroke/ Transient ischemic attack	4 (10%)
Fever	2 (5%)
Collapse	1 (2%)
Physical examination	
Body mass index	26.2 ± 4.5
Body surface area	1.9 ± 0.2
New murmur†	12 (29%)
Systemic embolization	4 (10%)
Laboratory results, ‡	
Hemoglobine, g/dL	11.9 ± 2.3
White blood cell count, *10^9/L	7.8 ± 3.0
C-reactive protein >10mg/L / n cases elevated >10mg/L	10 [3-35] / 10 (24%)
International normalized ratio	2.6 ± 1.3
Glomerular filtration rate < 60 ml/min/1.73m^2	12 (29%)
PHV position	
Aortic	27 (64%)
Mitral	8 (19%)
Aortic and mitral	7 (17%)
PHV type	
Mechanical	40 (82%)
Biological	9 (18%)
PHV manufacturer	
ATS	1 (2%)
Björk-Shiley	4 (8%)
Carbomedics	13 (27%)
Duromedics	4 (8%)
Edwards-Sapien (transcatheter)	1 (2%)
ON-X	1 (2%)
Medtronic Hall	1 (2%)
Medtronic Mosaic	3 (6%)
Mitroflow	2 (4%)
Perimount	3 (6%)
Sorin bileaflet	4 (8%)
St. Jude	12 (25%)
Time TTE to MDCT, days	6 [1-37]
Time TEE to MDCT, days	2 [0-10]
Clinical follow-up, months	23 [11-38]

Data are presented as number (percentage), mean ± standard deviation or median [interquartile range]
* with normal heart rate 60-110 beats per minute, one patient with a mitral prosthesis had a substantially high pressure gradient in the LVOT tract; †known in 36/42 patients; ‡if clinically available within one month from TTE and/or CT imaging
PHV= prosthetic heart valve; TEE= transesophageal echocardiography; TTE= transthoracic echocardiography TPG= transprosthetic pressure gradient

The majority of studied PHVs were mechanical (42/49; 82%) in aortic position (34/49; 69%). The primary reason for suspected dysfunction and inclusion in the study was: aortic TPG increase (n=21), an elevated mitral mean TPG with normal heart rate (n=3), restricted leaflet motion (n=1) with collapse (n=1), cerebral stroke or transient ischemic attack (n=4) and abnormal (peri) prosthetic regurgitation (n=12). Thus, 30 patients were included in the PHV obstruction group and 12 patients in the PHV regurgitation group. Median time between TTE and TEE imaging was 7 days [IQR 0-29]. Mean heart rates during TTE and TEE were 71±13 and 75±12 beats per minute, respectively. Fluoroscopy was performed in 22 patients (26/40 mechanical PHVs). Median time between TEE and MDCT was 2 days [IQR 0-10]. Two patients were imaged at the Academic Medical Center, Amsterdam using 64-slice MDCT and 40 patients at the University Medical Center Utrecht using the 256-slice system. Mean heart rate during MDCT acquisition was 69±13 beats per minute. Five patients received beta-blockers before imaging. Median radiation exposure was 11.6mSv [IQR 10.8-14.4]. According to routine work-up, PHV-related pathology was present in 35/42 patients. No valve related pathology was found in six patients and in one patient, echocardiography images were scored as non-diagnostic. Additional MDCT imaging showed incremental value to routine diagnostic work-up in 33/42 patients and resulted in an altered therapeutic strategy in 11 patients (*Figure 2*).

PHV obstruction

The detected PHV-related pathology in patients with suspected PHV obstruction is presented in *Table 2*. The main diagnosis based on routine work-up and the diagnosis including additional MDCT was similar in 16 patients, different in 6 and in 8 patients routine work-up deemed incomplete since the clinician could not identify the cause of obstruction. In the latter 8 patients, MDCT showed pannus and/or thrombus (n=6) and a subvalvular membrane (n=2) as the cause of obstruction. In the 6 patients with disagreement in diagnosis, MDCT changed the diagnosis to PHV pathology being present by detecting pannus and/or thrombus (n=2) and to no PHV-pathology in two patients with suspected structural valve deterioration and thrombus. Furthermore, MDCT showed pannus and/or thrombus in one patient with non-diagnostic routine imaging and in one patient with suspected PHV vegetation. Overall, additional MDCT was considered valuable in 26/30 patients (*Figure 2*) for providing insight on the cause of obstruction and for indicating no PHV-related pathology. In 23/26 cases this concerned mechanical valve patients.

Inclusion	
Obstruction N=30	Regurgitation N=12
Diagnosis - Routine work-up	
5 No PHV-related pathology 16 Thrombus / Pannus 3 SVD 1 PPM 1 Vegetation (non-obstructive) 1 Vegetation (with obstruction) 2 LVOT obstruction (mitral PHV n=1, unknown cause n=1) 1 Non-diagnostic	1 No PHV-related pathology 8 Periprosthetic regurgitation 1 Periprosthetic regurgitation (suspected endocarditis) 1 Prosthetic regurgitation 1 Pseudoaneurysm with active fistula
Diagnosis - Routine work-up & MDCT	
5 No PHV-related pathology 18 Thrombus / Pannus 2 SVD 1 PPM 1 Vegetation (non-obstructive) 3 LVOT obstruction (mitral PHV n=1, subvalvular membrane n=2)	1 No PHV-related pathology 6 Periprosthetic regurgitation 1 Prosthetic regurgitation 1 Periprosthetic regurgitation & pseudoaneurysm 1 Periprosthetic regurgitation (suspected endocarditis) 1 Pseudoaneurysm 1 Pseudoaneurysm with active fistula
MDCT showed incremental value	
26 Yes 4 No	7 Yes 5 No
MDCT changed therapeutic strategy	
8 Yes 22 No	3 Yes 9 No

Figure 2 | Results. Routine work-up: transthoracic echocardiography, transesophageal echocardiography, (+/-) fluoroscopy.
LVOT= left ventricular outflow tract; MDCT= multidetector-row computed tomography; PHV= prosthetic heart valve; PPM= patient prosthesis mismatch; SVD= structural valve deterioration.

Table 2 | Diagnosis and therapy in suspected PHV obstruction

SID	Diagnosis routine work-up	Diagnosis with additional MDCT	MDCT value	Change in therapeutic strategy†
1	Thrombus / LVOT obstruction (subvalvular membrane)	LVOT obstruction (subvalvular membrane)	Showed cause of LVOT obstruction	Yes†, surgery indicated
2	LVOT obstruction (unknown cause)	LVOT obstruction (subvalvular membrane)	Confirmed LVOT obstruction and showed its cause	Yes†, surgery indicated
3	Thrombus / Pannus	Pannus	Detected pannus and excluded thrombus	Yes, no heparin indicated
4	No PHV-related pathology	No PHV-related pathology	Excluded presence of pannus/thrombus	Yes, indication for wait and see
5	No PHV-related pathology	Pannus	Detected pannus	Yes†, surgery indicated
6	Thrombus / Pannus	Thrombus	Detected thrombus	Yes, heparin/fibrinolysis indicated
7	Pannus	Pannus	Confirmation of pannus	Yes†, surgery indicated
8	Pannus	Pannus	Showed evident pannus	Yes†, surgery indicated
9	SVD with restricted leaflet motion	No PHV-related pathology	Showed absence of PHV-related pathology	- (Follow-up remained indicated)
10	Non-Diagnostic	Pannus	Echocardiography was non-diagnostic	- (Follow-up remained indicated)
11	PPM	PPM & tilted PHV position	Excluded obstruction due to mass and showed a tilted PHV position	-
12	Pannus	Pannus	Increased certainty of diagnosis	-
13	Vegetation with obstruction	Thrombus / Pannus	Showed thrombus/pannus, clinical endocarditis suspicion was rejected	- (Emergency surgery remained indicated)
14	Thrombus / Pannus	Thrombus	Excluded pannus and confirmed intercurrent thrombus	-
15	LVOT obstruction by mitral PHV	LVOT obstruction by mitral PHV	Confirmed diagnosis	-
16	Pannus	Thrombus and Pannus	Detected superposing thrombus in addition to pannus	- (Elective surgery remained indicated)

17	No PHV-related pathology	No PHV-related pathology	Excluded presence of PHV-related pathology	-
18	No PHV-related pathology	Thrombus / Pannus	Detected pannus/thrombus	- (TTE follow-up remained indicated)
19	Pannus	Pannus	Confirmed solely aortic PHV-problem with mitral PHV present	-
20	Thrombus / Pannus	Thrombus and Pannus	Showed extent of thrombus and detected pannus	-
21	SVD	SVD & tilted PHV position	Provided insight on SVD & showed a tilted PHV position	-
22	Pannus	Pannus	Limited, MDCT confirmed no other PHV-related pathology	-
23	Thrombus / Pannus	Pannus	Excluded thrombus	-
24	Thrombus	No PHV-related pathology	Showed good leaflet motion and absence of thrombus	- (Heparin remained indicated‡)
25	Vegetation (non-obstructive)	Vegetation (non-obstructive)	Excluded abcesses/aneurysms	-
26	No PHV-related pathology	No PHV-related pathology	Endocarditis unlikely	-
27	Pannus	Pannus	- (CT was non-diagnostic due to PHV-related artifacts)	-
28	SVD	SVD	-	-
29	Thrombus	Thrombus	-	-
30	Thrombus	Thrombus	-	-

† indicates a major change in therapy defined as change from no thrombolysis to thrombolysis and vice versa and/or from conservative to surgical/percutaneous treatment and vice versa

‡ MDCT showed no PHV-related pathology but did show irregularity of the proximal part of the ascending aortic prosthesis (differential diagnosis adherent thrombus)

LVOT= left ventricular outflow tract; PHV= prosthetic heart valve; SID= study subject identification; SVD= structural valve deterioration

No incremental value was found for MDCT in one case of structural valve deterioration and in two cases of thrombus as already detected by routine imaging. In one case with suspected pannus, MDCT evaluation was hampered by beam hardening PHV-related artifacts from a Sorin bileaflet prosthesis. Examples of routine work-up and additional MDCT are presented in *Figures 3-5*.
In PHV obstruction, MDCT lead to a change in treatment plan in eight patients, all with mechanical valves. Treatment strategy with MDCT (theoretically) resulted in surgery for five patients, indication for thrombolysis (one patient), no indication for heparin (one patient) and watchful waiting in a last patient.

PHV regurgitation

The detected pathology in patients with suspected PHV regurgitation is presented in *Table 3*. The main diagnosis based on routine work-up compared with additional MDCT information was similar in 11/12 patients. In two patients, pseudoaneurysms were detected by MDCT. Overall, additional MDCT showed incremental value in 7/12 patients by excluding abscess/mycotic aneurysm formation, detecting additional pathology and providing information required for surgical planning. Four of these patients had biological valves and three had mechanical valves. No incremental value for MDCT imaging was found in 4 patients with periprosthetic regurgitation detected by routine imaging and in the single patient without PHV-related pathology. Moreover, MDCT missed regurgitation of the aortic PHV in a patient with two PHVs in which routine work-up showed periprosthetic regurgitation of both valves. Treatment strategy with MDCT (theoretically) changed into a watchful waiting approach in one patient with a bioprosthesis and in percutaneous repair of the periprosthetic mechanical valve leak in another patient. In one patient with a biological valve the surgical plan was altered. Examples of routine work-up and additional MDCT images are presented in *Figures 6 and 7*. The score for confidence of diagnosis and treatment is presented in *Supplement 2*.

Follow-up

Median clinical follow-up time after MDCT imaging was 23 months [IQR 11-38]. Thirteen patients underwent redo valve surgery and one patient underwent surgical valve inspection and ascending aorta replacement (*Table 4*). Median time between MDCT imaging and surgery was 73 days [IQR 6-157]. Eleven patients showed good PHV function and uncomplicated follow-up after redo valve surgery. One patient required antibiotic treatment based on surgical findings (no.13),

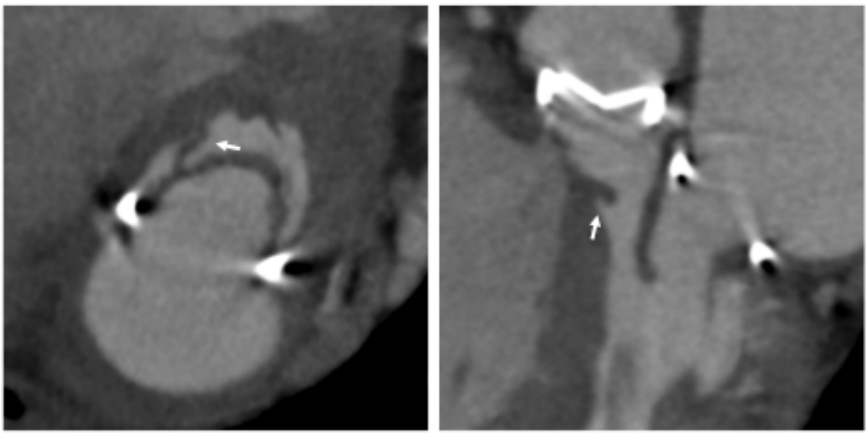

Figure 3 | Sixty-seven year old female with suspected dysfunction of the aortic Carbomedics 21mm prosthesis (study ID no.1). Echocardiography showed suspected dysfunction due to thrombus formation on the aortic prosthesis and possible obstruction of the left ventricular outflow tract (LVOT). MDCT showed the presence of a subvalvular membrane (arrows) causing obstruction of the LVOT.

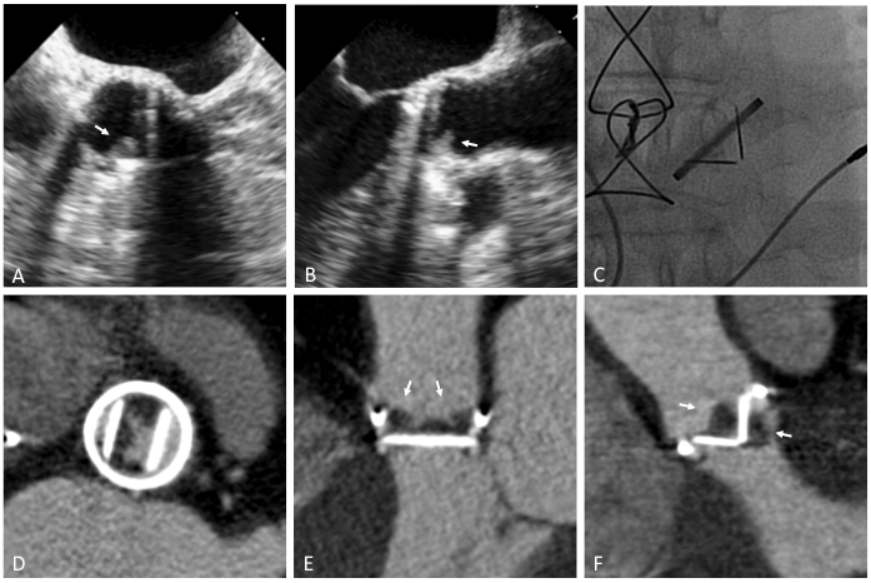

Figure 4 | Fifty-five year old female patient with a St. Jude in aortic position and suspected PHV obstruction based on thrombus/pannus formation (study ID no.20). Transesophageal echocardiography (A,B) showed a supraprosthetic mass (arrows) and fluoroscopy (C) showed restricted leaflet motion. Additional MDCT imaging (D-F) detected extensive thrombus formation at both the aortic and ventricular side of the PHV (arrows), showed restricted leaflet motion and presented subprosthetic pannus formation.

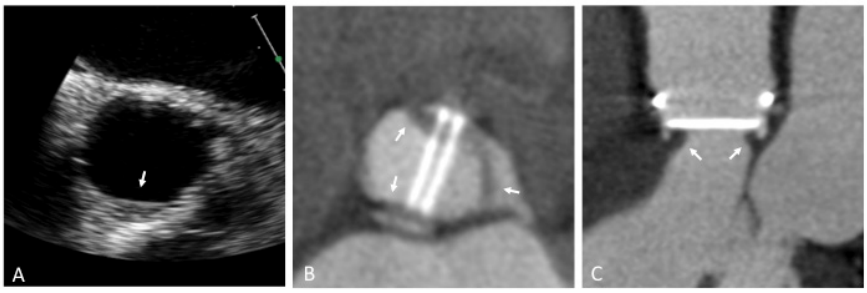

Figure 5 | Female aged 44 with a 21mm St. Jude prosthesis in aortic position (study ID no.8). Based on clinical presentation and routine echocardiography imaging (A) subprosthetic pannus (arrow) was suspected. MDCT (B, C) confirmed pannus (arrows) as the diagnosis and showed its extent whereupon surgery was indicated.

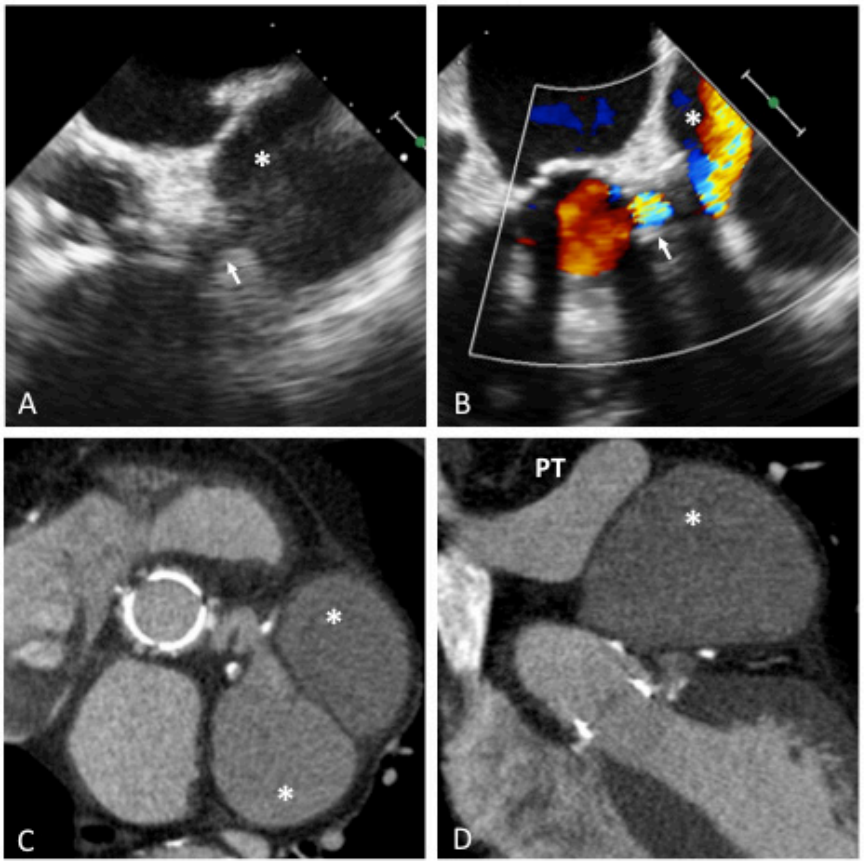

Figure 6 | Male patient aged 75 with a Perimount bioprosthesis in aortic position (study ID no.31). Transesophageal echocardiography (A) and Doppler imaging (B) showed an active fistula (arrow) and pseudoaneurysm (asterisk). MDCT (C, D) detected two large collections (pseudoaneurysms, asterisks) with compression of the pulmonary trunk (PT).

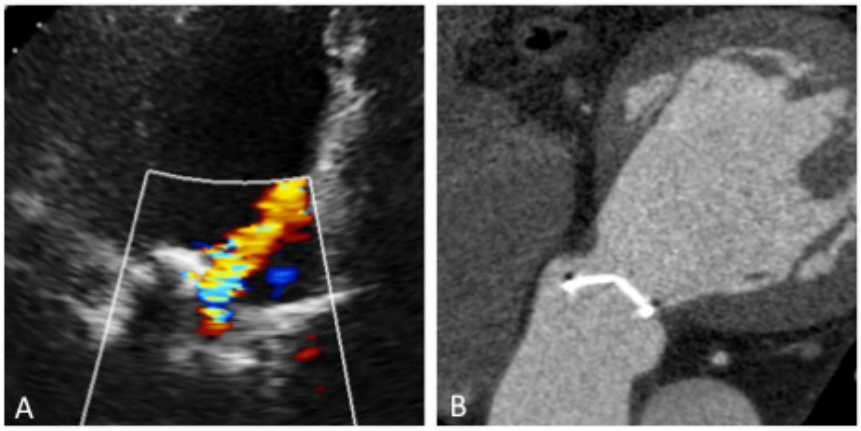

Figure 7 | Sixty-four year old male patient with an aortic St. Jude 27 mm and mitral St. Jude 31 mm prosthesis (study ID no.33). Echocardiography (A) detected aortic periprosthetic regurgitation. MDCT (B) visualized the periprosthetic leak and showed a small pseudoaneurysm. No pathology was found for the mitral prosthesis.

Table 3 | Diagnosis and therapy in suspected PHV regurgitation

SID	Diagnosis routine work-up	Diagnosis with additional MDCT	MDCT value	Change in therapeutic strategy†
31	Pseudoaneurysm and active fistula	Pseudoaneurysm and active fistula	For surgical planning	Yes, altered surgical strategy
32	Periprosthetic regurgitation (Dx in endocarditis)	Pseudoaneurysm	Detected pseudoaneurysm	Yes, wait and see indicated
33	Periprosthetic regurgitation	Periprosthetic regurgitation and pseudoaneurysm	Visualized leak & detected pseudoaneurysm	Yes†, percutaneous repair indicated
34	Periprosthetic regurgitation	Periprosthetic regurgitation	Excluded other PHV-related pathology‡	-
35	Periprosthetic regurgitation	Periprosthetic regurgitation	Excluded endocarditis complications, no abscesses present	-
36	Periprosthetic regurgitation (suspected endocarditis)	Periprosthetic regurgitation (suspected endocarditis)	Excluded abscess formation	-
37	Prosthetic regurgitation	Prosthetic regurgitation	Provided insight on SVD§	-
38	Periprosthetic regurgitation	Periprosthetic regurgitation	-	-
39	Periprosthetic regurgitation	Periprosthetic regurgitation	-	-
40	No PHV-related pathology	No PHV-related pathology	-	-
41	Periprosthetic regurgitation	Periprosthetic regurgitation	-	-
42	Periprosthetic regurgitation	Periprosthetic regurgitation	-	-

† indicates a major change in therapy defined as change from conservative to surgical/percutaneous treatment and vice versa
‡ in a patient with an aortic and mitral prosthetic valve, also regurgitation due to endocarditis (complications) was not likely
§ in a patient with an aortic and mitral bioprosthesis, also MDCT visualized periprosthetic details
PHV= prosthetic heart valve; SID= study subject identification; SVD= structural valve deterioration

Table 4 | Surgical findings

	SID	Pt*	PHV†	Diagnosis routine work-up	Diagnosis with additional MDCT	Days to surgery	Surgical findings
Obstruction	1	F-67	AVR CM 21	Thrombus / LVOT obstruction	LVOT obstruction (subvalvular membrane)	94	Obstructive fibrotic tissue in LVOT matching recurrent subvalvular membrane and prominent anterior mitral valve leaflet ridge
	3	M-54	AVR MH 25	Thrombus / Pannus	Pannus	3	Subvalvular pannus tissue and annular calcification
	6	M-66	MVR ATS 27	Thrombus / Pannus	Thrombus	51	No pannus, but restricted leaflet opening due to (unclear) mechanical valve failure
	13	F-60	MVR CM 31	Vegetation with obstruction	Thrombus / Pannus	1	Prosthetic endocarditis culture-negative, thrombus, no abundant pannus tissue
	19	F-61	AVR BS 19	Pannus	Pannus	348	Significant pannus tissue present
	20	F-55	AVR SJ 23	Thrombus / Pannus	Thrombus and Pannus	0	Extensive thrombus supraprosthetic and subprosthetic
	22	M-58	AVR DM 23	Pannus	Pannus	218	Pannus tissue and prominent anterior mitral valve leaflet ridge
	23	F-64	AVR CM 23	Thrombus / Pannus	Pannus	104	Pannus tissue causing significant obstruction
	25	F-55	AVR BS 23	Vegetation (non-obstructive)	Vegetation (non-obstructive)	136	No PHV-related pathology
	28	M-28	AVR P 27	SVD	SVD	573	SVD
Regurgitation	31	M-75	AVR P 23	Pseudoaneurysm & active fistula	Pseudoaneurysm & active fistula	22	Enormous aneurysm with pressure on pulmonary trunk
	38	M-69	MVR BS 31	Periprosthetic regurgitation	Periprosthetic regurgitation	119	Periprosthetic regurgitation with valve dehiscence and annular calcification
	40	M-53	AVR SO 23	No PHV-related pathology‡	No PHV-related pathology	7	Fibrous material on prosthesis and hingepoints
	42	F-70	AVR CM 31	Periprosthetic regurgitation	Periprosthetic regurgitation	26	Periprosthetic regurgitation and neointima formation over prosthesis ring

* patient gender and age (years)

† implanted prosthesis position, manufacturer and size

‡ no PHV-related pathology visualized, but intermittent PHV dysfunction on echocardiography

AVR= aortic valve; BS= Bjork-Shiley; CM= Carbomedics; DM= Duromedics; LVOT= left ventricular outflow tract; MH= Medtronic Hall; MVR= mitral valve; P= Perimount; PHV= prosthetic heart valve; SID= study subject identification; SJ= St. Jude; SO= Sorin bileaflet; SVD= structural valve deterioration

one patient showed recurrent periprosthetic regurgitation with hemolysis but was considered not suitable for re-redo surgery (no.42) and one patient died six days after redo surgery due to respiratory complications (no.1). One patient was scheduled to undergo surgery, but the PHV function normalized after intravenous heparin therapy. One patient died before surgery. Three patients underwent percutaneous paravalvular leak repair (n=3) with clinical improvement. The remaining patients were treated conservatively (n=23) with uncomplicated follow-up in 22/23 patients. One patient showed inflammatory abnormalities requiring corticosteroid drug treatment.

DISCUSSION

This is the first study that assessed the additional value of MDCT to routine imaging on clinical diagnosis and treatment decisions in patients with suspected PHV dysfunction in a daily clinical setting. The findings of this study are twofold. First, MDCT as additional routine imaging modality was valuable in the vast majority of patients with suspected PHV obstruction, mainly for detecting the cause of obstruction or indicating no PHV-related pathology. In addition, MDCT imaging resulted in a treatment change in a third of mechanical valve patients. Second, in patients with suspected PHV regurgitation MDCT may be useful to rule out (extensive) abscess formation and provide relevant information for treatment planning, but its role in PHV dysfunction diagnosis was less prominent.

Based on our findings, we believe MDCT may be considered in the routine diagnostic work-up of patients with suspected PHV dysfunction. Identification of the cause of obstruction is of great importance for successful therapy. In addition, redo valve surgery bears significant risks with mortality rates up to 30% in case of emergency surgery[15]. Routinely, fluoroscopy is used to assess mechanical leaflet motion and detect leaflet restriction, though positioning the beam perpendicular to the leaflets while performing image acquisition is challenging. Inadequate positioning will result in unreliable diagnostic assessment. Also, mechanical leaflet restriction detected with routine fluoroscopy is mainly present in case of PHV-thrombosis[3]. With dysfunction due to pannus, leaflet restriction may be absent in 5-33% of patients[3, 16].

MDCT may be more reliable than fluoroscopy for the assessment of leaflet motion and may also depict periprosthetic masses that cause the limitation in leaflet motion. In addition, MDCT may depict obstructive masses without restricted leaflet motion. Whilst echocardiography has many benefits as a routine diagnostic tool in

PHV patients, it may not differentiate pannus and thrombus[3-5]. In our study, MDCT provided additional information on the cause of obstruction. To date, five studies reported on MDCT in mechanical valve patients with suspected PHV obstruction or periprosthetic regurgitation[8, 9, 11, 17, 18]. None of these studies investigated the clinical role of MDCT in addition to echocardiography and fluoroscopy. Study samples were relatively small ranging from 7-25 patients and only one study included patients prospectively[11]. MDCT did however provide information for diagnosing the cause of mechanical PHV dysfunction by detecting: subprosthetic tissue - not specified (n=20), pannus (n=15), valvular mass - not specified (n=2), suture loosening with periprosthetic leak (n=4), narrowing of the LVOT due to mitral PHV protrusion (n=2) and tilted position of the PHV (n=1). Two recent MDCT studies in randomly selected aortic valve patients (i.e. not based on PHV dysfunction) detected pannus in 71/92 mechanical[16] and 17/88 mechanical and biological valves[19]. MDCT in dysfunctional bioprostheses was evaluated in one study (n=34) and showed leaflet thickening, calcifications and/or hypoattenuating adhesions (presumed thrombus)[20]. Very recently, Makkar et al. detected restricted leaflet motion and hypoattenuating leaflet tissue using MDCT in supposedly normal functioning aortic biological valves[21]. TTE failed to detected leaflet restriction or leaflet structure abnormalities in all of these cases and showed normal TPGs.

These findings support the use of MDCT in the evaluation of dysfunctional aortic bioprostheses.

In contrast, the role of MDCT in the detection of (peri)prosthetic regurgitation is limited[9, 22]. As demonstrated in this study, its strength was ruling out (infectious) complications, or, as we demonstrated in a previous study, detecting endocarditis complications and showing their relation to relevant anatomical structures such as the coronary arteries[12]. In both cases, MDCT imaging provided additional information relevant for surgical planning. Since the value of additional MDCT imaging in a clinical setting of suspected endocarditis was evaluated in a previous study[12], we did not repeatedly include endocarditis patients in our current study.

Limitations of the current study were: first, the lack of a gold standard, which is a well-known problem in studies concerning PHV dysfunction. This is due to the relatively low prevalence of PHV dysfunction disease and the fact that only a part of patients undergo redo valve surgery. Hence we could not evaluate the diagnostic

accuracy of MDCT for the differentiation of PHV obstruction cause compared with surgical findings in most patients. An expert panel determined the presence or absence of a specific diagnosis. We consider this the best available evidence and it resembles daily clinical practice in PHV dysfunction patients. Second, the time interval between MDCT imaging and redo surgery was long in some patients which may have induced time-related discrepancies. Third, the change in diagnosis and treatment strategy was assessed by the expert panel for study purposes only. Proposed changes did not lead to changes in the routine clinical patient care. Last, contrast-enhanced MDCT imaging may not be preferred in certain clinical conditions, though the severity of prosthetic valve related complications might outweigh this concern.

CONCLUSION

This cross-sectional study in patients with suspected PHV dysfunction shows that MDCT as routine additional imaging modality has incremental value for both diagnosing the cause of PHV dysfunction and for proposing a treatment strategy. Its additional value is most prominent in patients with suspected PHV obstruction, in which it may show the underlying mechanism of obstruction. In our study, MDCT resulted in a treatment change in a third of mechanical valve patients. In patients with suspected PHV regurgitation, additional MDCT imaging can be acquired for detecting infectious complications, but has limited value for regurgitation detection. We suggest that MDCT should be considered as a routine imaging tool in patients with suspected PHV obstruction and in selected patients with suspected PHV regurgitation.

REFERENCES

1. Nishimura RA, Otto CM, Bonow RO, Carabello BA, Erwin JP, 3rd, Guyton RA, et al. 2014 aha/acc guideline for the management of patients with valvular heart disease: A report of the american college of cardiology/american heart association task force on practice guidelines. *J Thorac Cardiovasc Surg*. 2014;148:e1-e132
2. Vahanian A, Alfieri O, Andreotti F, Antunes MJ, Baron-Esquivias G, Baumgartner H, et al. Guidelines on the management of valvular heart disease (version 2012): The joint task force on the management of valvular heart disease of the european society of cardiology (esc) and the european association for cardio-thoracic surgery (eacts). *Eur J Cardiothorac Surg*. 2012;42:S1-44
3. Tanis W, Habets J, van den Brink RB, Symersky P, Budde RP, Chamuleau SA. Differentiation of thrombus from pannus as the cause of acquired mechanical prosthetic heart valve obstruction by non-invasive imaging: A review of the literature. *Eur Heart J Cardiovasc Imaging*. 2014;15:119-129
4. Barbetseas J, Nagueh SF, Pitsavos C, Toutouzas PK, Quinones MA, Zoghbi WA. Differentiating thrombus from pannus formation in obstructed mechanical prosthetic valves: An evaluation of clinical, transthoracic and transesophageal echocardiographic parameters. *J Am Coll Cardiol*. 1998;32:1410-1417
5. Lin SS, Tiong IY, Asher CR, Murphy MT, Thomas JD, Griffin BP. Prediction of thrombus-related mechanical prosthetic valve dysfunction using transesophageal echocardiography. *Am J Cardiol*. 2000;86:1097-1101
6. Girard SE, Miller FA, Jr., Orszulak TA, Mullany CJ, Montgomery S, Edwards WD, et al. Reoperation for prosthetic aortic valve obstruction in the era of echocardiography: Trends in diagnostic testing and comparison with surgical findings. *J Am Coll Cardiol*. 2001;37:579-584
7. Habets J, Budde RP, Symersky P, van den Brink RB, de Mol BA, Mali WP, et al. Diagnostic evaluation of left-sided prosthetic heart valve dysfunction. *Nat Rev Cardiol*. 2011;8:466-478
8. Teshima H, Aoyagi S, Ueda T, Takagi K, Shojima T, Tanaka H. Evaluation of advancing the standard valve dysfunction by multidetector-row ct. *J Artif Organs*. 2014;17:162-168
9. Symersky P, Budde RP, de Mol BA, Prokop M. Comparison of multidetector-row computed tomography to echocardiography and fluoroscopy for evaluation of patients with mechanical prosthetic valve obstruction. *Am J Cardiol*. 2009;104:1128-1134
10. LaBounty TM, Agarwal PP, Chughtai A, Kazerooni EA, Wizauer E, Bach DS. Hemodynamic and functional assessment of mechanical aortic valves using combined echocardiography and multidetector computed tomography. *J Cardiovasc Comput Tomogr*. 2009;3:161-167
11. Tsai IC, Lin YK, Chang Y, Fu YC, Wang CC, Hsieh SR, et al. Correctness of multi-detector-row computed tomography for diagnosing mechanical prosthetic heart valve disorders using operative findings as a gold standard. *Eur Radiol*. 2009;19:857-867
12. Habets J, Tanis W, van Herwerden LA, van den Brink RB, Mali WP, de Mol BA, et al. Cardiac computed tomography angiography results in diagnostic and therapeutic change in prosthetic heart valve endocarditis. *Int J Cardiovasc Imaging*. 2014;30:377-387
13. Deak PD, Smal Y, Kalender WA. Multisection ct protocols: Sex- and age-specific conversion factors used to determine effective dose from dose-length product. *Radiology*. 2010;257:158-166
14. Suchá D, Daans CG, Symersky P, Planken RN, Mali WP, van Herwerden LA, et al. Reliability, agreement, and presentation of a reference standard for assessing implanted heart valve sizes by multidetector-row computed tomography. *Am J Cardiol*. 2015;116:112-120

15. Piazza N, Bleiziffer S, Brockmann G, Hendrick R, Deutsch MA, Opitz A, et al. Transcatheter aortic valve implantation for failing surgical aortic bioprosthetic valve: From concept to clinical application and evaluation (part 1). *JACC Cardiovasc Interv*. 2011;4:721-732
16. Suh YJ, Kim YJ, Lee S, Hong YJ, Lee HJ, Hur J, et al. Utility of cardiac computed tomography for evaluation of pannus in mechanical aortic valve. *Int J Cardiovasc Imaging*. 2015;31:1271-1280
17. Teshima H, Hayashida N, Fukunaga S, Tayama E, Kawara T, Aoyagi S, et al. Usefulness of a multidetector-row computed tomography scanner for detecting pannus formation. *Ann Thorac Surg*. 2004;77:523-526
18. Ueda T, Teshima H, Fukunaga S, Aoyagi S, Tanaka H. Evaluation of prosthetic valve obstruction on electrocardiographically gated multidetector-row computed tomography--identification of subprosthetic pannus in the aortic position. *Circ J*. 2013;77:418-423
19. Han K, Yang DH, Shin SY, Kim N, Kang JW, Kim DH, et al. Subprosthetic pannus after aortic valve replacement surgery: Cardiac ct findings and clinical features. *Radiology*. 2015;276:724-731
20. Chenot F, Montant P, Goffinet C, Pasquet A, Vancraeynest D, Coche E, et al. Evaluation of anatomic valve opening and leaflet morphology in aortic valve bioprosthesis by using multidetector ct: Comparison with transthoracic echocardiography. *Radiology*. 2010;255:377-385
21. Makkar RR, Fontana G, Jilaihawi H, Chakravarty T, Kofoed KF, de Backer O, et al. Possible subclinical leaflet thrombosis in bioprosthetic aortic valves. *N Engl J Med*. 2015;373:2015-2024
22. Grunenfelder J, Plass A, Alkadhi H, Genoni M. Evaluation of biological aortic valve prostheses by dual source computer tomography and anatomic measurements for potential transapical valve-in-valve procedure. *Interact Cardiovasc Thorac Surg*. 2008;7:195-200

SUPPLEMENTARY MATERIAL

Certainty of diagnosis and treatment strategy

To get an impression of the impact of additional MDCT on the clinicians confidence in the decision-making, the expert was asked to score the certainty of diagnosis and therapeutic strategy based on a subjective 4-point scale: (1) uncertain, (2) some doubt, (3) reasonably certain, (4) absolutely sure. The change in confidence of diagnosis and/or therapy was evaluated and the Wilcoxon-signed rank test was used to analyze these results (level of significance $P<0.05$). Routine diagnostic work-up included transthoracic and transesophageal echocardiography +/- fluoroscopy.

In PHV obstruction

In patients with suspected PHV obstruction, the score for certainty of diagnosis was median [IQR] 2 - some doubt - [2-3] after routine diagnostic work-up and 3 - reasonably certain - [3-4] after additional MDCT imaging ($P=0.001$). For treatment strategy decisions, median certainty score was 3 - reasonably certain - [3-4] for both routine and additional MDCT work-up ($P=0.008$).

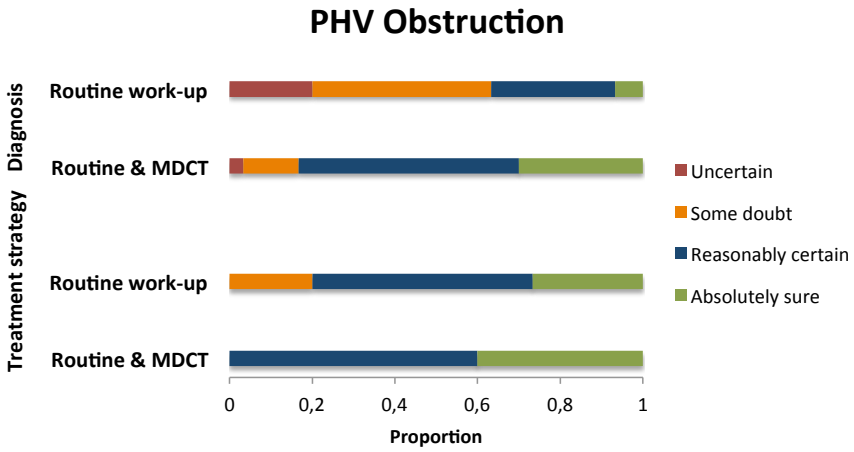

In PHV regurgitation

For patients with suspected PHV regurgitation, the median score for certainty of diagnosis was 4 - absolutely sure - [3-4] after both routine imaging work-up and with additional MDCT information (P=1.000). For treatment strategy decisions, median score was 3 - reasonably certain - [3-4] with routine work-up and 3.5 - reasonably certain/absolutely sure - [3-4] including additional MDCT work-up (P=0.083).

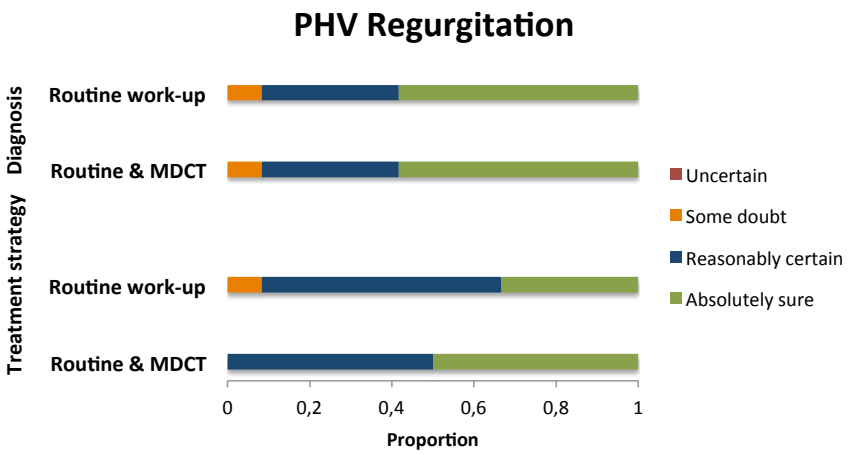

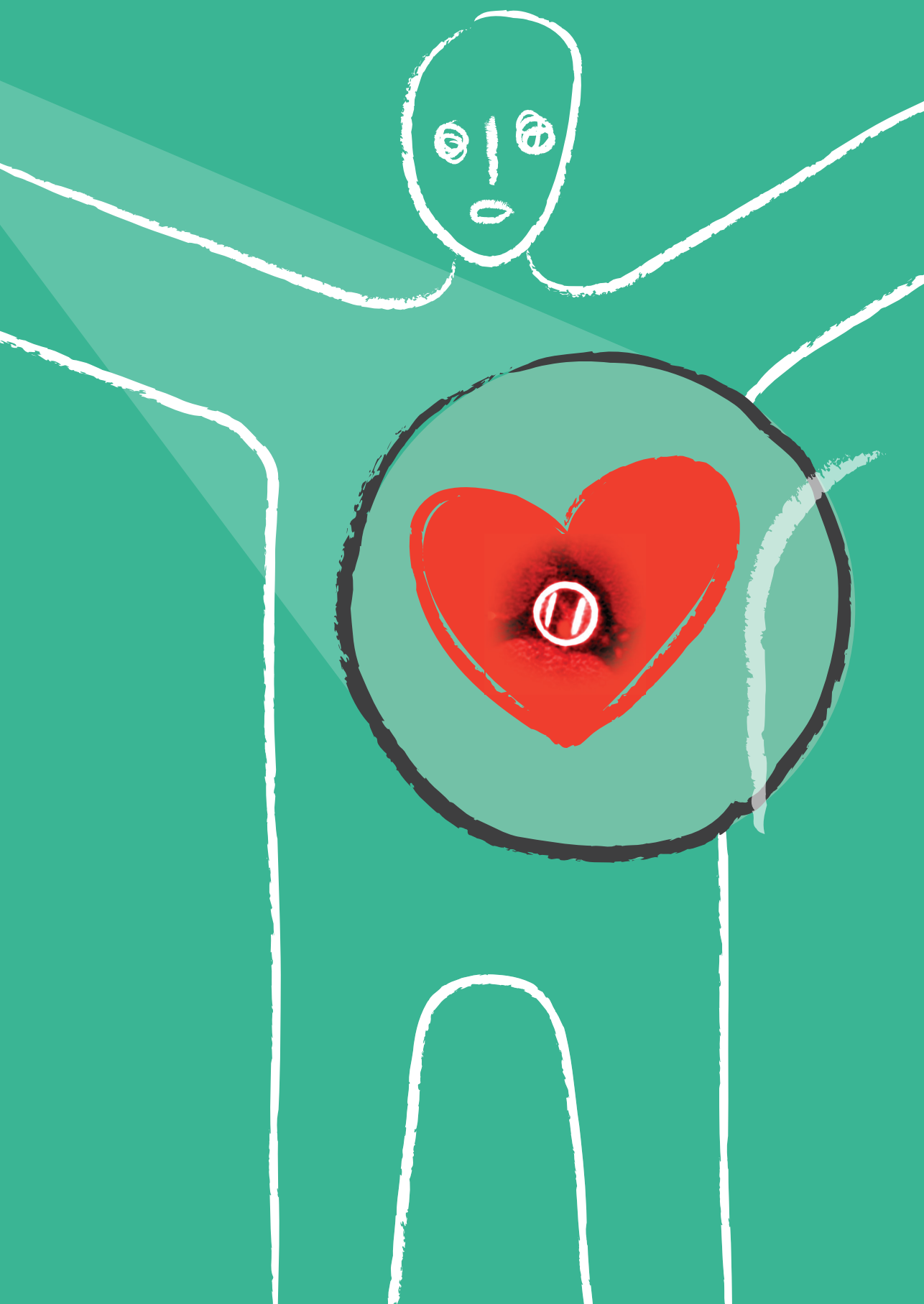

CHAPTER 9

Reliability, agreement and presentation of a reference standard for assessing implanted heart valve sizes by multidetector-row computed tomography

Dominika Suchá
Ceranza G. Daans
Petr Symersky
R. Nils Planken
Willem P.Th.M. Mali
Lex A. van Herwerden
Ricardo P.J. Budde

Published in the American Journal of Cardiology, 2015

ABSTRACT

The implanted prosthetic heart valve (PHV) size is vital for the evaluation of suspected PHV dysfunction and in case of reoperation or valve-in-valve transcatheter approaches. The labeled size is not always known and discrepancies exist between manufacturers' labeled sizes and true sizes. Reproducible methods for non-invasive PHV size assessment are lacking. We determined the reliability and agreement of PHV size measurements using multidetector-row computed tomography (MDCT) and provide reference values of MDCT measurements compared to manufacturer specifications. In vitro, 15 different PHV types in available sizes (total n=63) were imaged. In vivo, available PHV patient MDCT acquisitions were retrospectively gathered in 2 centers and 230 patients with 249 PHVs were included. Inner valve area and area-derived diameter were measured in all PHVs. For mechanical PHVs, the inner diameter was also measured. Data were analyzed using the intraclass correlation coefficient (ICC) and Bland-Altman plots and related to manufacturer specifications. Measurements could be obtained for all PHV types, except the Björk-Shiley (n=7) due to severe valve-related artifacts hampering the image quality. Intra-rater and inter-rater reliability was excellent for biological and mechanical PHVs (ICCs ≥0.903). Agreement was good for all measurements with an overall maximal mean difference (95% confidence-interval) of -2.61 mm^2 (-37.9- 32.7), -0.1 mm (-1.1- 1.0) and 0 mm (-0.4- 0.3) for valve area, area-derived diameter and inner diameter, respectively. MDCT reliably discriminated consecutive PHV sizes as labeled by the manufacturer since the absolute ranges for the measurements never overlapped. In conclusion, MDCT allows assessment of the implanted PHV size with excellent reliability and agreement and can discriminate between PHV sizes for contemporary prostheses. MDCT can be used to non-invasively identify the manufacturer labeled PHV size.

INTRODUCTION

For the analysis of prosthetic heart valve (PHV) function the labeled prosthesis size may help to discriminate between valve stenosis and patient prosthesis mismatch[1,2]. Both the size and type of the PHV are important for the decision to replace a dysfunctional PHV to prevent patient prosthesis mismatch and predict the potential gain of replacing the PHV[3,4]. For transcatheter valve-in-valve procedures, knowledge of the PHV size is paramount for choosing the size of the valve to be implanted since direct measurement as used during conventional surgery cannot be performed[5]. In addition, valve-in-valve replacement in small sizes of biological PHV may lead to excessively high transprosthetic gradients[6,7]. Sometimes, the labeled size may not be documented in the patients' medical files and obtaining medical records from other hospital centers can be difficult or even impossible. In addition, the manufacturer labeled PHV size does not reflect the true prosthetic internal diameter, effective valve area[4,8], or the external PHV tissue diameter[8] and important differences may exist between valve types of the same labeled size[9]. Non-invasive assessment of the valve size may improve the interpretation of echocardiography results and optimize the patient-specific decision-making process. Conventional echocardiography is a readily available non-invasive modality, but may provide unsatisfactory results for prosthetic size assessment due to its two-dimensional nature[10] and impaired image quality due to prosthetic components causing acoustic shadowing[2]. In our daily practice, preoperative multidetector-row computed tomography (MDCT) is routinely performed to assess the cause or extension of PHV pathology and for the determination of re-entry strategy before redo surgery[11,12]. Since MDCT offers three-dimensional information, it might be a promising modality for concomitant non-invasive PHV size assessment. The purpose of this study was (a) to assess the reliability and agreement of PHV size measurements using MDCT acquisitions in vitro and in vivo and (b) to provide a reference overview of MDCT size measurements compared to manufacturer specifications.

METHODS

In vitro, we evaluated 8 mechanical and 7 biological PHVs from various manufacturers and in different sizes (17 to 33mm). A total of 63 PHVs were included. The complete list of studied PHVs is presented in *Appendix 1*. All valves remained in the original packaging and were imaged in non-pulsatile setting.

Images were acquired with either a 256-slice or 64-slice MDCT scanner (Philips Healthcare, Best, The Netherlands) using retrospective ECG-gating with an ECG-

simulator and the following parameters: slice collimation of 128 or 64 x 0.625, pitch of 0.2, gantry rotation time of 0.27 or 0.40 sec, tube voltage of 120 kV and tube current-time product of 150 mAs. All raw data were reconstructed with filtered back projection. Since images were acquired in still valve position, only the 75% phase of the RR-interval was used for analysis. Reconstructed image thickness was 0.9 mm with an increment of 0.45 mm.

For the in vivo study, all patients with biological and mechanical PHVs and available cardiac MDCT imaging performed between January 2007 and March 2014 were retrieved from the medical archives of the University Medical Center Utrecht and the Academic Medical Center Amsterdam, The Netherlands. Both retrospective ECG-gated and prospective ECG-triggered acquisitions routinely used for cardiac imaging and performed on a 64-slice or 256-slice MDCT scanner (Philips Healthcare, Best, The Netherlands) were included for analysis. The majority of images in this study were acquired at 120 kV (95%), the remaining at 100kV (4%) and 140kV (1%). Our MDCT acquisitions are reconstructed using filtered back projection. For patients with multiple MDCT acquisitions, only one was included. Data on implanted PHV type and size were obtained for each patient from the medical records and served as the reference standard. Exclusion criteria were unknown valve type or size, annuloplasty rings and stentless valves since these do not contain a radiopaque structure which can serve as a reference point. MDCT acquisitions of all included patients were collected and sent to a dedicated workstation for analysis. Informed consent was waived by the local medical ethical committee.

Images were analyzed by 2 observers independently using commercially available software (Extended Brilliance Workstation version 4.5, Philips Healthcare, Best, The Netherlands). The observers were blinded for the nominal PHV size. For each PHV, images were reconstructed in 3 planes: 1 in plane with the PHV (short axis) and 2 perpendicular to the PHV of which one plane was set perpendicular to the valve leaflets (long axis, *Figure 1*). All measurements were performed using a default window for bone, with a window level of 800 and window width of 2000 Hounsfield units, in order to obtain standardized measurements and limit measurement errors due to blooming of the PHV components. The cardiac phase providing the best MDCT image quality of the PHV was used for analysis. Image magnification was conducted at the discretion of the reader.

For all valves, the inner PHV area was measured on the transverse plane using a circular region of interest (ROI) tool available in the software. The circle ROI was drawn either within the narrowest inner part of the radiopaque valve ring or, if no ring was visible, within the 3 tops of the biological valve struts (*Figure 2*). If a complete

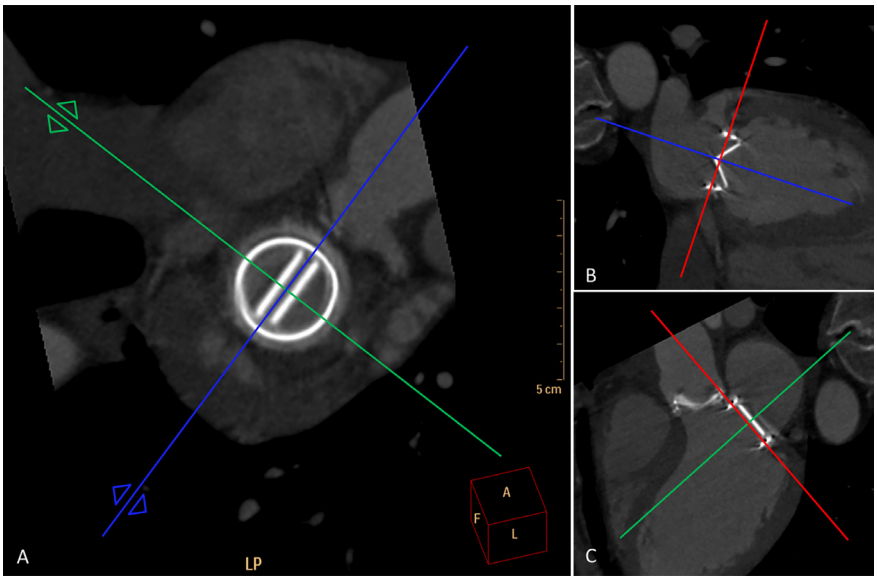

Figure 1 | Multidetector-row computed tomography reconstruction planes. Reconstruction planes used for prosthetic valve measurement in an ON-X mechanical valve in the mitral position providing a short axis view (A) and long axis view perpendicular and parallel to the leaflets (B and C, respectively).

circular ROI was not possible due to (biological valve) ring deformation, the inner valve area was defined manually by drawing points connected into a spline curve (*Figure 2C*). For each PHV, the inner valve area (mm^2) and area-derived diameter (mm) were documented. In case of mechanical PHVs, the plane perpendicular to the valve leaflets was used additionally to measure the inner valve diameter using the straight line tool from the inner edge of the PHV ring to the inner edge on the opposing side of the ring (*Figure 2D*). For in vivo acquisitions, the image quality was scored on a 3-point scale: (0) poor, (1) fair and (2) good (*Figure 3*).

Two readers with 2 and 6 years' experience in cardiac MDCT independently measured all in vitro acquisitions (DS and PS, respectively). After 1 month, 1 reader (DS) measured all in vitro images again for the intra-rater analysis.

All measurements in the patient acquisitions were performed by 1 observer with 1 year experience (CD) and repeated in a random sample of 70% of patients after a period of at least 3 weeks. In addition, a second observer (DS) measured a random sample of 10% of the patient acquisitions for the inter-rater analysis.

Collected data were analyzed using IBM SPSS Statistics 20.0 for Windows. Intra-rater and inter-rater reliability was assessed by the two-way random intraclass correlation

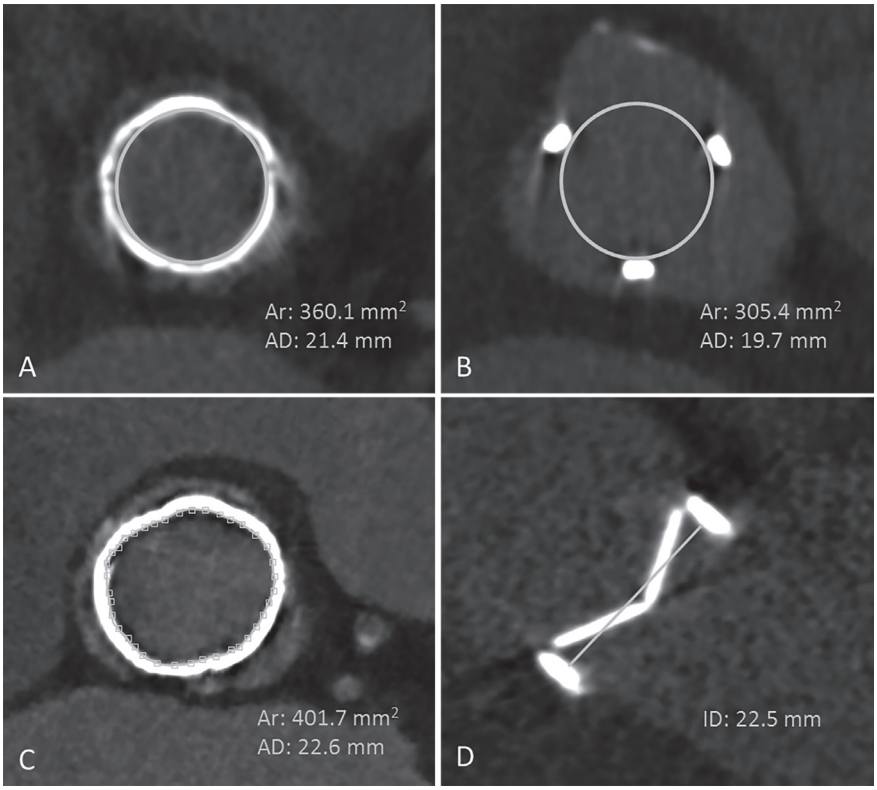

Figure 2 | Prosthetic heart valve inner area and diameter measurements. Computed tomography measurements in a biological valve: valve area (Ar) and area-derived diameter (AD) measured in plane in a prosthetic valve with a radiopaque valve ring (A) and a prosthetic valve with only radiopaque struts (B). The ROI circle (A, B) and ROI spline (C) are drawn on the inner edge of the radiopaque PHV ring. For mechanical valves also the inner diameter (ID) is measured in the plane perpendicular to the PHV leaflets (D). All measurements were performed using a default setting with a window level of 800 and window width of 2000 Hounsfield units. *AD= area-derived diameter; AR=valve area; ID= inner diameter*

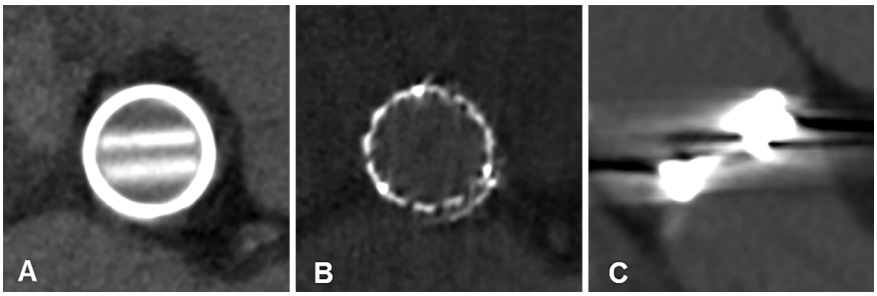

Figure 3 | Examples of the image quality scores. Example of good (A), fair (B) and poor (C) image quality in in the Carbomedics mechanical, Edwards Sapien transcatheter and Björk-Shiley monoleaflet valve, respectively.

coefficient (ICC) with absolute agreement. Intra-rater and inter-rater agreement was evaluated using the Bland-Altman plots with 95% limits of agreement. The possibility to discriminate consecutive PHV sizes was studied in all PHV subgroups by the median and maximal absolute range.

RESULTS

Both intra-rater and inter-rater reliability for the in vitro measurements was excellent for valve area, area-derived diameter and inner diameter (ICC ≥ 0.995). Agreement within and between raters was excellent as well (*Table 1*). The greatest difference found for diameter measurements between readers was 0.8mm. This is less than the minimal difference between two studied consecutive PHV sizes (1.5 mm) with differing internal diameters as provided by the manufacturers.

Table 1 | In vitro agreement and reliability

		Mean Δ (SD)	95% CI	ICC
Intra-rater	Area	-0.7 (5.5)	-11.5 – 10.1	0.999
	AD	0 (0.2)	-0.4 – 0.4	0.999
	ID	0 (0.1)	-0.2 – 0.2	1.000
Inter-rater	Area	6.3 (10.6)	-14.5 – 27.1	0.995
	AD	0.2 (0.3)	-0.4 - 0.8	0.995
	ID	0 (0.2)	-0.4 – 0.4	1.000

AD= area-derived internal diameter; CI=Confidence interval; ICC= intraclass correlation coefficient; ID= inner valve diameter; SD= standard deviation

A total of 230 patients with available MDCT imaging were included comprising 249 PHVs: 166 mechanical and 83 biological valves. The position of the implanted PHV was: 200 aortic, 43 mitral, 5 tricuspid and 1 pulmonary. The image quality was scored as good in 164 (66%), fair in 52 (21%) and poor in 33 (13%) PHVs. In the latter group, poor image quality due to valve related artifacts precluded assessment of the inner valve diameter in 6 valves (all Björk-Shiley) and in 1 valve also the area measurements could could not be performed due to extensive valve related artifacts (Björk-Shiley). In total, 48 PHVs (31 mitral) were assessed in systolic phase (10%-40% of the RR-interval) and 200 (184 aortic) in diastolic phase (70%-0% of the RR-interval). The vast majority was assessed in closed valve position.

Results of the intra-rater and inter-rater reliability for the in vivo measurements are presented in *Table 2*. An excellent correlation was found for both mechanical and biological valves (ICC ≥ 0.903). Good intra-rater and inter-rater agreement was found in general, and after stratification by main PHV type.

Table 2 | In patient agreement and reliability by prosthetic valve type

	Mechanical			Biological		
	Mean Δ (SD)	95% CI	ICC	Mean Δ (SD)	95% CI	ICC
Intra-rater						
Area	2.4 (11.8)	-20.7 – 25.5	0.993	1.6 (12.1)	-22.1 – 25.3	0.988
AD	0.1 (0.4)	-0.7 – 0.9	0.992	0 (0.3)	-0.6 – 0.6	0.988
ID	0.1 (0.3)	-0.5 – 0.7	0.994	n/a		
Inter-rater						
Area	-4.8 (12.7)	-29.7 – 20.1	0.991	0.1 (23.4)	-45.8 – 46.0	0.910
AD	-0.1 (0.3)	-0.7 – 0.5	0.993	0 (0.7)	-1.4 – 1.4	0.903
ID	0 (0.2)	-0.4 – 0.4	0.998	n/a		

AD= area-derived diameter; CI=Confidence interval; ICC= intraclass correlation coefficient; ID= inner valve diameter; n/a= not applicable; SD= standard deviation

All differences for diameter measurements within and between readers were less than the minimal difference between 2 consecutive sizes. The results on measurement agreement are presented in *Table 2* and *Figure 4*.

MDCT examples of the most common valves are presented in *Figure 5* and *Figure 6*. The reference overview in *Table 3* shows the median and range of the valve area and inner diameter measured in vitro and in patients for all studied mechanical valves obtained from the first measurements of observer 1 (CD). For biological valves, the median and range for the inner valve area and area-derived diameter are presented in *Table 4*. When available, results are compared to the dimensions provided by the manufacturers. As shown, the maximal range for specific PHV size measurements does not overlap with the consecutive labeled PHV size, thus PHV sizes can be discriminated. This is valid for consecutive labeled PHVs that truly differ in diameter of area as provided by the manufacturer.

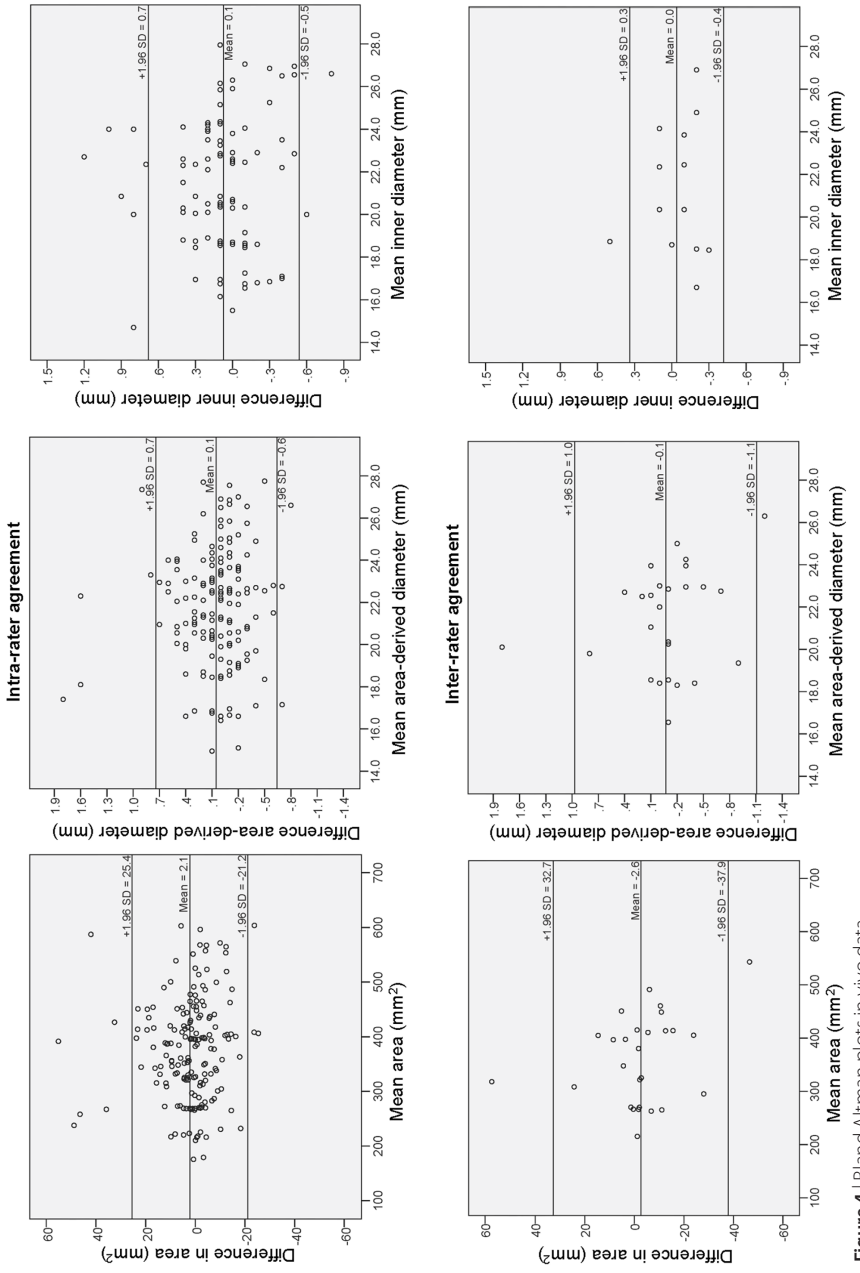

Figure 4 | Bland Altman plots in vivo data

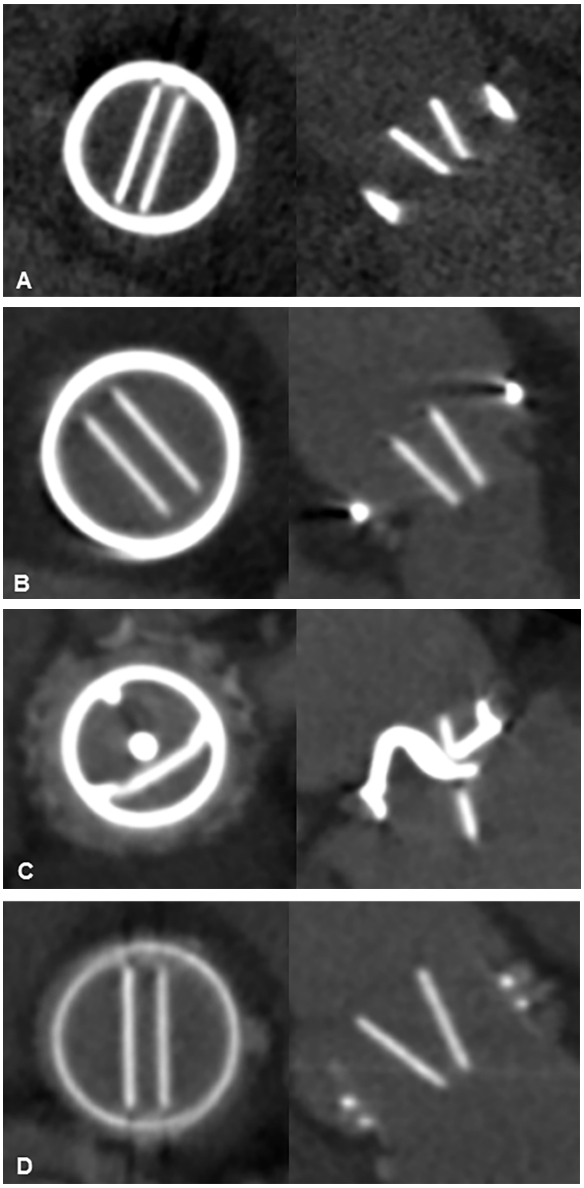

Figure 5 | Overview of the most common mechanical valves included in the study. Standard MDCT reconstructions of an (A) aortic Carbomedics 27mm (B) aortic St. Jude Regent 25mm, (C) mitral Medtronic-Hall monoleaflet 25mm and (D) aortic ON-X 23mm valve. An example of the Björk-Shiley monoleaflet valve which is related to poor image quality is shown in *Figure 3C*.

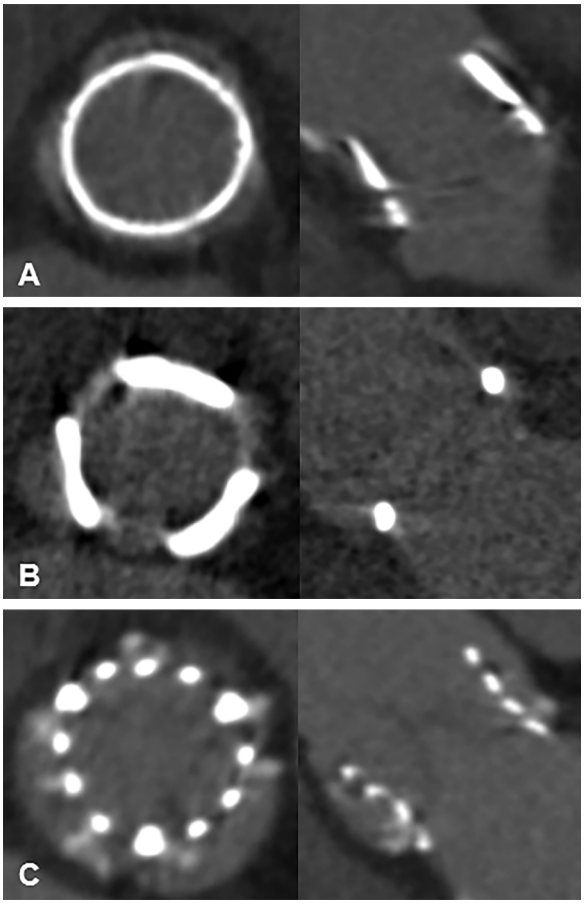

Figure 6 | Overview of the most common biological valves included in the study. Standard MDCT reconstructions of an (A) aortic Carpentier-Edwards Perimount 23mm (B) aortic Sorin Mitroflow 23mm and (C) Edwards Sapien transcatheter valve 23mm.

Table 3 | Results and reference list for mechanical heart valves

Manufacturer	Size	N*	Area † (mm^2)			ID (mm)		
			MFR	*In vitro*	In vivo	MFR	*In vitro*	In vivo
Carbomedics	21	6	207	*223.8*	218.3 [212.4-235.8]	16.7	*16.8*	16.9 [16.4-17.3]
	23	21	256	*275.6*	267.7 [261.1-276.6]	18.5	*18.8*	18.6 [18.1-18.8]
	25	18	316	*346.0*	325.9 [307.7-335.1]	20.5	*21*	20.4 [19.6-20.8]
	27	17	384	*414.2*	395.6 [364.1-410.4]	22.5	*23.0*	22.5 [22.0-23.1]
	29	5	444	*468.7*	454.3 [440.7-463.6]	24.2	*24.5*	23.9 [23.5-24.4]
	31	5	444	*473.3*	450.8 [439.5-455.3]	24.2	*24.4*	23.8 [23.6-24.2]
	33	2	444	*479.7*	449.7 [440.6-458.7]	24.2	*25.1*	24.0 [23.7-24.2]
St.Jude Regent	17	-	187	*209.3*	-	15.9	*16.9*	-
	19	-	239	*270*	-	17.8	*18.6*	-
	21	5	290	*328.3*	328.0 [319.6-342.5]	19.6	*20.6*	20.3 [19.9-21.2]
	23	9	345	*394.1*	386.2 [381.0-395.8]	21.4	*22.5*	22.2 [22.0-22.6]
	25	7	402	*461.7*	447.5 [439.5-469.5]	23.0	*24.3*	23.9 [23.4-24.1]
	27	2	469	*530.6*	525.5 [525.3-525.5]	24.9	*26.1*	26.0 [25.9-26.1]
	29	2	544	*624.2*	599.7 [599.4-599.7]	26.8	*28.4*	28.1 [27.9-28.2]
St.Jude Masters	25	-	309	*359.4*	-	20.4	*21.2*	-
	27	2	367	*428.7*	405.4 [398.5-412.3]	22.5	*23.4*	22.8 [22.4-23.2]
	29	-	441	*505.3*	-	24.2	*25.3*	
	31	5	518	*583.1*	552.7 [535.2-576.7]	26.1	*27.2*	26.9 [26.3-27.2]
	33	3	518	*586.7*	566.3 [559.4-569.6]	26.1	*27.1*	27.0 [26.7-27.1]
St.Jude HP	21	1	255	-	270.6	18.6	-	18.3
St.Jude Silzone	23	1	n/a	-	333.7	n/a	-	20.8
St.Jude CAVG	25	2	309	-	267.3 [256.0-267.3]	20.4	-	18.2 [18.0-18.3]
Sorin Slimline	19	-	233	*209.9*	-	17.6	*16.2*	-
	21	-	291	*260.6*	-	19.6	*18.4*	-
	23	1	355	*321.9*	317.2	21.7	*20.3*	19.9
	25	2	426	*388.9*	368.4 [346.1-390.6]	23.8	*22.1*	21.1
	27	-	512	*474.6*	-	26.1	*24.7*	-
Sorin Fitline	25	1	355	*326.0*	303.0	21.3	*20*	19.9
	27	-	426	*388.2*	-	23.3	*22.6*	-
	29	2	512	*470.4*	483.8 [476.8-490.8]	25.6	*24.3*	24.9 [24.2-25.6]
	31	1	512	*472.0*	452.6	25.6	*24.5*	23.7
	33	-	512	*473.4*	-	25.6	*24.6*	-
ON-X	19	-	222	*290.4*	-	17.4	*19.1*	-
	21	1	279	*354.7*	333.6	19.4	*21.3*	20.4
	23	3	342	*439.9*	435.5 [429.9-439.9]	21.4	*23.3*	23.2 [23.0-23.4]
	25	5	409	*504.0*	503.8 [491.9-525.5]	23.4	*25.3*	25.4 [24.9-25.8]
	27/29	3	409	*505.6*	494.3 [491.0-503.2]	23.4	*25.1*	25.1 [25.0-25.6]
	31/33	-	409	*501.4*	-	23.4	*25.3*	-

Table 3 | Continued

Manufacturer	Size	N*	Area † (mm^2)			ID (mm)		
			MFR	*In vitro*	In vivo	MFR	*In vitro*	In vivo
Medtronic-Hall	20	1	201	-	186.5	16	-	14.9
	22	7	254	-	220.2 [210.5-238.1	18	-	16.7 [16.1-17.0]
	23	5	254	-	215.8 [212.1-222.3]	18	-	16.6 [16.5-16.8]
	25	3	314	-	266.3 [256.6-280.6]	20	-	18.6 [18.6-18.8]
	27	2	380	-	349.3 [342.4-356.1]	22	-	20.8 [20.6-20.9]
	29	1	452	-	402.8	24	-	22.8
Duromedics	21	2	n/a	-	178.1 [175.4-180.0]	n/a	-	14.9 [14.3-15.5]
	23	1	n/a	-	241.3	n/a	-	17.3
	25	1	n/a	-	257.4	n/a	-	17.1
	29	1	n/a	-	394.0	n/a	-	22.0
	31	1	n/a	-	381.4	n/a	-	21.3
ATS	23	1	256	-	282.3	18.8	-	19.2
	27	1	384	-	400.2	22.8	-	22.9
Björk-Shiley	19	2	n/a	-	125.7 [117.1-134.2]	n/a	-	Poor IQ
	23	1	n/a	-	Poor IQ	n/a	-	Poor IQ
	25	2	n/a	-	224.2 [213.4-234.9]	n/a	-	Poor IQ
	29	1	n/a	-	455.2	n/a	-	Poor IQ
	31	1	n/a	-	381.1	n/a	-	Poor IQ

* N represents the number of prosthetic heart valves studied in vivo per valve type and size

† For in vitro results the mean of the measurements by two observers is presented. For in vivo results, the median and the total range is presented as measured by one observer in multiple PHVs. All measurements were performed at a window level of 800 and window width of 2000 Hounsfield units. MDCT measurements do not detect radiolucent structures and may differ from manufacturer reference data.

Area= valve area of the prosthesis; ID= internal diameter of the prosthesis; IQ= image quality; MFR= manufacturer

Table 4 | Results and reference list for biological heart valves

Manufacturer	Size	N*	Area† (mm^2)		ID (mm)	AD (mm)	
			In vitro	In vivo	MFR	*In vitro*	In vivo
CE Perimount Aortic	19	-	*229.7*	-	18	*17.1*	-
	21	3	*285.6*	286.2 [249.3-290.5]	20	*19.1*	19.2 [19.4-19.4]
	23	16	*345.7*	350.5 [324.2-363.5]	22	*21.0*	21.1 [20.3-21.5]
	25	19	*408.6*	415.2 [395.7-436.8]	24	*22.8*	23.0 [22.4-23.6]
	27	6	*490.7*	480.1 [465.8-495.6]	26	*25.0*	24.7 [24.4-25.1]
	29	2	*565.9*	564.8 [560.5-569.0]	28	*26.8*	26.8 [26.7-26.9]
CE Perimount Mitral	27	1	*472.1*	494.8	27	*24.5*	25.1
	29	1	*548.7*	559.7	29	*26.4*	26.7
	31	2	*619.2*	622.7 [615.6-629.8]	31	*28.1*	28.2 [28.0-28.3]
	33	1	*618.2*	597.3	31	*28.1*	27.6
CE Porcine	27	1	-	389.3	25	-	22.3
Medtronic Mosaic	23	1	*305.0*	272.3	20.5	*19.7*	18.6
	25	1	*356.3*	305.4	22.5	*21.3*	19.7
	27	2	*406.1*	392.1 [372.2-412.0]	24.0	*22.7*	22.4 [21.8-22.9]
	29	-	*484.8*	-	26.0	*24.8*	-
	31	-	*555.1*	-	28.0	*26.6*	-
Sorin Mitroflow	19	-	*252.1*	-	15.4	*17.9*	-
	21	8	*307.8*	305.6 [293.5-332.2]	17.3	*19.8*	19.7 [19.3-20.6]
	23	5	*380.1*	359.8 [341.2-372.1]	19	*22*	21.4 [20.8-21.8]
	25	1	*456.1*	413.0	21	*24.1*	22.9
	27	2	*530.5*	522.9 [514.5-522.9]	22.9	*26.0*	25.8 [25.6-26.0]
	29	-	*643.2*	-	24.7	*28.6*	-
Sorin Pericarbon More	25	-	*402.3*	-	21	*22.6*	-
	27	-	*478.6*	-	23	*24.7*	-
	29	1	*557.0*	567.4	25	*26.6*	26.9
	31	-	*656.9*	-	27	*28.9*	-
	33	-	*741.5*	-	29	*30.8*	-
Edwards Sapien	23	4	-	294.5 [289.5-311.4]	-	-	19.4 [19.2-19.9]
	26	6	-	392.8 [381.3-418.9]	-	-	22.4 [22.0-23.1]

* N represents the number of prosthetic heart valves studied in vivo per valve type and size
† For in vitro results the mean of the measurements by two observers is presented. For in vivo results, the median and the total range is presented as measured by one observer in multiple PHVs. All measurements were performed at a window level of 800 and window width of 2000 Hounsfield units. MDCT measurements do not detect radiolucent structures and may differ from manufacturer reference data.
AD= area-derived internal diameter of the prosthesis; Area= valve area of the prosthesis; CE= Carpentier-Edwards; ID= internal diameter of the prosthesis; MFR= manufacturer

DISCUSSION

We present the first reliability and agreement study that assessed the reproducibility for measuring the PHV diameter and area using MDCT imaging. Measurements of the inner diameter and valve area were highly reproducible in both in vitro and in patients. MDCT may be used as a tool for the assessment of PHV size and a reference table is presented for mechanical and biological valves.

For mechanical valves, both inner diameter and area-derived diameter showed high correlation and agreement. Thus in daily practice, both methods could be used for PHV size assessment according to the clinicians' preference. Few studies evaluated measurements of the internal and/or external PHV ring or annulus diameter using MDCT[13-15]. LaBounty et al. found a good inter-rater agreement for external diameter measurement, with a mean difference of 0.1mm (95%CI -1.7 – 1.9)[13], despite some underestimation of both external diameter and valve area by MDCT compared to the manufacturer dimensions. Their study included only the monoleaflet Medtronic Hall and bileaflet St. Jude mechanical valves and the actual PHV sizes were not described. Lee et al. assessed the agreement between MDCT and manufacturers' values for leaflet length and valve area of the St. Jude bileaflet[14]. Though, in this study both the use of the statistical analysis method and the choice for leaflet length assessment are questionable. Bazeed et al. showed that non-enhanced MDCT assessment of the external PHV diameter of mechanical bileaflet PHVs correlates well with manufacturers specifications[15]. However, reliability and agreement were not assessed, thus no information about structural bias was provided and the PHV types were not specified. Moreover, none of the abovementioned studies on mechanical valves assessed the reliability of the MDCT measurements[13-15].

For biological valves, one study assessed the reliability of measuring the maximal valve opening area and found a high intra-rater and inter-rater correlation (ICC 0.97 and 0.96 respectively) with a mean difference of -0.029cm^2 (95%CI -0.225 - 0.167)[16]. The PHV opening area was assessed and compared to the effective orifice area as measured with echocardiography. In our study, we measured the radiopaque structure of the PHV instead of the leaflet opening and the results are not comparable.

Bapat et al. stated that the internal PHV diameter as given by the manufacturer or measured with non-invasive imaging may not present the true internal diameter as measured using Hegar dilators, which is most relevant for valve-in-valve implantation[17]. However in case that the implanted PHV size is unknown, MDCT can reliably assess the internal diameter and retrieve the labeled size. Hence,

our results may help in the sizing for transcatheter valve-in-valve procedures. As valve-in-valve results for stentless valves have been erratic because of significant coronary occlusion risks, these valves were considered of lesser importance and excluded[6]. Moreover, they do not contain a radiopaque reference point and their dimensions are primarily determined by the aortic root geometry and implantation technique[18].

A strength of this study is the large group of included patients, especially of those with biological valves, considering biological PHV size assessment has not been evaluated previously. The in vivo measurements demonstrated a low inter-rater variability which suggests that MDCT readings are highly reproducible. Although the image quality was scored as decreased (fair or poor) in 34% of patient acquisitions, the images still allowed for size measurements except for all the Björk-Shiley valves. These valves are known to demonstrate severe valve related artifacts[18]. We deliberately used the inner diameter as a reference measure for PHV size assessment. Another alternative as was used in the studies of Bazeed et al. and LaBounty et al. is the external valve diameter[13, 15]. For PHV size assessment the external MDCT diameter could be related to the tissue annulus diameter as often provided by the manufacturer. However, several other external diameters are presented by the manufacturers as well, such as the external sewing ring diameter, cuff diameter and flare diameter, which can be confusing and complex for daily clinical practice.

As for inner diameter only one value is presented by the manufacturer and thus this dimension seems most clear and convenient. Importantly, the MDCT reference standard as presented shows again the discrepancies in labeled PHV sizes for true dimensions[8]. Our study has proven that for specific valve types such as all the St. Jude valves, the aortic Sorin and the Carpentier-Edwards biological valves one needs the specific PHV subtype to assess the implanted labeled PHV size. Furthermore, it is essential to use standardized window level settings to prevent measurement errors and inconsistencies due to metal blooming effects. We therefore used a window level of 800 and window width of 2000 Hounsfield units for all measurements.

A limitation of this study is the retrospective study design. With this, we had to exclude patients from analysis since the PHV manufacturer or size of the implanted valve was not documented correctly or not reported at all in the medical files.

Although we tried to be as comprehensive as possible, we do not have MDCT data on all available prosthetic valves. Furthermore, only one acquisition was performed per PHV for the in vitro study. However, these measurements were compared to the in vivo measurements where most PHVs were available in multiple patient

acquisitions. Lastly, this study comprised images acquired mainly at 120 kV and reconstructed with standard filtered back projection. We have not evaluated whether the reference values alter with the use of iterative reconstruction techniques or different tube voltage levels.

REFERENCES

1. Nishimura RA, Otto CM, Bonow RO, Carabello BA, Erwin JP, Guyton RA, et al. 2014 aha/acc guideline for the management of patients with valvular heart disease: A report of the american college of cardiology/american heart association task force on practice guidelines. *J Thorac Cardiovasc Surg*. 2014;148:e1-e132
2. Zoghbi WA, Chambers JB, Dumesnil JG, Foster E, Gottdiener JS, Grayburn PA, et al. Recommendations for evaluation of prosthetic valves with echocardiography and doppler ultrasound: A report from the american society of echocardiography's guidelines and standards committee and the task force on prosthetic valves, developed in conjunction with the american college of cardiology cardiovascular imaging committee, cardiac imaging committee of the american heart association, the european association of echocardiography, a registered branch of the european society of cardiology, the japanese society of echocardiography and the canadian society of echocardiography, endorsed by the american college of cardiology foundation, american heart association, european association of echocardiography, a registered branch of the european society of cardiology, the japanese society of echocardiography, and canadian society of echocardiography. *J Am Soc Echocardiogr*. 2009;22:975-1014
3. Shibata T, Inoue K, Ikuta T, Bito Y, Yoshioka Y, Mizoguchi H. Which valve and which size should we use in the valve-on-valve technique for re-do mitral valve surgery? *Interact Cardiovasc Thorac Surg*. 2009;8:206-210
4. Chambers JB, Oo L, Narracott A, Lawford PM, Blauth CI. Nominal size in six bileaflet mechanical aortic valves: A comparison of orifice size and biologic equivalence. *J Thorac Cardiovasc Surg*. 2003;125:1388-1393
5. Webb JG, Wood DA, Ye J, Gurvitch R, Masson JB, Rodes-Cabau J, et al. Transcatheter valve-in-valve implantation for failed bioprosthetic heart valves. *Circulation*. 2010;121:1848-1857
6. Dvir D, Webb J, Brecker S, Bleiziffer S, Hildick-Smith D, Colombo A, et al. Transcatheter aortic valve replacement for degenerative bioprosthetic surgical valves: Results from the global valve-in-valve registry. *Circulation*. 2012;126:2335-2344
7. Seiffert M, Conradi L, Baldus S, Knap M, Schirmer J, Franzen O, et al. Impact of patient-prosthesis mismatch after transcatheter aortic valve-in-valve implantation in degenerated bioprostheses. *J Thorac Cardiovasc Surg*. 2012;143:617-624
8. Christakis GT, Buth KJ, Goldman BS, Fremes SE, Rao V, Cohen G, et al. Inaccurate and misleading valve sizing: A proposed standard for valve size nomenclature. *Ann Thorac Surg*. 1998;66:1198-1203
9. Doenst T, Amorim PA, Al-Alam N, Lehmann S, Mukherjee C, Faerber G. Where is the common sense in aortic valve replacement? A review of hemodynamics and sizing of stented tissue valves. *J Thorac Cardiovasc Surg*. 2011;142:1180-1187
10. Ng AC, Delgado V, van der Kley F, Shanks M, van de Veire NR, Bertini M, et al. Comparison of aortic root dimensions and geometries before and after transcatheter aortic valve implantation by 2- and 3-dimensional transesophageal echocardiography and multislice computed tomography. *Circ Cardiovasc Imaging*. 2010;3:94-102
11. Imran Hamid U, Digney R, Soo L, Leung S, Graham AN. Incidence and outcome of re-entry injury in redo cardiac surgery: Benefits of preoperative planning. *Eur J Cardiothorac Surg*. 2014;1–5
12. Kamdar AR, Meadows TA, Roselli EE, Gorodeski EZ, Curtin RJ, Sabik JF, et al. Multidetector computed tomographic angiography in planning of reoperative cardiothoracic surgery. *Ann Thorac Surg*. 2008;85:1239-1245

13. LaBounty TM, Agarwal PP, Chughtai A, Bach DS, Wizauer E, Kazerooni EA. Evaluation of mechanical heart valve size and function with ecg-gated 64-mdct. *AJR Am J Roentgenol*. 2009;193:W389-396
14. Lee DH, Youn HJ, Shim SB, Lee SH, Jung JI, Jung SE, et al. The measurement of opening angle and orifice area of a bileaflet mechanical valve using multidetector computed tomography. *Korean Circ J*. 2009;39:157-162
15. Bazeed MF, Moselhy MS, Rezk AI, Al-Murayeh MA. Low radiation dose non-contrast cardiac ct: Is it of value in the evaluation of mechanical aortic valve. *Acta Radiol*. 2012;53:389-393
16. Chenot F, Montant P, Goffinet C, Pasquet A, Vancraeynest D, Coche E, et al. Evaluation of anatomic valve opening and leaflet morphology in aortic valve bioprosthesis by using multidetector ct: Comparison with transthoracic echocardiography. *Radiology*. 2010;255:377-385
17. Bapat VN, Attia R, Thomas M. Effect of valve design on the stent internal diameter of a bioprosthetic valve: A concept of true internal diameter and its implications for the valve-in-valve procedure. *JACC Cardiovasc Interv*. 2014;7:115-127
18. Tsai IC, Lin YK, Chang Y, Fu YC, Wang CC, Hsieh SR, et al. Correctness of multi-detector-row computed tomography for diagnosing mechanical prosthetic heart valve disorders using operative findings as a gold standard. *Eur Radiol*. 2009;19:857-867

SUPPLEMENTARY MATERIAL

Appendix 1 | Heart valve prostheses evaluated in vitro

Prosthetic valve	Manufacturer	Sizes
Mechanical, aortic		
Carbomedics Reduced	Sorin Group, Arvada, CO	21, 23, 25, 27
Sorin Bicarbon Slimline	Sorin Group, Arvada, CO	19, 21, 23, 25, 27
St. Jude Regent FlexCuff	St. Jude Medical Inc, St. Paul, MN	17, 19, 21, 23, 25, 27, 29
ON-X	ON-X Life Technologies Inc, Austin, TX	19, 21, 23, 25
Mechanical, mitral		
Carbomedics Standard	Sorin Group, Arvada, CO	27, 29, 31, 33
Sorin Bicarbon Fitline	Sorin Group, Arvada, CO	25, 27, 29, 31, 33
St. Jude Master Series Standard Cuff	St. Jude Medical Inc, St. Paul, MN	25, 27, 29, 31, 33
ON-X	ON-X Life Technologies Inc, Austin, TX	25, 27/29, 31/33
Biological, aortic		
Carpentier-Edwards Perimount 2900	Edwards Lifesciences, Irvine, CA	19, 21, 23, 25, 27, 29
Medtronic Mosaic (Cinch II)	Medtronic Inc, Minneapolis, MN	23, 25, 27
Sorin Mitroflow	Sorin Group, Arvada, CO	19, 21, 23, 25, 27, 29
Biological, mitral		
Carpentier-Edwards Perimount Magna Ease	Edwards Lifesciences, Irvine, CA	27, 29, 31
Carpentier-Edwards Perimount Magna	Edwards Lifesciences, Irvine, CA	33
Medtronic Mosaic (Cinch)	Medtronic Inc, Minneapolis, MN	29,31
Sorin Pericarbon More	Sorin Group, Arvada, CO	25, 27, 29, 31, 33

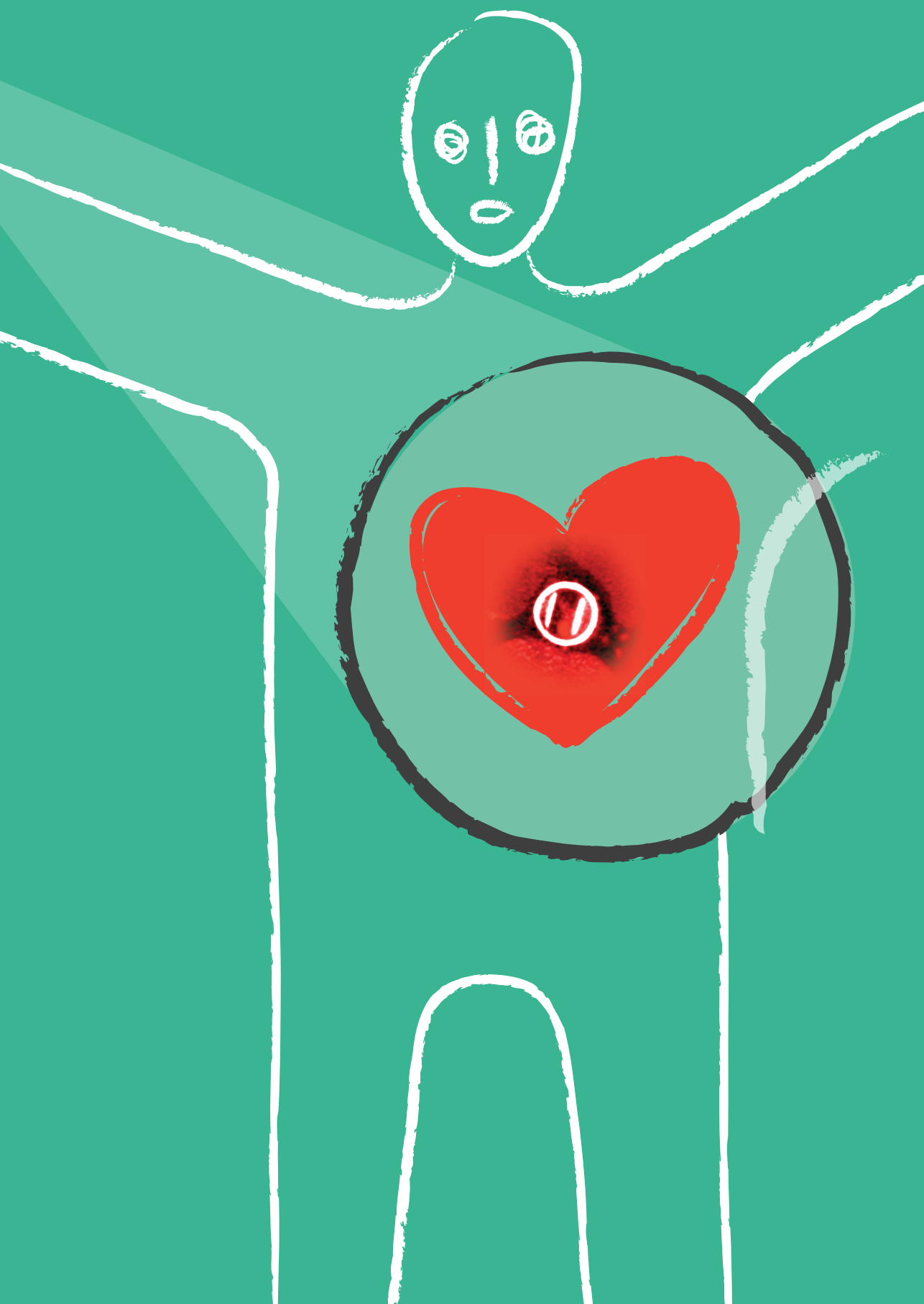

CHAPTER 10

Aortic bioprostheses deform after implantation: insights from multidetector-row computed tomography

Dominika Suchá
Petr Symersky
Linda M. de Heer
Willem P.Th.M. Mali
Lex A. van Herwerden
Ricardo P.J. Budde

Submitted

ABSTRACT

BACKGROUND

Distortion of biological aortic prosthetic heart valve geometry after implantation might affect leaflet coaptation, alter mechanical stress distribution and impact valve durability. Although much has been published on the distortion of transcatheter prostheses, little is known about the prevalence and degree of distortion of surgical aortic bioprostheses. The aim of this study was to assess deformation of aortic bioprostheses using multidetector-row computed tomography (MDCT).

METHODS

A retrospective search was performed in our database between 2007 and 2014 to acquire all patients with an aortic biological heart valve that underwent MDCT imaging. MDCT images were used to measure minimal and maximal valve diameters and the eccentricity index (EI, ratio of minimal and maximal valve ring diameter) was calculated as a measure of deformation. A prosthetic EI of <5% was considered none or trivial deformation, 5-10% mild deformation and ≥10% non-circular. Calcifications of the periprosthetic region were assessed using a visual 4-point scale (none, mild, moderate, severe).

RESULTS

Fifty-six aortic biological prostheses (45 Perimount, 7 Mitroflow, 4 Medtronic Mosaic) were included. Bioprostheses showed mild eccentricity in 16/56 (29%) of cases and non-circularity in 7/56 (13%) of cases. Median prosthetic EI was 4.5% [interquartile range 3.0-7.8%]. Periprosthetic calcifications were present in 44/56 (79%) of bioprostheses. There was no relation between eccentricity and periprosthetic calcifications (p=0.61). Median time from surgical implant to MDCT was 3 months [interquartile range 1-22].

CONCLUSIONS

Aortic biological valve geometry was deformed in 41% of cases and considered non-circular in 13% of studied valves. Deformation was not related to periprosthetic calcifications in this cohort.

INTRODUCTION

The introduction of transcatheter aortic valve implantation as a routine treatment for selected high risk patients with heart valve disease has entailed a great scientific interest in the evaluation of transcatheter heart valves (THVs) using different imaging modalities. One of the key concerns assessed by various imaging studies, is the eccentricity of THVs after implantation[1-3]. The native aortic annulus has shown to undergo dynamic change throughout the cardiac cycle, being predominantly oval in diastole and circular in systole[4, 5]. After THV implantation, non-circularity of the prosthesis has been described in up to a third of cases[6-8]. Undersizing and especially oversizing of THVs may have consequences as this can result in incomplete stent deployment[3, 9] and, amongst other things, incomplete leaflet expansion[10]. In addition, valve durability may be affected by the eccentricity of the prosthesis as prosthetic deformation can alter mechanical stress distribution and accelerate valve leaflet calcification[11, 12]. Similarly, deformation of surgically implanted aortic bioprostheses (ABPs) may impact durability as well. Although much attention has focused on anticalcification treatment of leaflet tissue, no work has specifically focused on implantation issues that may impact long-term durability. In analogy to THVs, deformation of valve geometry may alter the mechanical stresses on the tissue leaflets and accelerate valve degeneration. Deformation of stented aortic bioprotheses is related to the unequal distribution of stress on the suture ring and may be due to an improper implantation technique. For example, inadequate spacing of the sutures on the prosthetic ring in relation the aortic annulus may distort the stent that supports the leaflets. The aim of this study was to assess the eccentricity of biological valves after surgical implantation using multidetector-row computed tomography (MDCT) and evaluate the frequency of valve deformation.

METHODS

Study subjects

We retrospectively searched the medical database of our institution for patients with an aortic biological heart valve and available MDCT imaging between 2007 and 2014. Stentless valves and prosthetic valves in mitral, tricuspid and/or pulmonary position were excluded. Only one acquisition was included for analysis in patients with multiple MDCT acquisitions. The implanted valve type and size, the reason for MDCT acquisition and time from implantation to MDCT imaging were collected. Both prospectively ECG-triggered and retrospectively ECG-gated MDCT acquisitions were included. Given the retrospective nature of the study the need for informed consent was waived by the Medical Ethics Committee.

Image and data analysis

For each bioprosthesis, we selected the systolic and diastolic cardiac phase with least amount of PHV-related artifacts present and most optimal subjective image quality. For patients with prospectively ECG-triggered scans only the diastolic phase was available for analysis. Images were reconstructed in three planes using the multiplanar tool available on the dedicated workstation and software (Extended Brilliance Workstation, version 4.5; Philips Healthcare). Images were reconstructed exactly in plane with the prosthetic valve. This plane was used to obtain all measurements. One observer measured the maximal and minimal inner valve diameter for each valve in systole and diastole, if available, as presented in *Figure 1*.

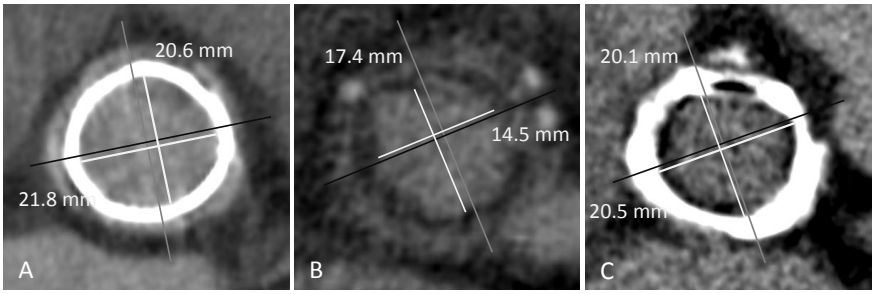

Figure 1 | Measurements. Example of in plane measurements of the minimal and maximal inner valve diameter in a Carpentier-Edwards Perimount (A), Sorin Mitroflow (B) and Medtronic Mosaic bioprosthesis in aortic position (C).

All measurements were performed at the level of the valve ring and/or stent where it was visible as a complete (circular) structure.

The eccentricity index (EI) was calculated for both cardiac phases as EI = 1 - (minimal diameter/maximal diameter)*100%. The eccentricity of the bioprosthesis was considered none/trivial (circular) with an EI <5%, mild with an EI 5-10% and non-circular with an EI of ≥10%. Calcification of the periprosthetic area was visually graded based on previously used methods by two observers[13-15]. The following grades of calcification were assigned: 0: no calcification, 1: mild with small isolated spots of calcification, 2: moderate with multiple larger spots of calcification, 3: severe with extensive calcification (*Figure 2*). Consensus was reached in case of disagreement between the observer scores.

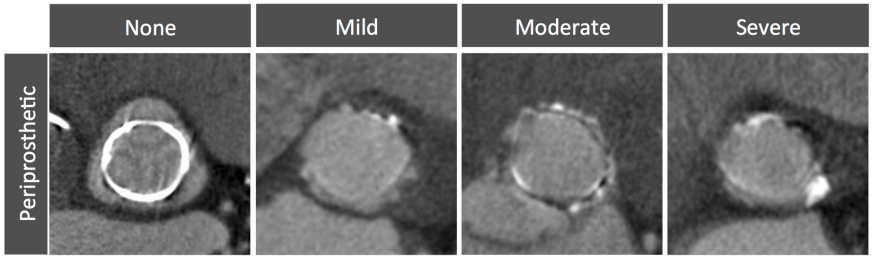

Figure 2 | Calcification score. Calcification visual grading score for the periprosthetic/annular region in patients with aortic biological valves.
None= no calcifications; Mild= mild calcifications with small isolated spots of calcification; Moderate= moderate calcifications with multiple larger spots of calcification; Severe= severe, extensive calcifications calcification.

Statistical analysis

IBM SPSS Statistics 22.0 software was used for analysis. QQ-plots and Kolmogorov-Smirnov tests were performed to evaluated data distribution. Categorical data are presented as number and percentage, continuous data as mean ± standard deviation or median and interquartile range [IQR] as appropriate. The Wilcoxon signed rank test was used to compare paired systolic and diastolic EI measurements and the Fisher's exact test was used to evaluate significant differences between patients for the periprosthetic calcification grade (none and ≥ mild) and the eccentricity score (none/trivial and ≥ mild eccentricity). A P-value of <0.05 was considered significant.

RESULTS

In total, 70 patients with 71 stented biological valves and available MDCT imaging were identified. Of these, five prostheses were not in the aortic position and 10 were THVs and excluded from further analysis. Hence, our search yielded 56 ABPs. An overview of the included bioprostheses and reasons for MDCT imaging is presented in *Table 1*. The vast majority of studied valves concerned the Carpentier-Edwards Perimount valve (80%). In 57% of cases MDCT imaging was performed for suspected ABP dysfunction (of any kind) and in 43% MDCT was performed in supposedly normal functioning ABPs for research purposes or for other reasons than prosthetic valve assessment. Median time between bioprosthesis implant and MDCT imaging was 3 months [IQR 1-22].

Overall, surgical bioprostheses showed ≥ mild eccentricity in 19/46 (41%) valves measured in the systolic phase and in 23/56 (41%) measured in the diastolic phase. Non-circular ABPs were found in 6/46 (13%) cases using systolic measurements and 7/56 (13%) using diastolic measurements (*Table 2*).

Table 1 | Studied surgical valves

	Total N=56
Bioprosthesis type	
Carpentier-Edwards Perimount	45 (80%)
Medtronic Mosaic	4 (7%)
Sorin Mitroflow	7 (13%)
Prosthesis size	
21 mm	6 (11%)
23 mm	20 (36%)
25 mm	19 (34%)
27 mm	9 (16%)
29 mm	2 (4%)
Main reason MDCT	
Research purpose (no pathology)	20 (36%)
Suspected endocarditis	15 (27%)
Suspected obstruction	8 (14%)
Suspected leakage (non-endocarditis)	3 (5%)
Suspected dysfunction (general)	6 (11%)
Non PHV-related	4 (7%)
Time implant to MDCT, months	3 [1-22]

Data presented as number (percentage) or median [interquartile range]

Table 2 | Deformation of aortic bioprostheses

Surgical valves	Systolic phase	Diastolic phase
	N=46	N=56
None/trivial eccentricity	27 (59%)	33 (59%)
Mild eccentricity	13 (28%)	16 (29%)
Non-circular	6 (13%)	7 (13%)

Eccentricity was defined as: none/trivial <5%, mild 5-10% and non-circular ≥10% eccentricity

Examples of all ABP types are shown in *Figure 3*. Median (systolic) eccentricity of the ABPs was 4.5% [3.0-7.8%] (*Table 3*). No significant differences were found for the EI between all systolic and diastolic measurements (all $P \geq 0.11$).

Examples of the calcification scores are presented in *Figure 2*. In 12/56 cases (21%) no periprosthetic calcifications were present. Patients with ABPs predominantly

showed mild calcifications of the periprosthetic region (28/56, 50%). Any periprosthetic calcifications were present in 44/56 (79%) ABPs, of which 5/56 (9%) were considered severe. No significant difference was found between valves with none/trivial eccentricity and ≥ mild eccentricity and none or ≥ mild calcifications of the periprosthetic region (P=0.61).

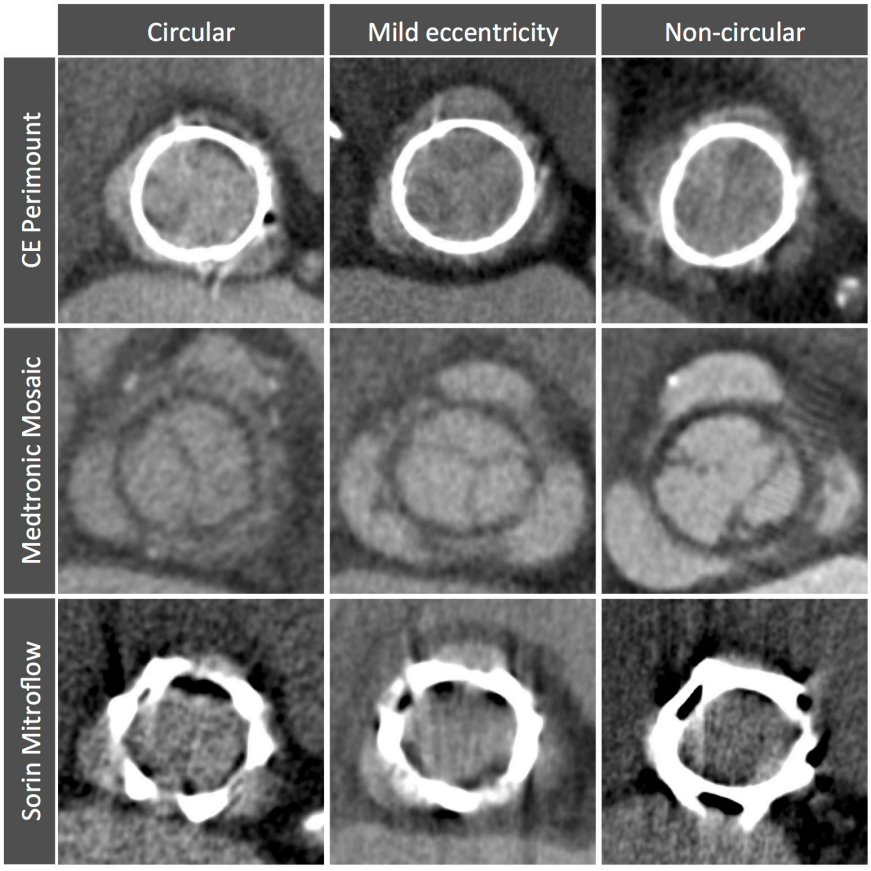

Figure 3 | Eccentricity in biological surgical valves. Overview of the eccentricity of the aortic biological valves: Carpentier-Edwards Perimount, Medtronic Mosaic and Sorin Mitroflow. Eccentricity was defined as: none/trivial (circular) <5%, mild 5-10% and non-circular ≥10% eccentricity based on the eccentricity index calculated as (1 - (minimal diameter/maximal diameter))*100.

Table 3 | Biological valve eccentricity

	Eccentricity*				
	N	Systolic	N	Diastolic	P-value
Biological valves	46	4.5% [3.0-7.8%]	56	4.3% [2.4-6.6%]	0.39
Carpentier-Edwards Perimount	36	4.1% [2.1-6.6%]	45	4.1% [2.4-5.8%]	0.36
Medtronic Mosaic	3	7.7% [NA]	4	5.9% [2.4-10.7%]	0.11
Sorin Mitroflow	7	9.3% [3.2-12.1%]	7	7.8% [4.7-14.0%]	0.61

* Presented as median [interquartile range], measured as (1 - (minimal diameter/maximal diameter))*100
N=total number valves evaluated; NA=not available due to count

DISCUSSION

In the current study we evaluated the eccentricity of biological valves after surgical implantation using MDCT and found a considerable amount of aortic bioprostheses to show deformation. At least mild eccentricity was found in 23/56 (41%) biological valves of which 7/56 (13%) were considered non-circular. No significant difference was found between patients for the presence of periprosthetic calcifications and none/trivial deformation or ≥ mild prosthesis deformation.

Previous studies have shown that mechanical stress can impact (pathological) tissue calcification, which affects valve durability[11, 12, 16, 17]. It has also been suggested that structural deformation might contribute to the valve calcification process[11, 18].

As deformation of the prosthetic stent can impact leaflet composition and stress distribution, bioprostheses with significant deformation may be more prone to early structural valve deterioration. Literature on the prevalence and degree of deformation of surgical bioprostheses is, however, scarce. In our study, we found a considerable portion of implanted valves to show valve deformation of any extent. In contrast to surgical valves, the eccentricity of THVs was evaluated in several studies. For balloon-expandable THVs a circular prosthesis was found in most patients, showing a non-circular prosthesis in 0-34% of the studied population[1-3, 6, 8, 9, 19, 20]. In contrast, the self-expandable CoreValve was non-circular in 87% of patients at ventricular level and in 67% at the nadir of leaflets. One study found no differences for stent frame EI within different balloon-expandable THV types (Sapien (XT) and Cribier-Edwards)[3], though results on balloon-expandable and self-expandable THVs may not be comparable. One factor that may impact EI results is the stent level selected for EI measurement as a trend has been shown for most deformation at ventricular site and most circularity (least eccentricity) at the

aortic site for the Edwards Sapien[3, 6, 9], St. Jude Portico[20] and Corevalve THVs[7]. In our study, the biological valve diameters were measured at the level of the annulus. The native aortic annulus has shown to change shape throughout the cardiac cycle[5]. For biological valves, we did not find significant differences between systolic and diastolic EI measurements. The bioprosthetic stent ring is a rigid structure and may therefore be less subject to cardiac phase-related deformation. Surgical valves also differ fundamentally from THVs. Hence the underlying mechanism of deformation is likely to differ between surgical and transcatheter valves. With surgical valves, native annular calcifications are resected before valve implantation, whereas for transcatheter implantation a certain amount and distribution is needed for prosthesis positioning and deployment. In THVs, annular calcifications have been reported to impact stent deployment and eccentricity[2, 3]. Since calcifications are resected during surgical implantation, this mechanism is not likely to account for deformation in bioprostheses. In this study, we also did not find a significant difference for the degree of deformation and presence of periprosthetic calcifications. However, deformation might be induced by the implantation technique itself. It seems plausible that the biological valve can undergo deformation due to the force exerted by surgical sutures on the sewing ring. Should the tension by the sutures be distributed unequally at implant, the biological valve may adopt to a (slightly) non-circular shape. If it were assumed that valve deformation is predictive for clinically suboptimal results or valve dysfunction over time, it would be interesting to evaluate specific surgical techniques. Furthermore, future studies may provide insight on differences between specific surgical bioprostheses types and the degree of deformation and/or structural deterioration.

Study limitations

First, due to selection of the valves with 57% imaged due to suspected dysfunction, our study sample may not be representative of a normal consecutive surgical cohort. Also, the sample size of the Medtronic Mosaic and Sorin Mitroflow valves was small; therefore a subanalysis for bioprosthesis type and amount of deformation could not be performed. Second, the median time from implant to MDCT was only three months. Third, we did not perform a reliability and agreement analysis for EI measurements in the current study. However, MDCT has been used repeatedly to assess the EI in THVs[1-3, 6, 8, 9, 19, 20] and the reliability and agreement for diameter measurements in biological valves was assessed previously[21]. In addition, no difference between MDCT and three-dimensional transesophageal echocardiography was found with annular eccentricity assessment in THVs[22].

To conclude, surgical ABPs in this study showed valve deformation in 42% of cases as assessed with MDCT at a median of 3 months [IQR 1-22] after implantation. Future studies are required to evaluate the prognostic value of biological valve deformation on valve durability and assess differences within different valve types.

REFERENCES

1. Binder RK, Webb JG, Toggweiler S, Freeman M, Barbanti M, Willson AB, et al. Impact of post-implant sapien xt geometry and position on conduction disturbances, hemodynamic performance, and paravalvular regurgitation. *JACC Cardiovasc Interv*. 2013;6:462-468
2. Delgado V, Ng AC, van de Veire NR, van der Kley F, Schuijf JD, Tops LF, et al. Transcatheter aortic valve implantation: Role of multi-detector row computed tomography to evaluate prosthesis positioning and deployment in relation to valve function. *Eur Heart J*. 2010;31:1114-1123
3. Willson AB, Webb JG, Gurvitch R, Wood DA, Toggweiler S, Binder R, et al. Structural integrity of balloon-expandable stents after transcatheter aortic valve replacement: Assessment by multidetector computed tomography. *JACC Cardiovasc Interv*. 2012;5:525-532
4. de Heer LM, Budde RP, van Prehn J, Mali WP, Bartels LW, Stella PR, et al. Pulsatile distention of the nondiseased and stenotic aortic valve annulus: Analysis with electrocardiogram-gated computed tomography. *Ann Thorac Surg*. 2012;93:516-522
5. Suchá D, Tuncay V, Prakken NH, Leiner T, van Ooijen PM, Oudkerk M, et al. Does the aortic annulus undergo conformational change throughout the cardiac cycle? A systematic review. *Eur Heart J Cardiovasc Imaging*. 2015
6. Caudron J, Fares J, Hauville C, Cribier A, Dacher JN, Tron C, et al. Evaluation of multislice computed tomography early after transcatheter aortic valve implantation with the edwards sapien bioprosthesis. *Am J Cardiol*. 2011;108:873-881
7. Schultz CJ, Weustink A, Piazza N, Otten A, Mollet N, Krestin G, et al. Geometry and degree of apposition of the corevalve revalving system with multislice computed tomography after implantation in patients with aortic stenosis. *J Am Coll Cardiol*. 2009;54:911-918
8. Wood DA, Tops LF, Mayo JR, Pasupati S, Schalij MJ, Humphries K, et al. Role of multislice computed tomography in transcatheter aortic valve replacement. *Am J Cardiol*. 2009;103:1295-1301
9. Binder RK, Rodes-Cabau J, Wood DA, Mok M, Leipsic J, De Larochelliere R, et al. Transcatheter aortic valve replacement with the sapien 3: A new balloon-expandable transcatheter heart valve. *JACC Cardiovasc Interv*. 2013;6:293-300
10. Abbasi M, Azadani AN. Leaflet stress and strain distributions following incomplete transcatheter aortic valve expansion. *J Biomech*. 2015;48:3672-3678
11. Schoen FJ, Levy RJ. Calcification of tissue heart valve substitutes: Progress toward understanding and prevention. *Ann Thorac Surg*. 2005;79:1072-1080
12. Thubrikar MJ, Deck JD, Aouad J, Nolan SP. Role of mechanical stress in calcification of aortic bioprosthetic valves. *J Thorac Cardiovasc Surg*. 1983;86:115-125
13. Grunenfelder J, Plass A, Alkadhi H, Genoni M. Evaluation of biological aortic valve prostheses by dual source computer tomography and anatomic measurements for potential transapical valve-in-valve procedure. *Interact Cardiovasc Thorac Surg. 2008;7:195-200*
14. Rosenhek R, Binder T, Porenta G, Lang I, Christ G, Schemper M, et al. Predictors of outcome in severe, asymptomatic aortic stenosis. *N Engl J Med*. 2000;343:611-617
15. Takx RA, Zanen P, Leiner T, van der Graaf Y, de Jong PA, group Ss. The interdependence between cardiovascular calcifications in different arterial beds and vascular risk factors in patients at high cardiovascular risk. *Atherosclerosis*. 2015;238:140-146
16. Bernacca GM, Fisher AC, Wilkinson R, Mackay TG, Wheatley DJ. Calcification and stress distribution in bovine pericardial heart valves. *J Biomed Mater Res*. 1992;26:959-966

17. Smith DB, Sacks MS, Pattany PM, Schroeder R. Fatigue-induced changes in bioprosthetic heart valve three-dimensional geometry and the relation to tissue damage. *J Heart Valve Dis*. 1999;8:25-33
18. van Nooten G, Ozaki S, Herijgers P, Segers P, Verdonck P, Flameng W. Distortion of the stentless porcine valve induces accelerated leaflet fibrosis and calcification in juvenile sheep. *J Heart Valve Dis*. 1999;8:34-41
19. Blanke P, Reinohl J, Schlensak C, Siepe M, Pache G, Euringer W, et al. Prosthesis oversizing in balloon-expandable transcatheter aortic valve implantation is associated with contained rupture of the aortic root. *Circ Cardiovasc Interv*. 2012;5:540-548
20. Willson AB, Rodes-Cabau J, Wood DA, Leipsic J, Cheung A, Toggweiler S, et al. Transcatheter aortic valve replacement with the st. Jude medical portico valve: First-in-human experience. *J Am Coll Cardiol*. 2012;60:581-586
21. Suchá D, Daans CG, Symersky P, Planken RN, Mali WP, van Herwerden LA, et al. Reliability, agreement, and presentation of a reference standard for assessing implanted heart valve sizes by multidetector-row computed tomography. *Am J Cardiol*. 2015;116:112-120
22. Ng AC, Delgado V, van der Kley F, Shanks M, van de Veire NR, Bertini M, et al. Comparison of aortic root dimensions and geometries before and after transcatheter aortic valve implantation by 2- and 3-dimensional transesophageal echocardiography and multislice computed tomography. *Circ Cardiovasc Imaging*. 2010;3:94-102

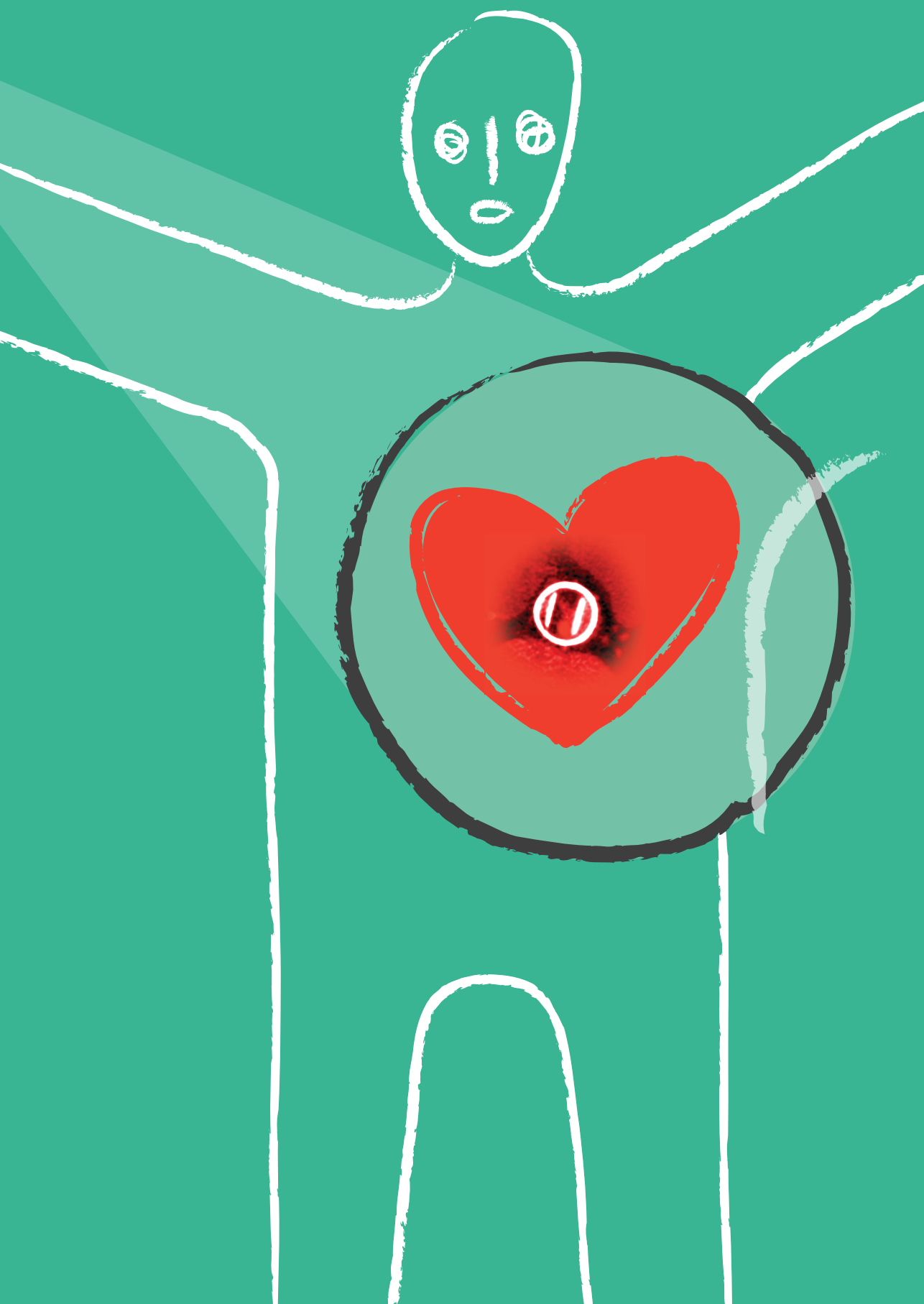

CHAPTER 11

MDCT diagnosis of early severe structural degeneration of a Mitroflow aortic bioprosthesis

Dominika Suchá
Ricardo P.J. Budde
Ronald T.A. van den Bosch
Petr Symersky

Submitted

BACKGROUND

Recently concerns have been raised on the performance of the Mitroflow biological valve as a seemingly increased prevalence of relatively early structural valve deterioration (SVD) has been reported in young (≤ 30 years)[1] and elderly (≥65 years)[2] patients. A hypothesis for this is the absence of anticalcification therapy of the Mitroflow prosthesis. Furthermore, severe patient prosthesis mismatch (PPM) may be related to SVD in the absence of abnormalities on transthoracic echocardiography (TTE)[3]. We present a case of a 58-year old woman with very severe SVD without PPM only 16 months after valve replacement surgery and imaged with TTE, transesophageal echocardiography (TEE) and multidetector-row computed tomography (MDCT).

CASE PRESENTATION

A 58-year old female with severe symptomatic aortic stenosis underwent aortic valve replacement with a Mitroflow 21mm bioprosthesis in a supra-annular position. The patient received anticoagulation therapy with low-molecular-weight heparin until hospital discharge and continued daily aspirin therapy without any oral anticoagulation therapy. Baseline TTE 3 days after valve implantation showed a maximal transprosthetic gradient (TPG) of 17 mmHg.

Sixteen months after aortic valve replacement the patient was referred to our center with complaints of fatigue, dyspnea (New York Heart Association Class II) and occasional chest pain during exercise. She had a medical history of Diabetes Mellitus type II and severe obesity (body mass index of 36.7 kg/m^2, body surface area 2.16m^2). Physical examination revealed a murmur over the aortic area radiating into the neck. At clinical presentation, the patients' normalized international ratio was 0.90. The electrocardiogram at a mean sinus rhythm of 79 beats per minute detected a new left bundle branch block. TTE showed a maximal TPG of 89 mmHg and a mean TPG of 56 mmHg. Aortic valve area was 0.43 cm^2 with a dimensionless valve index of 16%. In addition, a moderate aortic insufficiency was detected, possibly of paravalvular origin (*Figure 1*). The underlying pathological mechanism was unclear. TEE was unsuccessful at this moment since the patient experienced too much discomfort related to the examination.

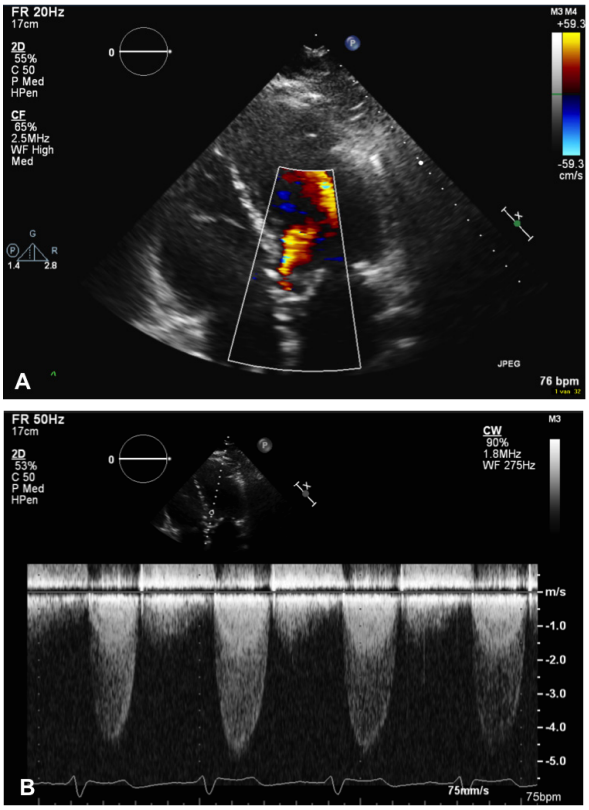

Figure 1 | Transthoracic echocardiography. Color Doppler TTE detected mild regurgitation (A) of the Mitroflow bioprosthesis in aortic position and continuous-wave Doppler TTE images showed severe prosthetic stenosis with high transprothetic gradients (B).

The patient underwent additional MDCT imaging. Non-enhanced prospective ECG-triggered imaging showed extensive calcifications of the right coronary artery, left anterior descending artery and circumflex artery. Retrospective ECG-gated imaging showed no signs of prosthetic valve obstruction (no pannus or thrombus). Despite of high image noise and valve-related artifacts, extensive calcifications of the prosthetic leaflets were suggested (*Figure 2*). MDCT also showed extensive mitral valve annulus calcifications.

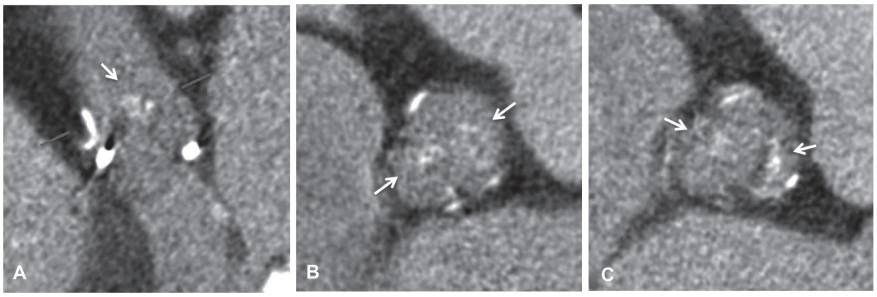

Figure 2 | Multidetector-row computed tomography. MDCT images of the 21 mm Mitroflow valve in aortic position in diastole (A and B) and systole (C). Lines in (A) indicate the level of images (B) and (C). Despite the relatively high amount of image noise (body mass index of 36) substantial valve leaflet calcification can be appreciated. Furthermore, no adherent thrombus mass or pannus is detected as cause of valve dysfunction.

Hereupon, the patient underwent TEE under general anesthesia. No pannus or thrombus was detected. TEE showed calcifications of all three leaflets of the Mitroflow valve with restricted leaflet opening and mild transprosthetic aortic insufficiency (*Figure 3*). Furthermore, mild mitral valve insufficiency was detected. Systolic left ventricular function was good.

The patient was referred for redo aortic valve surgery with a mechanical prosthesis. Unfortunately, the patient died during hospital admission while waiting for redo surgery.

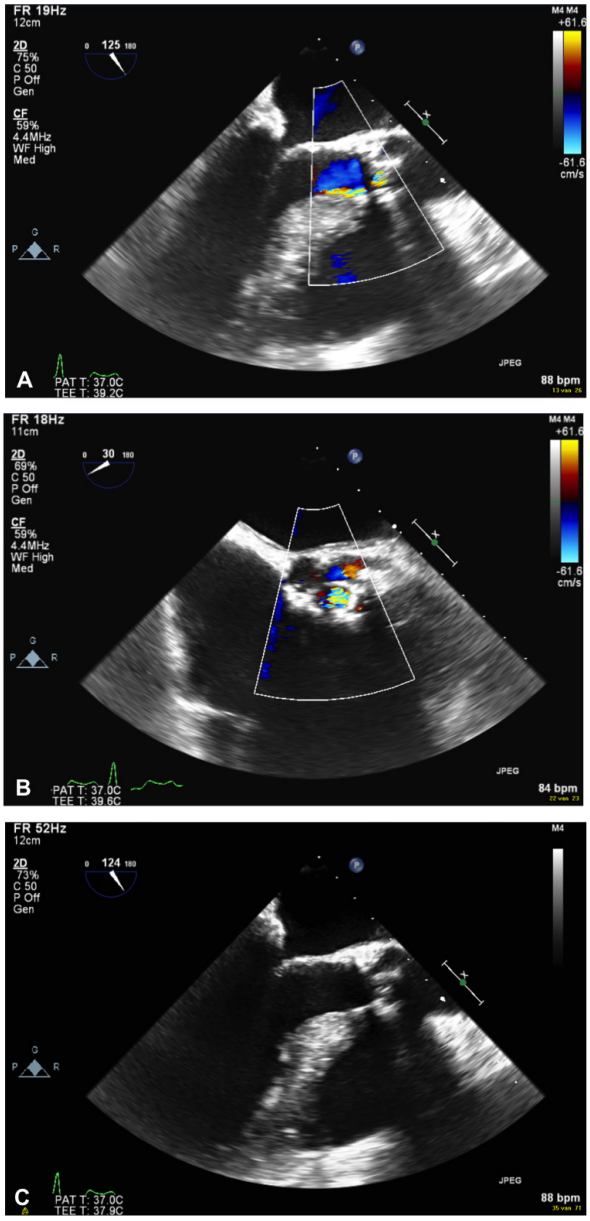

Figure 3 | Transesophageal echocardiography. TEE color Doppler detected transprosthetic regurgitation (A and B). Furthermore, TEE showed leaflet thickening of all three prosthetic cusps with restricted leaflet motion.

DISCUSSION

The aortic biological Mitroflow valve has been implanted frequently over the past years. Early SVD in patients aged over 65 years occurred (mean) 45 months after implantation in the study of Senage et al.[2] and 75 months in Luk et al[4]. It has been suggested that biological valves in younger patients may be more prone to SVD[5], possibly because of a more aggressive autoimmune response. Saleeb et al. reported early SVD occurring in children and young adults between 19-33 months after valve implantation[1]. In our case very severe SVD was shown only 16 months after implantation without PPM in a patient aged 58 years. Early SVD of a 21 mm Mitroflow may be related to the absence of valve leaflet anticalcification treatment and possibly to early non-occlusive leaflet thrombosis as reported by Makkar et al.[6] In accordance with previous results, our case seems to stress the need for earlier and more frequent follow-up after Mitroflow implantation, in all patients. Because of the architecture of the Mitroflow prosthesis, with the valve leaflets secured on the outside of three polyester valve struts, the inner diameter of the 21 mm prosthesis is 17 mm. Therefore, transcatheter approaches may result in significant residual transprosthetic gradients. Additionally, due to the supra-annular Mitroflow implantation, transcatheter valve-in-valve procedures may also result in obstruction of the coronary ostia[7]. Hence, surgical replacement may be the only appropriate approach. It remains important to identify the underlying pathologic mechanism. In this patient, TTE detected severe dysfunction, though the specific cause could not be identified. MDCT is a non-invasive modality rapidly available that can be used in case routine work-up is inconclusive or cannot be performed. In this case, MDCT suggested SVD by showing leaflet calcifications and made thrombus and pannus unlikely as the cause of dysfunction.

REFERENCES

1. Saleeb SF, Newburger JW, Geva T, Baird CW, Gauvreau K, Padera RF, et al. Accelerated degeneration of a bovine pericardial bioprosthetic aortic valve in children and young adults. *Circulation*. 2014;130:51-60
2. Senage T, Le Tourneau T, Foucher Y, Pattier S, Cueff C, Michel M, et al. Early structural valve deterioration of mitroflow aortic bioprosthesis: Mode, incidence, and impact on outcome in a large cohort of patients. *Circulation*. 2014;130:2012-2020
3. Pfeiffer S, Fischlein T, Santarpino G. Letter by pfeiffer et al regarding article, "early structural valve deterioration of mitroflow aortic bioprosthesis: Mode, incidence, and impact on outcome in a large cohort of patients". *Circulation*. 2015;132:e152
4. Luk A, Cusimano RJ, Butany J. Pathologic evaluation of 28 mitroflow pericardial valves: A 12-year experience. *Ann Thorac Surg*. 2015;99:48-54
5. Anantha Narayanan M, Suri RM, Ugur M, Greason KL, Stulak JM, Dearani JA, et al. Predictors of survival and modes of failure after mitroflow aortic valve replacement in 1,003 adults. *Ann Thorac Surg*. 2015;100:560-567
6. Makkar RR, Fontana G, Jilaihawi H, Chakravarty T, Kofoed KF, de Backer O, et al. Possible subclinical leaflet thrombosis in bioprosthetic aortic valves. *N Engl J Med*. 2015;373:2015-2024
7. Gurvitch R, Cheung A, Bedogni F, Webb JG. Coronary obstruction following transcatheter aortic valve-in-valve implantation for failed surgical bioprostheses. *Catheter Cardiovasc Interv*. 2011;77:439-444

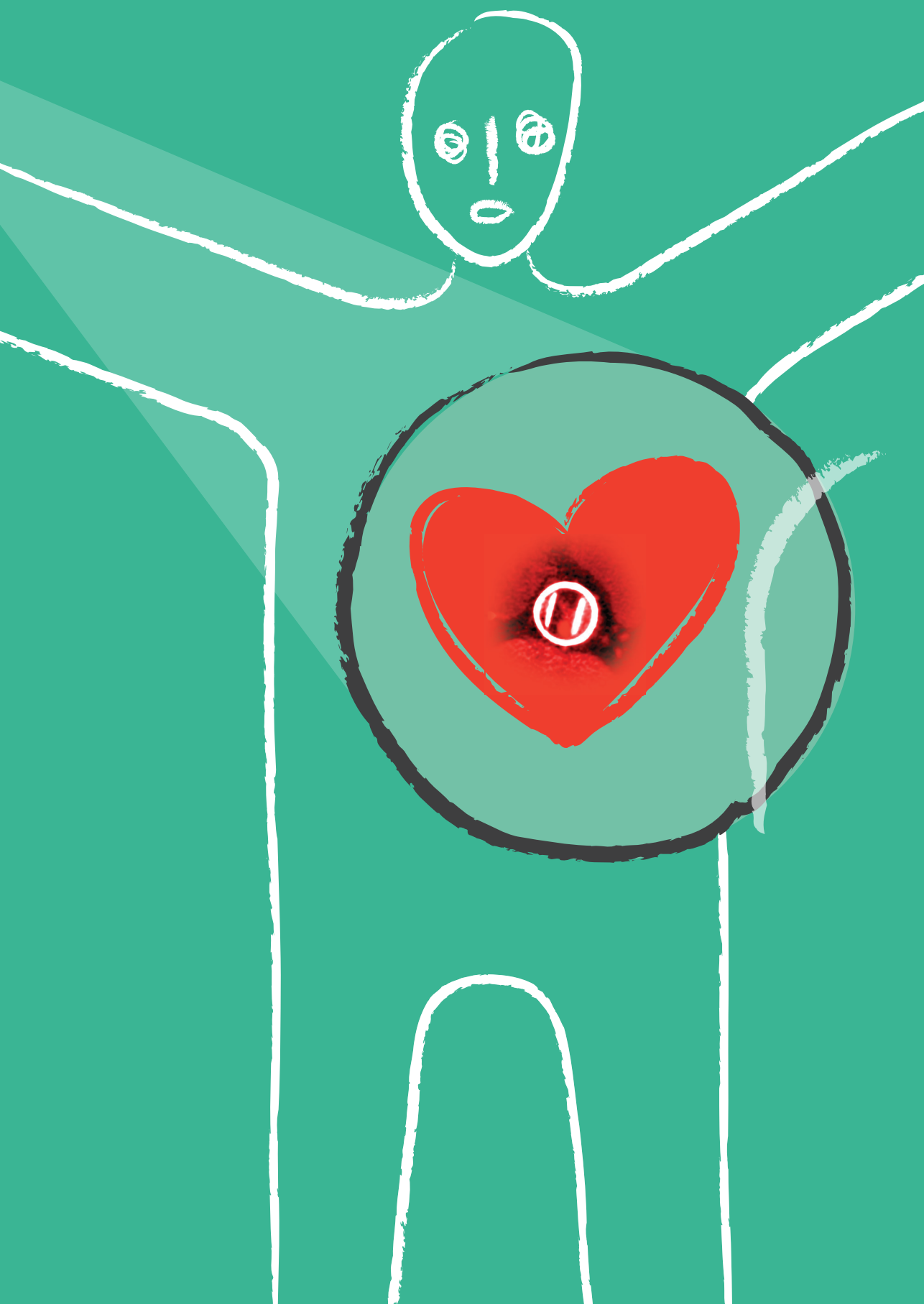

CHAPTER 12

Multidetector-row computed tomography for prosthetic heart valve dysfunction: is concomitant non-invasive coronary angiography possible before redo-surgery?

Dominika Suchá*
Wilco Tanis*
Eduard M. Laufer
Jesse Habets
Lex. A. van Herwerden
Petr Symersky
Steven A.J. Chamuleau
Ricardo P.J. Budde

*Both authors contributed equally to this paper

Published in European Radiology, 2015

ABSTRACT

PURPOSE

Retrospective ECG-gated multidetector-row computed tomography (MDCT) is increasingly used for the assessment of prosthetic heart valve (PHV) dysfunction. The purpose is to determine whether MDCT performed in PHV work-up for potential redo valve surgery is feasible for concomitant coronary artery stenosis assessment and can replace invasive coronary angiography (CAG).

METHODS

PHV patients with CAG and MDCT imaging were identified. Based on medical history, two groups were created: (I) patients with no known coronary artery disease (CAD), (II) patients with known CAD. All images were scored for the presence of significant (>50%) stenosis. CAG was the reference test.

RESULTS

Fifty-one patients were included. In group I (n=38), MDCT accurately ruled out significant stenosis in 19/38 (50%) patients, but could not replace CAG in the remaining 19/38 (50%) patients due to non-diagnostic image quality (n=16) or significant stenosis (n=3) detection. In group II (n=13), MDCT correctly found no patients without significant stenosis, requiring CAG imaging in all. MDCT assessed patency in 16/19 (84%) grafts and detected a hostile anatomy in two.

CONCLUSIONS

Retrospective MDCT performed for PHV dysfunction assessment can replace CAG imaging in approximately half of patients without previously known CAD for its excellent accuracy of ruling out significant coronary stenosis.

INTRODUCTION

Recently retrospectively ECG-gated multidetector-row computed tomography (MDCT) has shown additional diagnostic value (compared to echocardiography) for the evaluation of prosthetic heart valve (PHV) dysfunction and detection of PHV endocarditis[1-8]. As a result, PHV patients frequently undergo MDCT imaging before potential redo valve surgery[9]. According to the guidelines, preoperative invasive coronary angiography (CAG) is often required to detect significant coronary obstructions which may require concomitant bypass surgery. Although, MDCT may provide all aforementioned preoperative required information including coronary artery assessment, CAG is the reference standard for this indication[10]. In case of a vegetation or thrombus on an aortic PHV, however, mechanical manipulation by an invasive catheter may be undesirable since it can be complicated by distal embolization[10]. Furthermore, impaired renal function may be a relative contraindication for performing both MDCT and CAG imaging, hence omitting one of these examinations would be beneficial for the patient. As MDCT has a high negative predictive value for coronary artery obstructions in patients with a low or intermediate risk of coronary artery disease (CAD), it may replace CAG in patients with no known CAD[11, 12]. Unfortunately, coronary artery assessment by MDCT in PHV patients may be hampered by metallic artifacts or motion artifacts due to elevated or irregular heart rates which are frequently present in PHV dysfunction patients[13].

Moreover, beta-blockers are not routinely administered before PHV assessment by MDCT. Also, MDCT images for PHV assessment are acquired with retrospectively ECG-gating, in contrast to MDCT images for coronary artery assessment, which are preferably acquired using prospective ECG-triggering[9, 12]. For the above-mentioned reasons MDCT performed for PHV dysfunction assessment could result in non-diagnostic results for coronary assessment[13]. Although clinically relevant, to our best knowledge no studies have been published that investigated the diagnostic role of MDCT in patients with PHVs for the exclusion of significant CAD. Therefore, the purpose of this explorative study is to determine whether non-invasive angiography with retrospectively ECG-gated MDCT is feasible and can replace CAG in the diagnostic work-up of PHV patients before redo valve surgery.

METHODS

Patient selection

We reviewed all patients with a left-sided mechanical or biological PHV who underwent CAG and retrospectively ECG-gated MDCT primarily performed for

PHV dysfunction assessment. Patients were selected from the database of the Department of Radiology of the University Medical Center Utrecht, the Netherlands. The search was performed from January 2009 until June 2013 with a maximum allowed interval of six months between CAG and MDCT. Patients who underwent coronary revascularization between CAG and MDCT were excluded. Additional patient information was retrieved from the patient medical records. Informed consent was waived by the local Medical Ethical Committee. Patients were divided in two groups. Group I consisted of patients with no known CAD defined by an absent medical history of: (a) myocardial ischemia due to known coronary artery obstructions, (b) percutaneous coronary intervention (PCI) or (c) coronary artery bypass grafting (CABG). Group II consisted of patients with known CAD defined by a positive medical history of (a) myocardial ischemia due to known coronary artery obstructions, (b) PCI or (c) CABG.

MDCT acquisition

Retrospectively ECG-gated MDCT images were acquired using scan parameters as applied with PHV patients in our daily practice. A comprehensive description of our standard clinical protocol has been presented previously[4]. In short, our most recent clinical 256-slice MDCT acquisition protocol consisted of a scout view and unenhanced prospectively ECG-triggered acquisition of the PHV region followed by the contrast-enhanced retrospectively ECG-gated acquisition with the following parameters: 120 kV, 600-700 mAs, collimation 128 x 0.625, gantry rotation time 270-330 ms and pitch 0.16-0.18. Gantry rotation time and pitch were dependent on the heart rate. Beta-blockers in PHV dysfunction patients are usually not administrated before MDCT acquisition, but this is case dependent. Nitroglycerine was not administered to PHV patients given their physical condition, suspected dysfunction and possible complications. For contrast-enhanced imaging our clinical triphasic contrast administration protocol was applied, as described previously[4]. In brief, this usually comprised contrast medium, a mixture of 30% contrast medium and 70% saline and a saline flush, respectively. Images were reconstructed at each 10% of the RR-interval.

Invasive coronary angiography and image analysis

CAG was performed according to currently available guidelines via radial or femoral access[14, 15]. Fractional flow reserve (FFR) was occasionally performed if visual assessment of an obstruction was inconclusive[16]. Coronary arteries were scored as: (1) present significant stenosis (>50 %) or FFR < 0.80, (2) absent stenosis or non-significant stenosis (<50 %) or FFR > 0.80[10, 15]. Coronary arteries judged as

significantly obstructed were regarded as requiring a bypass graft. The location of the stenosis was documented and categorized in proximal or distal coronary stenosis of the right coronary artery (RCA), left main (LM), left descending artery (LDA) or left circumflex artery (LCx). Bypass grafts were assessed as patent or significantly obstructed/occluded as well. CAG's were reviewed by the cardiologist who performed the CAG and an independent observer (WT). Both observers were not aware of the MDCT results for coronary artery obstructions. In case of incongruent results, a consensus was reached. Based on this procedure the reference standard result was defined.

MDCT image analysis

Assessment of the MDCT images was performed on a dedicated workstation (Extended Brilliance Workstation, Philips Healthcare, Best, the Netherlands). The best systolic and diastolic image phase for coronary assessment was selected for each coronary artery segment. All coronary artery segments were assessed according to the 18-segment SCCT model and scored as present or absent[17]. Present coronary artery segments were scored as: 1. non-diagnostic (not sufficiently visualized to perform diagnostic assessment) or 2. diagnostic (stenosis grade of the segment can be assessed). Reasons for non-diagnostic segments were classified as: PHV-related artifacts, low contrast enhancement, pacemaker lead artifacts, technical failure, superimposing vein, motion artifacts and noise. Very small coronary segments (of approximately 1 mm diameter) are clinically not relevant as these segments are not eligible for concomitant bypass grafting. Therefore segments that were approximately 1 mm in diameter and too small for MDCT intraluminal evaluation, and thus for grafting, were excluded from analysis. Only if a MDCT acquisition was diagnostic for all present coronary artery segments larger than 1 mm, the MDCT images were used for the detection of: 1. presence of significant stenosis (>50 %) or 2. absence of stenosis or non-significant stenosis (<50 %). For stenosed coronary arteries the location of the stenosis was documented and categorized into proximal or distal coronary stenosis of the RCA, LM, LAD or LCx.

The main reason for non-diagnostic MDCT was determined per patient. In case of multiple non-diagnostic reasons, the reviewers chose the artifact which was mainly responsible for hampered coronary visualization. Since no full cardiac unenhanced acquisitions were performed the Agatston calcium score could not be assessed. As calcified plaques may interfere with the correct interpretation of coronary artery obstructions, the amount of calcium was scored on a qualitative visual calcium score per coronary artery (LM/LAD/RCA/LCx) as follows; 0. absent (no calcium), 1. mild (small and few calcium spots), 2. moderate (extended and larger calcified

plaques) or 3. severe (extremely calcified). For analysis, per patient overall calcium score was calculated by adding the visual calcium scores of the individual four coronary arteries. As a result, the total score varied between 0 as minimum and 12 as maximum per patient.

For coronary bypasses, the graft patency was scored even when MDCT scans were non-diagnostic for the native coronary arteries. Since MDCT was acquired for PHV imaging, the most proximal part of the (arterial) bypass graft was not available for analysis in some patients. Bypasses were scored as: 1. non-diagnostic, 2. patent or 3. occluded/significantly obstructed (>50%). All MDCT scoring was performed independently by two reviewers (DS and EL). Reviewers were blinded for CAG results. A consensus was reached for discordant MDCT results. The data analysis was based on the consensus score.

Data analysis

Data analysis was restricted to descriptive statistics. Categorical data were presented in total numbers or percentages. Based on the data distribution, continuous data were reported as mean ± standard deviation (SD) or median and interquartile range (IQR). CAG was the reference test for detection of significant stenosis. The MDCT results for coronary artery stenosis assessment were matched to the results of the CAG assessment to evaluate MDCT accuracy on patient level in terms of sensitivity, specificity, positive predictive value (PPV) and negative predictive value (NPV) (95% confidence interval; CI). Only diagnostic MDCT scans were compared with the reference standard; CAG ± FFR. In group II, coronary bypass patency assessment on MDCT was compared to CAG results even when MDCT scans were non-diagnostic for the native coronary arteries. If MDCT found an absent or non-significant stenosis and if this was in agreement with CAG results, MDCT was considered to accurately rule out significant CAD or bypass graft obstruction.

RESULTS

We identified 51 patients with 53 left sided PHVs; 45 aortic and eight mitral valves. Thirty-eight patients had a history of no known CAD (group I) and 13 patients had known CAD (group II; 12 coronary bypass surgery and one PCI). Median time between CAG and MDCT was 86 days (IQR 22-129 days). Other baseline characteristics are shown in *Table 1*. Two of 51 patients (4%) received beta-blockers before MDCT imaging. The mean heart rate during the MDCT acquisition was 71 ± 16 beats per minute (bpm). In 14/51 (27%) patients, the heart rate during the MDCT scan was unknown. Five (14%) patients had an arrhythmia during MDCT acquisition. A flowchart of the results is provided in *Figure 1*.

Table 1 | Patient characteristics

	No known CAD N = 38	Known CAD N = 13
Age, mean ±SD	62.9 ± 12.2	70.9 ± 7.8
Male (%)	29 (76%)	9 (69%)
CABG (grafts)	0	12 (19)
PCI	0	1
Time (days) CAG-MDCT, median (IQR)	99 (43-134)	27 (9-95)
Valve position (%)		
Aortic	32 (84%)	11 (85%)
Mitral	4 (11%)	2 (15%)
Aortic and Mitral	2 (5%)	0
Mechanical valves (%)	29 (71%)	8 (62%)
ATS	1	0
Björk-Shiley	2	0
Carbomedics	12	2
Duromedics	1	0
ON-X	2	1
Sorin bicarbon	2	0
St. Jude	9	5
Biological valves (%)	10 (26%)	5 (39%)
CE Perimount	8	3
Medtronic Mosaic	0	1
Mitroflow	2	1
TAVI valves (%)	1 (3%)	0
Edwards Sapien	1	0

CABG = coronary artery bypass graft; CAD = coronary artery disease; IQR = interquartile range; MDCT = multidetector-row computed tomography; PCI = percutaneous coronary intervention; SD = standard deviation; TAVI = transcatheter aortic valve implantation

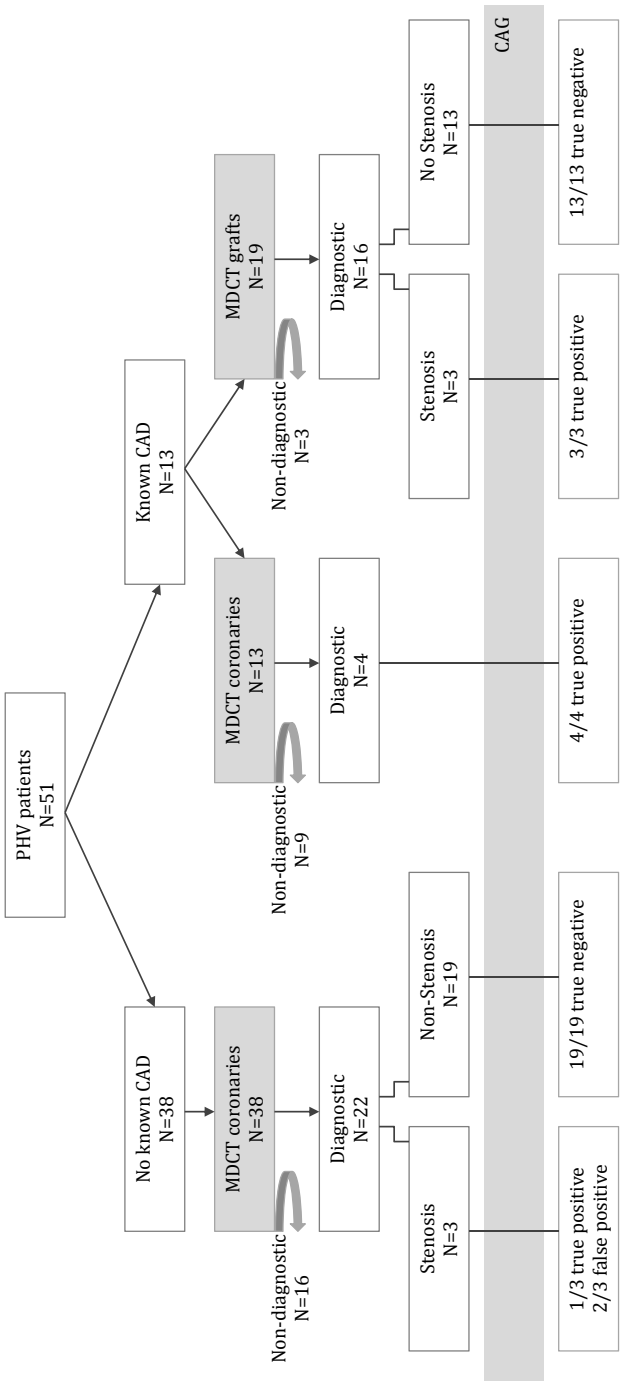

Figure 1 | Flowchart of the results

Group one

CAG images identified 36/38 patients without significant coronary artery stenosis. In two of these patients FFR was required to exclude a significant obstruction. Two patients revealed significant stenoses on CAG: one patient with distal RCA and distal LAD stenosis, the other with a LM and proximal and distal RCA stenosis. An example of a CAG versus a MDCT image is presented in *Figure 2*.

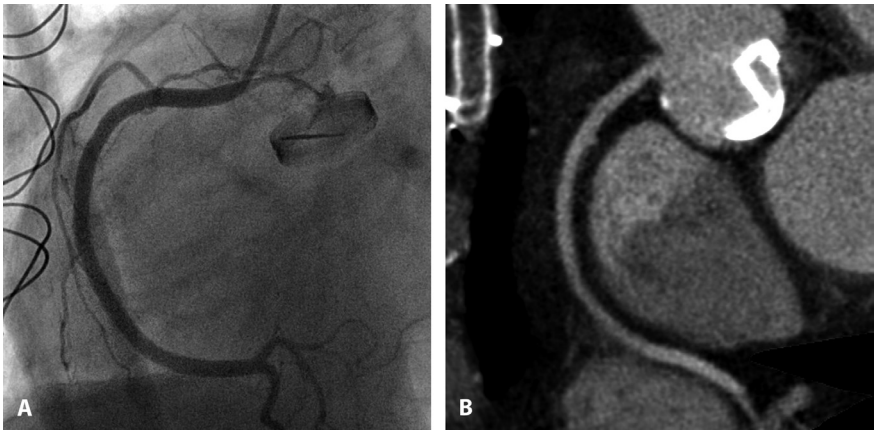

Figure 2 | Invasive versus non-invasive coronary angiography in a PHV patient. Invasive angiography (A) and computed tomography angiography (B) image showing the patent right coronary artery in a patient with a prosthetic aortic valve.

Mean heart rate during MDCT examinations was 70 ± 16 bpm. The calcium score analyzed per patient was overall 3 ± 3 (mild). MDCT in accordance with the CAG, results correctly ruled out significant coronary obstructions in 19/38 patients (50%). In the remaining 19/38 patients (50%) MDCT was non-diagnostic (n=16) or revealed a coronary obstruction (n=3). In one patient with coronary artery obstructions, MDCT correctly detected significant distal RCA and LAD stenoses. The other two patients with significant obstructions on MDCT proved to be false positive. In the first false positive case MDCT revealed a stenosis in the proximal LAD in which the calcium score was judged as severe. In the other false positive case MDCT revealed proximal LAD and LCx stenoses with calcium scored as moderate and mild, respectively. Overall, diagnostic MDCT sensitivity was 100% (95% CI 17%-100%), specificity 90% (95% CI 70%-99%), PPV 33% (95% CI 5%-88%) and NPV 100% (95% CI 82%-100%). For the 16 patients in which significant stenosis was ruled out,

MDCT can be considered as useful and sufficient for CAD assessment, whereas with non-diagnostic image quality and/or positive findings further assessment with CAG remains required.
PHV-related artifacts were the main reason for non-diagnostic MDCT in only 5/16 patients (31%). Other reasons for non-diagnostic assessment were due to more common MDCT errors such as noise artifacts (n=5), motion artifacts (n=5) and technical failure (n=1). Mean heart rate during MDCT was 67 ± 11 bpm for patients with a diagnostic MDCT compared to 76 ± 20 bpm for patients with a non-diagnostic MDCT. Mean calcium score analysed per patient was overall 2 ± 2 (mild) for patients with a diagnostic MDCT and 3 ± 4 (mild) for patients with a non-diagnostic MDCT.

Group two

CAG showed one or more significant obstruction of the native coronary arteries in all patients (n=13). In this group mean heart rate during MDCT examinations was 72 bpm ± 16. The calcium score per patient was 9 ± 3 (moderate-severe). In 9/13 patients (69%) the MDCT scan was non-diagnostic for evaluation of native coronary arteries. PHV-related artifacts were the main reason for non-diagnostic MDCT in solely 1/9 patients (11%). MDCT errors accounted for the remaining non-diagnostic images: noise artifacts (n=3), motion artifacts (n=3), superimposing vein (n=1) and pacemaker artifacts (n=1) (*Figure 3*). MDCT was diagnostic in the other four patients and revealed significant coronary artery stenoses in all. Of note, besides these correctly diagnosed stenoses, MDCT also revealed false positive stenoses in other severely calcified segments in all these four patients.
In total, 19 bypass grafts were present in 12 CABG patients. CAG revealed 3/19 non-patent and 16/19 patent grafts. All patent bypass grafts were free of calcifications. During MDCT analysis, three bypass grafts (all internal mammary artery grafts) were excluded due to small graft vessel size (n=2) and limited MDCT graft image acquisitions (n=1). For the diagnostic grafts (n=16), MDCT correctly identified 3/3 (100%) non-patent grafts and 13/13 (100%) patent bypass grafts. Thus, bypass graft patency was correctly identified by MDCT in all 16/16 (100%) assessable bypass grafts whereas 3/19 grafts (16%) needed additional CAG analysis since MDCT was non-diagnostic. Furthermore, MDCT detected a hostile anatomy in two bypass grafts (both to the right posterior descending artery) showing a direct retrosternal course.

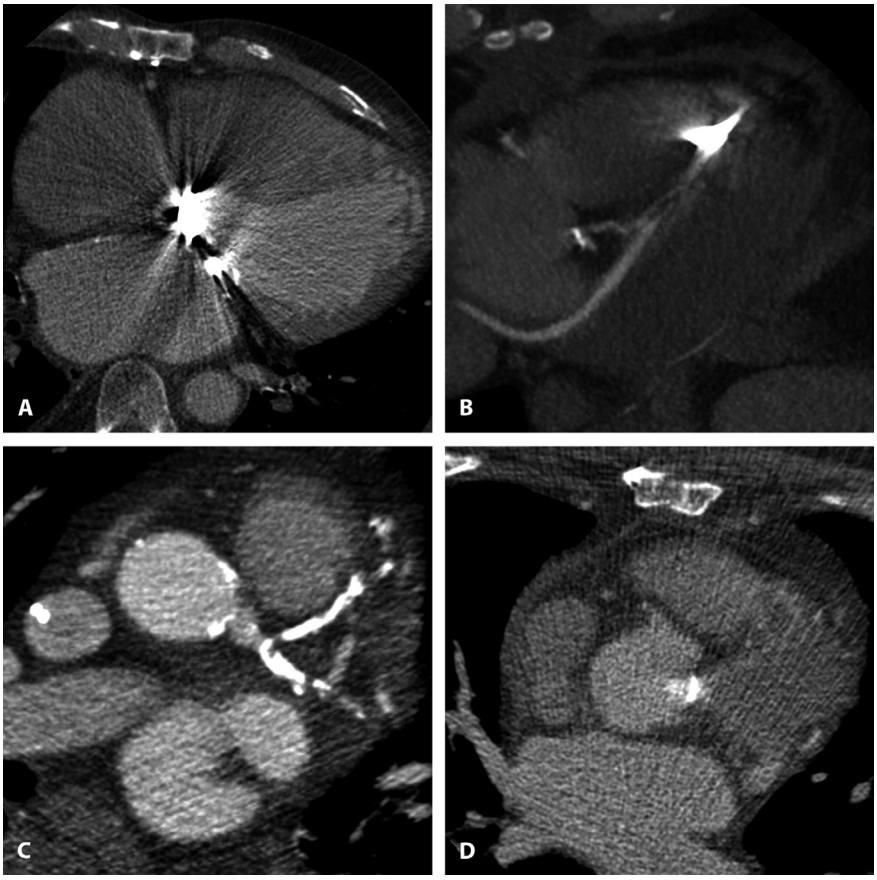

Figure 3 | Artifacts encountered in non-invasive angiography by MDCT. (A) Computed tomography (CT) image of a patient showing prosthetic heart valve artifacts due to the Björk-Shiley valve. (B) Pacemaker artifact hampering assessment of the right posterior descending artery. (C) Calcifications in the left coronary system with blooming artifacts impairing adequate stenosis evaluation. (D) Non-diagnostic CT image due to image noise.

DISCUSSION

The main findings of this study were twofold. First, retrospectively ECG-gated MDCT primarily performed for the detection of PHV dysfunction may replace invasive coronary artery assessment to rule out CAD in a substantial part (50%) of patients with no known CAD. Second, in patients with known CAD, MDCT appeared to be effective in assessing the patency of bypass grafts and hostile graft anatomy, but CAG is still required for native coronary artery assessment in this group.

The results of our study may be of significant clinical impact as MDCT is increasingly performed for the detection of PHV endocarditis or the morphological cause of PHV obstruction (thrombus and pannus)[1-4]. In case of PHV replacement, MDCT may also replace preoperative invasive angiography. This would save patient radiation dose, contrast exposure, costs and exposure to risk of invasive catheterization.

For patients with thrombi or vegetations attached to aortic PHVs, a CAG may be relatively contraindicated as manipulation with invasive catheters may result in distal embolization[10]. In these specific cases, non-invasive coronary assessment is of even more clinical value. We previously assessed the effect of PHVs on coronary MDCT assessment. In that study, MDCT results were analysed per coronary segment for image quality[13]. Overall, 17/89 (19%) PHVs caused non-diagnostic images. Common aortic PHVs showed no relevant artifacts, despite the close relationship of the PHV and proximal coronaries. However, cobalt-chrome containing PHVs (Björk-Shiley, Sorin tilting disc and Duromedics bileaflet) encountered major artifacts hampering coronary assessment[13]. Furthermore, mitral PHVs also caused relevant artifacts hampering coronary assessment. In this study we found similar results with only 6/51 patients (12%) with non-diagnostic images due to PHV artifacts. A reason for the small difference might be the inclusion of less cobalt-chrome containing PHVs (6% versus 8%) and analysis on patient level instead of on PHV level.

In agreement with studies investigating non-invasive identification of coronary artery lesions by MDCT in non-PHV patients, MDCT is also of limited value in PHV patients with known CAD. It has the tendency to overestimate the significance of stenosis and therefore a CAG is required when a significant stenosis is observed by MDCT[11, 18]. As a consequence, native coronary artery assessment by MDCT is not advised in patients already known with ischemic heart disease. However, MDCT may have additional value for the surgeon and the candidates for cardiac reoperation after CABG. In agreement with the study of Weustink et al. which investigated non-PHV patients, our study showed good diagnostic accuracy for MDCT in the assessment of bypass grafts and their patency[18]. This finding may be of additional clinical value before a CAG is performed. For example, in case of graft obstruction already detected by MDCT, attempts to find the graft during invasive CAG can be omitted, which saves catheter manipulations in the aorta, procedure time and contrast exposure. Furthermore, details on the position of the graft in relation to other anatomical landmarks may help the surgeon to avoid injuring a graft during a reoperation. This was also shown in this study as MDCT detected two grafts with a direct retrosternal course.

Compared to standard coronary MDCT studies in non-PHV patients, the present study showed a relative high percentage of non-diagnostic scans. This was also observed in the group of patients with no known CAD (n=38) with relatively low calcium score and low incidence of coronary artery obstructions (2/38). Most non-diagnostic coronary acquisitions were however due to common MDCT errors, as noise and motion were the most important causes for inconclusive MDCT assessment. This might be explained by the fact that the acquisition protocol is optimized for PHV assessment, comprising retrospective ECG-gating and no or infrequent administration of nitroglycerine and beta-blockers, respectively.

For coronary artery assessment, current prospective acquisitions provide most optimal results. In PHV assessment, prospectively triggered scans result in less PHV artifacts as well[19]. Though, retrospectively ECG-gated images are favoured in PHV assessment because they provide images of all cardiac phases and hence dynamic PHV information. Retrospectively gated MDCT has a higher total radiation dose compared to prospectively triggered acquisitions, but the relative radiation dose per cardiac phase is lower. Whereas with prospective triggering one cardiac phase receives the full dose, with retrospective gating the dose is spread over ten cardiac phases. A relatively lower radiation dose may account for the higher amount of image noise. The high percentage of non-diagnostic coronary arteries is probably also caused by higher heart rates inducing motion artifacts, as beta-blockers were given in only 4% (2/51) of the total study group and a large number of patients with PHV dysfunction have arrhythmias. Administration of beta-blockers before MDCT acquisition might significantly improve image quality and reduce PHV or motion related artifacts. Though, caution must be taken in PHV patients and especially in patients with PHV dysfunction. Close collaboration between the radiologist and cardiologist is essential to optimize heart rate before acquisition.

This study has several limitations. First, our study concerns a retrospective analysis containing various PHV types represented in only small numbers and mainly placed in the aortic position. Second, only four patients with known CAD showed a diagnostic image quality. Statistical measures of MDCT accuracy were therefore not calculated in this group. Third, objective calcium scoring according to Agatston was not possible. As a result a visual calcium score was provided. Fourth, beta-blockers were not routinely administered before MDCT. This may have reduced the image quality of the depicted coronary segments. However, beta-blockers could be contraindicated in patients with PHV dysfunction because of possible hemodynamic deterioration and conduction disturbances.

In conclusion, in PHV patients with no known CAD MDCT primarily performed to diagnose PHV dysfunction can replace invasive angiography for the exclusion of significant CAD in approximately half of these patients. When conclusive for coronary assessment, MDCT stenosis rule out is highly accurate. In PHV patients with known CAD, MDCT is not able to replace CAG reliably for the assessment of the native coronary artery system. However, coronary artery bypass graft patency can be reliably determined in the majority of patients.

REFERENCES

1. Habets J, Tanis W, Mali WP, Chamuleau SA, Budde RP. Imaging of prosthetic heart valve dysfunction: Complementary diagnostic value of tee and mdct? *JACC Cardiovasc Imaging*. 2012;5:956-961
2. Ueda T, Teshima H, Fukunaga S, Aoyagi S, Tanaka H. Evaluation of prosthetic valve obstruction on electrocardiographically gated multidetector-row computed tomography--identification of subprosthetic pannus in the aortic position. *Circ J*. 2013;77:418-423
3. Tanis W, Habets J, van den Brink RB, Symersky P, Budde RP, Chamuleau SA. Differentiation of thrombus from pannus as the cause of acquired mechanical prosthetic heart valve obstruction by non-invasive imaging: A review of the literature. *Eur Heart J Cardiovasc Imaging*. 2014;15:119-129
4. Habets J, Tanis W, van Herwerden LA, van den Brink RB, Mali WP, de Mol BA, et al. Cardiac computed tomography angiography results in diagnostic and therapeutic change in prosthetic heart valve endocarditis. *Int J Cardiovasc Imaging*. 2014;30:377-387
5. Fagman E, Perrotta S, Bech-Hanssen O, Flinck A, Lamm C, Olaison L, et al. Ecg-gated computed tomography: A new role for patients with suspected aortic prosthetic valve endocarditis. *Eur Radiol*. 2012;22:2407-2414
6. Teshima H, Hayashida N, Fukunaga S, Tayama E, Kawara T, Aoyagi S, et al. Usefulness of a multidetector-row computed tomography scanner for detecting pannus formation. *Ann Thorac Surg*. 2004;77:523-526
7. Feuchtner GM, Stolzmann P, Dichtl W, Schertler T, Bonatti J, Scheffel H, et al. Multislice computed tomography in infective endocarditis: Comparison with transesophageal echocardiography and intraoperative findings. *J Am Coll Cardiol* . 2009;53:436-444
8. Tanis W, Habets J. Images in clinical medicine. The silence of the leaflets. *N Engl J Med*. 2013;368:e21
9. Habets J, Mali WP, Budde RP. Multidetector ct angiography in evaluation of prosthetic heart valve dysfunction. *Radiographics*. 2012;32:1893-1905
10. Vahanian A, Alfieri O, Andreotti F, Antunes MJ, Baron-Esquivias G, Baumgartner H, et al. Guidelines on the management of valvular heart disease (version 2012): The joint task force on the management of valvular heart disease of the european society of cardiology (esc) and the european association for cardio-thoracic surgery (eacts). *Eur J Cardiothorac Surg*. 2012;42:S1-44
11. Meijboom WB, Mollet NR, Van Mieghem CA, Kluin J, Weustink AC, Pugliese F, et al. Pre-operative computed tomography coronary angiography to detect significant coronary artery disease in patients referred for cardiac valve surgery. *J Am Coll Cardiol*. 2006;48:1658-1665
12. Meijboom WB, Meijs MF, Schuijf JD, Cramer MJ, Mollet NR, van Mieghem CA, et al. Diagnostic accuracy of 64-slice computed tomography coronary angiography: A prospective, multicenter, multivendor study. *J Am Coll Cardiol*. 2008;52:2135-2144
13. Habets J, van den Brink RB, Uijlings R, Spijkerboer AM, Mali WP, Chamuleau SA, et al. Coronary artery assessment by multidetector computed tomography in patients with prosthetic heart valves. *Eur Radiol*. 2012;22:1278-1286
14. Jolly SS, Amlani S, Hamon M, Yusuf S, Mehta SR. Radial versus femoral access for coronary angiography or intervention and the impact on major bleeding and ischemic events: A systematic review and meta-analysis of randomized trials. *Am Heart J*. 2009;157:132-140
15. Kolh P, Wijns W, Danchin N, Di Mario C, Falk V, Folliguet T, et al. Guidelines on myocardial revascularization. *Eur J Cardiothorac Surg*. 2010;38 Suppl:S1-S52

16. Tonino PA, De Bruyne B, Pijls NH, Siebert U, Ikeno F, van' t Veer M, et al. Fractional flow reserve versus angiography for guiding percutaneous coronary intervention. *N Engl J Med*. 2009;360:213-224
17. Raff GL, Abidov A, Achenbach S, Berman DS, Boxt LM, Budoff MJ, et al. Scct guidelines for the interpretation and reporting of coronary computed tomographic angiography. *J Cardiovasc Comput Tomogr*. 2009;3:122-136
18. Weustink AC, Nieman K, Pugliese F, Mollet NR, Meijboom WB, van Mieghem C, et al. Diagnostic accuracy of computed tomography angiography in patients after bypass grafting: Comparison with invasive coronary angiography. *JACC Cardiovasc Imaging*. 2009;2:816-824
19. Symersky P, Habets J, Westers P, de Mol BA, Prokop M, Budde RP. Prospective ecg triggering reduces prosthetic heart valve-induced artefacts compared with retrospective ecg gating on 256-slice ct. *Eur Radiol*. 2012;22:1271-1277

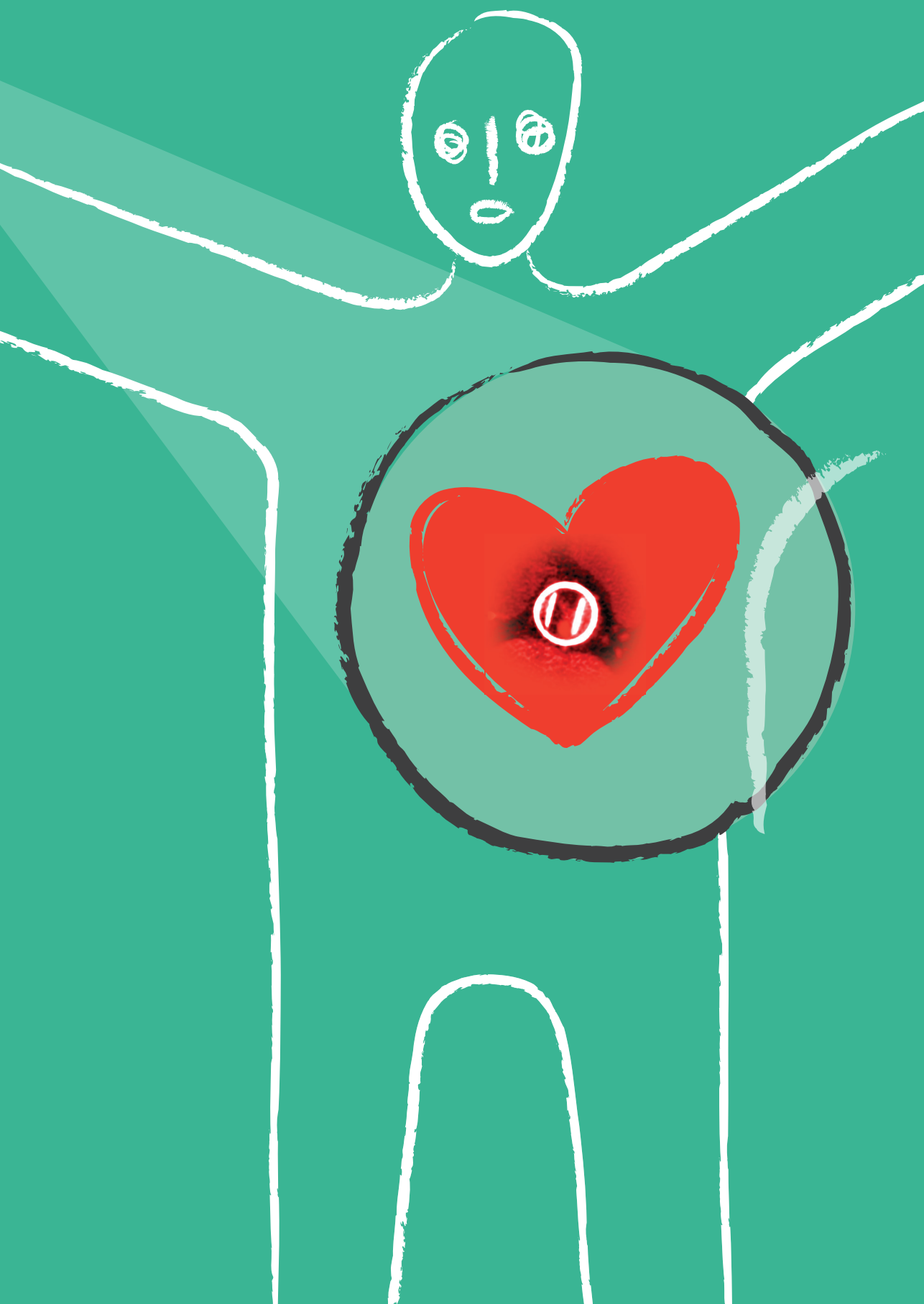

CHAPTER 13
General discussion

Current guidelines recommend transthoracic echocardiography (TTE) after prosthetic heart valve replacement as baseline reference[1-3]. Biological valves require annual follow-up with TTE after the first five years post implantation for monitoring potential structural valve deterioration, whereas follow-up imaging for mechanical valves is only advised if valve dysfunction is suspected based on clinical symptoms. TTE should be performed in all cases of suspected prosthetic valve dysfunction.
If results are inconclusive, transesophageal echocardiography (TEE) is advised as it offers higher spatial resolution and better anatomic views because of its close relation to the heart. Traditionally, fluoroscopy can be added to routine work-up for the assessment of mechanical valve leaflet excursions if prosthetic obstruction is suspected. All routine imaging modalities as introduced above have specific limitations that may result in an inconclusive diagnostic work-up of patients with prosthetic heart valves (PHVs). In this thesis the role of computed tomography (CT) as a novel imaging modality in patients with PHVs was evaluated.

In *Chapter 2* the potentials and pitfalls of novel imaging modalities for PHV assessment are discussed based on a systematic review of current literature on CT and magnetic resonance imaging (MRI). According to the current guidelines, the role of CT for PHV evaluation is limited and MRI has not been included in the guidelines at all.

CT ACCORDING TO GUIDELINES

The main role of CT as presented in the guidelines is evaluation of mechanical leaflet motion in case echocardiography and fluoroscopy are inconclusive[1-3]. With certain pathology, valve leaflet excursions can be restricted, for example due to adherent thrombus, vegetations or pannus. Restricted leaflet motion might be one of the few signs of suspected PHV obstruction, and, if present, leaflet restriction may only be very subtle[4]. Fluoroscopy can be used to evaluate valve leaflet excursions, since manufacturers impregnate mechanical PHV leaflets with tungsten to provide radiopacity. It is however widely recognized that fluoroscopy may be challenging since valve torsion due to cardiac motion and certain PHV positions may hinder perpendicular X-ray alignment. Fluoroscopy is therefore limited to aortic mechanical valves. Although additional CT imaging has been proposed as an alternative for the evaluation of mechanical valve leaflet angles, its accuracy has not been determined. *Chapter 3* shows that CT-based evaluation of valve leaflet excursions has excellent reliability compared with fluoroscopy in contemporary monoleaflet and bileaflet PHVs in normal and dysfunctional

conditions. CT more accurately detected and ruled out restricted leaflet motion compared with fluoroscopy. The maximal mean difference between CT and fluoroscopy was 2 degrees. CT could thus be used to detect even subtle leaflet restriction. In patients, the margin of error of CT measurements could be larger, due to poor image quality because of PHV-related artifacts or cardiac motion and low temporal resolution. In *Chapter 7*, CT was used to obtain leaflet angles in patients with supposedly normal functioning PHVs. Leaflet angles of mechanical valves in aortic position differed maximal (median) 2 degrees compared with manufacturers' values. For prostheses in mitral position, this difference was 5 degrees for opening and 2 degrees for closing angle measurements, respectively. These results show that CT in patients is reliable in aortic and mitral valves and indicate the margin of error that should be taken into account when evaluating leaflet angles with CT. One finding that should be highlighted is that the ON-X valve leaflet opening angles were remarkably decreased compared to manufacturer values (76 versus 90 degrees, respectively), and has been described previously in fluoroscopy studies. Hence, one should keep in mind that reduced opening angles of the ON-X valve do not necessarily indicate underlying pathology. Although leaflets of the Perimount valve were not assessable with CT early after implantation, CT can potentially be used to evaluate biological valves with leaflet thickening and calcifications (*Chapter 10* and *Chapter 11*). Compared with fluoroscopy, CT offers a lot more information that may be used to detect pathology because of its full cardiac acquisition. In the 2014 version of the AHA/ACC guidelines, it is suggested that additional CT may be considered if echocardiography (both TTE and TEE) are inconclusive in patients with suspected structural valve deterioration, PHV obstruction or periprosthetic infections[1]. The results presented in this thesis underline the importance of CT in PHV dysfunction.

CT AT BASELINE

Guidelines recommend baseline TTE imaging as a patient-specific reference for follow-up in suspected PHV dysfunction. Similarly, it would be helpful to compare baseline findings to CT performed for suspected PHV dysfunction. In general, it is only truly possible to detect pathology if physiologic and pathologic conditions can be discriminated. It is thus required to know the CT appearance of PHVs and PHV-related anatomy under normal, uncomplicated circumstances. With this objective, a prospective study was conducted in which 46 patients were imaged with CT in addition to routine echocardiography (TTE) approximately six weeks after PHV implantation *(Chapter 7*). First, this study shows that despite the presence

of PHV-related artefacts, CT images can be used to reliably assess PHVs and related anatomy relevant for the evaluation of PHV-related pathology. Second, CT showed that normal, baseline findings early after implantation include moderate pericardial effusion and prominent pericardial and pleural hematoma. Importantly, six-week baseline CT shows induration of the periaortic fat tissue in 83% of patients after aortic valve replacement. Apparently, this can be considered a normal CT imaging finding, though it is unknown how long this indurated appearance lasts.

Periaortic tissue induration may however also be related to PHV endocarditis and differentiation early after implantation may be challenging. In patients with early suspected PHV endocarditis without infectious complications, additional CT imaging by itself could therefore be of limited value. In contrast, baseline CT showed incremental value by detecting three cases of pathology not detected with routine TTE imaging; aspecific subprosthetic tissue, pseudoaneurysms and valve dehiscence. The latter case had to undergo redo valve surgery, which would not have been planned based on routine baseline imaging. The patient in whom CT detected aspecific subprosthetic tissue after uncomplicated PHV implantation shows the importance of baseline imaging. Whereas persistent native valve tissue is likely, late follow-up imaging alone might suggest other, acquired, causes of pathology. Another CT finding that may be relevant at follow-up is the detection of a tilted PHV position in relation to the left ventricular outflow tract. A tilted position may have hemodynamic consequences and may result in increased transprosthetic gradients, though the tilted position may not be evident on echocardiography.

This study is too preliminary to conclude that CT should be included routinely as baseline imaging tool in all patients. CT as screening modality should however be considered in patients with complicated PHV implantation or with any higher suspicion for developing PHV-related complications. The prevalence of abovementioned CT findings does yet need to be confirmed in larger studies as well as the value of CT in the diagnostic work-up of suspected PVH dysfunction.

CT IN SUSPECTED PHV DYSFUNCTION

CT can be used to detect restricted leaflet excursions as an indication of PHV obstruction, but its role in functional PHV assessment remains limited. However, CT may provide complementary information to echocardiography on PHV-related anatomy and pathology because of its three-dimensional nature and high spatial resolution. In a prospective study in patients with suspected PHV endocarditis, CT showed incremental value for detecting and showing the extent of endocarditis related complications.[5] Potential value for CT has also been suggested in suspected

PHV obstruction[6-10], but no prospective study had been conducted to evaluate CT in addition to routine work-up. In *Chapter 8* such a cross-sectional study is presented in patients with suspected PHV obstruction and periprosthetic regurgitation (non endocarditis). CT showed incremental value in addition to routine work-up with TTE and TEE (+/- fluoroscopy) in most cases, and especially for mechanical PHVs. In patients with suspected PHV obstruction, CT provided an indication of the underlying cause of obstruction by showing subvalvular membrane, pannus and/or thrombus. In mechanical PHVs, CT also resulted in a change of the treatment strategy in a third of patients. In patients with suspected PHV regurgitation, the strength of complementary CT was its ability to detect or exclude infectious complications in both mechanical and biological valves. Furthermore, CT provided information relevant for planning redo surgery and percutaneous periprosthetic leak closure. Overall, the role of complementary CT imaging in patients with suspected dysfunction is greater in suspected PHV obstruction. It is important to identify the cause of PHV obstruction since both fibrinolysis and redo valve surgery bear significant risks. A limitation of this study is that surgical findings were only available in a third of patients. Though in the absence of a reference test an expert panel evaluated all cases, surgical or pathological confirmation may improve differentiation between pannus and thrombus. Regardless, the findings of this study indicate that CT should be implemented in the routine diagnostic work-up of patients with suspected PHV obstruction. A recent study showed CT to detect restricted leaflet motion with hypoattenuating leaflet structures in aortic biological valves early after implantation.TTE did not detect restricted motion or leaflet abnormalities and showed normal transprosthetic pressure gradients[11]. The pathological findings may be related to insufficient post implantation anticoagulation therapy, but the results of this study stress the urge of CT in PHV obstruction. In patients with suspected PHV regurgitation, the role of CT may be limited. CT can however be considered to rule out extensive (infectious) complications, detect valve dehiscence (*Chapter 7*) or for planning redo valve surgery. As PHV-related pathology is complex and diagnostic work-up can be challenging, multidisciplinary collaboration is needed to provide high quality and state of the art care.

In biological valves, structural deterioration is the main cause of PHV dysfunction over time. The durability of biological PHVs may be affected by the geometry of the prostheses. Deformation of a prosthesis may impact leaflet coaptation and alter mechanical stress distribution, which has been related to the process of valve leaflet

calcification and degeneration[12]. In *Chapter 10*, CT was used to assess the geometry of biological PHVs after surgical aortic valve implantation. The prosthetic valve eccentricity index (calculated using the ratio of the minimal and maximal valve diameters) showed that biological valve geometry was at least mildly deformed in 41% of cases. Significant prosthesis deformation (non-circular, defined as an eccentricity index ≥10%) was present in 13% of all cases. Should valve deformation lead to suboptimal PHV function or early structural valve deterioration, these findings may require evaluation of surgical implantation techniques to improve biological valve durability. *Chapter 11* presents a case of unexpected early structural valve deterioration of the biological Mitroflow valve implanted in aortic position. TTE showed signs of PHV dysfunction and regurgitation, though the underlying mechanism was unclear. As TEE imaging was unsuccessful because of patient discomfort CT was performed.
Despite high CT image noise and valve-related artifacts, extensive calcifications of the prosthetic leaflets were seen.

CT PRIOR TO PHV (REDO) PROCEDURES

In patients requiring surgical valve replacement, the size of the prosthesis is determined based on direct measurements of the annulus during surgery. However, with the introduction of transcatheter procedures, sizing of transcatheter valves relies completely on pre-procedural or peri-procedural imaging. It is not known whether the aortic annulus undergoes conformational change throughout the cardiac cycle, and if so, whether this impacts PHV sizing. Accurate sizing is crucial to minimize the risk of complications such as periprosthetic regurgitation. Results from the systematic literature review presented in *Chapter 6* show that in general, the aortic annulus is more circular during the systolic phase and predominantly oval during the diastolic phase. Using only the systolic phase for annular size assessment in patients with significant conformational change may result in undersizing of transcatheter valves. However, the cardiac phase in which the annular dimensions were maximal differed between patients and in some, the largest dimensions were found in diastole. Hence, the complex annular anatomy and behavior throughout the cycle calls for patient evaluation using three-dimensional imaging modalities to reduce sizing error. An advantage of CT is that it can show annular calcifications that may impact sizing in patients potentially eligible for two valve sizes[13]. Three-dimensional TEE might be helpful in patients with contraindications for contrast-enhanced imaging, though TEE may underestimate annular dimensions compared with CT-derived measurements[13-15].

CT images obtained for PHV dysfunction evaluation may provide even more useful, complementary information. When deciding upon therapy in PHV dysfunction, it is essential to know the size of the current dysfunctional prosthesis. As over the years valve-in-valve procedures have been introduced, selected patients with dysfunctional PHVs may be eligible for transcatheter treatment. Only with knowledge of the implanted PHV size it can be evaluated whether there is potential gain in replacing the PHV and prevent patient prosthesis mismatch. In daily practice, the PHV size is not always known and significant discrepancies exist between manufacturers' PHV labels and the true dimensions. Non-invasive, reproducible methods to retrieve the PHV-size were lacking. In *Chapter 9* it is shown that CT is a reliable tool for measuring the PHV area and diameter in predefined window-levels setting. CT also allows for discrimination between consecutive PHV sizes and can thus be used to non-invasively obtain the size of the implanted PHV. This is true for all studied PHVs except the Björk-Shiley valve, which is known to give rise to significant PHV-related artifacts. With the reference overview presented, CT may aid in the interpretation of echocardiography results and the pre-procedural work-up in PHV dysfunction.

Chapter 7 briefly showed that CT initially performed for PHV evaluation could also be relevant for concomitant evaluation of coronary arteries, as CT in one patient detected a coronary anomaly with significant tapering which required further diagnostic work-up. Routinely, CT for coronary artery disease (CAD) is acquired using prospective ECG-triggered acquisition as it provides good diagnostic image quality. In contrast, retrospective ECG-gated acquisition is favored for PHV evaluation since it provides dynamic information, though image quality may be reduced due to noise. Despite this, a previous study showed that CT image quality for coronary artery segments is not substantially hampered by contemporary PHVs[16]. However, this study did not evaluate the diagnostic feasibility of CT. In *Chapter 12* the performance of retrospective ECG-gated CT for the rule out of CAD was compared with invasive coronary angiography (CAG) results. CT was able PHV to rule out CAD in approximately half of PHV patients without a history of CAD. In the remaining patients CAG remains required for accurate CAD rule out or detection. In addition, CT showed its ability to adequately assess coronary bypass graft patency and to detect hostile graft anatomy with retrosternal coursing grafts. As CAG is often required before redo valve surgery, available CT information could be used to omit CAG in a substantial part of PHV patients. This saves associated risks for distant embolization of thrombi or vegetations due to manipulation by the

catheter. Furthermore, this avoids unnecessary exposure to contrast agent, which may even be a contraindication for performing both examinations. Replacing CAG by available CT imaging will even save patient radiation dose.

CT OPTIMIZATION

Although the use of CT in patients with prosthetic heart valves is promising, a major drawback is the relatively high radiation dose that is related to retrospective ECG-gated acquisitions. CT radiation dose reduction would allow a far more widespread use of CT as a PHV assessment tool. In the prospective studies presented in *Chapter 7* and *Chapter 8*, the mean effective radiation dose with retrospective ECG-gated CT imaging was 11.3 and 11.6 mSv, respectively. Prospective ECG-triggered imaging is associated with a lower radiation dose and may reduce PHV-related artifacts[17]. Its impact on PHV-artifacts is however valve type and heart rate dependent and it does not provide dynamic information. With prospective triggering, images are retrieved during one, pre-specified cardiac phase. As shown in *Chapter 7*, the optimal cardiac phases for PHV-evaluation (acquired with retrospective gating) included 30% and 40% systolic and 75%, 80% and 90% diastolic reconstructions. Predicting the optimal imaging phase can thus be challenging. In addition, prospective gating requires low and stable heart rates. Beta-blockers might optimize heart rates, but caution must be taken as especially in PHV (dysfunction) patients administration can be contraindicated. All considered, the use of prospective ECG-triggering as optimization method is currently limited.

In the study presented in *Chapter 4* an attempt is made to optimize retrospective ECG-gated CT image quality and to reduce the radiation dose. For this, different image reconstruction algorithms were evaluated in a phantom setting.
Reconstruction algorithms are used to process raw CT data into images. Filtered-back projection (FBP) is a conventional algorithm used routinely in CT imaging, Additional novel iterative reconstruction (IR) techniques have been introduced over the last years comprising relatively simple and more advanced, 'model-based' algorithms. *Chapter 4* shows that IR techniques allow for up to 75% radiation dose reduction while maintaining image quality and reducing image noise. These results are promising, though for clinical implementation it is required to evaluate these algorithms under pulsatile PHV circumstances.

To allow for further evaluation of PHVs in a controlled in vitro setting, a novel mock circulation loop was developed and presented in *Chapter 5*. The mock loop system is based on a five-element Windkessel model, which means that

the arterial and venous compliance, peripheral resistance, aortic impedance and inertia of blood are taken into account when simulating the cardiac system. With this mock circulation loop various physiologic and pathologic flow conditions can be simulated in both biological and mechanical valves. Moreover, this mock circulation loop was constructed using non-ferromagnetic materials ensuring a magnetic resonance imaging (MRI) safe PHV assessment. The advanced mock loop can be used to further optimize CT acquisition protocols and test image reconstruction techniques. Importantly, MRI acquisition can be optimized to allow for PHV assessment without any radiation dose and potentially provide functional information.

FUTURE PERSPECTIVES

CT has shown incremental value to routine imaging for the diagnostic work-up of patients with suspected PHV dysfunction and for planning (redo) valve surgery or transcatheter procedures and is a reliable tool for anatomical and PHV-related measurements. CT performed for PHV evaluation can be used to retrieve additional information such as on CAD. The main concern related to additional CT imaging is the radiation dose. Different scanning techniques such as high pitch acquisition protocols, tube current modulation, tube voltage modulation and prospective ECG-triggering may allow radiation dose reduction, though each technique has drawbacks that may restrict the use to specific conditions. IR reconstruction techniques are favorable, but clinical studies are needed to evaluate the diagnostic performance in PHV patients in daily practice. Another concern is that cardiac CT requires contrast-enhanced imaging. This involves risks of developing contrast-induced nephropathy while a substantial part of PHV patients have an impaired renal function. In these patients a tailor-made approach may reduce such risks and allow for contrast-enhanced CT imaging in a larger group of patients. Furthermore, PHV-related artifacts may obscure periprosthetic regions that are relevant for the evaluation of suspected PHV dysfunction. Larger studies are needed to more specifically differentiate underlying PHV-pathology. With CT, the tissue attenuation value (in Hounsfield Units) may aid in discrimination of pannus from thrombus, though this has not yet been established. Future CT studies in patients with PHV obstruction with available surgical or pathological conformation will allow evaluation of pannus and thrombus differentiation based on reference test results. Considering the relatively low prevalence of PHV-complications and the fact that not all patients undergo redo valve surgery, a multicenter or even multinational study approach seems required. Furthermore, clinical CT studies early after PHV implantation may further clarify the prevalence of unexpected (pathological)

findings and the correlation with complications at follow-up. Based on those results, implementation of CT as baseline screening tool after PHV implantation may be justified. Future efforts to improve and implement CT in PHV patients should therefore be aimed at: (I) radiation dose reduction, (II) contrast agent restriction, (III) heart rate optimization, (IV) PHV-artifact reduction, and (V) tissue characterization.

NOVEL CT TECHNIQUES

CT technology is developing rapidly which is particularly promising for cardiac imaging in general as well as for the evaluation of PHV patients in specific. All CT imaging in this thesis was performed using single source, multidetector-row CT.
Most recent CT technology comprises dual energy CT and photon-counting CT. Dual energy CT has already been implemented in daily practice in several clinical centers but only lately photon-counting CT has become commercially available.
Dual energy CT is an old concept proposed at the very start of the CT imaging era but has only been introduced clinically over the past few years[18]. Some basic understanding of this system is helpful to appreciate it. As its name implies, dual energy CT (DECT) allows for the use of two X-ray (photon) energies, usually 80kV and 140kV. Whereas low energy X-rays provide good contrast (and more noise), high energy X-rays provide less noise (and little contrast). Though several DECT techniques exist, the general basic principle of DECT is that X-ray attenuation differences resulting from two different energies can be used to characterize tissue, i.e. allow for material decomposition. As certain tissues can be recognized, image reconstruction can be modified using this specific information. For instance, non-enhanced images can be (virtually) reconstructed from contrast-enhanced images after subtracting iodine (contrast) signal. In PHV assessment, which is based on contrast-enhanced imaging, virtually non-enhanced DECT may allow concomitant evaluation of annular and valve leaflet calcifications and aid in the diagnostic work-up of structural valve deterioration. Likewise, iodine signal may be colored on virtual non-enhanced reconstructions and used to detect enhancing tissue (e.g. infection) or evaluate myocardial perfusion. These features may have potential to differentiate between underlying PHV pathology in suspected PHV dysfunction and provide additional cardiac information. Furthermore, material decomposition together with virtual (monochromatic) reconstructions may also be used to reduce beam-hardening artifacts and potentially improve image quality in PHV assessment. In addition, monochromatic reconstructions might allow for restricted contrast-agent administration while maintaining sufficient image quality[19, 20].
Dual source CT has a higher temporal resolution (66-75ms) compared with single source CT (~150ms) and is thus less susceptible for cardiac motion artifacts, which

could be beneficial for PHV-artifact reduction as well. The impact of DECT on the effective radiation dose in PHV-assessment needs to be clarified.
The most recent breakthrough in the field of CT technology is spectral CT, also known as photon-counting CT. Spectral CT may allow for even better, more advanced material decomposition since more energy levels can be differentiated.
This improved tissue characterization is based on the implementation of special, cadmium zinc telluride detectors that allow individual counting of photons. Whereas DECT may be beneficial compared with single source multidetector-row CT, spectral CT systems seem even more promising compared with DECT for radiation dose efficiency and tissue characterization.
These developments in suggest improvement on all aspects required for a more widespread use of CT in PHV assessment. Furthermore, advances in computational fluid dynamics may allow simulation of PHV specific hemodynamics, which might be used for patient-specific treatment planning. Only future research will show whether these expectations can be fulfilled.

OTHER IMAGING TECHNIQUES

Additional imaging modalities with potential for the evaluation of PHV patients include three-dimensional transesophageal echocardiography (3D-TEE), fluorine fluorodesoxyglucose positron emission tomography and CT (^{18}F-FDG PET/CT) and last but not least, MRI. The potential role of MRI for PHV assessment has yet been highlighted in *Chapter 2*. In short, MRI may provide additional information on prosthetic valve function since it allows assessment of valve orifice area and regurgitation[21, 22]. More MRI studies are needed to verify its reproducibility for valve orifice area measurements in a larger variety of biological valves and to assess its diagnostic value in dysfunctional valves. Likewise, optimization and validation should be pursued for the assessment of regurgitation using MRI[23]. Especially with the growing interest in transcatheter procedures and related increase in regurgitation prevalence, methods for regurgitation quantification are needed. Four-dimensional MRI is a promising technique for this matter[24]. Furthermore, 4D-MRI may also be helpful in the assessment of valve hemodynamics after PHV implantation or in planning redo valve surgery.
The first studies evaluating 3D-TEE in patients with suspected PHV dysfunction have been published recently[25-27].Though results are promising, larger studies may confirm the use of complementary 3D-TEE imaging to aid in the detection of thrombus in PHV obstruction or vegetations and periprosthetic abscesses in PHV endocarditis.

Although this thesis was not focused on PHV endocarditis as underlying cause of PHV dysfunction, it should be noted that ^{18}F-FDG PET/CT may be useful in these patients as it provides metabolic information. In patients with periaortic fat tissue induration on CT images (*Chapter 7*), FDG PET/CT may be the only imaging modality to potentially differentiate between early PHV endocarditis and a normal postoperative aspect. Studies on the performance of FDG PET/CT in PHV patients are however yet lacking and so are normal reference values. For this, the PROSPECTA study was initiated and results will be available soon.

GENERAL CONCLUSIONS OF THIS THESIS

In patients with prosthetic heart valves, CT has incremental value to echocardiography and fluoroscopy. CT as additional imaging modality should therefore always be considered in all patients with suspected PHV dysfunction and may be considered in selected patients at baseline. Detecting the underlying cause of PHV dysfunction remains challenging, though advances in imaging techniques are rapid and promising. CT provides complementary, readily available information that is helpful for planning redo surgery or transcatheter procedures.

REFERENCES

1. Nishimura RA, Otto CM, Bonow RO, Carabello BA, Erwin JP, 3rd, Guyton RA, et al. 2014 aha/acc guideline for the management of patients with valvular heart disease: Executive summary: A report of the american college of cardiology/american heart association task force on practice guidelines. *J Am Coll Cardiol*. 2014;63:2438-2488
2. Vahanian A, Alfieri O, Andreotti F, Antunes MJ, Baron-Esquivias G, Baumgartner H, et al. Guidelines on the management of valvular heart disease (version 2012): The joint task force on the management of valvular heart disease of the european society of cardiology (esc) and the european association for cardio-thoracic surgery (eacts). *Eur J Cardiothorac Surg*. 2012;42:S1-44
3. Zoghbi WA, Chambers JB, Dumesnil JG, Foster E, Gottdiener JS, Grayburn PA, et al. Recommendations for evaluation of prosthetic valves with echocardiography and doppler ultrasound: A report from the american society of echocardiography's guidelines and standards committee and the task force on prosthetic valves, developed in conjunction with the american college of cardiology cardiovascular imaging committee, cardiac imaging committee of the american heart association, the european association of echocardiography, a registered branch of the european society of cardiology, the japanese society of echocardiography and the canadian society of echocardiography, endorsed by the american college of cardiology foundation, american heart association, european association of echocardiography, a registered branch of the european society of cardiology, the japanese society of echocardiography, and canadian society of echocardiography. *J Am Soc Echocardiogr*. 2009;22:975-1014
4. Tanis W, Habets J, van den Brink RB, Symersky P, Budde RP, Chamuleau SA. Differentiation of thrombus from pannus as the cause of acquired mechanical prosthetic heart valve obstruction by non-invasive imaging: A review of the literature. *Eur Heart J Cardiovasc Imaging*. 2014;15:119-129
5. Habets J, Tanis W, van Herwerden LA, van den Brink RB, Mali WP, de Mol BA, et al. Cardiac computed tomography angiography results in diagnostic and therapeutic change in prosthetic heart valve endocarditis. *Int J Cardiovasc Imaging*. 2014;30:377-387
6. Symersky P, Budde RP, de Mol BA, Prokop M. Comparison of multidetector-row computed tomography to echocardiography and fluoroscopy for evaluation of patients with mechanical prosthetic valve obstruction. *Am J Cardiol*. 2009;104:1128-1134
7. Teshima H, Hayashida N, Fukunaga S, Tayama E, Kawara T, Aoyagi S, et al. Usefulness of a multidetector-row computed tomography scanner for detecting pannus formation. *Ann Thorac Surg*. 2004;77:523-526
8. Teshima H, Aoyagi S, Ueda T, Takagi K, Shojima T, Tanaka H. Evaluation of advancing the standard valve dysfunction by multidetector-row ct. *J Artif Organs*. 2014;17:162-168
9. Tsai IC, Lin YK, Chang Y, Fu YC, Wang CC, Hsieh SR, et al. Correctness of multi-detector-row computed tomography for diagnosing mechanical prosthetic heart valve disorders using operative findings as a gold standard. *Eur Radiol*. 2009;19:857-867
10. Ueda T, Teshima H, Fukunaga S, Aoyagi S, Tanaka H. Evaluation of prosthetic valve obstruction on electrocardiographically gated multidetector-row computed tomography--identification of subprosthetic pannus in the aortic position. *Circ J*. 2013;77:418-423
11. Makkar RR, Fontana G, Jilaihawi H, Chakravarty T, Kofoed KF, de Backer O, et al. Possible subclinical leaflet thrombosis in bioprosthetic aortic valves. *N Engl J Med*. 2015;373:2015-2024

12. Schoen FJ, Levy RJ. Calcification of tissue heart valve substitutes: Progress toward understanding and prevention. *Ann Thorac Surg*. 2005;79:1072-1080
13. Husser O, Holzamer A, Resch M, Endemann DH, Nunez J, Bodi V, et al. Prosthesis sizing for transcatheter aortic valve implantation--comparison of three dimensional transesophageal echocardiography with multislice computed tomography. *Int J Cardiol*. 2013;168:3431-3438
14. Jilaihawi H, Doctor N, Kashif M, Chakravarty T, Rafique A, Makar M, et al. Aortic annular sizing for transcatheter aortic valve replacement using cross-sectional 3-dimensional transesophageal echocardiography. *J Am Coll Cardiol*. 2013;61:908-916
15. Ng AC, Delgado V, van der Kley F, Shanks M, van de Veire NR, Bertini M, et al. Comparison of aortic root dimensions and geometries before and after transcatheter aortic valve implantation by 2- and 3-dimensional transesophageal echocardiography and multislice computed tomography. *Circ Cardiovasc Imaging*. 2010;3:94-102
16. Habets J, van den Brink RB, Uijlings R, Spijkerboer AM, Mali WP, Chamuleau SA, et al. Coronary artery assessment by multidetector computed tomography in patients with prosthetic heart valves. *Eur Radiol*. 2012;22:1278-1286
17. Symersky P, Habets J, Westers P, de Mol BA, Prokop M, Budde RP. Prospective ecg triggering reduces prosthetic heart valve-induced artefacts compared with retrospective ecg gating on 256-slice ct. *Eur Radiol*. 2012;22:1271-1277
18. Fleischmann D, Boas FE. Computed tomography--old ideas and new technology. *Eur Radiol*. 2011;21:510-517
19. Carrascosa P, Capunay C, Rodriguez-Granillo GA, Deviggiano A, Vallejos J, Leipsic JA. Substantial iodine volume load reduction in ct angiography with dual-energy imaging: Insights from a pilot randomized study. *Int J Cardiovasc Imaging*. 2014;30:1613-1620
20. Raju R, Thompson AG, Lee K, Precious B, Yang TH, Berger A, et al. Reduced iodine load with ct coronary angiography using dual-energy imaging: A prospective randomized trial compared with standard coronary ct angiography. *J Cardiovasc Comput Tomogr*. 2014;8:282-288
21. von Knobelsdorff-Brenkenhoff F, Rudolph A, Wassmuth R, Bohl S, Buschmann EE, Abdel-Aty H, et al. Feasibility of cardiovascular magnetic resonance to assess the orifice area of aortic bioprostheses. *Circ Cardiovasc Imaging*. 2009;2:397-404
22. Crouch G, Bennetts J, Sinhal A, Tully PJ, Leong DP, Bradbrook C, et al. Early effects of transcatheter aortic valve implantation and aortic valve replacement on myocardial function and aortic valve hemodynamics: Insights from cardiovascular magnetic resonance imaging. *J Thorac Cardiovasc Surg*. 2015;149:462-470
23. Orwat S, Diller GP, Kaleschke G, Kerckhoff G, Kempny A, Radke RM, et al. Aortic regurgitation severity after transcatheter aortic valve implantation is underestimated by echocardiography compared with mri. *Heart*. 2014;100:1933-1938
24. von Knobelsdorff-Brenkenhoff F, Trauzeddel RF, Barker AJ, Gruettner H, Markl M, Schulz-Menger J. Blood flow characteristics in the ascending aorta after aortic valve replacement--a pilot study using 4d-flow mri. *Int J Cardiol*. 2014;170:426-433
25. Anwar AM, Nosir YF, Alasnag M, Chamsi-Pasha H. Real time three-dimensional transesophageal echocardiography: A novel approach for the assessment of prosthetic heart valves. *Echocardiography*. 2014;31:188-196

26. Tanis W, Teske AJ, van Herwerden LA, Chamuleau S, Meijboom F, Budde RP, et al. The additional value of three-dimensional transesophageal echocardiography in complex aortic prosthetic heart valve endocarditis. *Echocardiography*. 2015;32:114-125
27. Ozkan M, Gursoy OM, Astarcioglu MA, Gunduz S, Cakal B, Karakoyun S, et al. Real-time three-dimensional transesophageal echocardiography in the assessment of mechanical prosthetic mitral valve ring thrombosis. *Am J Cardiol*. 2013;112:977-983

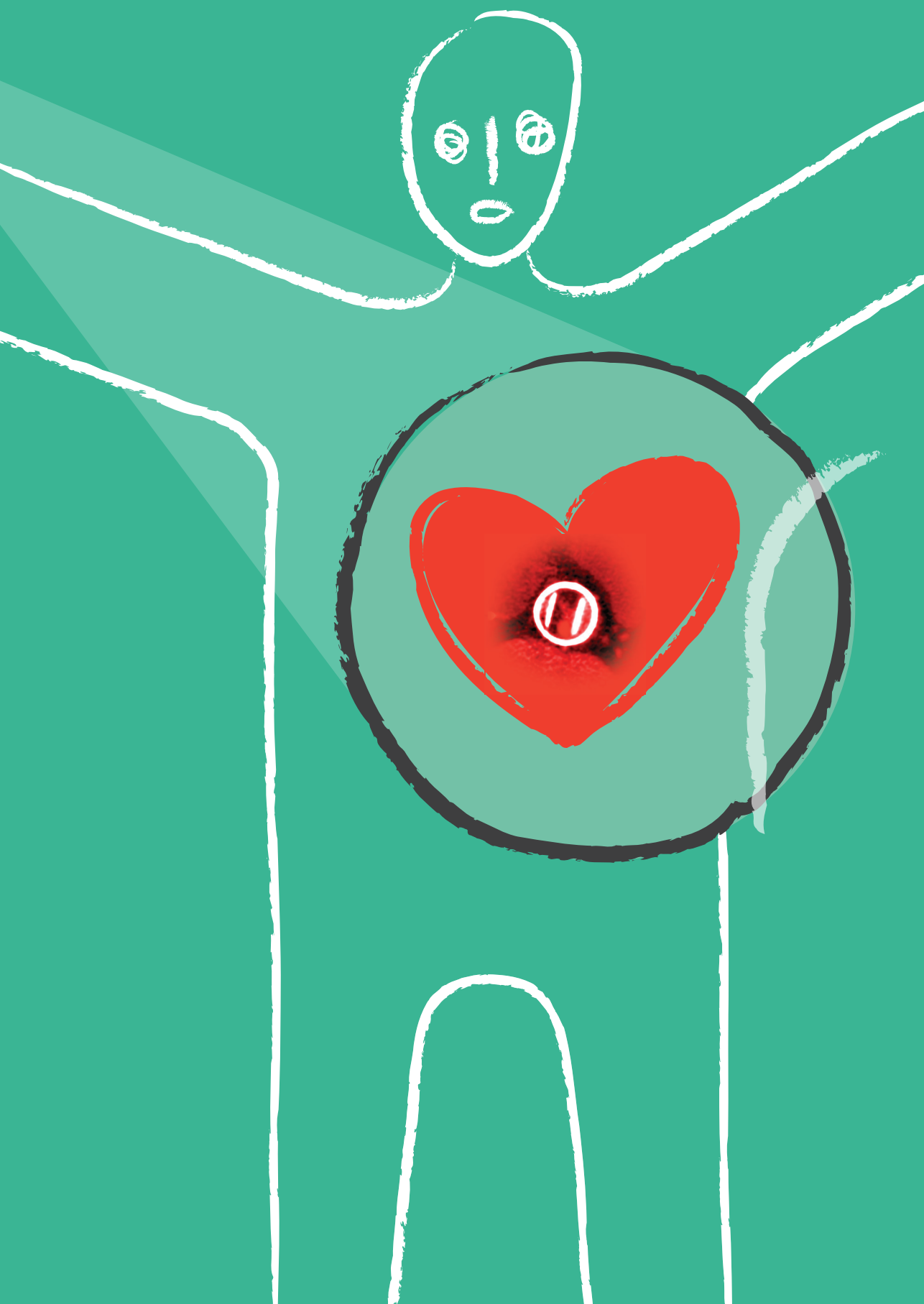

CHAPTER 14

Dutch summary
Review committee
List of abbreviations
Biography
List of publications
Acknowledgements

CHAPTER 14

Dutch summary

Review committee
List of abbreviations
Biography
List of publications
Acknowledgements

Bij patiënten met hartklepprothesen (kunstkleppen) wordt kort na implantatie beeldvorming met transthoracale echocardiografie (TTE) geadviseerd als basis referentiepunt[1-3]. Bij patiënten met een biologische kunstklep is vanaf vijf jaar na implantatie jaarlijkse follow-up met TTE noodzakelijk om eventuele structurele klepdysfunctie op te sporen. Mechanische kunstkleppen behoeven follow-up beeldvorming enkel bij verdenking op klepdysfunctie op basis van klinische symptomen. TTE dient te worden verricht in alle gevallen van verdenking op klepdysfunctie. Wanneer TTE onvoldoende uitsluitsel geeft wordt transoesophageale echocardiografie (TEE) geadviseerd. TEE heeft een hogere spatiële resolutie en biedt een beter anatomisch overzicht vanwege de nauwe relatie met het hart. Fluoroscopie kan van meerwaarde zijn ter beoordeling van klepbladbewegingen bij een verdenking op kunstklepobstructie. Alle bovengenoemde traditionele beeldvormende technieken hebben specifieke beperkingen die kunnen leiden tot niet conclusieve diagnostische resultaten in patiënten met kunstkleppen. In dit proefschrift werd de rol van computertomografie (CT) als nieuwe beeldvormende techniek bij patiënten met een kunstklep onderzocht.

In *Hoofdstuk 2* worden de mogelijkheden en valkuilen van nieuwe beeldvormende technieken voor kunstklepevaluatie besproken, gebaseerd op een systematisch overzicht van de huidige literatuur op het gebied van CT en magnetische resonantie beeldvorming (MRI). Volgens de huidige richtlijnen is de rol van CT voor kunstklepevaluatie slechts beperkt en wordt MRI zelfs helemaal niet geopperd.

CT VOLGENS HUIDIGE RICHTLIJNEN

De voornaamste rol van CT, zoals dat wordt gepresenteerd in de richtlijnen, is evaluatie van mechanische klepbladbewegingen wanneer echocardiografie en fluoroscopie niet conclusief zijn[1-3]. Bepaalde pathologie zoals een thrombus, vegetatie of pannus kan de klepbladbeweging beperken. Restrictie van klepbladbeweging kan een van de weinige tekenen zijn van kunstklepobstructie en kan slechts zeer subtiel aanwezig zijn[4]. Fluoroscopie kan worden gebruikt om klepbladbewegingen te beoordelen, omdat klepfabrikanten mechanische klepbladen impregneren met Wolfraam (radiopaak). Fluoroscopie vereist een loodrechte positie van de röntgenstraal ten opzichte van de kunstklep, wat erg lastig kan zijn in bepaalde klepposities en bij rotatie van de kunstklep door bewegingen van het hart. Derhalve is het gebruik van fluoroscopie beperkt tot mechanische kunstkleppen in aortapositie. Ondanks dat in de richtlijnen CT als alternatief middel wordt gesuggereerd om mechanische kunstklepbeweging te beoordelen, is de nauwkeurigheid van deze techniek niet vastgesteld. *Hoofdstuk 3* toont dat CT

uitstekende betrouwbaarheid en overeenstemming heeft met fluoroscopie voor het beoordelen van klepbladbewegingen van hedendaagse monoleaflet en bileaflet kunstkleppen in normale en dysfunctionele omstandigheden. CT detecteerde met een hogere nauwkeurigheid beperkte klepbladbeweging. Ook sloot CT met een hogere nauwkeurigheid beperkte klepbladbeweging uit. Het maximale gemiddelde verschil tussen CT en fluoroscopie voor de gemeten klephoeken was 2 graden. CT kan derhalve gebruikt worden om zelfs subtiele bewegingsrestrictie te detecteren. In patiënten kan de foutmarge van CT groter zijn bij een verminderde beeldkwaliteit door kunstklepgerelateerde artefacten en beweging van het hart bij een lage temporele resolutie. In *Hoofdstuk 7* werd CT gebruikt om klepbladuitslagen te meten bij patiënten met een normaal veronderstelde klepfunctie. Gemeten klephoeken van mechanische kunstkleppen in aortapositie verschilden maximaal (gemiddeld) 2 graden met fabrikantgegevens. Voor prothesen in mitraalpositie was het gemeten verschil 5 graden voor openingshoeken en 2 graden voor sluitingshoeken. Deze resultaten tonen dat CT ook in patiënten betrouwbaar is in zowel aorta- als mitraalkleppen en geven de meetfout aan van CT waar in praktijk rekening mee dient te worden gehouden. Een bevinding die aandacht verdient is dat de openingshoeken van de ON-X klep beduidend minder waren vergeleken met fabrikantsgegevens (resp. 76 versus 90 graden), eerder ook beschreven in fluoroscopie-studies. Men dient dus in gedachten te houden dat een verminderde opening van de ON-X klep geen teken van onderliggende pathologie hoeft te zijn. Alhoewel klepbladen van de Perimount klep niet beoordeelbaar bleken met CT vroeg na implantatie, kan CT mogelijk wel gebruikt worden voor de evaluatie van biologische kunstkleppen bij klepbladverdikking en -calcificatie (*Hoofdstuk 10* en *Hoofdstuk 11*). Vanwege de complete cardiale acquisitie biedt CT vergeleken met fluoroscopie veel meer informatie die gebruikt kan worden om pathologie te detecteren. In de AHA/ACC 2014 richtlijnen wordt geopperd dat wanneer echocardiografie (TTE en TEE) niet conclusief is, aanvullende CT beeldvorming kan worden overwogen bij patiënten met een verdenking op structurele klepdysfunctie, klepobstructie en periprosthetische infecties[1]. De resultaten gepresenteerd in dit proefschrift benadrukken het belang van CT in klepdysfunctie.

CT NA IMPLANTATIE

Na implantatie wordt TTE geadviseerd als patiënt-specifieke referentie voor follow-up beeldvorming bij verdenking op klepdysfunctie. Ook zou het nuttig zijn om CT beelden verricht na implantatie te kunnen vergelijken met CT in het kader van klepdysfunctie. Het is echter pas mogelijk pathologie te detecteren wanneer fysiologische en pathologische omstandigheden van elkaar onderscheiden

kunnen worden. Daarom is het een primair vereiste een referentie te hebben van kunstkleppen en gerelateerde anatomie in normale omstandigheden. Met dit doel werd een prospectieve studie verricht waarin 46 patiënten met CT werden onderzocht in aanvulling op routine TTE zes weken na kunstklepimplantatie (*Hoofdstuk 7*). Ten eerste toont deze studie dat, ondanks de aanwezigheid van klepgerelateerde artefacten, CT kan worden gebruikt om betrouwbaar kunstkleppen en omliggende anatomie in klepdysfunctie te evalueren. Ten tweede toont CT dat matige pericardeffusie en prominente pericardiale en pleurale hematomen normale bevindingen zijn vroeg na implantatie. Ten derde wordt met CT zes weken na aortakunstklep implantatie in 83% van de patiënten induratie van het peri-aortale vetweefsel gevonden. Dit kan als een normale bevinding worden beschouwd, alhoewel niet bekend is hoelang deze geïndureerde verschijning aanwezig blijft. Induratie van het peri-aortale vetweefsel kan echter ook gerelateerd zijn aan kunstklependocarditis en differentiatie vroeg na implantatie kan daarom lastig zijn. Bij patiënten met verdenking op vroege klependocarditis zonder infectieuze complicaties is aanvullende CT mogelijk van beperkte waarde. Daarentegen toonde CT na implantatie toegevoegde waarde door het detecteren van drie gevallen van pathologie, die niet werden gedetecteerd met routine TTE: aspecifiek subprosthetisch weefsel, pseudoaneurysmata en klepdehiscentie. Laatstgenoemde casus vereiste een heroperatie, die niet gepland zou zijn gebaseerd op routine diagnostiek. De patiënt met aspecifiek subprosthetisch weefsel toont het belang van beeldvorming na implantatie. Waarschijnlijk betreft het een restant van de natieve annulus, echter bij verdenking op klepdysfunctie zou hetzelfde CT beeld verworven pathologie kunnen suggereren. Een andere bevinding die relevant is voor follow-up CT is detectie van een geanguleerde kunstkleppositie ten opzichte van de LVOT. Een geanguleerde positie kan hemodynamische consequenties hebben en leiden tot een verhoogde transprosthetische drukgradiënt, alhoewel deze angulatie vaak niet zichtbaar is met echocardiografie. Op basis van de gepresenteerde studie kan nog niet worden geconcludeerd dat CT routinematig bij elke patiënt na implantatie zou moeten worden verricht. CT als screeningstechniek zou echter wel overwogen moeten worden bij patiënten met een gecompliceerde kunstklepimplantatie of met een hogere verdenking op het ontwikkelen van klepgerelateerde complicaties na implantatie. De prevalentie van bovengenoemde bevindingen en de toegevoegde waarde van CT bij patiënten met verdenking op klepdysfunctie moeten worden bevestigd in nadere studies.

CT BIJ VERDENKING OP KLEPDYSFUNCTIE

CT kan worden gebruikt om restrictie van klepbeweging te detecteren als indicator voor klepobstructie, maar de nadere rol van CT voor functionele klepevaluatie blijft beperkt. Vanwege zijn driedimensionale aard en hoge spatiële resolutie kan CT echter wel aanvullende informatie verschaffen op het gebied van anatomie en aanwezige pathologie. In een prospectieve studie bij patiënten met verdenking op kunstklependocarditis toonde CT toegevoegde waarde in aanvulling op echocardiografie voor het detecteren en tonen van de uitgebreidheid van endocarditis gerelateerde complicaties[5]. Een potentiele meerwaarde van CT wordt ook gesuggereerd in verdenking op kunstklepobstructie[6-10], alhoewel prospectief onderzoek met CT in aanvulling op routine diagnostiek ontbreekt. In *Hoofdstuk 8* wordt een dergelijke cross-sectionele studie gepresenteerd bij patiënten met verdenking op kunstklepobstructie en periprosthetische lekkage (niet endocarditis gerelateerd). CT toont in de meeste gevallen toegevoegde waarde bovenop routine TTE en TEE beeldvorming (+/- fluoroscopie), en voornamelijk in mechanische kunstkleppen. Bij patiënten met verdenking op klepobstructie gaf CT een indicatie van de onderliggende oorzaak van obstructie door het tonen van een subvalvulair membraan, pannus en/of trombus. In mechanische kunstkleppen leidde CT tot een verandering van het beleid bij een derde van de patiënten. Bij patiënten met verdenking op kunstkleplekkage was de kracht van CT het detecteren of uitsluiten van eventuele infectieuze complicaties in zowel mechanische als biologische kunstkleppen. Daarnaast gaf CT aanvullende informatie relevant voor de planning van een heroperatie of percutane sluiting van het lek. De rol van aanvullende CT diagnostiek is het grootst bij patiënten met verdenking op klepobstructie.

Het is namelijk zeer belangrijk de onderliggende oorzaak van obstructie te kunnen detecteren, gezien zowel fibrinolyse als heroperatie aanzienlijke risico's met zich meebrengen. Een limitatie van bovengenoemde studie is dat chirurgische bevindingen slechts in een derde van alle patiënten beschikbaar waren. Alhoewel een deskundige jury alle patiënten heeft beoordeeld, zou chirurgische of pathologische bevestiging (referentietest) nadere differentiatie tussen pannus en trombus kunnen verbeteren. Desondanks toont deze studie dat CT zou moeten worden ingevoerd als standaard diagnostisch middel bij alle patiënten met verdenking op kunstklepobstructie. In een recente studie detecteerde CT kort na implantatie in biologische kunstkleppen beperkte klepbewegingsuitslagen en pathologische klepbladstructuren. TTE had deze afwijkingen niet gedetecteerd en toonde normale transprosthetische drukgradiënten[11]. De pathologische bevindingen in deze studie kunnen gerelateerd zijn aan een inadequaat

antistollingsbeleid na implantatie, maar hoe dan ook bevestigen de bevindingen het belang van CT in klepobstructie. Alhoewel de rol van CT bij patiënten met kunstkleplekkage beperkter is, kan CT wel worden overwogen om complicaties uit te sluiten, klepdehiscentie te detecteren (*Hoofdstuk 7*) of een heroperatie te plannen. Voor een kwalitatieve en state-of-the-art patiëntenzorg is een multidisciplinaire aanpak een vereiste, gezien de complexiteit van kunstkleppathologie en diagnostiek.

In biologische kunstkleppen is structurele dysfunctie de hoofdoorzaak van dysfunctie na verloop van tijd. De duurzaamheid van biologische kleppen zou mogelijk beïnvloed kunnen worden door de vorm van de protheses. Deformatie van de kunstklep kan invloed hebben op de ontplooiing van klepblaadjes en de verdeling van mechanische drukken, wat in verband is gebracht met het proces van klepbladcalcificatie en degeneratie[12]. In *Hoofdstuk 10* werd CT gebruikt om de vorm van biologische kunstkleppen na implantatie na te gaan. De excentriciteitindex (gebaseerd op de ratio van de minimale en maximale klepdiameters) toonde dat biologische kunstkleppen minstens mild gedeformeerd waren in 41% van de gevallen. Significante deformatie (niet-circulair, gedefinieerd als een excentriciteitindex ≥10%) was aanwezig in 13% van de gevallen. Mocht klepdeformatie leiden tot suboptimale klepfunctie of vroege structurele dysfunctie, vragen deze resultaten mogelijk om een re-evaluatie van chirurgische technieken om de duurzaamheid van de biologische kleppen te verhogen.
In *Hoofdstuk 11* wordt een casus gepresenteerd met onverwacht vroege structurele dysfunctie van de biologische Mitroflow klep, geïmplanteerd in aortapositie. TTE toonde tekenen van klepdysfunctie en lekkage, maar slaagde er niet in de onderliggende oorzaak aan te wijzen. TEE was niet succesvol omdat de patiënt het invasieve onderzoek niet verdroeg, waarna CT werd verricht. Ondanks de aanwezigheid van beeldruis en klepgerelateerde artefacten toonde CT uitgebreide klepbladcalcificaties.

CT VOORAFGAAND AAN KUNSTKLEP (HER)PROCEDURES

In chirurgische klepimplantaties wordt de maat van de kunstklep gebaseerd op directe metingen van de annulus tijdens de ingreep. Bij transcatheter procedures is bepaling van de maat echter volledig afhankelijk van informatie verkregen bij beeldvorming. Het is onbekend of gedurende de hartcyclus de annulus van vorm verandert en of dit gevolgen heeft voor het kiezen van de juiste klepmaat. Het kiezen van de juiste maat is essentieel om complicaties zoals paravalvulaire lekkage

te voorkomen. Resultaten van het systematische literatuuroverzicht gepresenteerd in *Hoofdstuk 6* tonen dat in het algemeen de annulus meer circulair is tijdens de systole en meer ovaal tijdens de diastole. Het gebruik van enkel systolische metingen voor het bepalen van de klepmaat bij patiënten met een significante vormverandering tijdens de hartcyclus kan daarom leiden tot een te kleine kunstklep. De exacte fase waarin de annulus het grootst is, verschilt echter tussen patiënten en betreft in sommige gevallen de diastole. De complexe anatomie van de annulus en de vormverandering gedurende de hartcyclus vereisen daarom gebruik van driedimensionale modaliteiten voor het verkrijgen van de juiste kunstklepmaat. Een voordeel van CT is dat het ook annulaire calcificaties kan tonen die van belang kunnen zijn bij patiënten die in een range van twee klepmaten vallen[13]. Driedimensionale TEE kan een goed alternatief van CT zijn bij patiënten met een contrastmedium allergie, alhoewel TEE de annulus dimensies kan onderschatten vergeleken met CT[13-15].

CT verricht in het kader van kunstklepdysfunctie kan nuttige aanvullende informatie geven. Bij de besluitvorming omtrent therapie bij dysfunctie is de maat van de huidige kunstklep essentieel. Vrij recent zijn klep-in-klep procedures geïntroduceerd waardoor sommige patiënten met biologische klepdysfunctie nu in aanmerking kunnen komen voor een transcatheter (her)procedure. Echter, enkel met kennis van de huidige klepmaat kan besloten worden of potentiele winst te halen valt met een herprocedure en kan patiënt prothese mismatch voorkomen worden. In de praktijk is de maat echter niet altijd bekend en daarnaast bestaan discrepanties tussen de maat gegeven door de fabrikant en werkelijke dimensies. Niet-invasieve, reproduceerbare methoden om de geïmplanteerde kunstklepmaat te achterhalen ontbreken. *Hoofdstuk 9* toont dat CT een betrouwbaar instrument is om de klepdiameter en oppervlak te meten. CT maakt het ook mogelijk om opeenvolgende klepmaten te onderscheiden en kan dus gebruikt worden om non-invasief de maat van de geïmplanteerde klep te achterhalen. Dit geldt voor alle onderzochte kustkleppen behalve de (monoleaflet) Björk-Shiley, die bekend is om zijn significante CT klepartefacten. Het gepresenteerde CT overzicht kan gebruikt worden om bij klepdysfunctie echocardiografie resultaten te interpreteren en herprocedures te plannen.

Hoofdstuk 7 toonde dat CT verricht voor kunstklepevaluatie ook bruikbaar kan zijn voor gelijktijdige beoordeling van de coronairarteriën, gezien CT in een patiënt een coronaire anomalie detecteerde met significante tapering

die nadere diagnostiek vereiste. Normaliter wordt voor coronair evaluatie CT verricht met prospectieve ECG-triggering vanwege de goede diagnostische beeldkwaliteit. Daarentegen heeft retrospectieve ECG-gating de voorkeur voor kunstklepevaluatie, omdat dit dynamische informatie verschaft, ook al kan de beeldkwaliteit verminderd zijn door beeldruis. Desondanks toonde een eerdere studie dat de beeldkwaliteit van CT voor coronairarteriën niet substantieel wordt verstoord door hedendaagse kunstkleppen[16]. Deze studie onderzocht echter niet de diagnostische waarde van CT. In *Hoofdstuk 12* wordt CT vergeleken met invasieve coronairangiografie (CAG) voor het uitsluiten van coronairlijden. CT was in staat coronairlijden uit te sluiten in ongeveer de helft van de patiënten zonder een voorgeschiedenis met coronairziekten. Bij de overige patiënten zal CAG vereist blijven om verdere coronairziekte aan te tonen of uit te sluiten. Wel toonde CT adequaat de doorgankelijkheid van coronaire bypass grafts en detecteerde een maligne verloop van een graft direct retrosternaal. Beschikbare CT informatie zou daarom gebruikt kunnen worden om het CAG voor heroperatie in een aanzienlijk deel van de patiënten te mijden. Dit bespaart risico's op distale embolizatie van de thrombus of vegetatie door manipulatie van de katheter. Bovendien wordt hiermee onnodige bloostelling aan contrast vermeden waar twee contrastonderzoeken zelfs gecontraïndiceerd kunnen zijn. Het vervangen van CAG met al beschikbare CT beeldvorming zal ook de stralingsdosis verlagen.

CT OPTIMALISATIE

De toepassing van CT bij patiënten met kunstkleppen is veelbelovend, maar een groot nadeel is de hoge stralingsdosis die te wijten is aan retrospectieve ECG-gated acquisities. Een verlaging van de stralingsdosis zou het gebruik van CT als diagnostisch middel op een grotere schaal toestaan. In de prospectieve studies getoond in *Hoofdstuk 7* en *Hoofdstuk 8* was de gemiddelde stralingsdosis resp. 11.3 mSv en 11.6 mSv. Prospectieve ECG-triggering heeft een lagere stralingsdosis en kan klepartefacten verminderen[17], alhoewel dit afhankelijk is van het hartritme en kleptype. Met prospectieve ECG-triggering worden beelden verkregen gedurende één vooraf bepaalde fase van de hartcyclus en daarom is er geen dynamische informatie beschikbaar. Zoals getoond in *Hoofdstuk 7* was de optimale fase voor kunstklepevaluatie 30-40% systolisch en 75%, 80% en 90% diastolisch. Het voorspellen van de optimale fase kan dus lastig zijn. Daarnaast vereist prospectief scannen een lage en stabiele hartslag. Bètablokkers kunnen de hartslag optimaliseren, maar voorzichtigheid is geboden aangezien deze zeker in patiënten met klepdysfunctie gecontraïndiceerd kunnen zijn. Al met al is de rol van prospectieve ECG-triggering als optimalisatiemethode op dit moment beperkt.

In de studie gepresenteerd in *Hoofdstuk 4* wordt gepoogd retrospectieve ECG-gating CT te optimaliseren middels verbetering van de beeldkwaliteit en verlaging van de stralingsdosis. Hiervoor werden verschillende beeldreconstructie-algoritmen onderzocht in een fantoomopstelling. Reconstructie-algoritmen worden gebruikt om ruwe CT data te converteren in beelden. Filtered-back projection (FBP) is een conventioneel algoritme en wordt standaard gebuikt in CT beeldvorming. Additionele nieuwe iteratieve reconstructie (IR) technieken zijn de laatste jaren geïntroduceerd en behelzen zowel relatief simpele als meer geavanceerde 'model-based' algoritmen. *Hoofdstuk 4* toont dat IR technieken tot 75% verlaging van de stralingsdosis toelaten met behoud van de beeldkwaliteit en vermindering van beeldruis. Deze resultaten zijn veelbelovend, maar de algoritmen dienen in pulsatiele kunstkleppen gevalideerd te worden voordat deze standaard klinisch gebruikt kunnen worden.
Om verdere evaluatie van kunstkleppen in een in vitro omgeving mogelijk te maken werd een nieuw pulsatiel fantoom (mock loop) ontwikkeld en gepresenteerd in *Hoofdstuk 5*. Deze mock loop is gebaseerd op een vijf-elementen Windketel model. Dat houdt in dat bij het simuleren van het cardiale systeem rekening wordt gehouden met de arteriële en veneuze compliantie, perifere weerstand, aorta impedantie en inertie van bloed. Met deze mock loop kunnen verschillende fysiologische en pathologische omstandigheden worden nagebootst in zowel mechanische als biologische kunstkleppen. Bovendien is de mock loop geconstrueerd uit enkel niet-ferromagnetische materialen, waardoor kunstkleppen ook veilig met MRI kunnen worden bestudeerd. Deze geavanceerde mock loop kan worden gebruikt om acquisitieprotocollen te optimaliseren en beeldreconstructie-algoritmen te testen. MRI beeldvorming kan worden geoptimaliseerd, waardoor kunstklepevaluatie zonder enige stralingsdosis mogelijk wordt en ook functionele informatie kan bieden.

TOEKOMSTPERSPECTIEVEN

CT heeft meerwaarde als toevoeging op routine diagnostiek bij patiënten met verdenking op klepdysfunctie en voor het plannen van heroperaties of transcatheter procedures. Daarnaast is CT een betrouwbaar middel voor anatomische en klepgerelateerde metingen. CT verricht in het kader van klepdysfunctie kan worden gebruikt om extra informatie te vergaren zoals coronairlijden. De voornaamste zorg bij CT is de stralingsdosis. Verschillende scantechnieken zoals een hoge tafelbeweging (high pitch), buisspanning modulatie en prospectieve ECG-triggering kunnen de stralingsdosis verlagen, alhoewel iedere techniek bezwaren kent die de toepassing tot specifieke situaties beperkt. IR technieken zijn

bevorderlijk, maar klinische studies zijn nodig om bij patiënten met kunstkleppen de diagnostische toepasbaarheid in de dagelijkse praktijk te beoordelen. Een andere zorg is dat CT van het hart toediening van contrastmiddel vereist. Dit brengt risico's met zich mee in het ontwikkelen van contrast geïnduceerde nefropathie, terwijl een aanzienlijk deel van de kunstkleppatiënten al een verminderde nierfunctie heeft. Bij deze patiënten zou een op maat gemaakte aanpak dergelijke risico's kunnen verminderen en contrast CT in een grotere groep patiënten toestaan.
Daarnaast kunnen klepgerelateerde artefacten periprosthetische gebieden, die belangrijk zijn voor de beoordeling van klepdysfunctie, overschaduwen. Grotere studies zijn nodig om meer specifiek te differentiëren tussen onderliggende kunstkleppathologie. Bij CT kan de attenuatie in weefsels (gemeten in Hounsfield Units) helpen in het differentiëren van pannus en trombus. Dit is echter nog niet gevalideerd. Toekomstige studies in patiënten met kunstklepobstructie én chirurgische of pathologische bevestiging als referentie zullen deze nadere differentiatie eventueel mogelijk maken. Gezien de lage prevalentie van klepgerelateerde complicaties en het feit dat niet alle patiënten een heroperatie ondergaan, lijkt een multicentrische of zelfs multinationale studie noodzakelijk.
Verder kunnen klinische CT studies vroeg na kunstklepimplantatie de prevalentie van onverwachte (pathologische) bevindingen verduidelijken en correleren met complicaties bij follow-up. Gebaseerd op die resultaten kan de implementatie van CT als screeningsmiddel na klepimplantatie gerechtvaardigd zijn. Al met al, in de nabije toekomst zal aandacht dienen te worden besteed aan (I) stralingsdosis verlaging, (II) contrastmiddel restrictie, (III) hartslag optimalisatie, (IV) klepartefact-reductie en (V) weefsel karakterisering.

NIEUWE CT TECHNIEKEN

CT technologie ontwikkelt zich snel, wat bijzonder veelbelovend is voor beeld-vorming van het hart in het algemeen en specifiek voor patiënten met kunstkleppen. Al het CT onderzoek in dit proefschrift werd verricht met een single-source multidetector-row CT (MDCT) systeem. De meest recente CT technologie omhelst dual energy CT en photon-counting CT. Dual energy CT is reeds in verscheidene klinische centra geïmplementeerd en photon-counting CT is slechts zeer recentelijk commercieel beschikbaar geworden. Dual energy CT is een relatief oud concept dat stamt uit het begin van de CT tijd, alhoewel dit pas sinds enkele jaren in de dagelijkse praktijk is geïntroduceerd[18]. Enige basiskennis van dit system is nuttig om de mogelijkheden ervan in te zien. Zoals de naam impliceert, is dual energy CT (DECT) gebaseerd op het gebruik van twee röntgen (foton) energieën, gebruikelijk 80 kV

en 140 kV. Lage fotonenergie geeft een goed weefselcontrast (en meer beeldruis), daarentegen leidt hoge fotonenergie tot minder beeldruis (maar ook minder weefselcontrast). Alhoewel verschillende DECT technieken beschikbaar zijn, is het basisprincipe dat de twee verschillende röntgenenergieën leiden tot verschillen in weefselattenuatie en dus kunnen worden gebruikt voor weefselkarakterisatie, ook wel weefseldecompositie. Aangezien bepaalde weefsels daarmee kunnen worden herkend, kan met gebruik van deze informatie de reconstructie van beelden worden aangepast. Bijvoorbeeld, uit CT met contrast kunnen (virtueel) beelden zonder contrast worden gereconstrueerd door substractie van jodium (contrast) signaal. Bij contrast CT van kunstkleppen zouden virtueel gereconstrueerde non-contrastbeelden gelijktijdige beoordeling van annulus- en klepbladcalcificaties kunnen toelaten en bijdragen aan de diagnostiek van structurele klepdysfunctie. Op dezelfde manier kan het jodium signaal op virtuele reconstructies worden gekleurd en gebruikt voor de detectie van aankleurend (infectieus) weefsel of voor de evaluatie van myocardperfusie. Deze technieken bieden de mogelijkheid om te differentiëren tussen onderliggende oorzaken van kunstkleppathologie en kunnen aanvullende informatie bieden. Weefseldecompositie in combinatie met virtuele (monochromatische) reconstructies kan potentieel ook worden gebruikt om beam-hardening artefacten te reduceren en de beeldkwaliteit te verbeteren. Daarnaast kunnen monochromatische reconstructies potentieel ook worden gebruikt om de hoeveelheid benodigd contrast te beperken met behoud van beeldkwaliteit[19, 20].
Dual source CT heeft een hogere temporele resolutie (66-75ms) vergeleken met single source CT (~150ms) en is daarom minder gevoelig voor artefacten door beweging van het hart, wat ook effectief kan zijn voor het verminderen van kunstklepartefacten. Het effect van DECT op de stralingsdosis in beeldvorming van kunstkleppen dient te worden vastgesteld.
De meest recente doorbraak in CT technologie is photon-counting CT, ook bekend als spectrale CT. Spectrale CT zou nog betere, meer geavanceerde weefseldecompositie kunnen toestaan omdat multipele energieniveaus kunnen worden gedifferentieerd. Deze geavanceerde weefselkarakterisatie is gebaseerd op de implementatie van speciale, cadmium telluride zinkdetectoren die individuele fotondetectie (counting) mogelijk maken. Waar DECT profijtelijk kan zijn vergeleken met single source MDCT, lijkt photon-counting CT nog veelbelovender vergeleken met DECT voor stralingsdosisverlaging en weefselkarakterisatie.
Bovengenoemde ontwikkelingen suggereren een verbetering in alle aspecten noodzakelijk voor het implementeren van CT voor kunstklepevaluatie in een grotere groep patiënten. Daarnaast zijn ook ontwikkelingen op het gebied van numerieke

stromingsleer (computational fluid dynamics) veelbelovend, omdat deze hemodynamische simulatie mogelijk kunnen maken waarmee patiënt-specifieke behandelpannen zouden kunnen worden opgesteld. Alleen uit vervolgonderzoek zal blijken of deze verwachtingen kunnen worden waargemaakt.

OVERIGE BEELDVORMENDE TECHNIEKEN

Aanvullende potentiele beeldvormende technieken voor de evaluatie van patiënten met kunstkleppen zijn driedimensionale TEE (3D-TEE), fluorine fluorodeoxyglucose positronemissietomografie (^{18}F-FDG PET/CT) en MRI. De rol van MRI voor het beoordelen van kunstkleppen is reeds belicht in *Hoofdstuk 2*. Kort samengevat kan MRI aanvullende functionele informatie bieden gezien het kunstklep openingsoppervlak en eventuele kleplekkage kunnen worden beoordeeld[21, 22]. Nadere MRI studies zijn nodig om de reproduceerbaarheid van de metingen te valideren in een bredere groep biologische kleptypen en de diagnostische waarde in dysfunctionele kleppen vast te stellen. Ook zou optimalisatie en validatie voor het beoordelen van kunstkleplekkage met MRI moeten worden nagestreefd[23].

Gezien de groeiende belangstelling in transcatheter procedures en daarmee ook de stijging in prevalentie van kunstkleplekkage zijn methoden om lekkage te kwantificeren onmisbaar. Vierdimensionale MRI is hiervoor een veelbelovende techniek[24] en zou daarnaast ook geschikt kunnen zijn voor het beoordelen van kunstklep hemodynamica na klepimplantatie of voor het plannen van een heroperatie.

Onlangs zijn de eerste studies gepubliceerd die 3D-TEE hebben onderzocht in patiënten met verdenking op kunstklepdysfunctie[25-27]. De eerste resultaten lijken veelbelovend, maar grotere studies zijn nodig om 3D-TEE als aanvullend middel voor detectie van thrombus in klepobstructie of vegetaties en abcessen in kunstklependocarditis te bevestigen.

Alhoewel in dit proefschrift de aandacht niet uitging naar endocarditis als onderliggende oorzaak van klepdysfunctie, dient te worden opgemerkt dat aanvullende ^{18}F-FDG PET/CT zinvol kan zijn in deze patiënten omdat dit metabole informatie verstrekt. In patiënten met induratie van het peri-aortale vetweefsel op CT (*Hoofdstuk 7*) zou mogelijk ^{18}F-FDG PET/CT als enige modaliteit kunnen differentiëren tussen een vroege kunstklependocarditis en een normaal postoperatief beeld. Studies om de diagnostische waarde van FDG PET/CT vast te stellen en normaalwaarden te presenteren ontbreken. Hiervoor is de PROSPECTA studie gestart waarvan de resultaten op korte termijn beschikbaar zullen zijn.

ALGEMENE CONCLUSIES VAN DIT PROEFSCHRIFT

Bij patiënten met een kunsthartklep heeft CT in aanvulling op echocardiografie en fluoroscopie duidelijk meerwaarde. Aanvullende diagnostiek met CT zou daarom altijd overwogen moeten worden bij alle patiënten met een verdenking op kunstklepdysfunctie en zou overwogen kunnen worden als referentie kort na implantatie van een kunstklep. Alhoewel detectie van de onderliggende oorzaak van kunstklepdysfunctie een uitdaging blijft, zijn huidige ontwikkelingen in beeldvormende technieken snel en veelbelovend. Tevens verschaft CT aanvullende, reeds beschikbare informatie die gebruikt kan worden voor het plannen van een heroperatie of transcatheter procedure.

REFERENTIES

1. Nishimura RA, Otto CM, Bonow RO, Carabello BA, Erwin JP, 3rd, Guyton RA, et al. 2014 aha/acc guideline for the management of patients with valvular heart disease: Executive summary: A report of the american college of cardiology/american heart association task force on practice guidelines. *J Am Coll Cardiol*. 2014;63:2438-2488
2. Vahanian A, Alfieri O, Andreotti F, Antunes MJ, Baron-Esquivias G, Baumgartner H, et al. Guidelines on the management of valvular heart disease (version 2012): The joint task force on the management of valvular heart disease of the european society of cardiology (esc) and the european association for cardio-thoracic surgery (eacts). *Eur J Cardiothorac Surg*. 2012;42:S1-44
3. Zoghbi WA, Chambers JB, Dumesnil JG, Foster E, Gottdiener JS, Grayburn PA, et al. Recommendations for evaluation of prosthetic valves with echocardiography and doppler ultrasound: A report from the american society of echocardiography's guidelines and standards committee and the task force on prosthetic valves, developed in conjunction with the american college of cardiology cardiovascular imaging committee, cardiac imaging committee of the american heart association, the european association of echocardiography, a registered branch of the european society of cardiology, the japanese society of echocardiography and the canadian society of echocardiography, endorsed by the american college of cardiology foundation, american heart association, european association of echocardiography, a registered branch of the european society of cardiology, the japanese society of echocardiography, and canadian society of echocardiography. *J Am Soc Echocardiogr*. 2009;22:975-1014
4. Tanis W, Habets J, van den Brink RB, Symersky P, Budde RP, Chamuleau SA. Differentiation of thrombus from pannus as the cause of acquired mechanical prosthetic heart valve obstruction by non-invasive imaging: A review of the literature. *Eur Heart J Cardiovasc Imaging*. 2014;15:119-129
5. Habets J, Tanis W, van Herwerden LA, van den Brink RB, Mali WP, de Mol BA, et al. Cardiac computed tomography angiography results in diagnostic and therapeutic change in prosthetic heart valve endocarditis. *Int J Cardiovasc Imaging*. 2014;30:377-387
6. Symersky P, Budde RP, de Mol BA, Prokop M. Comparison of multidetector-row computed tomography to echocardiography and fluoroscopy for evaluation of patients with mechanical prosthetic valve obstruction. *Am J Cardiol*. 2009;104:1128-1134
7. Teshima H, Hayashida N, Fukunaga S, Tayama E, Kawara T, Aoyagi S, et al. Usefulness of a multidetector-row computed tomography scanner for detecting pannus formation. *Ann Thorac Surg*. 2004;77:523-526
8. Teshima H, Aoyagi S, Ueda T, Takagi K, Shojima T, Tanaka H. Evaluation of advancing the standard valve dysfunction by multidetector-row ct. *J Artif Organs*. 2014;17:162-168
9. Tsai IC, Lin YK, Chang Y, Fu YC, Wang CC, Hsieh SR, et al. Correctness of multi-detector-row computed tomography for diagnosing mechanical prosthetic heart valve disorders using operative findings as a gold standard. *Eur Radiol*. 2009;19:857-867
10. Ueda T, Teshima H, Fukunaga S, Aoyagi S, Tanaka H. Evaluation of prosthetic valve obstruction on electrocardiographically gated multidetector-row computed tomography--identification of subprosthetic pannus in the aortic position. *Circ J*. 2013;77:418-423
11. Makkar RR, Fontana G, Jilaihawi H, Chakravarty T, Kofoed KF, de Backer O, et al. Possible subclinical leaflet thrombosis in bioprosthetic aortic valves. *N Engl J Med*. 2015;373:2015-2024

12. Schoen FJ, Levy RJ. Calcification of tissue heart valve substitutes: Progress toward understanding and prevention. *Ann Thorac Surg*. 2005;79:1072-1080
13. Husser O, Holzamer A, Resch M, Endemann DH, Nunez J, Bodi V, et al. Prosthesis sizing for transcatheter aortic valve implantation--comparison of three dimensional transesophageal echocardiography with multislice computed tomography. *Int J Cardiol*. 2013;168:3431-3438
14. Jilaihawi H, Doctor N, Kashif M, Chakravarty T, Rafique A, Makar M, et al. Aortic annular sizing for transcatheter aortic valve replacement using cross-sectional 3-dimensional transesophageal echocardiography. *J Am Coll Cardiol*. 2013;61:908-916
15. Ng AC, Delgado V, van der Kley F, Shanks M, van de Veire NR, Bertini M, et al. Comparison of aortic root dimensions and geometries before and after transcatheter aortic valve implantation by 2- and 3-dimensional transesophageal echocardiography and multislice computed tomography. *Circ Cardiovasc Imaging*. 2010;3:94-102
16. Habets J, van den Brink RB, Uijlings R, Spijkerboer AM, Mali WP, Chamuleau SA, et al. Coronary artery assessment by multidetector computed tomography in patients with prosthetic heart valves. *Eur Radiol*. 2012;22:1278-1286
17. Symersky P, Habets J, Westers P, de Mol BA, Prokop M, Budde RP. Prospective ecg triggering reduces prosthetic heart valve-induced artefacts compared with retrospective ecg gating on 256-slice ct. *Eur Radiol*. 2012;22:1271-1277
18. Fleischmann D, Boas FE. Computed tomography--old ideas and new technology. *Eur Radiol*. 2011;21:510-517
19. Carrascosa P, Capunay C, Rodriguez-Granillo GA, Deviggiano A, Vallejos J, Leipsic JA. Substantial iodine volume load reduction in ct angiography with dual-energy imaging: Insights from a pilot randomized study. *Int J Cardiovasc Imaging*. 2014;30:1613-1620
20. Raju R, Thompson AG, Lee K, Precious B, Yang TH, Berger A, et al. Reduced iodine load with ct coronary angiography using dual-energy imaging: A prospective randomized trial compared with standard coronary ct angiography. *J Cardiovasc Comput Tomogr*. 2014;8:282-288
21. von Knobelsdorff-Brenkenhoff F, Rudolph A, Wassmuth R, Bohl S, Buschmann EE, Abdel-Aty H, et al. Feasibility of cardiovascular magnetic resonance to assess the orifice area of aortic bioprostheses. *Circ Cardiovasc Imaging*. 2009;2:397-404
22. Crouch G, Bennetts J, Sinhal A, Tully PJ, Leong DP, Bradbrook C, et al. Early effects of transcatheter aortic valve implantation and aortic valve replacement on myocardial function and aortic valve hemodynamics: Insights from cardiovascular magnetic resonance imaging. *J Thorac Cardiovasc Surg*. 2015;149:462-470
23. Orwat S, Diller GP, Kaleschke G, Kerckhoff G, Kempny A, Radke RM, et al. Aortic regurgitation severity after transcatheter aortic valve implantation is underestimated by echocardiography compared with mri. *Heart*. 2014;100:1933-1938
24. von Knobelsdorff-Brenkenhoff F, Trauzeddel RF, Barker AJ, Gruettner H, Markl M, Schulz-Menger J. Blood flow characteristics in the ascending aorta after aortic valve replacement--a pilot study using 4d-flow mri. *Int J Cardiol*. 2014;170:426-433
25. Anwar AM, Nosir YF, Alasnag M, Chamsi-Pasha H. Real time three-dimensional transesophageal echocardiography: A novel approach for the assessment of prosthetic heart valves. *Echocardiography*. 2014;31:188-196

26. Tanis W, Teske AJ, van Herwerden LA, Chamuleau S, Meijboom F, Budde RP, et al. The additional value of three-dimensional transesophageal echocardiography in complex aortic prosthetic heart valve endocarditis. *Echocardiography*. 2015;32:114-125
27. Ozkan M, Gursoy OM, Astarcioglu MA, Gunduz S, Cakal B, Karakoyun S, et al. Real-time three-dimensional transesophageal echocardiography in the assessment of mechanical prosthetic mitral valve ring thrombosis. *Am J Cardiol*. 2013;112:977-983

CHAPTER 14

Dutch summary
Review committee
List of abbreviations
Biography
List of publications
Acknowledgements

Prof. dr. W.J.L. Suyker
Professor of Cardiothoracic Surgery
Department of Cardiothoracic Surgery, University Medical Center Utrecht

Dr. R.B.A. van den Brink
Cardiologist
Department of Cardiology, Amsterdam Medical Center

Prof. dr. A.J.J.C. Bogers
Professor of Cardiothoracic Surgery
Department of Cardiothoracic Surgery, Erasmus Medical Center Rotterdam

Prof. dr. P.A.F.M. Doevendans
Professor of Cardiology
Department of Cardiology, University Medical Center Utrecht

Prof. dr. T. Leiner
Professor of Cardiovascular Radiology
Department of Radiology, University Medical Center Utrecht

CHAPTER 14

Dutch summary
Review committee
List of abbreviations
Biography
List of publications
Acknowledgements

ABP	Aortic biological valve prosthesis
AS	Aortic stenosis
AVR	Aortic valve replacement
BMI	Body mass index
BPM	Beats per minute
CABG	Coronary artery bypass graft
CAG	Invasive coronary angiography
CAD	Coronary artery disease
CT	Computed tomography
ECG	Electrocardiography
EI	Eccentricity index
EOA	Effective orifice area
ES	Edwards Sapien XT
FBP	Filtered back projection
FFR	Fractional flow reserve
FGRE	Fast gradient echo
GOA	Geometric orifice area
HU	Hounsfield units
ICC	Intraclass correlation coefficient
IMR	Model-based iterative reconstruction
IR	Hybrid iterative reconstruction
IQR	Interquartile range
LCx	Left circumflex artery
LDA	Left descending artery
LM	Left main artery
LVOT	Left ventricular outflow tract
MDCT	Multidetector-row computed tomography
MH	Medtronic Hall
MRI	Magnetic resonance imaging
NPV	Negative predictive value
PCI	Percutaneous coronary intervention
PHV	Prosthetic heart valve
PPV	Positive predictive value
RCA	Right coronary artery
SD	Standard deviation
SJ	St. Jude
SSFP	Steady-state free-precession
SVD	Structural valve deterioration
TAVI	Transcatheter aortic valve implantation
TEE	Transesophageal echocardiography
THV	Transcatheter heart valve
TTE	Transthoracic echocardiography
VTI	Velocity time integral

CHAPTER 14

Dutch summary
Review committee
List of abbreviations
Biography
List of publications
Acknowledgements

Dominika Suchá was born on April 30, 1987 in Prague, Czechoslovakia. In 2005, she obtained her Gymnasium degree at the Lorentz Casimir Lyceum in Eindhoven, the Netherlands. That same year, she started medical school at Utrecht University. As part of her medical training, she completed a clinical internship in Gynaecology and Obstetrics in Melbourne, Australia. During medical school, she conducted stroke imaging research under supervision of Prof. dr. J. Hendrikse in the Department of Radiology at the University Medical Center (UMC) Utrecht. After graduation in 2012, she started her work as a PhD student, investigating computed tomography imaging in patients with prosthetic heart valves in the Departments of Radiology and Cardiothoracic Surgery, UMC Utrecht under supervision of Prof. dr. W.P.Th.M. Mali, Prof. dr. L.A. van Herwerden, Dr. R.P.J. Budde and Dr. P. Symersky. Upon completion of her PhD research, she worked at Stanford University for six months in stroke imaging research under supervision of Dr. M. Lansberg. For this, she was awarded personal travel grants from Circulatory Health, the van Wijck-Stam Casper Foundation, the JoKolk Foundation and the Doctor Catharina van Tussenbroek Foundation. Concomitantly, she is finishing her Master of Science degree in Clinical Epidemiology at Utrecht University. In 2016, she will continue her research as a postdoctoral scholar in cardiovascular imaging at Stanford University under supervision of Prof. dr. D. Fleischmann. Upon returning in November 2016, she will begin her Radiology residency under supervision of Dr. K. Droogh at Gelre Ziekenhuizen, Apeldoorn and UMC Utrecht.

CHAPTER 14

Dutch summary
Review committee
List of abbreviations
Biography
List of publications
Acknowledgements

PEER REVIEWED PUBLICATIONS

Suchá D, Chamuleau SA, Symersky P, Meijs MF, van den Brink RB, de Mol BA, Mali WP, Habets J, van Herwerden LA, Budde RP. Baseline MDCT findings after prosthetic heart valve implantation provide important complementary information to echocardiography for follow-up purposes. *Eur Radiol.* 2015; [Epub ahead of print]

Suchá D, Symersky P, Tanis W, Mali WP, Leiner T, van Herwerden LA, Budde RP. Multimodality imaging of prosthetic heart valves. *Circ Cardiovasc Imaging.* 2015; [Epub ahead of print]

Suchá D, Tuncay V, Prakken NH, Leiner T, van Ooijen PM, Oudkerk M, Budde RP. Does the aortic annulus undergo conformational change throughout the cardiac cycle? A systematic review. *Eur Heart J Cardiovasc Imaging.* 2015;16:1307-1317

Takx RA, **Suchá D**, Park J, Leiner T, Hoffmann. Sublingual nitroglycerin administration in coronary computed tomography angiography: a systematic review. *Eur Radiol.* 2015;25:3536-3542

Suchá D, Daans SG, Symersky P, Planken RN, Mali WP, van Herwerden LA, Budde RPJ. Reliability, agreement and presentation of a reference standard for assessing implanted heart valve sizes by multidetector-row computed tomography. *Am J Cardiol.* 2015;116:112-120

Tanis W, **Suchá D**, Laufer EM, Habets J, van Herwerden LA, Symersky P, Chamuleau SA, Budde RP. Multidetector-row computed tomography for prosthetic heart valve dysfunction: is concomitant non-invasive coronary angiography possible before redo-surgery? *Eur Radiol.* 2015;25:1623-1630

Suchá D, Willemink MJ, de Jong PA, Schilham AM, Leiner T, Symersky P, Budde RP. The impact of a new model-based iterative reconstruction algorithm on prosthetic heart valve related artifacts at reduced radiation dose mdct. *Int J Cardiovasc Imaging*. 2014;30:785-793

Suchá D, Symersky P, Vonken EJ, Provoost E, Chamuleau SA, Budde RP. Multidetector-row computed tomography allows accurate measurement of mechanical prosthetic heart valve leaflet closing angles compared with fluoroscopy. *J Comput Assist Tomogr*. 2014;38:451-456

CONFERENCE PROCEEDINGS - ORAL PRESENTATIONS (presenter only)

Suchá D, Symersky P, van den Brink RB, Tanis W, Meijs FL, Habets J, Chamuleau SA, van Herwerden LA, Budde RP. Routine MDCT results in an increased diagnostic certainty and a therapeutic change in patients with suspected prosthetic heart valve dysfunction. *European Congress Radiology (ECR) 2016, Vienna*

Suchá D, Symersky P, de Heer LM, Mali WP, van Herwerden LA, Budde RP. Biological aortic heart valves deform after surgical implantation: a multidetector-row computed tomography study. *European Congress Radiology (ECR) 2016, Vienna*

Suchá D, Symersky P, van den Brink RB, Tanis W, Laufer EM, Meijs FL, Habets J, de Mol BA, Mali WPT, Chamuleau SA, van Herwerden LA, Budde RP. Multidetector-row computed tomography in patients with suspected prosthetic valve dysfunction: a prospective study. *Radiological Society of North America (RSNA) 2015, Chicago*

Suchá D, Chamuleau SA, Symersky P, van den Brink RB, de Mol BA, Mali WP, Habets J, van Herwerden LA, Budde RP. The incremental value of multi-detector row computed tomography early after prosthetic heart valve implantation. *Nederlandse Vereniging Thoraxchirurgie (NVT) 2015, Utrecht*

Suchá D, Daans CG, Symersky P, Planken RN, Mali WPThM, van Herwerden LA, Budde RPJ. Valve-in-valve transcatheter implantation work-up: CT can accurately determine the implanted bioprosthesis size. *European Congress Radiology (ECR) 2015, Vienna*

Suchá D, Chamuleau SA, Symersky P, van den Brink RB, de Mol BA, Mali WP, Habets J, van Herwerden LA, Budde RP. Multidetector-row CT findings six weeks post prosthetic heart valve implantation: results of the IMPACT Study. *Radiological Society of North America (RSNA) 2014, Chicago*

Suchá D, Daans CG, Symersky P, Planken RN, Mali WP, van Herwerden LA, Budde RP. The size of the implanted prosthetic heart valve can accurately and non-invasively be determined by multidetector-row computed tomography. *European Society of Cardiac Radiology (ESCR) 2014, Paris*

Suchá D, Tanis W, Laufer EM, Habets J, van Herwerden LA, Symersky P, Chamuleau SA, Budde RP. Multidetector-row CT for prosthetic heart valve evaluation can replace invasive coronary angiography in selected patients. R*adiologendagen 2014, 's-Hertogenbosch*

Suchá D, Willemink MJ, de Jong PA, Schilham AM, Leiner T, Symersky P, Budde RP. The impact of a novel iterative model-based reconstruction algorithm on prosthetic heart valve related artifacts at reduced radiation dose multidetector-row CT. *European Congress Radiology (ECR) 2014, Vienna*

Suchá D, Symersky P, Vonken EJ, Provoost E, Chamuleau SA, Budde RP. Assessment of leaflet closing angles in mechanical prosthetic heart valves with multidetector-row CT compared to cinefluoroscopy: an in vitro study. *Radiological Society of North America (RSNA) 2013, Chicago*

Suchá D, Symersky P, Vonken EJ, Provoost E, Chamuleau SA, Budde RP. Comparison of multidetector-row CT to cinefluoroscopy for leaflet closing angle measurements in mechanical prosthetic heart valves: an in vitro study. *European Society of Cardiac Radiology (ESCR) 2013, London*

Suchá D, Symersky P, Mali WP, van Herwerden LA, Leiner T, Budde RP. Assessment of prosthetic heart valves with cardiac CT and MRI: capabilities and pitfalls. *Radiologendagen 2013, 's-Hertogenbosch*

Suchá D, van der Kolk AG, Brundel M, Biessels GJ, Luijten PR, Hendrikse J. Blood-brain-barrier leakage on 7.0 Tesla MRI in patients after transient ischemic attack and stroke. *Radiologendagen 2012, 's-Hertogenbosch*

CONFERENCE PROCEEDINGS - POSTER PRESENTATIONS

Den Harder AM, **Suchá D**, Martens JPJ, van Hamersvelt RW, Schilham AM, Bos C, Budde RP, Breur JM, Leiner T. Optimal imaging of pediatric aortic stents: computed tomography versus magnetic resonance imaging. *Netherlands Heart Days 2016, Piscadera Bay*

Dijkshoorn ML, **Suchá D**, Nieman K, Bogers AJ, Budde RP. Comprehensive evaluation of mechanical heart valves with third generation dual source CT. *Radiological Society of North America (RSNA) 2015, Chicago*

Suchá D, Tuncay V, Prakken NH, Leiner T, van Ooijen PM, Oudkerk M, Budde RP. The dynamic behavior of the aortic annulus and its implications for TAVI prosthesis sizing: a systematic review. *Society of Cardiovascular Computed Tomography (SCCT) 2015, Las Vegas*

den Harder AM, **Suchá D**, Breur JM, Martens JP, Budde RP, Bos, C, Leiner T. Reliability and agreement of pediatric stent diameter measurements with computed tomography. *European Society of Cardiac Radiology (ESCR) 2014, Paris*

Suchá D, Chamuleau SA, Symersky P, van den Brink BA, de Mol BA, Mali WP, Habets J, van Herwerden LA, Budde RP. Imaging characteristics of prosthetic heart valves acquired with MDCT six weeks post implant: the IMPACT study. *European Society of Cardiology (ESC) 2014, Barcelona*

CHAPTER 14

Dutch summary
Review committee
List of abbreviations
Biography
List of publications
Acknowledgements

Graag wil ik iedereen bedanken die heeft bijgedragen aan de totstandkoming van dit proefschrift. Enkele personen wil ik in het bijzonder bedanken.

PROMOTOREN EN COPROMOTOREN

Prof. dr. W.P.Th.M. Mali, geachte promotor, beste professor, ik wil u zeer hartelijk bedanken voor de mogelijkheid die u mij heeft geboden dit promotietraject te starten. Alhoewel u met zo een grote groep promovendi niet altijd op de voorgrond aanwezig kon zijn, was u toch oprecht betrokken. U nam op essentiële momenten beslissingen die tot dit mooie proefschrift hebben geleid. Ook wil ik u bedanken voor uw vertrouwen en aanmoediging een onderzoeksstage in het buitenland na te streven.

Prof. dr. L.A. van Herwerden, geachte promotor, beste professor, ik ben zeer dankbaar dat u mijn tweede promotor bent. U bent uiterst betrokken geweest bij mijn promotie en ik kon vanaf het eerste moment altijd rekenen op uw klinische kritische blik. Dank voor uw enthousiasme, begeleiding en uw inzet waarmee u een nauwe wetenschappelijke samenwerking tussen de Cardiothoracale chirurgie en Radiologie heeft gerealiseerd.

Dr. R.P.J. Budde, geachte copromotor, beste Ricardo, al voordat ik zelf wist waar ik aan begon had je mijn proefschrift voor ogen. Elke promovendus zal bij jou kennismaken met het uiterst georganiseerde en motiverende 'lijstje' aan mogelijke projecten. Dank voor je vertrouwen toen je me nog als geneeskundestudent aannam en je begeleiding tijdens mijn promotie. Ik heb altijd op je duidelijke uitleg, hulp, geduld en oplossingen voor problemen kunnen rekenen, zelfs nadat je naar Rotterdam vertrok.

Dr. P. Symersky, geachte copromotor, beste Petr, je enthousiasme en klinische blik zijn een must geweest voor mijn proefschrift. Dank voor je bereidheid te helpen bij mijn studies, manuscripten en (vele) revisies. Je kan als geen ander elk stuk net die extra relevante boodschap meegeven die ik zo belangrijk vind. Dank voor je tijd en energie die je hebt gestoken in onze hartklepstudies en je motiverende woorden wanneer ik die nodig had.

BEOORDELINGSCOMMISSIE

Geachte leden van de beoordelingscommissie, Prof. dr. W.J.L. Suyker, Prof. dr. T. Leiner, Prof. dr. P.A.F.M. Doevendans, Prof. dr. A.J.J.C. Bogers, Dr. R.B.A. van den Brink, hartelijk dank voor uw tijd en bereidheid mijn proefschrift kritisch te lezen en te beoordelen.

Geachte opponenten, hartelijk dank voor het plaatsnemen in de oppositie.

CO-AUTEURS

Prof. dr. T. Leiner, professor, beste Tim, je was niet direct betrokken bij mijn promotietraject maar toch ben je een mentor geweest. Altijd wanneer dat nodig is ben je bereid steun of advies te geven. Je onuitputtelijke enthousiasme en gedrevenheid voor (cardiovasculair) onderzoek zijn buitengewoon motiverend. Bedankt voor je vertrouwen en voor alle kansen die je me biedt en vooral ook gunt.

Dr. R.B.A. van den Brink, beste Renee, dank voor uw bereidheid mijn proefschrift te beoordelen en in de commissie zitting te nemen. Uw kennis en ervaring met betrekking tot kunstkleppathologie zijn zeer waardevol, zo niet onmisbaar geweest voor mijn onderzoek. Veel dank voor uw betrokkenheid en uw kritische blik op mijn manuscripten en abstracts.

Prof. dr. B.A.J.M. de Mol, professor, beste Bas, ik wil u bedanken dat u mij de mogelijkheid heeft geboden op uw afdeling onderzoek te doen. U was altijd zeer positief en enthousiast betrokken bij de klinische studie, zelfs tijdens de tijdrovende taak als panel expert. Dank voor uw interesse in de beeldvorming. Hopelijk kunnen we de samenwerking in de toekomst voortzetten.

Dr. Steven Chamuleau, beste Steven, samen de echo's doornemen voor de IMPACT I was voor mij ontzettend leuk en leerzaam. Dank voor al je tijd en enthousiasme, ik weet hoe druk je het had.

Dr. Wilco Tanis, beste Wilco, ik ben blij dat we samen een mooi klinisch stuk hebben kunnen schrijven. Ik waardeer het zeer dat je ook nu vanuit Den Haag nog altijd bereid bent je in te zetten voor de kunstklepprojecten. Het was een plezier de

IMPACT casussen een voor een met je door te nemen. Met je enthousiasme en energie weet ik zeker dat jij de beeldvorming in deze patiëntengroep in de kliniek verder op de kaart zal zetten. Ook dank voor de goede gesprekken die we hebben kunnen voeren.

Drs. Hanna Talacua, beste Hanna, je was vanaf het begin mijn mock loop maatje en daar ben ik heel blij mee. Wat een uren hebben we samen daaraan besteed. Dank voor je gezelligheid. Ook jij bent bijna daar, je verdiende PhD. Succes met de laatste loodjes en ik hoop dat we elkaar weer snel treffen.

Dr. Linda de Heer, beste Linda, jij hebt eerder al met je proefschrift de Radiologie en Cardiothoracale chirurgie nader tot elkaar gebracht. Ik hoop dat we deze lijn in het UMC Utrecht kunnen vasthouden. Dank dat je altijd zin en energie hebt mee te denken en te helpen met allerlei projecten naast je drukke opleiding.

Drs. Eduard Laufer, beste Ward, het was altijd gezellig samenwerken met je. Veel succes met het afronden van je eigen onderzoeken en ik hoop dat we binnenkort weer een studie samen kunnen doen.

Dr. Matthijs Meijs, na je kliniek nog met mij casussen doornemen tot ver in de avond en dat vol overgave tot de allerlaatste patiënt. Dank voor je inzet en bereidheid altijd op korte termijn klaar te staan.

Dr. Jesse Habets, je hebt als mijn voorganger de toon gezet. Vol enthousiasme heb je de klinische hartklepstudies opgezet, dank daarvoor. Ik hoop dat je tevreden kan terugkijken op al onze klepprojecten.

Jolanda Kluin, Marc Buijsrogge, Pim de Jong, Arnold Schilham, Martin Willemink, Nils Planken, professor Oudkerk, Niek Prakken, Peter van Ooijen, Esther Provoost, Volkan Tuncay, Marco Stijnen, Ronald van den Bosch, Ceranza Daans, bedankt voor jullie tijd, hulp commentaar en suggesties op onze manuscripten.

COLLEGA'S EN BETROKKENEN

Prof. dr. J. Hendrikse, beste Jeroen, je enthousiasme voor de neuroradiologie is aanstekelijk. Dank voor je steun en alle mogelijkheden die je me hebt geboden, als coassistent, bij mijn afstuderen en toen ik tijdens mijn promotie bij je kwam met de wens naar het buitenland te gaan.

Radiologen en assistenten van het UMC Utrecht, in het bijzonder dr. Evert-Jan Vonken en dr. Birgitta Velthuis, bedankt voor jullie inzet tijdens de klinische studie en alle andere hartklepprojecten.

CT laboranten, veel dank voor de energie die jullie hebben gestoken in de IMPACT studie. In het bijzonder Karin Thijn, Jamal Moumni en Robert Valkenburg, dank voor alle avonden en weekenden die jullie aan mijn hartklepprojecten hebben besteed.

Echolaboranten, cardiologen, thoraxchirurgen en assistenten van de afdeling Cardiologie en Cardiothoracale chirurgie van het UMC Utrecht, bedankt voor jullie bijdrage aan de studies gepresenteerd in dit proefschrift.

Stafleden, fellows en assistenten van de afdelingen Cardiothoracale chirurgie, Cardiologie en Radiologie van het AMC, dank voor jullie inzet tijdens de IMPACT studie.

Trialbureau Radiologie, Lenny, Saskia, Anneke, Shanta en Cees. Dank voor jullie inzet bij alle hartklepstudies. In het bijzonder, Shanta en Cees dank voor jullie onmisbare hulp bij de administratie en opzet van de database. Anneke dank voor het inplannen van alle CT onderzoeken.

Marco Stijnen en Sjoerd van Tuijl, bedankt dat jullie altijd bereid waren te helpen met de mock loop.

Prof. dr. van der Graaf, beste Yolanda, dank voor uw interesse in de kunstklepstudies en voor het lezen en beoordelen van mijn eindproject van de master Clinical Epidemiology.

Collega's van de Cardiovasculaire Radiologie in Nederland, bedankt voor de samenwerking, inspiratie en gesprekken tijdens congressen en andere gelegenheden.

Maatschap Radiologie Gelre Ziekenhuizen, Apeldoorn. Ik had me geen betere semi-arts tijd kunnen wensen. Dr. Gratama, in het bijzonder wil ik u bedanken voor uw enthousiasme, hulp en betrokkenheid. Dr. Droogh-de Greve, beste Kitty, veel dank voor de kans en tijd die ik krijg om na mijn promotie naar Stanford terug te keren als postdoc. Ik kijk er ook ontzettend naar uit daarna mijn opleiding in Apeldoorn te starten.

Graag wil ik het secretariaat Radiologie en in het bijzonder Marja Kool bedanken voor alle hulp. Marja, je hebt ontzettend veel voor me gedaan en me enorm geholpen, zeker toen ik in het buitenland verbleef en het einde van mijn promotietraject naderde. Dank daarvoor.

Chris, Karin, Jan en Roy, fotografie team, dank voor jullie hulp bij de opmaak van mijn figuren en foto's. Roy Sanders, dank voor de opmaak van mijn proefschrift.

Technisch cluster, 57000, bedankt voor het aanzetten van mijn computer en het oplossen van andere technische problemen waar ik jullie écht voor nodig had. Kees van Kesteren, dank voor het redden van de data op mijn USB-stick.

COLLEGA-ONDERZOEKERS

Onderzoekers van de Radiologie, bedankt voor de leuke congressen, fantastische borrels, heerlijke koffiemomenten en wandelingen. Zeker ook bedankt voor alle te slechte en te vaak herhaalde grappen en verhalen, een ware bron van inspiratie. Ik hoop dat we elkaar nog veel gaan zien.

Jip Prince, je bent altijd bereid te helpen, zelfs op grote afstand. Andor van den Hoven, dank voor de leuke tijd in Californië en alle 'Dutchies' momenten. Richard Takx, niets is hetzelfde zonder, of is alles anders met, thanks. Floor Knuttel, het was briljant, niet alleen tijdens maar ook buiten werktijden. Nu moeten we echt werken. Dank dat je mijn paranimf wilt zijn.

Suzanne, Merel, Charlotte, Thijs, Tom, Alexander, Maarten B., Joost, Herwie (Marnix), Wouter, Maarten S., Joris, Gisela, Annemarie, Anouk E., Anouk G., Cecile, Josephine, Martin, Bjorn, Alexandra, Esther, Remko, Anja, Jill, Bertine, Pushpa, Arthur, Nolan, Marlijne, Hanke, bedankt voor alle fijne momenten en wijze adviezen.

Sophie, Danny, alle collega's van de radiotherapie, collega's van het ISI, het was gezellig.

Raluca, we will run into each other again.

INTERNATIONAL COLLEAGUES

Dr. M. Lansberg, dear Maarten, thank you for giving me the opportunity to come to Stanford University and work with you in stroke imaging research. Thank you for your kind and generous help.

Thanks to everyone at the Stanford Stroke Center, thank for your help with my stroke projects and your interest in my PhD. Søren Christensen, Sun Kim, Jenny Tsai, Christian Federau, thanks for being great colleagues and making my time so enjoyable.

Prof. dr. D. Fleischmann, dear Dominik, it is a privilege to be working with you as a postdoc at Stanford. Thank you for your enthusiasm, trust and your encouragement for cardiovascular imaging. I am grateful for all the opportunities you provided and I am looking forward to all our future research projects.

I would also like to express my thanks to the entire team of the Cardiovascular Imaging Section at Stanford. Special thanks to prof. dr. Hans-Christoph Becker, Dr. Frandics Chan and prof. dr. Robert Herfkens for having me at the department. Recai Aktay, Michael Kadoch, Aya Kino, Jia Wang, Lior Molvin, thank you for your interest, time and willingness to help.

VRIENDEN EN FAMILIE

Lieve jaarclub, Gorenje, vrienden uit Eindhoven en Utrecht, bedankt voor jullie interesse in mijn onderzoek maar voornamelijk voor alle fantastische momenten die we samen hebben en voor alle bijzondere dingen die we meemaken. Dank voor jullie vriendschap.

Tijme, bedankt voor alle leuke afleiding, onze reizen en je luisterend oor tijdens mijn promotietijd.

Merel Dirkx, naast de gezelligheid een extra dank voor je betrokkenheid bij het afronden van mijn promotie, je hulp bij de Nederlandse samenvatting en dat je mijn paranimf wilt zijn.

Geoff Naylor, thank you for designing my thesis cover.

Friends from the Bay Area, roomies and Hackmann House. Thanks for all the good times, SF nights, family dinners and road trips.

Sjimmie, zelfs duizenden kilometers ver weg weten we elkaar te vinden. Of jij mij. Hoe dan ook, bedankt voor je geduld, steun en zorgzaamheid.

V neposlední řadě bych chtěla poděkovat svým rodičům, bratrovi a celé rodině za všestrannou pomoc a podporu.